Composites Science and Technology

Mohammad Jawaid
Ahmad Hamdan
Mohamed Thariq Hameed Sultan *Editors*

# Structural Health Monitoring System for Synthetic, Hybrid and Natural Fiber Composites

Springer

# Composites Science and Technology

**Series Editor**

Mohammad Jawaid, Lab of Biocomposite Technology, Universiti Putra Malaysia, INTROP, Serdang, Malaysia

**Composites Science and Technology (CST)** book series publishes the latest developments in the field of composite science and technology. It aims to publish cutting edge research monographs (both edited and authored volumes) comprehensively covering topics shown below:

- Composites from agricultural biomass/natural fibres include conventional composites-Plywood/MDF/Fiberboard
- Fabrication of Composites/conventional composites from biomass and natural fibers
- Utilization of biomass in polymer composites
- Wood, and Wood based materials
- Chemistry and biology of Composites and Biocomposites
- Modelling of damage of Composites and Biocomposites
- Failure Analysis of Composites and Biocomposites
- Structural Health Monitoring of Composites and Biocomposites
- Durability of Composites and Biocomposites
- Biodegradability of Composites and Biocomposites
- Thermal properties of Composites and Biocomposites
- Flammability of Composites and Biocomposites
- Tribology of Composites and Biocomposites
- Bionanocomposites and Nanocomposites
- Applications of Composites, and Biocomposites

To submit a proposal for a research monograph or have further inquries, please contact springer editor, Ramesh Premnath (ramesh.premnath@springer.com).

More information about this series at http://www.springer.com/series/16333

Mohammad Jawaid · Ahmad Hamdan ·
Mohamed Thariq Hameed Sultan
Editors

# Structural Health Monitoring System for Synthetic, Hybrid and Natural Fiber Composites

Springer

*Editors*
Mohammad Jawaid
Laboratory of Biocomposite Technology,
INTROP
Universiti Putra Malaysia
Serdang, Selangor, Malaysia

Mohamed Thariq Hameed Sultan
Department of Aerospace Engineering,
Faculty of Engineering
Universiti Putra Malaysia
Serdang, Selangor, Malaysia

Ahmad Hamdan
Department of Aeronautical Engineering,
Faculty of Mechanical and Manufacturing
Engineering
Universiti Tun Hussein Onn Malaysia
Parit Raja, Johor, Malaysia

Composites Science and Technology
ISBN 978-981-15-8839-6 ISBN 978-981-15-8840-2 (eBook)
https://doi.org/10.1007/978-981-15-8840-2

© Springer Nature Singapore Pte Ltd. 2021
This work is subject to copyright. All rights are reserved by the Publisher, whether the whole or part of the material is concerned, specifically the rights of translation, reprinting, reuse of illustrations, recitation, broadcasting, reproduction on microfilms or in any other physical way, and transmission or information storage and retrieval, electronic adaptation, computer software, or by similar or dissimilar methodology now known or hereafter developed.
The use of general descriptive names, registered names, trademarks, service marks, etc. in this publication does not imply, even in the absence of a specific statement, that such names are exempt from the relevant protective laws and regulations and therefore free for general use.
The publisher, the authors and the editors are safe to assume that the advice and information in this book are believed to be true and accurate at the date of publication. Neither the publisher nor the authors or the editors give a warranty, expressed or implied, with respect to the material contained herein or for any errors or omissions that may have been made. The publisher remains neutral with regard to jurisdictional claims in published maps and institutional affiliations.

This Springer imprint is published by the registered company Springer Nature Singapore Pte Ltd.
The registered company address is: 152 Beach Road, #21-01/04 Gateway East, Singapore 189721, Singapore

# Preface

Structural analysis is a crucial element in engineering. The analysis is employed in many fields such as building, marine, automotive, and aerospace. Composite material is one of the materials applied to those applications. Most of the time, synthetic fiber such as glass fiber, kevlar, and carbon fiber are consumed as fiber-reinforced in composite. Interestingly, natural fiber-reinforced composite gains serious attention due to the 'green' concept. It starts to substitute the synthetic fiber in a hybrid approach or replace the existing synthetic fiber. However, the knowledge in the structural analysis needs further discussion and exploration. Therefore, the discussion will be focussing on analysis methods like simulation, predictive analysis, experimental data, and structural health monitoring system.

Besides that, the structural analysis is crucial as well during the usage or on running application condition. However, how are we going to monitor the structural condition? Therefore, the maintenance scheduling needs to be conducted to the engineering structure. Interestingly, Structural Health Monitoring has gained popularity in evaluating the performance of a structural application in recent trends. The Structural Health Monitoring system occurs in real-time or in an online situation. Hence, it also has advantages for damage detection, damage localization, damage assessment, and life prediction compared to the Non-Destructive Test which is conducted offline.

The simulation and modeling analysis gain new exciting especially to predict and identify the material properties. It involved a combination of several materials and need a special definition and assumption. Experimental data is very important to investigate the feasibility and the properties of composite, especially, in natural fiber and synthetic fiber-based hybrid composites. The analysis of the prototype will give better information on the material properties of ready to commercialize products. The book contains recent works on Sensing device technology in recent industrial applications, Modeling and Analysis of Functionally Graded Biocomposite Plate Structure using Higher Order Kinematics, Natural fiber and hybrid composite for structural application, Damage Characterization of Composite Stiffened Panel Subjected to Low-Velocity Impact, Numerical Simulation Techniques for Damage Response Analysis in Composites, Modeling of damage

evaluation and failure of laminated composite materials, Fatigue responses of Fiber-reinforced polymer composite, Predictive engineering in structural Application, design of a Low-Resolution Thermography Camera system for Subsurface defect detection of a thin composite plate, The Energy Absorption Performances of the Rectangular Composite Crash Boxes, and Numerical and experimental assessment of water absorption of red mud—an industrial waste reinforced sisal/polyester hybrid polymer composite.

We are thankful to all authors who share their knowledge and expertise on Structural health monitoring for natural fiber and hybrid composite and make editors thoughts into reality. Besides that we are also thankful to Springer-Nature team for continuous support during the whole project without that it is difficult to complete the Project.

Serdang, Malaysia — Mohammad Jawaid
Batu Pahat, Malaysia — Ahmad Hamdan
Serdang, Malaysia — Mohamed Thariq Hameed Sultan

# Contents

# About the Editors

**Dr. Mohammad Jawaid** is currently working as Senior Research Fellow (Professor) at Biocomposite Technology Laboratory, Institute of Tropical Forestry and Forest Products (INTROP), Universiti Putra Malaysia, Serdang, Selangor, Malaysia. He has more than 10 years of experience in teaching, research and industries. His area of research interests includes hybrid reinforced/filled polymer composites and advance materials. So far, he has published 40 books, 65 book chapters, more than 350 peer-reviewed international journal papers and several published review papers under top 25 hot articles in science direct during 2013–2018. He also obtained 2 Patents and 6 Copyrights. H-index and citation in Scopus are 51 and 12100, and in Google scholar, H-index and citation are 61 and 16736. He is founding Springer Series Editor of Composite Science and Technology Book and Series Editor of Springer Proceedings in Materials. He is also International Advisory Board member of Springer Series on Polymer and Composite Materials. His several published review papers under top 25 hot articles in science direct during 2013–2020. He is reviewer of several high impact ISI journals (84 journals). Recently Dr. Mohammad Jawaid received Excellent Academic Award in Category of International Grant-Universiti Putra Malaysia-2018 and also Excellent Academic Staff Award in industry High Impact Network (ICAN 2019) Award. Beside that Gold Medal-Community and Industry Network (JINM Showcase) at Universiti Putra Malaysia. He also Received Publons Peer Review Awards 2017, and 2018 (Materials Science), Certified Sentinel of science Award Receipient-2016 (Materials Science) and 2019 (Materials Science and Cross field). He is also Winner of Newton-Ungku Omar Coordination Fund: UK-Malaysia Research and Innovation Bridges Competition 2015. He is Fellow and Charted Scientist of Institute of Materials, Minerals and Mining, UK. He is also life member of Asian Polymer Association, and Malaysian Society for Engineering and Technology. He has professional membership of American Chemical Society (ACS), and Society for polymers Engineers (SPE), USA.

**Dr. Ahmad Hamdan** obtained his Ph.D. in Aerospace Engineering from Universiti Putra Malaysia in 2015. Presently, he is working as a Senior Lecturer at Universiti Tun Hussein Onn Malaysia, Malaysia. His research focuses mainly on turbine blade aerodynamics, structural health monitoring system, biocomposites fabrication, structure vibration, cutting tool technology and cooling system. He was awarded with Gold Medal for his project, Automatic Thermocyclic Dipping Machine (ATDM) at ITEX 2011. He already published 1 book, 5 book chapters, 14 proceeding papers and more than 12 international journal papers.

**Prof. Ir. Ts. Dr. Mohamed Thariq Hameed Sultan** is a Professor at Aerospace Department, Universiti Putra Malaysia. He received his Ph.D. from the University of Sheffield, UK. He has about 15 years of experience in teaching as well as in research. His area of research interests includes hybrid composites, advanced materials, structural health monitoring and impact studies. So far, he has published more than 300 international journal papers and received many awards locally and internationally. Currently, he is also attached to the Institution of Engineers Malaysia (IEM) as the Chairman in the Engineering Education Technical Division (E2TD).

# Structural Health Monitoring: Sensing Device Technology in Recent Industrial Applications


**Muhammad Imran Najeeb and Mohamed Thariq Hameed Sultan**

**Abstract** With continuous rapid development of sensor technology, structural health monitoring system (SHMS) managed to be developed and employed in various kind of structures or component. The aim of this chapter is to give a brief review on recent sensing technology that had been used in structural health monitoring system towards industrial application. There are various field of engineering that utilize different kind of sensor to measure and evaluate in real-time assessment on the structural behaviour/performance under such loads for further maintenance actions or in optimizing a design. Even though SHMS showed many advantages in take care of the structure, it also shows several drawback that causing it not been used widely. However, it is believe that in the next 15 years, the SHMS will become a needs in multi-industry and sub industry level in their structures or components, as the world are now moving towards industrial 4.0.

**Keywords** SHMS · NDT · Structural health monitoring sensor · Structural integrity · Strain gauge · Bridge · Flyover · Transportation

M. I. Najeeb
Faculty of Engineering, Department of Aerospace Engineering, Universiti Putra Malaysia, Serdang, Selangor, Malaysia

M. T. H. Sultan (✉)
Laboratory of Biocomposite Technology, Institute of Tropical Forestry and Forest Products (INTROP), UPM, 43400 Serdang, Selangor Darul Ehsan, Malaysia
e-mail: thariq@upm.edu.my

Faculty of Engineering, Department of Aerospace Engineering, Universiti Putra Malaysia, 43400 Serdang, Selangor Darul Ehsan, Malaysia

Aerospace Malaysia Innovation Centre (944751-A), Prime Minister's Department, MIGHT Partnership Hub, Jalan Impact, 63000 Cyberjaya, Selangor Darul Ehsan, Malaysia

© Springer Nature Singapore Pte Ltd. 2021

M. Jawaid et al. (eds.), *Structural Health Monitoring System for Synthetic, Hybrid and Natural Fiber Composites*, Composites Science and Technology,
https://doi.org/10.1007/978-981-15-8840-2_1

## 1 An Overview

Safety of buildings and other structures is of paramount importance, as structural integrity may be compromised with the passage of time due to internal and external load pressure. Among factors attributing to defects include environmental stress. Apart from periodic maintenance, early identification of structural defect is crucial to ensure safety of a structure or component. However, identifying and assessing the extent of internal damage, and its precise location can be very challenging. Therefore application of structural health monitoring system (SHMS) is crucial for long-term assessment of safety and security. Structural health monitoring involve continuous observation of structural integrity over a period of time by using an array of connected sensors during the duration of service life of the structure [1]. Routine structural monitoring is important to secure the safety of a structure or component for daily use. Through the monitoring process, potential problems could be detected early, even in normally occluded areas, prior to structural damage. Structural monitoring can also be applied to understand how best to maintain a structure to extend its design life, or to gauge if the construction or maintenance works were progressing as planned.

SHMS offers a more proactive maintenance approach compared to conventional maintenance routine where repair works are carried out only after the occurrence of any form of damage [1]. Usually damages are detected upon visual inspection or when a machinery breaks down. Such structural or machinery failure have far-reaching implication on life-cyclecost, apart from draining resources. For example, Taiwan's Nanfang'ao bridge suddenly collapsed in 2019, without any early warning sign indicating structural defect and subsequent failure. It was a tragedy that killed six people. It was reported that the possible causes of failure were due to rust, as well as wear and tear [2]. The same year, a significant structural failing of the Hammersmith bridge in London was visually detected, as cracks appeared at the pedestal. Access to the bridge was closed to facilitate repair works that cost an estimated €120 million [3]. To overcome such unforeseen circumstances, it is better to adopt the SHMS to help identify and quantify potential structural defects at early stages locally and globally. Early detection and the right maintenance measures taken could help prevent major damage that could lead to eventual structural failure.

Over the decades the SHMS has evolved, thanks to advances in sensing, power, communication, storage, signal processing algorithm and health evaluation algorithm technologies. Together with such technologies, SHMS had been applied in various civil industry as well as the transportation sector, including bridge, dams, building and railways. Sensing technology is the pulse of SHMS. Various types of sensing technologies are available, and it continues to evolve to further improve monitoring of structural conditions based on real data collection [4]. With the availability of various types of sensors with different functions, engineers should identify and set up the proper array of sensors according to the designed sensing system so that it can properly capture the targeted data during the real-time monitoring process.

## 2 Sensing Technology by Application

### *2.1 Civil*

Civil structures constantly bear the load pressure from multiple directions. Therefore it is vital to systematically assess structural behaviour for early detection of damage, to ensure the structures continue to function well. Traditionally, scheduled visual inspection are carried out to detect damages on the surface of a structure. However, this does not provide the best solution because internal signs of damages could not be seen with the naked eyes. Early detection is vital so that corrective measures could be taken in order to extend the life span of a structure. Therefore it is important to periodically monitor the structural health of a structure to detect anomalies in time. This will help optimise maintenance and reduce the overall operating cost. The latest SHMS applications in several sub-sectors of civil architecture are discussed below.

SHMS had been used to monitor various kind of infrastructure such as bridge. Manhattan bridge in New York City state had applied SHMS to monitor the bridge in real-time because the bridge floor beams had developed distortion-induced cracks due to repeated train loads. In the first stage, the engineers conducting visual inspection along the bridge from the sidewalk. They observed a clearly joints misalignment and the sound of train wheels impacting the rails end. To gain understanding the nature of coupled dynamic system between the train and bridge, over twenty accelerometers (PCB 393A03 accelerometer) were installed along the selected location of the floor beams. Then they monitor the data of 30 train crossing over the bridge to quantify the impact of this amplification on the strain responses of the transit stringers and floor beams. The results obtain seems agreed the visual inspection results where there are misalignment and the impact sound from the wheels and the rail. In 2nd stage, the objective was to estimate the impact of the distortion on the long-term bridge performances. They had installed 14 strain gages to anaylze flexural stress, 16 strain gages to capture shear stress, 6 temperature sensor and 4 crack gages. The crack gages was employed at locations that are suspected to have fatigue cracking. With these sensors, they can identify if there were presence of opening of the distortion-induced cracks and to provide a baseline data that could be used to quantify the efficacy of mitigation strategies [5]. By having the SHSM, the structural integrity of the bridge can be preserve in long-run and the life-cycle maintenance cost can be reduced.

The SHMS technology is also applied to ensure longterm safety of the Hammersmith flyover in London. The four-lane flyover stretching 622 m long was built in 1961. Reinforced concrete piers support the flyover bridge [6]. And roller bearings at the base of each pier allow thermal expansion and accommodate both rotation and translation movement in longitudinal direction so that the stress acting on the structure is reduced [7]. Findings during decades of maintenance services reflect cause for concern over structural integrity, as corrosion was observed at the prestressing tendons. The rapid corrosion is believed to have occurred because of deicing salts application during winter, apart from failure of the water-proofing system. Further visual inspection also showed deterioration of roller bearing, and this posed a grave

concern as the bearing serve a critical function to reduce stress in a structure. Therefore it is important to fix sensors to enable monitoring, interpretation and analysis of relevant data so that remedial action can be taken to address defect at the specific area. An acoustic emission sensor is used to detect wire breaks, while linear potentiometric displacement transducers (LPDT) are used to measure pier-bearing horizontal displacement and temperature readings [6]. It is not feasible to use longitudinal strain measurements to detect changes caused by even a large number of wire breaks in the bridge deck because it is impossible to ascertain if prestress losses have occurred in view of noise in data due to live load effects [6].

Besides bridge and flyover, the SHMS can also be used on offshore structures like an example in Bremerhaven, Germany offshore wind power plant that located in open sea. There power plant consist of two component which were the carrying structure (jacket + tower) and the nacelle with the rotor blades [8]. The structures were subjected to rough sea stress such as wind, waves and saltwater. There were 70 strain gage installed on the jacket to analyse the static and dynamic behaviour of the newly developed cast-iron nodes. Two type of sensor that had employed at the stressed points of the jacket namely electrical strain gages and fiber-optical strain gages. The electrical resistance working principle is simple where it depending on the changes of electrical resistance experience by the strain gages when it compressed and strectched. The changes in the electrical resistance gives value of strain. Fiber optical strain gages is used to also measure strain and temperature. However, this sensor had advantages as it can allocate many sensing point along a single fiber optic making it can provide local and global strain of a structure [9].

The SHMS application can also be used to enhance productivity and efficiency of machine performance, apart from monitoring damages and evaluating structural behavior under loading pressure. In Europe, SHMS is applied to enhance efficiency of turbine blades in hydropower plants. Two types of strain gauges are installed directly onto the turbine blade at input stage. Strain gauges are used because they are durable, thus providing long-term stability. The first type of strain gauge, HBM XY41-3/700, is used to measure torque movement. And the second type of strain gauge, XY31-3/350, is used to measure the axial force and speed at the turbine input stage. The installed strain gauges are enveloped in a special cover for electrical protection as well as to prevent electromagnetic interferences. All the information based on real-time calculation, measurements, and diagnosis are analysed using PMX data acquisition system. With such setting, the efficiency of the hydro powerplant is increased up to 10% [10].

The SHMS application is also used in underground construction works to monitor changes in soil characteristics. Uncertainties over soil characteristics pose a major challenge in the underground construction sector [11]. For example, Avenue2, a consortium of Strukton and Ballast Nedam, carried out tunneling works right below Maastricht in a move to re-route A2 motorway. Soil characteristics and excavation works at a depth of 22 m below ground posed various challenges. To ensure stability during the excavation process, various types of sensors were installed in the surrounding areas to enable real-time monitoring, and raise alert if signs of subsidence emerge. Three types of sensors were installed to monitor the conditions of

external walls of buildings near the excavation site. Sensors installed are automatic clinometers to measure elevation angles above horizontal, pressure sensor to measure water tension in vertical tubes, and strain gauges to measure the load on horizontal props [12]. Using these sensors, site engineers can carry out real-time monitoring and keep contractors informed on forces at play during construction works so that remedial action can be taken immediately to keep the surrounding structures strong and safe, while enabling work to progress rapidly as planned and save cost.

## *2.2 Air Transportation*

Damages to a structure do not necessarily result in visible dents and cracks. Therefore SHMS application is needed to detect possible structural flaws although the surface may appear smooth and undamaged. For example, sensors are positioned in the aircraft landing gear shock strut to continuously monitor tyre pressure, brake temperature and hydraulic pressure [13]. Safran, one of the leading high-technology industry players, have developed a an extremely light miniaturised micro-electro-mechanical system (MEMS), weighing a mere two grams. This system enables a wide range of parameter measurements including acceleration, pressure, and magnetic field. Compared to conventional MEMS, the newly invented tiny and extremely light sensor can be applied to monitor performance of engines, brakes, landing gear, and many other critical components [14].

Apart from MEMS, comparative vacuum monitoring (CVM) sensors and piezo-electric sensor arrays (PZT) are also applied in SHMS programmes to automatically and remotely assess an aircraft's structural condition in real time, and raise an alert when the need for maintenance arise [15]. The CVM sensor is used to detect crack. It is mounted on aircraft parts that are prone to experience fatigue. It is bonded to the surface of the structure with an adhesive, sealing off the atmosphere, thus creating a vacuum inside the gallery. When a tiny crack intersects with the gallery, the sensor records the changes in pressure, and alerts the operator before the cracks pose safety issues. Besides that, for PZT, the sensors are strategically located throughout smart layers, adhered to the aircraft structure. The sensors function by transmitting and receiving ultrasonic surface waves (Lamb waves) to one another, where its creates a mini network system. When a damage occur, it will disrupt the signal pattern (compared with baseline signal pattern) and the measurement and analysis are made using software [15]. Hence the SHM system showcases the real-time condition of an aircraft, and raise maintenance alert accordingly. It promotes condition-based maintenance rather than the conventional time-based maintenance.

Apart from MEMS, CVM and PZT applications, strain gauge sensors are also used in monitoring structural integrity of aircraft. A French aircraft manufacturing company firm, LISA Airplanes, utilise SHMS in their latest light-weight aircraft AKOYA. AKOYA is built using hybrid with composite materials that offers good flexibility and stability. As this is a newly developed aircraft, the manufacturer carried out comprehensive structural and component tests especially on various stress acting

on the structure at various stages of flight [16]. Therefore, it is important to ascertain the desired parameters for measurements. Strain gauge were installed in quater-, half- and full-bridge configurations on the aircraft wings. Generally, a simple quater bridge is used to measure strain on a tension/compression bar or on a bending beam. Half-bridge strain gauge can measure axial/bending strain or bending strain only, while full-bridge strain gauge can measure bending or axial strain only. Besides measuring the various parameters, the choice of strain gauge configuration is also important, as changing the bridge configuration can improve strain sensitivity [17].

On top of that, aircraft airframe are vulnerable to corrosion, potentially leading to material degradation, and eventually causing fatigue crack. Generally, aircraft structures are well coated. However, the aircraft are exposed to various type of impact and damage during daily services. Three methods are available to monitor and measure corrosion. The first method involve direct measurement of corrosion effects using electrochemical sensors such as Electrochemical Impedance Spectroscopy (EIS) sensor. The second method involve measurement of corrosivity environment, where corrosive condition of underlying structures are evaluated. For example, galvanic sensors are used to monitor the corrosion of metallic elements through the changes in electrical resistance of the sensor. The third method involve measurement of corrosion using chemical sensors [18]. This sensor can detect the presence of specific ion from a corroded component/structure. However, this sensor is not very reliable because to date it could not demonstrate long-term stability or resistance to poisoning caused by contaminants. Table 1 summarize application of structural health monitoring ‘s sensor in industries.

## 3 Challenges in Implementing SHMS

SHMS application in various industries, showcasing a positive impact in the long run both in safety and maintenance cost. However, the technology has its limitations due to several factors including SHMS cost. The technology and installation of this system is costly, and beyond the affordability of many small and medium industries [1]. Therefore, the engineers must verify specific parameters that are highly likely to affect structural integrity so that only necessary sensors are used instead of using multiple sensors to measure all sorts of parameters. A study concluded that corrosion sensor is not cost-effective, and that the current ground inspection of aircraft is already sufficient, for now, to detect corrosion [18]. However, application of corrosion sensor is much more cost effective in hard to access areas such as undersea/subterranean pipelines and offshore structures. Next was on the interperation of the test result. Since the SHMS enable real-time monitoring, the size of data collected can be very big. It can prove challenging for engineers to analyse and interpret the big data. A special set of skills is needed to utilise the data to facilitate decision-making [1].

**Table 1** Structural health monitoring 's sensor application

| Type of sensor | Application | References |
|---|---|---|
| Accelerometer | Bridge-floor beams | [5] |
| Strain gauges | Bridge, power plant, Subterranean, aircraft | [5, 10, 11, 16] |
| Crack gauges | Bridge | [5 |
| Acoustic emission | Flyover | [7] |
| Linear potentiometric displacement transducers (LPDT) | | |
| Electrical strain gauges | Power plant | [8] |
| Optical strain gauges | | |
| Automatic clinometers | Subterranean | [11] |
| Pressure sensor | | |
| Micro-electro-mechanical system (MEMS) | Aircraft | [14] |
| Comparative vacuum monitoring (CVM) | | [15] |
| Piezoelectric sensor arrays (PZT) | | [15] |
| Electrochemical impedance spectroscopy (EIS) sensor | | [18] |
| Galvanic sensors | | [18] |
| Chemical sensors | | [18] |

## 4 Conclusion

This paper discuses advances in the use of various sensors complementing the SHMS applications in both civil and aviation industries. A variety of sensors, and integrated sensor networks are available to evaluate the performance of a desired system including structural elements, electronics, hydraulics, avionics and others. Smaller size matters in the advent of sensor technology, as innovators continue to minimise the size of sensors to enable embedding in various structures and remote locations. It is important for the engineers to determine crucial parameters, and analyse the big date to gauge structural integrity and performance. It is important to verify where to measures, and translate the data obtained into useful information in decision-making process in order to optimise the maintenance process. It is also crucial to select the desired sensor based on its usage, and ascertain if it is practical and effective in obtaining reliable data that are free from noise disturbance.

**Acknowledgments** The authors would like to thank Universiti Putra Malaysia for the financial support through the Geran Putra Berimpak, GPB 9668200. The authors would like to thank the Department of Aerospace Engineering, Faculty of Engineering, Universiti Putra Malaysia and Laboratory of Biocomposite Technology, Institute of Tropical Forestry and Forest Product (INTROP), Universiti Putra Malaysia (HICOE) for the close collaboration in this research.

## References


1. Why We Need Structural Health Monitoring? (2019, March 12) https://www.fprimec.com/why-we-need-structural-health-monitoring/. Accessed 18 May 2020
2. Greenwood M (2019) What caused Taiwan'S Nanfang'Ao bridge to collapse? https://www.engineering.com/BIM/ArticleID/19645/What-Caused-Taiwans-Nanfangao-Bridge-to-Collapse.aspx. Accessed 18 May 2020
3. BBC News (2019) Hammersmith bridge repairs 'Could Cost £120M'. https://www.bbc.com/news/uk-england-london-49564267. Accessed 18 May 2020
4. FPrimeC Solutions Inc. (2020) Sensors for structural health monitoring|Fprimec Solutions Inc. https://www.fprimec.com/sensors-for-structural-health-monitoring/. Accessed 18 May 2020
5. McAnulty K (2020) Structural health monitoring of representative cracks in the Manhattan bridge. Doctoral dissertation, Rutgers, The State University of New Jersey
6. Webb GT, Vardanega PJ, Fidler PRA, Middleton CR (2014) Analysis of structural health monitoring data from Hammersmith flyover. J Bridge Eng 19(6):05014003
7. The Constructor (n.d.) Bridge bearings -types of bearings for bridge structures and details. https://theconstructor.org/structures/bridge-bearings-types-details/18062/. Accessed 18 May 2020
8. HBM (n.d.) HBM technology and service for building up the first germ. https://www.hbm.com/en/3316/hbm-technology-and-service-for-building-up-the-first-german-offshore-wind-farm/. Accessed 18 May 2020
9. Berrocal CG, Fernandez I, Rempling R (2020) Crack monitoring in reinforced concrete beams by distributed optical fiber sensors. Struct Infrastruct Eng 1–16
10. HBM (n.d.) Iron gate dam: measuring the efficiency of turbine blades. https://www.hbm.com/en/6833/dam-monitoring-with-pmx/. Accessed 18 May 2020
11. HBM (n.d.) Strukton: monitoring changes in the soil characteristics. https://www.hbm.com/en/4583/strukton-monitoring-changes-in-the-soil-characteristics/. Accessed 18 May 2020
12. Calvert JB (2003) The clinometer. https://mysite.du.edu/~jcalvert/astro/abney.htm. Accessed 18 May 2020
13. Safran (n.d.) Monitoring system. Safran Landing Systems. https://www.safran-landing-systems.com/monitoring-system. Accessed 18 May 2020
14. Safran (2015) Revolutionary micro-sensors. https://www.safran-group.com/media/20151020_revolutionary-micro-sensors. Accessed 18 May 2020
15. Aerospace Manufacturing and Design (2014) Structural health monitoring. https://www.aerospacemanufacturinganddesign.com/article/structural-health-monitoring-maintenance-122914/. Accessed 18 May 2020
16. HBM (n.d.) LISA airplanes: many technological innovations. https://www.hbm.com/en/3246/lisa-airplanes-many-technological-innovations/. Accessed 18 May 2020
17. Ni.com (2019) Measuring strain with strain gages—National instruments. https://www.ni.com/en-my/innovations/white-papers/07/measuring-strain-with-strain-gages.html. Accessed 18 May 2020
18. Harris SJ, Mishon M, Hebbron M (2006) Corrosion sensors to reduce aircraft maintenance. In: Rto avt-144 workshop on enhanced aircraft platform availability through advanced maintenance concepts and technologies, Vilnius, Lithuania

# Modeling and Analysis of Functionally Graded Biocomposite Plate Structure Using Higher-Order Kinematics


**V. R. Kar, A. Karakoti, S. Jena, P. Tripathy, K. Jayakrishna, M. Rajesh, D. Mallikarjuna Reddy, and M. T. H. Sultan**

**Abstract** In this study, finite element modeling and analysis of functionally graded biocomposite structures are performed. Here, biocompatible materials are utilized throughout in the analysis to model biocomposite structures. Three types of material models, i.e., titanium, zirconia and titanium-zirconia biocomposites are considered. The material properties of titanium-zirconia biocomposites are evaluated Voigt's rule-of-mixture homogenization via power-law function. The strain field of the present model is based on higher-order equivalent single-layer kinematics. However, the motion equations are governed by minimizing total potential energy of the system. The final equilibrium equations are obtained using 2D Lagrangian finite element formulation. To confirm the correctness of the proposed finite element model, the present results are compared with the reported results. In addition, various numerical illustrations are demonstrated to exhibit the significance of different geometrical and material parameters on the deformation behavior of biocomposite structures under uniform pressure, and discussed in detail.

**Keywords** Biocomposites · FGM · Micromechanics · Deformation · Higher-order · FEM

V. R. Kar (✉) · A. Karakoti
Department of Mechanical Engineering, National Institute of Technology, Jamshedpur 831014, Jharkhand, India
e-mail: visheshkar@gmail.com; vishesh.me@nitjsr.ac.in

S. Jena · K. Jayakrishna · M. Rajesh · D. Mallikarjuna Reddy
School of Mechanical Engineering, VIT, Vellore 632014, Tamil Nadu, India

P. Tripathy
Department of Mechanical Engineering, National Institute of Technology, Rourkela 769008, Odisha, India

M. T. H. Sultan
Faculty of Engineering, Department of Aerospace Engineering, University Putra Malaysia (UPM), 43400 Serdang, Selangor Darul Ehsan, India

© Springer Nature Singapore Pte Ltd. 2021

M. Jawaid et al. (eds.), *Structural Health Monitoring System for Synthetic, Hybrid and Natural Fiber Composites*, Composites Science and Technology,
https://doi.org/10.1007/978-981-15-8840-2_2

## 1 Introduction

The capabilities of the advanced composite materials always attracted the researchers for design implementation in various structures/components of weight-sensitive areas. In past few years, replacement of conventional biomaterials with biocomposites is being the prime concern due to durability and performance. Typical functionally graded materials (FGMs) are known as advanced materials with smooth material gradation which replicate skin, bone, etc. like materials, and can be utilized effectively in bio-medical sectors [1]. The modeling and analysis of these types of advanced material structures always attract scientists and researchers. Many studies have been reported in past to examine various mechanical behavior of FGM type structures using various material, kinematic and solution schemes.

Thai and Vo [2] analyzed the bending, vibration and buckling behavior of FGM plates by employing a new sinusoidal shear deformation theory with four unknowns only. Governing equations and material properties were obtained using Hamilton's principle and power-law formulation, respectively. Reddy et al. [3] employed first order shear deformation theory (FSDT) to analyze the bending and stretching of FGM solid and annular plates. Brischetto and Carrera [4] proposed a model based on Reissner's mixed variation theorem (RMVT). FGM plates were transversely loaded and properties were graded according to Legendre's polynomial. Compelling results of RMVT shows the improvement when compared with the models based on principle of virtual displacement (PVD). Zidi et al. [5] used a four variable refined plate theory without shear correction factor for bending analyses of FGM plates experiencing hygro-thermo-mechanical load. Governing equations were obtained using principle of virtual displacement and material properties varied according to the simple rule of mixture. Della Croce and Venini [6] developed an extended model employing Reissner-Mindlin plate theory to manipulate the shear-locking phenomenon. Material properties were determined using power law formulation and variational principle derived the governing equations. Kar and Panda [7] obtained non-linear bending responses for FGM spherical panels using higher-order finite element approach.

The present study focuses the finite element modeling of different functionally graded biocomposite (FGB) structures, followed by their analysis to examine the deformation behavior under different sets of conditions. Here, zirconia and titanium materials are considered individually and also in combined form with smooth gradation. The smooth gradation is achieved using power-law function whereas the overall spatial elastic properties are obtained using Voigt's rule-of-mixture scheme. The kinematic model is developed using higher-order equivalent single-layer theory and the equation of motions are obtained using principle of total minimum potential energy. The final solutions are obtained using 2D finite element formulation. In later section, numerical examples are presented to demonstrate the impact of various geometrical parameters on the deformation behavior of different biocomposite structures under uniform pressure.

## 2 Mathematical Modeling of FGB Structure

### 2.1 Micromechanics of FGB Material

In the present work, three different material profiles, namely pure zirconia ($ZrO_2$), FGB ($ZrO_2$/Ti) and pure titanium (Ti) are considered as shown in Fig. 1. The moduli of elasticity of zirconia and titanium are $E_{Zr}$ and $E_{Ti}$, respectively. However the elastic modulus of FGB material ($E_{FGB}$) is evaluated using Voigt's rule-of-mixture

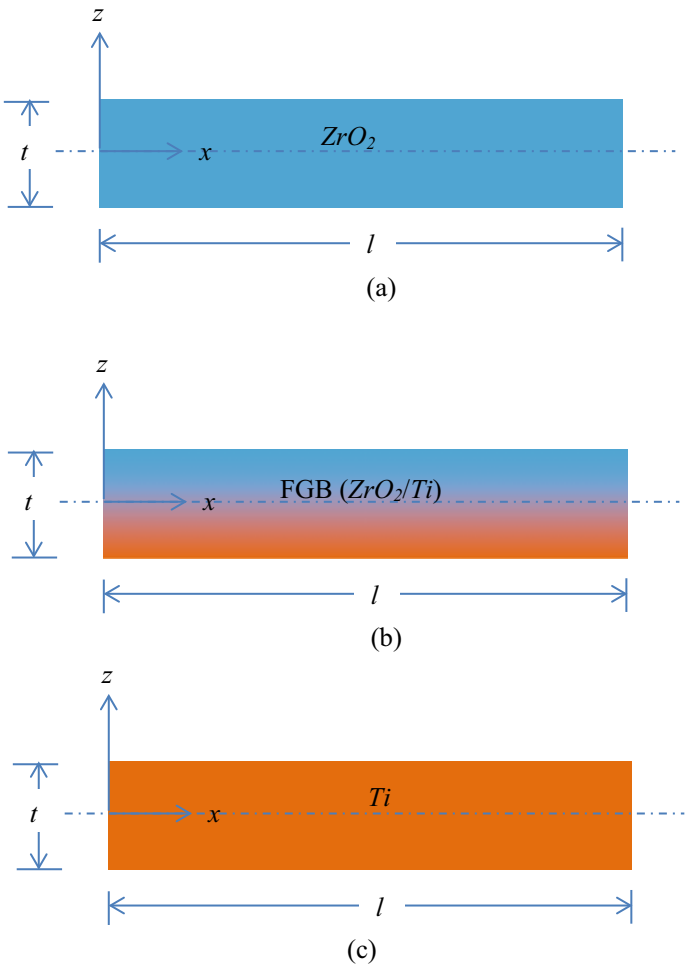


**Fig. 1** Description of different biocomposite structures **a** zirconia, **b** FGB (zirconia/titanium) and **c** titanium plate

micromechanical scheme [8, 11], as

$$E_{FGB} = (E_{\mathrm{Zr}} - E_{\mathrm{Ti}})V_{\mathrm{Zr}} + E_{\mathrm{Ti}} \tag{1}$$

where, $V_{\mathrm{Zr}}$ is the volume fraction of zirconia and this can be evaluated micromechanically using power-law function [8, 11], as follows

$$V_{\mathrm{Zr}} = \left(\frac{2z+t}{2t}\right)^{n} \tag{2}$$

where, volume fraction coefficient ($n$) controls the material distribution along the thickness direction of the structure and it can be any real value.

## 2.2 Kinematic and Constitutive Models

The strain tensor $\left(\{\varepsilon\} = \lfloor\, \varepsilon_{xx}\ \varepsilon_{yy}\ \varepsilon_{yz}\ \varepsilon_{zx}\ \varepsilon_{xy}\, \rfloor^{T}\right)$ of FGB plate can be written as,

$$\left.\begin{array}{l} \varepsilon_{xx} = \bar{\varepsilon}_1 + z\overline{\alpha_1} + z^2\overline{\beta_1} + z^3\overline{\gamma_1} \\ \varepsilon_{yy} = \bar{\varepsilon}_2 + z\overline{\alpha_2} + z^2\overline{\beta_2} + z^3\overline{\gamma_2} \\ \varepsilon_{yz} = \frac{1}{2}\left(\bar{\varepsilon}_4 + z\overline{\alpha_4} + z^2\overline{\alpha_4}\right) \\ \varepsilon_{zx} = \frac{1}{2}\left(\bar{\varepsilon}_5 + z\overline{\alpha_5} + z^2\overline{\alpha_5}\right) \\ \varepsilon_{xy} = \frac{1}{2}\left(\bar{\varepsilon}_6 + z\overline{\alpha_6} + z^2\overline{\alpha_6} + z^3\overline{\gamma_6}\right) \end{array}\right\} \tag{3}$$

$$\{\varepsilon\} = [\hbar]\{\bar{\varepsilon}\} \tag{4}$$

where, $\{\bar{\varepsilon}\} = \lfloor\, \bar{\varepsilon}_1\ \bar{\varepsilon}_2\ \bar{\varepsilon}_4\ \bar{\varepsilon}_5\ \bar{\varepsilon}_6\ \bar{\alpha}_1\ \bar{\alpha}_2\ \bar{\alpha}_4\ \bar{\alpha}_5\ \bar{\alpha}_6\ \bar{\beta}_1\ \bar{\beta}_2\ \bar{\beta}_4\ \bar{\beta}_5\ \bar{\beta}_6\ \bar{\gamma}_1\ \bar{\gamma}_2\ \bar{\gamma}_6\, \rfloor^{T}$ is mid-plane strain matrix and $[\hbar]$ is the spatial $z$-matrix.

Here, the mid-plane strain terms contain three translation ($u_1$, $v_1$, $w_1$), two rotation ($u_2$, $v_2$) and two higher-order ($u_3$, $v_3$, $u_4$, $v_4$) terms at any arbitrary point within the mid-plane ($z = 0$) of FGB plate which are based on the higher-order equivalent single-layer theory [12].

The stress field $\left(\{\sigma\} = \lfloor\, \sigma_{xx}\ \sigma_{yy}\ \sigma_{yz}\ \sigma_{zx}\ \sigma_{xy}\, \rfloor^{T}\right)$ at any point within FGB plate structure is written, as

$$\begin{Bmatrix} \sigma_{xx} \\ \sigma_{yy} \\ \sigma_{yz} \\ \sigma_{zx} \\ \sigma_{xy} \end{Bmatrix} = \begin{bmatrix} R_{11} & R_{12} & 0 & 0 & 0 \\ R_{21} & R_{22} & 0 & 0 & 0 \\ 0 & 0 & R_{44} & 0 & 0 \\ 0 & 0 & 0 & R_{55} & 0 \\ 0 & 0 & 0 & 0 & R_{66} \end{bmatrix} \begin{Bmatrix} \varepsilon_{xx} \\ \varepsilon_{yy} \\ \varepsilon_{yz} \\ \varepsilon_{zx} \\ \varepsilon_{xy} \end{Bmatrix} = [R]\{\varepsilon\} \tag{5}$$

where, [R] represents elastic material matrix and the individual terms are given as

$$R_{11} = R_{22} = \frac{E_{FGB}}{\left(1-\upsilon^2\right)}; \quad R_{12} = R_{21} = \frac{\upsilon E_{FGB}}{\left(1-\upsilon^2\right)}; \quad R_{55} = R_{44} = R_{66} = \frac{E_{FGB}}{2(1+\upsilon)}.$$

In this study, the equations of equilibrium of FGB plate structure under uniform pressure ($q$) are obtained using principle of total minimum potential energy in finite element form, as

$$[K]^e\{\lambda\}^e = \{F\}^e \tag{6}$$

where, $[K]^e = \int_{-1}^{1}\int_{-1}^{1} [B]^T[D][B]Jd\xi d\eta$ is the elemental stiffness matrix

$\{F\}^e = \int_{-1}^{1}\int_{-1}^{1} [S]^T\{q\}Jd\xi d\eta$ is the elemental force matrix.

Here, $[B]$, $[D]$ and $[S]$ are the strain-displacement, rigidity and interpolation function matrices, respectively.

## 3 Results and Discussion

A customized computer code is prepared from the developed finite element formulations to compute the desired responses of FGB structure. In the entire study, titanium and zirconia materials are utilized to model the said structure and the elastic properties are mentioned in Table 1. Here, different support conditions are considered on the edges of the FGB plate structure, such as fully clamped (*CCCC*), fully simply supported (*SSSS*), clamped-simply supported (*CSCS*), and clamped-free (*CFCF*). The unconstrained and constrained degrees-of-freedom (*d.o.f.*) for these support cases are mentioned in Table 2. Through the analysis, centerline deflections are computed and presented in non-dimensional form.

**Table 1** Elastic properties of bio-compatible materials [10]

| Materials | Properties | |
|---|---|---|
| | Young's modulus $E$ (GPa) | Poisson's ratio ($\upsilon$) |
| Zirconia ($ZrO_2$) | 200 | 0.3 |
| Titanium (Ti) | 110 | 0.3 |

**Table 2** Different support conditions on the edges of FGB plate structure

| Support conditions | Edges | Unconstrained *d.o.f.* | Fully constrained *d.o.f.* |
|---|---|---|---|
| SSSS | $x = 0, l$ | $u_1, u_2, u_3, u_4$ | $v_1, v_2, v_3, v_4, w_1$ |
| | $y = 0, b$ | $v_1, v_2, v_3, v_4$ | $u_1, u_2, u_3, u_4, w_1$ |
| CSCS | $x = 0, l$ | – | $u_1, u_2, u_3, u_4, v_1, v_2, v_3, v_4, w_1$ |
| | $y = 0, b$ | $v_1, v_2, v_3, v_4$ | $u_1, u_2, u_3, u_4, w_1$ |
| CFCF | $x = 0, l$ | – | $u_1, u_2, u_3, u_4, v_1, v_2, v_3, v_4, w_1$ |
| | $y = 0, b$ | $u_1, u_2, u_3, u_4, v_1, v_2, v_3, v_4, w_1$ | – |
| CCCC | $x = 0, l$ | – | $u_1, u_2, u_3, u_4, v_1, v_2, v_3, v_4, w_1$ |
| | $y = 0, b$ | – | $u_1, u_2, u_3, u_4, v_1, v_2, v_3, v_4, w_1$ |

## *3.1 Mesh Refinement*

Firstly, the convergence rate of discretized finite element model of FGB structure is confirmed through appropriate mesh refinement process. For this purpose, non-dimensional central deflection ($w/t$) of a fully clamped FGB plates ($a/h = 100$, $a/b = 1$) under uniform pressure ($q = 0.1$ MPa) are analyzed at various mesh densities, i.e., from $3 \times 3$ to $7 \times 7$ using uniform $h$-refinement scheme (see Fig. 2). Here, zirconia ($n = 0$), FGB-I ($n = 0.5$), FGB-II ($n = 2$) and titanium ($n = \infty$) plates are utilized. This mesh refinement of the FGB plate confirms that the desired responses can be computed efficiently at $5 \times 5$ mesh. Therefore, in the upcoming computational works, $5 \times 5$ mesh is adopted to discretize the FGB plate structures, if not mentioned otherwise.

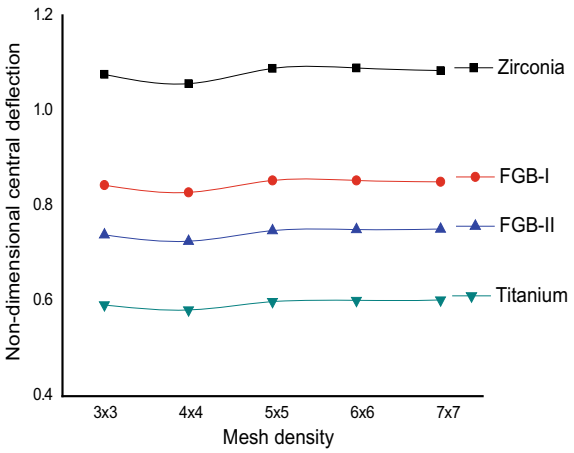


**Fig. 2** Mesh refinement of fully clamped FGB plate ($a/h = 100$, $a/b = 1$) structures under uniform pressure

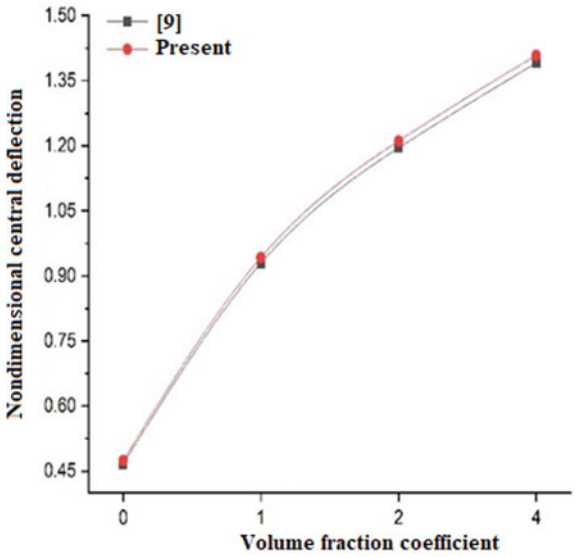


**Fig. 3** Deflection responses of a typical FGM plate under uniform pressure

## *3.2 Verification Study*

The correctness of the present work has been verified by comparing present results with the earlier reported work. Due to unavailability of the bending results of FGB plate structure in previous work, a simply supported FGM (aluminium and alumina) plate with $a/h = 10$ is analyzed under uniform load (see Fig. 3). The geometry and material properties are identical with reference [9]. Figure 3 confirms the accurateness of the present model and also demonstrates that the present model is flexible than the reference results because the compared results were evaluated using first-order kinematic theory.

## *3.3 Parametric Study*

In this section, the computational examples are established to demonstrate the deformation responses of FGB plate structure at various parametric values and conditions. Here, non-dimensional centerline deflections $w/t$ $(x, b/2)$ of FGB plate structures are computed under uniform pressure ($q = 0.1$ MPa). However, computations are executed for different volume fraction coefficients ($n = 0$, 0.5. 2 and $\infty$), side-to-thickness ratios ($l/t = 10$, 25, 50, 100), aspect ratios ($l/b = 1$, 1.4, 1.8, 2.2) and edge constraints (CCCC, CSCS, SSSS, CFCF) to reveal their individual and combined impact on the deformation behavior of FGB plate structures.

Table 3 exhibits the impact of side-to-thickness ratios ($l/t = 10$, 25, 50, 100) on the non-dimensional centerline deflections of different FGB plates ($l/b = 1$,

**Table 3** Effect of side-to-thickness ratio on the centerline deflection parameters of different FGB structures

| *l/t* | Material | *x/a* | | | | | | | | | | |
|---|---|---|---|---|---|---|---|---|---|---|---|---|
| | | 0 | 0.10 | 0.2 | 0.30 | 0.4 | 0.50 | 0.6 | 0.70 | 0.8 | 0.90 | 1 |
| 10 | $ZrO_2$ | 0 | 0.025e-3 | 0.068e-3 | 0.108e-3 | 0.135e-3 | 0.144e-3 | 0.135e-3 | 0.108e-3 | 0.068e-3 | 0.025e-3 | 0 |
| | FGB-I | 0 | 0.020e-3 | 0.053e-3 | 0.084e-3 | 0.106e-3 | 0.113e-3 | 0.106e-3 | 0.085e-3 | 0.053e-3 | 0.020e-3 | 0 |
| | FGB-II | 0 | 0.171e-4 | 0.461e-4 | 0.732e-4 | 0.916e-4 | 0.981e-4 | 0.918e-4 | 0.734e-4 | 0.377e-4 | 0.171e-4 | 0 |
| | Ti | 0 | 0.140e-4 | 0.376e-4 | 0.594e-4 | 0.743e-4 | 0.795e-4 | 0.744e-4 | 0.596e-4 | 0.377e-4 | 0.140e-4 | 0 |
| 25 | $ZrO_2$ | 0 | 0.0006 | 0.0019 | 0.0033 | 0.0043 | 0.0046 | 0.0043 | 0.0033 | 0.0019 | 0.0006 | 0 |
| | FGB-I | 0 | 0.0005 | 0.0015 | 0.0026 | 0.0034 | 0.0036 | 0.0034 | 0.0026 | 0.0015 | 0.0005 | 0 |
| | FGB-II | 0 | 0.0004 | 0.0013 | 0.0023 | 0.0029 | 0.0032 | 0.0029 | 0.0023 | 0.0013 | 0.0004 | 0 |
| | Ti | 0 | 0.0003 | 0.0011 | 0.0018 | 0.0024 | 0.0025 | 0.0024 | 0.0018 | 0.0011 | 0.0003 | 0 |
| 50 | $ZrO_2$ | 0 | 0.0073 | 0.0272 | 0.0492 | 0.0641 | 0.0696 | 0.0641 | 0.0494 | 0.0273 | 0.0073 | 0 |
| | FGB-I | 0 | 0.0057 | 0.0213 | 0.0386 | 0.0502 | 0.0545 | 0.0503 | 0.0387 | 0.0214 | 0.0057 | 0 |
| | FGB-II | 0 | 0.005 | 0.0186 | 0.0338 | 0.0439 | 0.0477 | 0.044 | 0.0338 | 0.0187 | 0.005 | 0 |
| | Ti | 0 | 0.004 | 0.015 | 0.0271 | 0.0352 | 0.0383 | 0.0353 | 0.0271 | 0.015 | 0.004 | 0 |
| 100 | $ZrO_2$ | 0 | 0.1059 | 0.415 | 0.7654 | 1.0001 | 1.0884 | 1.0012 | 0.767 | 0.416 | 0.1062 | 0 |
| | FGB-I | 0 | 0.083 | 0.3252 | 0.5999 | 0.7839 | 0.8532 | 0.7848 | 0.6012 | 0.3261 | 0.0832 | 0 |
| | FGB-II | 0 | 0.0726 | 0.2849 | 0.5258 | 0.6871 | 0.7478 | 0.6879 | 0.5269 | 0.2857 | 0.0728 | 0 |
| | Ti | 0 | 0.0582 | 0.2282 | 0.4209 | 0.5501 | 0.5986 | 0.5506 | 0.4218 | 0.2288 | 0.0584 | 0 |

**Table 4** Effect of aspect ratio on the centerline deflection parameters of different FGB structures

| *a/b* | Material | *x/a* | | | | | | | | | | |
|---|---|---|---|---|---|---|---|---|---|---|---|---|
| | | 0 | 0.10 | 0.2 | 0.30 | 0.4 | 0.50 | 0.6 | 0.70 | 0.8 | 0.90 | 1 |
| 1 | $ZrO_2$ | 0 | 0.1059 | 0.415 | 0.7654 | 1.0001 | 1.0884 | 1.0012 | 0.767 | 0.416 | 0.1062 | 0 |
| | FGB-I | 0 | 0.083 | 0.3252 | 0.5999 | 0.7839 | 0.8532 | 0.7848 | 0.6012 | 0.3261 | 0.0832 | 0 |
| | FGB-II | 0 | 0.0726 | 0.2849 | 0.5258 | 0.6871 | 0.7478 | 0.6879 | 0.5269 | 0.2857 | 0.0728 | 0 |
| | Ti | 0 | 0.0582 | 0.2282 | 0.4209 | 0.5501 | 0.5986 | 0.5506 | 0.4218 | 0.2288 | 0.0584 | 0 |
| 1.4 | $ZrO_2$ | 0 | 0.0486 | 0.1888 | 0.3422 | 0.4349 | 0.4663 | 0.4359 | 0.3437 | 0.1897 | 0.0489 | 0 |
| | FGB-I | 0 | 0.0381 | 0.148 | 0.2683 | 0.341 | 0.3655 | 0.3417 | 0.2694 | 0.1488 | 0.0383 | 0 |
| | FGB-II | 0 | 0.0333 | 0.1296 | 0.2351 | 0.2988 | 0.3203 | 0.2995 | 0.2361 | 0.1302 | 0.0335 | 0 |
| | Ti | 0 | 0.0268 | 0.1038 | 0.1882 | 0.2392 | 0.2565 | 0.2398 | 0.189 | 0.1044 | 0.0269 | 0 |
| 1.8 | $ZrO_2$ | 0 | 0.0236 | 0.0903 | 0.1596 | 0.1947 | 0.204 | 0.1954 | 0.1606 | 0.091 | 0.0238 | 0 |
| | FGB-I | 0 | 0.0185 | 0.0708 | 0.1251 | 0.1526 | 0.1599 | 0.1532 | 0.1259 | 0.0713 | 0.0187 | 0 |
| | FGB-II | 0 | 0.0162 | 0.0619 | 0.1096 | 0.1337 | 0.1401 | 0.1342 | 0.1103 | 0.0624 | 0.0163 | 0 |
| | Ti | 0 | 0.013 | 0.0496 | 0.0878 | 0.1071 | 0.1122 | 0.1075 | 0.0883 | 0.05 | 0.0131 | 0 |
| 2.2 | $ZrO_2$ | 0 | 0.0128 | 0.0479 | 0.0822 | 0.0956 | 0.0972 | 0.096 | 0.0829 | 0.0484 | 0.013 | 0 |
| | FGB-I | 0 | 0.0101 | 0.0376 | 0.0644 | 0.0749 | 0.0762 | 0.0753 | 0.065 | 0.0379 | 0.0102 | 0 |
| | FGB-II | 0 | 0.0088 | 0.0328 | 0.0564 | 0.0656 | 0.0667 | 0.0659 | 0.0569 | 0.0331 | 0.0088 | 0 |
| | Ti | 0 | 0.0071 | 0.0263 | 0.0452 | 0.0526 | 0.0535 | 0.0528 | 0.0456 | 0.0266 | 0.0071 | 0 |

CCCC) under uniform pressure. The computed results reveal the increasing trend of deflection values along the thickness ratios which is due to decrease in structural stiffness with increment in the side-to-thickness ratios. It is also confirmed through the computed results that pure zirconia plates exhibit maximum deflections whereas minimum is found in case of pure titanium plates.

Table 4 reveals the impact of aspect ratios ($l/b = 1, 1.4, 1.8, 2.2$) on the non-dimensional centerline deflections of different FGB plates ($l/t = 100$, CCCC) under uniform pressure. Here, a falling trend of deflections is observed with the increment of aspect ratios, which indicates that the stiffness of the structures is increasing with the increase in aspect ratios. Figure 4 shows the deformation behavior of different FGB plates under uniform pressure.

Table 5 exhibits the impact of support conditions (CCCC, CSCS, SSSS, CFCF) on the non-dimensional centerline deflections of different FGB plates ($l/b = 1, l/t = 100$) under uniform pressure. The results depict the significant of edge constraints on the deformation behavior of FGB plats. Here, decreasing trend of deflection parameters is found with the increase in number of constrained *d.o.f.*, i.e., structure with SSSS support demonstrate the maximum deflections whereas minimum in case of structure with CCCC conditions.

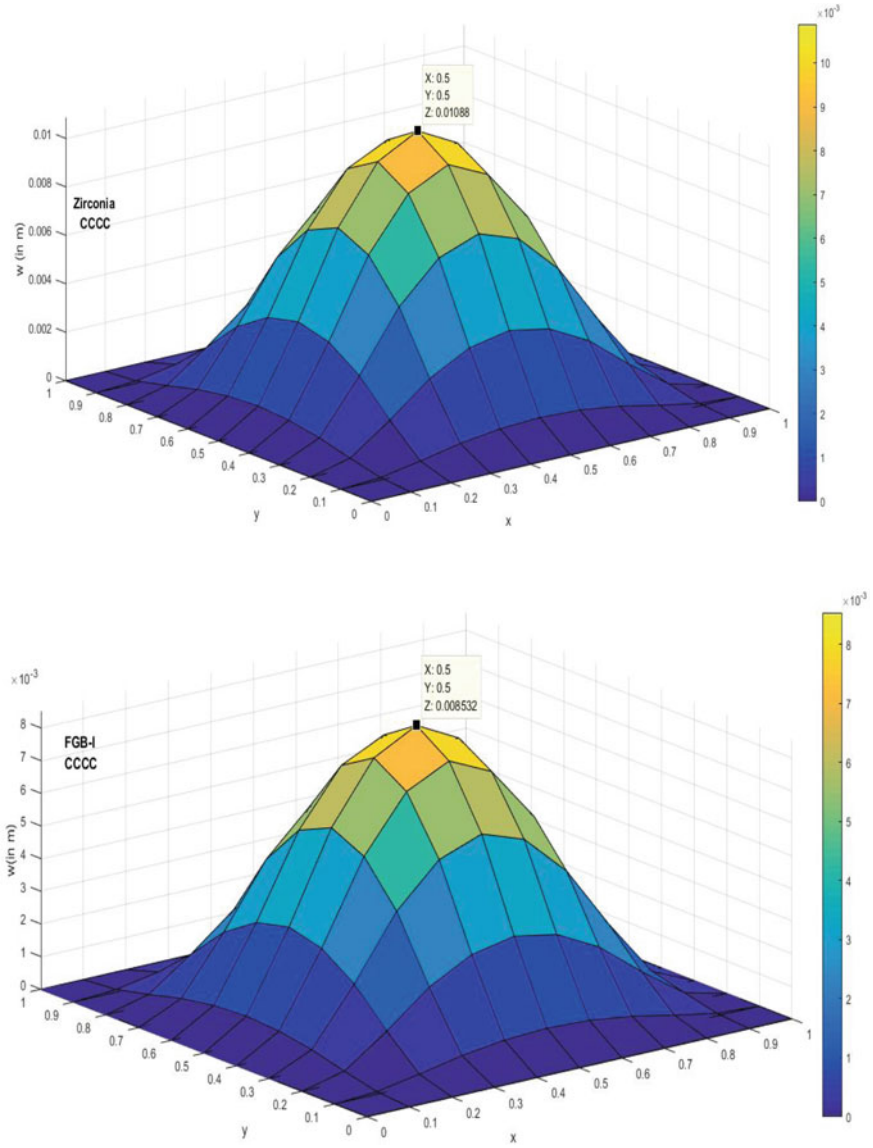


**Fig. 4** Deformation behaviour of clamed FGB plate structures under uniform pressure

## 4 Concluding Remarks

In this computational study, the deformation behavior of different FGB plate structures is analyzed under uniform pressure. Here, titanium and zirconia biocompatible materials are adopted to model the structure, whereas elastic properties of FGB

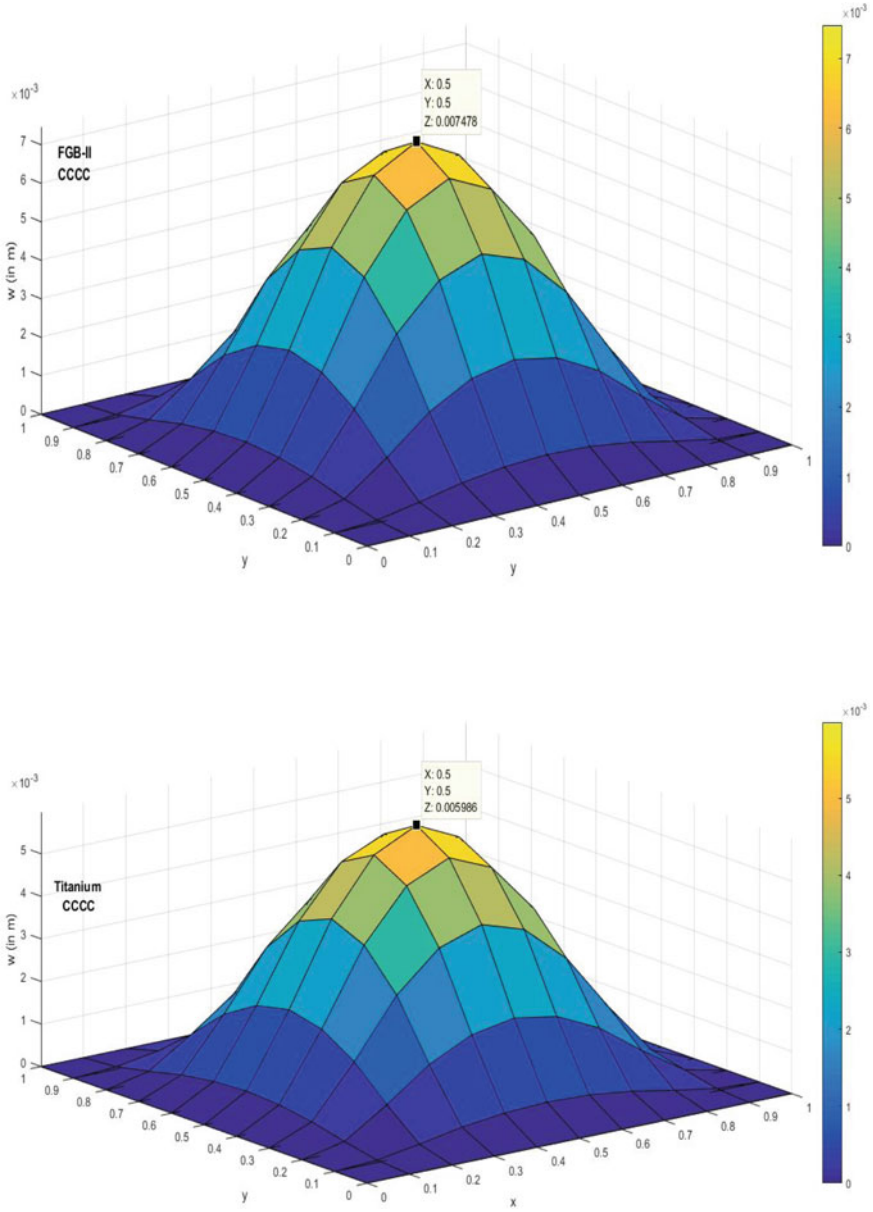


**Fig. 4** (continued)

**Table 5** Effect of edge constraints on the centerline deflection parameters of different FGB structures

| *a/b* | Material | *x/a* | | | | | | | | | | |
|---|---|---|---|---|---|---|---|---|---|---|---|---|
| | | 0 | 0.10 | 0.2 | 0.30 | 0.4 | 0.50 | 0.6 | 0.70 | 0.8 | 0.90 | 1 |
| SSSS | $ZrO_2$ | 0 | 1.2752 | 2.3875 | 3.2527 | 3.7886 | 3.9755 | 3.7948 | 3.263 | 2.3975 | 1.2815 | 0 |
| | FGB-I | 0 | 0.9995 | 1.8713 | 2.5494 | 2.9694 | 3.116 | 2.9743 | 2.5575 | 1.8792 | 1.0044 | 0 |
| | FGB-II | 0 | 0.8765 | 1.641 | 2.2356 | 2.604 | 2.7324 | 2.6082 | 2.2427 | 1.6479 | 0.8808 | 0 |
| | Ti | 0 | 0.7013 | 1.3131 | 1.7889 | 2.0837 | 2.1865 | 2.0871 | 1.7946 | 1.3186 | 0.7048 | 0 |
| CSCS | $ZrO_2$ | 0 | 0.5695 | 1.0474 | 1.406 | 1.6196 | 1.6908 | 1.6219 | 1.4098 | 1.051 | 0.5718 | 0 |
| | FGB-I | 0 | 0.4464 | 0.821 | 1.1021 | 1.2695 | 1.3253 | 1.2713 | 1.105 | 0.8238 | 0.4482 | 0 |
| | FGB-II | 0 | 0.3913 | 0.7197 | 0.9661 | 1.1129 | 1.1618 | 1.1145 | 0.9687 | 0.7222 | 0.3929 | 0 |
| | Ti | 0 | 0.3132 | 0.576 | 0.7733 | 0.8908 | 0.9299 | 0.8921 | 0.7754 | 0.5781 | 0.3145 | 0 |
| CFCF | $ZrO_2$ | 0 | 0.2042 | 0.8071 | 1.5092 | 2.0145 | 2.2174 | 2.0167 | 1.5125 | 0.8092 | 0.2047 | 0 |
| | FGB-I | 0 | 0.16 | 0.6326 | 1.1829 | 1.579 | 1.7381 | 1.5807 | 1.1854 | 0.6342 | 0.1604 | 0 |
| | FGB-II | 0 | 0.1401 | 0.5543 | 1.0369 | 1.3841 | 1.5235 | 1.3856 | 1.0391 | 0.5558 | 0.1405 | 0 |
| | Ti | 0 | 0.1123 | 0.4439 | 0.8301 | 1.108 | 1.2196 | 1.1092 | 0.8318 | 0.4451 | 0.1126 | 0 |
| CCCC | $ZrO_2$ | 0 | 0.1059 | 0.415 | 0.7654 | 1.0001 | 1.0884 | 1.0012 | 0.767 | 0.416 | 0.1062 | 0 |
| | FGB-I | 0 | 0.083 | 0.3252 | 0.5999 | 0.7839 | 0.8532 | 0.7848 | 0.6012 | 0.3261 | 0.0832 | 0 |
| | FGB-II | 0 | 0.0726 | 0.2849 | 0.5258 | 0.6871 | 0.7478 | 0.6879 | 0.5269 | 0.2857 | 0.0728 | 0 |
| | Ti | 0 | 0.0582 | 0.2282 | 0.4209 | 0.5501 | 0.5986 | 0.5506 | 0.4218 | 0.2288 | 0.0584 | 0 |

structure are computed using Voigt's micromechanical model via power-law function. The kinematics of the present model is developed using higher-order equivalent single layer theory. However, the equilibrium equations are obtained using principle of total minimum potential energy in conjunction with 2D finite element approach via Q9 Lagrangian elements. The computational tests are performed by developing the homemade computer algorithm. Through the *h*-type uniform mesh refinement process, a (5 × 5) mesh is confirmed to utilize further in the present study, whereas verification test reveals the correctness of the proposed finite element model. In addition, centerline deflections of different FGB plate structures under various sets of conditions are demonstrated through numerical examples. The exhaustive parametric study confirms that impact of side-to-thickness and aspect ratios, volume fraction coefficients and support conditions on the centerline deflections of FGB plate structures are noteworthy.

## References

1. Jha DK, Kant T, Singh RK (2013) A critical review of recent research on functionally graded plates. Compos Struct 96:833–849
2. Thai HT, Vo TP (2013) A new sinusoidal shear deformation theory for bending, buckling, and vibration of functionally graded plates. Appl Math Model 37:3269–3281
3. Reddy JN, Wang CM, Kitipornchap S (1999) Axisymmetric bending of functionally graded circular and annular plates. Eur J Mech A Solids 18:185–199
4. Brischetto S, Carrera E (2010) Advanced mixed theories for bending analysis of functionally graded plates. Comput Struct 88:1474–1483
5. Zidi M, Tounsi A, Houari MSA, Adda Bedia EA, Anwar Bég O (2014) Bending analysis of FGM plates under hygro-thermo-mechanical loading using a four variable refined plate theory. Aerosp Sci Technol 34:24–34
6. Della Croce L, Venini P (2004) Finite elements for functionally graded Reissner-Mindlin plates. Comput Methods Appl Mech Eng 193:705–725
7. Kar VR, Panda SK (2015) Large deformation bending analysis of functionally graded spherical shell using FEM. Struct Eng Mech 53:661–679
8. Shen H (2009) Nonlinear bending of functionally graded carbon nanotube-reinforced composite plates in thermal environments. Compos Struct 91:9–19
9. Singha MK, Prakash T, Ganapathi M (2011) Finite element analysis of functionally graded plates under transverse load. Finite Elem Anal Des 47:453–460
10. Bin Kadri NA, Osman NAA, Shirazi FS, Metselaar HSC, Mehrali M, Mehrali M (2013) Dental implants from functionally graded materials. J. Biomed. Mater Res Part A 101:3046–3057
11. Shen HS (2009) Functionally graded materials: nonlinear analysis of plates and shells. CRC Press, Taylor & Francis Group, Boca Raton
12. Reddy JN (2004) Mechanics of laminated composite plates and shells. CRC Press

# Natural Fiber Composite for Structural Applications


**Jayakrishna Kandasamy, A. Soundhar, M. Rajesh, D. Mallikarjuna Reddy, and Vishesh Ranjan Kar**

**Abstract** With emerging focus on sustainable product development researchers are now focusing on consumption of Natural Fibres (NF) directly or as reinforcement materials in polymer based materials. Natural fibers are being used since ages but in recent decades there exist a need to explore the properties of these fibres for varied applications subject to the requirement. Natural Fibre Reinforced Polymers (NFRP) are utilized in manufacturing several automotive, marine and aerospace low level structural applications. In order to use natural fibres in high level structural applications, it is necessary to understand the structural, mechanical and thermal properties of the fibre. But as the natural fibre are obtained in irregular size and shapes in their longitudinal direction and cross section its quite difficult to study their properties unlike advanced composites. Hydrophilic and hydrophobic properties of Natural Fibres (NF) distress the bonding interaction between the fibre and matrix. This chapter tries to analyse the different characteristics with respect to the application of Natural Fibers (NF) for real time applications and attempts to provide an insight for researchers and design engineers to understand the requirements of utilizing Natural Fibres Composites (NFC) for construction applications in future. This chapter also summarize the advantages of natural fibres on their bio degradability aspects.

**Keywords** Natural fibres · Fibre matrix bonding · Fibre reinforced composites · Mechanical properties · Structural applications

J. Kandasamy (✉) · A. Soundhar · M. Rajesh · D. Mallikarjuna Reddy
Vellore Institute of Technology, Vellore 632014, Tamil Nadu, India
e-mail: mail2jaikrish@gmail.com

V. R. Kar
National Institute of Technology, Jamshedpur 831014, Jharkhand, India

© Springer Nature Singapore Pte Ltd. 2021

M. Jawaid et al. (eds.), *Structural Health Monitoring System for Synthetic, Hybrid and Natural Fiber Composites*, Composites Science and Technology,
https://doi.org/10.1007/978-981-15-8840-2_3

## 1 Introduction

Researchers now focus upon NFC due to the potential environmental, health and end-of-life disposal benefits when compared with man-made composite materials. Man-made composite materials are also quite costly and high in density compared with NFC [1]. NFC are easily available, easy to process and easy to dispose. They are often produced using agricultural waste [2]. In the latter decades, the increased benefits of NF have found them wide applications in structural, naval and aerospace fields [3, 4]. As proof, NF such as flax, sisal, banana, jute, and hemp have replaced fibres like carbon, glass, boron and Kevlar in applications requiring low load carrying capacity [5]. NF can be characterized based on their resources such as plant, mineral and animal as presented in Table 1. Generally, the plant based fibers are the utmost frequently recognized fibers by the commerce, which is owing to the short progress period, availability and renewability.

Sen and Reddy [6] demonstrated the usage of natural fibres in several engineering applications, like bamboo fibre reinforced columns and pillars, special joints made of bamboo fibre composites, and packaging material based on jute fibre composites. Table 2 shows various natural fiber characteristics.

However, the major disadvantage related with NF is their inconsistent strength depending on the type of reinforcement, such as short fibre, fibre bundles and woven fibres [13]. Most of the researchers developed natural fibre composites by reinforcing the natural fibre of random orientation in short form within a polymer matrix, which leads to non-uniform stress distribution in composites because of fibre discontinuity [14]. To improve the mechanical properties, like the stiffness and load bearing capacity of the natural fibre composites, technical developments from the field of textiles were adopted, such as weaving, braiding and knitting [15, 16]. Sapuan and Maleque [7] explained the use of fabric woven from bananas in an epoxy matrix for the manufacture of telephone stands at low cost. Table 3 shows the chemical composition of various fibers. Alves et al. [8] also demonstrated the benefits of NFC in manufacturing car front bonnets by replacing fibreglass with jute fibre composites.

**Table 1** Natural fibre classsifation [2–5]

| | | |
|---|---|---|
| | Leaf | Pineapple, Banana, Abaca, Sisal |
| Lignocellulose/Cellulose | Bast | Flax, Hemp, Jute, Ramie, Kenaf |
| | Fruit | Coir |
| | Wood | Softwood, Hardwood |
| | Seed | Cotton, Kapok |
| | Grass/Reed | Bamboo, corn |
| | Stalk | Wheat, Maize, Oat, Rice |
| Mineral | – | Asbestos, Metal fibres, Ceramic fibres |
| Animal | Hair silk/Wool | Cashmere, Horse hair, Lamb wool, Goat hair |

**Table 2** Summary of Natural fiber characteristics [4–6]

| Fibre | Description |
|---|---|
| Coir | Among the various natural fibres, coir has more attraction, since it has strong resistant to salt water, durable, availability, free of chemical treatment |
| Cotton | Cotton Fibre (CF) has an outstanding permeability. Cotton signifies 46% world manufacture of chemical and natural fibres |
| Flax | On comparison with flax fibre, glass fibre has enhanced specific tensile, high strength, low density and stiffness |
| Jute | Jute fibre demonstrations high strength to weight ratio, high aspect ratio and better protection properties |
| Pineapple | Pineapple Fibre (PF) has outstanding physical, mechanical, and thermal properties |
| Sisal | Sisal cultivation takes short cultivation times. Fibre has great tensile intensity and tenacity, salt water resistance, abrasion resistance, alkali and acid resistance |
| Hemp | Hemp fibre has exceptional modulus of elasticity, insulation properties and mechanical strength |
| Ramie | Ramie fibre has enhanced specific strength and specific modulus compared to glass fibre. Because of its expensive pre-treatments, it is not extensively used |
| Eucalyptus | Eucalyptus fibre is extensively obtainable, but has less resistance towards fire. Thus, this fibres are suitable for protection purposes |

**Table 3** Chemical composition of common NF [7–10]

| Fibre | Cellulose (wt%) | Hemicellulose (wt%) | Lignin (wt%) | Waxes (wt%) |
|---|---|---|---|---|
| Flax | 72 | 19–21 | 2.2 | 1.5 |
| Sisal | 62–65 | 12 | 10 | 2 |
| Coir | 31–42 | 0.15–0.25 | 41–46 | – |
| Pineapple | 81 | – | 12.7 | – |
| Ramie | 68.6–76.2 | 13–16 | 0.6–0.7 | 0.3 |
| Jute | 60–72 | 13–19 | 10–13 | 0.5 |
| Kenaf | 72 | 21.3 | 8 | – |
| Bamboo | 25–44 | 30 | 20–31 | – |
| Hemp | 67 | 16 | 10 | 0.8 |
| Oil palm | 65 | – | 29 | – |
| Abaca | 56–63 | 20–25 | 7–9 | 3 |

Recently, researchers have been working on identifying potential plant fibres for use in low and medium load applications by characterising their mechanical properties [11]. The favourable properties of natural composites made up of woven fabric has increased their usage in aircraft, bio-medical, automotive and other applications [12]. Woven fabric NFC have extensive variety of applications because of properties inherently associated with them. Compared to unidirectional and randomly orientated fibres in natural composites, woven fabric natural fibres provide better properties, in

terms of strength and stiffness for the same quantity of fibres used. The use of woven fabric improves the fracture toughness of NFC [17, 18]. Riedel et al. reviewed the use of woven NFCs in different applications and reported that a stiff woven fabric will enhance the stiffness of the composites [19].

The goal of this chapter is to enlighten prevailing progress of NFC in structural applications.

## 2 Natural Fibre Composite

### *2.1 Mechanical Properties of NFCs*

In composite materials, especially in NFC, the mechanical properties such as impact strength, flexural and tensile depend on the fibre strength, fibre percentage in the matrix, orientation of the fibres, adhesion between fibre-matrix and type of treatment, and concentration [20, 21]. Decades ago, conventional materials such as aluminium, titanium and steel were utilized for engineering, automotive, aerospace, and civil applications. Favourable bulk strength and weight properties associated with woven natural fibre reinforced composites make them suitable replacement materials for conventional materials, and they exhibit superior strength and stiffness [22–24].

Khalil et al. [25] experimentally compared the flexural and tensile behaviour of tri-layer palm oil and woven jute fibre-epoxy composites with palm oil-epoxy and woven jute epoxy composites. Results indicated that hybrid tri-layer palm oil and woven jute fibre-epoxy composites possessed higher mechanical strength compared with similar composites made with individual fibre reinforcement. Mwaikambo et al. [26] used kapok and cotton fabric as a reinforcing material in a polypropylene matrix to investigate their mechanical properties. They found that the inclusion of the fabric improved the rigidity of the composite material. Sapuan et al. [27] examined the mechanical properties of banana composite/woven epoxy and consolidate that the woven banana composite yielded maximum strength and modulus. Bennet et al. [28] studied the outcome of the piling order of sansevieria cylindrical-coconut sheath polyester composites on their mechanical properties. They reported that due to hybridisation effects, the maximum modulus was observed when the mat fibre was kept as a skin layer and short fibre mat used as the core material. Table 4 shows the mechanical properties of various NF.

Carmisciano et al. [29] analyzed the basalt woven fibre reinforced vinyl ester composite flexural properties with a glass fibre composite, and concluded that the basalt woven fibre composites yielded higher values than the glass fibre composite. Venkateshwaran et al. [30] associated the mechanical properties of woven banana-epoxy-jute composites with different stacking sequence. They found that when jute fibres were placed as a core layer, the composite exhibited good tensile and flexural properties than the banana and jute composites individually. Mariatti et al. [31] reported the woven banana fabric composites flexural properties with composites

**Table 4** Mechanical properties of different NF used in composites [13, 15, 18, 25]

| Sl. no | Fibre | Density (g/cm$^3$) | Elongation (%) | Tensile strength (MPa) | Young's modulus (GPa) |
|---|---|---|---|---|---|
| 1 | Banana | – | 3 | 529–914 | 27–32 |
| 2 | Bamboo | 0.6–1.1 | – | 140–230 | 11–17 |
| 3 | Coir | 1.2 | 30 | 175 | 4.0–6.02 |
| 4 | Cotton | 1.4–1.6 | 6.0–8.0 | 287–597 | 5.5–12.6 |
| 5 | Hemp | 1.48 | 1.6 | 690 | 70 |
| 6 | Flax | 1.5 | 2.7–3.2 | 345–1035 | 27.6 |
| 7 | Jute | 1.3 | 1.5–1.8 | 393–773 | 26.5 |
| 8 | Oil palm | 0.7–1.55 | 3.2 | 248 | 25 |
| 9 | Sisal | 1.5 | 2.0–2.5 | 511–635 | 9.4–22.0 |
| 10 | Kenaf | 1.4 | 1.5 | 930 | 53 |

containing the same volume percentage of short fibres and found that the woven fabric composite exhibited the maximum strength and modulus at same volume percentage. Khan et al. [32] reported the mechanical properties of a plain-woven jute with a non-woven jute composite along the warp direction and concluded that the woven mat composite enhanced the mechanical properties in the warp direction better than the non-woven composite.

## *2.2 Dynamic Mechanical Properties of NFCs*

Dynamic mechanical properties such as loss modulus, damping factors and storage modulus of newly developed materials with respect to thermal and dynamic loading are important parameters to be analysed for structural applications [33]. In structural materials made of conventional materials, the interactions between molecules will be higher at higher temperatures, which increases the energy dissipation and reduces their stiffness. Dynamic properties of composite materials are reliant on the quantity of fibre present in the fibre, matrix or yarn arrangement, the gap between two fibres or yarn and adhesion between the reinforcement and matrix [34]. Rajesh and Pitchaimani [35] compared the dynamic mechanical properties of composite materials based on their weaving patterns and fibre strengths. They investigated that irrespective of the intertwining pattern, in glassy region the composite showed very little variation in storage modulus. After the glassy region, the basket style jute composite enhanced the storage modulus drastically when compared to the satin, plain weave, twill and huckaback woven composites. Results revealed that basket style composite enhanced the structural stiffness at higher temperatures and provided higher resistance against free molecule movement. It was also observed that the fibre

and yarn arrangement in the basket woven fabric carried more load and reduced the stress concentration between two successive yarns in the weft and warp directions.

Venkateshwaran and Elayaperumal [30] analysed the effect of weaving pattern on the dynamic mechanical behaviour of epoxy-banana composites. They found that the plain woven composite improved the storage modulus of the composite laminate associated with the twill and satin weaves, and did not affect the composite material glass transition temperature. From their results, they determined that the orientation of the fibres in the yarn in the warp and weft directions prejudiced the storage modulus of the plain woven composite. In the instance of plain weave, yarns alternate in the weft and warp directions, which provides better stability and considerable porosity [36]. The main problem associated with plain weave is the high crimp in both the warp and weft directions. However, compared to satin and twill, plain weave provides better stiffness and strength. Song et al. [37] analysed the viscoelastic behaviour of twill and plain woven hemp fibre reinforced polylactic acid composites and reported that twill weave improved the viscoelastic and mechanical properties of the composites, increased loss modulus and storage modulus. Results also revealed that woven fabric performed better as a reinforcement compared to randomly oriented short fibres in the composites. Gupta and Raghavan [38] investigated that plain weave composite improved the dynamic mechanical properties of the composite material more than short fibres. Jawaid et al. [39] reported dynamic mechanical analysis of oil palm empty fruit bunch/woven jute fibre epoxy hybrid composites and concluded that the storage modulus of the woven jute composite was more than the hybrid composites. Jawaid et al. [40] analysed the influence of jute fibre stacking on the dynamic mechanical behaviour of oil palm epoxy composites. Results revealed that the inclusion of jute fibre in the oil palm epoxy composites improved the storage modulus. It indicated that the inclusion of high strength jute fibre in the matrix enhanced the stiffness of the composite material at higher temperatures due to resistance against free molecule movement. Boccarusso et al. [41] studied the dynamic mechanical behaviour of biocomposites made of PLA-hemp. They found that higher fibre content in the PLA matrix enhanced glass transition temperature and storage modulus of the composite material. Huang and Netravali [42] analysed the dynamic behaviour of green composites made of woven flax fabric and an aliphatic-aromatic co-polyester matrix. Results proved that inclusion of woven fabric enhanced storage modulus of green composite drastically.

## *2.3 Braided and Knitted NFCs*

Progresses in the field of textiles greatly impact the field of composites to increase the stiffness and strength of composite materials, especially natural fibre composites. Braiding and knitting techniques have been employed to develop the performance of composite materials. The advantage of braiding over conventional weaving is that the modulus of elasticity of braided yarn is more than that of conventional yarn, this enhances the stiffness of braided fabrics [43]. Braided woven fabric reinforcement

are utilized in numerous engineering uses like rocket launch tubes, aircraft structural parts and air ducts. Similarly, the arrangement of fibres in the yarn of knitted fabrics contributes to energy dissipating behaviour [44]. Rajesh and Pitchaimani [45] analyzed the mechanical properties of braided, woven fabric and knitted reinforced composites. They discovered that braided woven jute fabric composites displayed enhanced mechanical properties compared with knitted and conventional woven fabric reinforcement. This was because the braided woven fabric enhanced the Young's modulus of the fabric, which therefore provided better resistance against loading. For confirmation, they experimentally computed the tensile strength of braided yarn, traditional yarn, braided and traditional woven fabrics, and knitted jute fabric. From the experimental results they found that braided woven fabric and its yarn had more modulus of elasticity compared to the other types, aided to increase the total enactment of the composite laminate. In addition, they compared jute-banana intra-ply composite with individual jute and banana woven fabrics. In case of the braided composite, the individual jute braided fabric enhanced the composite mechanical properties associated to the banana-jute intra-ply composite, while in the traditional woven fabric, intra-ply banana-jute woven fabric comparatively enhanced the composite material mechanical properties. From these outcomes, they determined that the type of yarn influenced the composite mechanical properties further than the fibre strength. The amount of fibre and the angle of twist defines the strength of the braided yarn [46–48]. Ayranci and Carey [49] studied the importance of braided composites and reported that braided composites can be employed in various fields without compromising strength, stiffness or stability behaviours, and represent good alternative materials to substitute conventional materials in components like shafts, structural columns, rods, pressure plates and vessels.

## *2.4 NFCs for Structural Application*

NFC have been employed in load-bearing applications in construction, automotive and electronics fields (Table 5).

**Table 5** Ten year challenge for natural fiber composites

| Bio-composites | Production (ton) | |
|---|---|---|
| | 2010 | 2020 |
| Construction [50] | 190,000 | 450,000 |
| Automotive [50] | 90,000 | 350,000 |
| Aerospace and marine [51] | 60,000 | 300,000 |

## 2.5 Construction Applications

Natural fibers extant sustainable and cheap alternative to the synthetic and metallic fibers utilized as building materials [52]. Lower ecological damage, light weight and bio-degradability are significant benefits of natural fibers. There are mainly two strategies achieved for the utilization of natural fibers in construction applications. In the main method, natural fiber reinforced polymeric composites was established for the diverse parts of building [53], conversely the subsequent method shows the usage of NF for concrete reinforcement.

Polymeric composites like as jute, sisal, hemp, kenaf, flax, ramie, coir, banana, straw, etc. have been advanced to construct various components of buildings such as roofs, beams, balcony, fire doors, floors, etc. Many composites have sandwich structures, to decrease weight and to attain improved flexural properties [54]. Mechanical evaluation of these composite structures have been categorised and the outcomes discovered their prospective for building construction [55].

Due to the steel corrosion difficulty, there is an accumulative necessity for concrete reinforcing resources which can interchange steel bars. Concrete has been reinforced with numerous natural fibers like coconut, bamboo, sisal, etc. for rising sustainable and economical constructions [56]. Inclusion of these natural fibers to concrete was observed to be supportive to increase various mechanical evaluations including impact resistance, flexural properties and fracture toughness [57].

Beams are made of reinforced concrete, timber, laminated veneer lumber or glulam, steel profiles. Latest advances have revealed the possible weight, installation, cost and time advantages of utilizing fiber composites beams [58]. Thus, a prospect occurs for the applications of NFC in the progress of pedestrian bridge girders and structural beams which needs moderate design loads. The awareness of utilizing natural fiber in beam improvement is incited by low density of NF, environmental benefits and lower cost [59].

NEC has established the leading mobile phone with an exterior casing produced from a biocomposite. The casing is prepared from a kenaf fibre reinforced PLA bio composite that comprises around 90% natural fibre. The extreme fibre content decreases the level of PLA used, develops heat deflection and doubles the impact resistance of the casing in contrast to unfilled PLA casing [60]. This is an inspiring creativity by the electronics segment, because millions of mobile phones are made every year with a lifetime of only $1 \pm 2$ years.

## 2.6 Automotive Applications

Nowadays, the improved significance of raw resources from recyclability and renewable sources of products is producing the conversion from petroleum to natural

**Table 6** Applications of natural fibers in automotive industry [66, 67]

| Natural fibres | Component description |
|---|---|
| Coir | Car seat covers, door mats, rugs, mattresses |
| Cotton | Sound proofing, insulation, trunk panel |
| Flax | Rear panel shelves, seatbacks, covers, floor trays, floor panels |
| Flax/Sisal | Door linings and panels |
| Wool | Seat coverings |
| Kenaf/flax | Door panel inserts and package trays |
| Hemp | Covered door panels carrier |
| Kenaf | Door inner panel |
| Kenaf/hemp | Covered door panels, carrier for armrest |
| Coconut | Seat bottoms, seat cushioning, interior trim and seat surfaces |

fibres in self-propelled applications [61]. NFCs hold important possible for motorized industry because the ultimatum for environmentally friendly and light-weight materials is advanced [4].

Studies show that NFCs can subsidise to a rate decrease of 20% and weight drop of 30% of motorized part. Light weight of machineries results in recycling opportunities, poor fuel consumption, greenhouse emissions and constricting in waste removal which are foremost reasons for usage of NF [62]. NFC are frequently utilized for internal portions such as dashboards, seat cushions, door panels, parcel shelves, cabin linings and backrests, however the usage of NFCs components for external applications is inadequate [63].

Various parts across the globe practise diverse types of NF and they export or import to further areas as well. For example, European motorized manufacturing mostly use hemp and flax, whereas kenaf and jute and are mostly imported from India and Bangladesh, sisal from United States, Brazil and South Africa and banana from Philippines [64]. Flax fibre has been the utmost appropriate NF for the German motorized industry. German motorized industry is the major significant shopper of NF components in the European automotive sector, where each car generated in Germany comprises 3.6 kg of natural fibers [65]. Table 6 indicates the applications of NFCs in automotive sector.

## *2.7 Future Market Trends*

In present market developments, NFCs are undergoing complete evolution with good potential in construction and automotive sector. Bast fiber such as hemp, kenaf, flax, etc., are ideal for automotive uses. In the case of wood plastic composite is the substantial of optimal for structure. Considering progresses of present scenario

Europe is projected to continue as major market for NFCs because of the large recognition of ecologically approachable composite materials by government agencies, automotive sectors and development in minor scale ecologically friendly industries. The development in materials enactment will motive the development of NFCs in new possible areas.

## *2.8 Conclusion*

NFRPC have useful properties such as reduced solidity, less expensive and low density when associated to synthetic products, providing benefits for use in viable applications (buildings, automotive industry and constructions). Utilizing NF as reinforcement for polymeric composites presents optimistic impact on the polymer mechanical behaviour. Textile technologies have now been absorbed into the development of fibre reinforced composites to enhance their strength and stiffness. From the literature, it was noted that NF in woven form enhanced the tensile strength, flexural strength and corresponding modulus, the fundamental natural frequency and storage modulus of composite materials. It was also noted that the alignment of fibres in the yarn in the weft and warp directions influenced the properties of the composites. In addition, the inclusion of more advanced weaving technology such as braiding and knitting have been summarised, and it was established that braided composites enhanced the composite properties material drastically, while knitted composites increased the energy dissipating properties of the composite materials, suggesting that braided fabric composites are appropriate for structural applications.

## References

1. Saheb DN, Jog JP (1999) Natural fiber polymer composites: a review. Adv Polym Technol: J Polym Process Inst 18(4):351–363
2. Venkateshwaran N, Elayaperumal A (2010) Banana fiber reinforced polymer composites-a review. J Reinf Plast Compos 29(15):2387–2396
3. Joshi SV, Drzal LT, Mohanty AK, Arora S (2004) Are natural fiber composites environmentally superior to glass fiber reinforced composites? Compos A Appl Sci Manuf 35(3):371–376
4. Holbery J, Houston D (2006) Natural-fiber-reinforced polymer composites in automotive applications. JOM 58(11):80–86
5. Reis RHM, Cândido VS, Nunes LF, Monteiro SN (2019) Chemical and morphological characterization of Guaruman fiber. In: Green materials engineering. Springer, Cham, pp 107–113
6. Sen T, Reddy HJ (2014) Flexural strengthening of RC beams using natural sisal and artificial carbon and glass fabric reinforced composite system. Sustain Cities Soc 10:195–206
7. Sapuan SM, Maleque MA (2005) Design and fabrication of natural woven fabric reinforced epoxy composite for household telephone stand. Mater Des 26(1):65–71
8. Alves C, Silva AJ, Reis LG, Freitas M, Rodrigues LB, Alves DE (2010) Ecodesign of automotive components making use of natural jute fiber composites. J Clean Prod 18(4):313–327

9. Davoodi MM, Sapuan SM, Ahmad D, Ali A, Khalina A, Jonoobi M (2010) Mechanical properties of hybrid kenaf/glass reinforced epoxy composite for passenger car bumper beam. Mater Des 31(10):4927–4932
10. Damodaran A, Mansour H, Lessard L, Scavone G, Babu AS (2015) Application of composite materials to the Chenda, an Indian percussion instrument. Appl Acoust 88:1–5
11. Wu M, Shuai H, Cheng Q, Jiang L (2014) Bioinspired green composite lotus fibers. Angew Chem Int Ed 53(13):3358–3361
12. Rao TV, Chowdary MS, Babu CSS, Sumanth CM (2019) Effect of bamboo fiber on mechanical properties of fly Ash with polypropylene composites. In: Advances in materials and metallurgy. Springer, Singapore, pp 437–446
13. Venkateshwaran N, Santhanam V, Alavudeen A (2019) Feasibility study of fly ash as filler in Banana fiber-reinforced hybrid composites. In: Processing of green composites. Springer, Singapore, pp 31–47
14. Sanyang ML, Ilyas RA, Sapuan SM, Jumaidin R (2018) Sugar palm starch-based composites for packaging applications. In: Bionanocomposites for packaging applications. Springer, Cham, pp 125–147
15. Sarikaya E, Çallioğlu H, Demirel H (2019) Production of epoxy composites reinforced by different natural fibers and their mechanical properties. Compos B Eng 167:461–466
16. Jariwala H, Jain P (2019) A review on mechanical behavior of natural fiber reinforced polymer composites and its applications. J Reinf Plast Compos 38(10):441–453
17. Habibi M, Laperrière L, Mahi Hassanabadi H (2019) Replacing stitching and weaving in natural fiber reinforcement manufacturing, Part 1: Mechanical behavior of unidirectional flax fiber composites. J Nat Fibers 16(7):1064–1076
18. Kumar R, Ul Haq MI, Raina A, Anand A (2019) Industrial applications of natural fibre-reinforced polymer composites–challenges and opportunities. Int J Sustain Eng 12(3):212–220
19. Riedel U, Chowanietz M, Deutsches Zentrum fur Luft-und Raumfahrt eV (1999) Fibre composite material and method of manufacture. U.S. Patent 5,948,706
20. Ramesh M, Deepa C (2019) Processing of green composites. In: Green composites. Springer, Singapore, pp 47–72
21. Shah DU (2013) Developing plant fibre composites for structural applications by optimising composite parameters: a critical review. J Mater Sci 48(18):6083–6107
22. Juarez C, Duran A, Valdez P, Fajardo G (2007) Performance of "Agave Lecheguilla" natural fiber in Portland cement composites exposed to severe environment conditions. Build Environ 42(3):1151–1157
23. Cavalcanti DKK, Banea MD, Neto JSS, Lima RAA, da Silva LFM, Carbas RJC (2019) Mechanical characterization of intralaminar natural fibre-reinforced hybrid composites. Compos B Eng 175:107149
24. Faruk O, Bledzki AK, Fink HP, Sain M (2014) Progress report on natural fiber reinforced composites. Macromol Mater Eng 299(1):9–26
25. Khalil HA, Jawaid M, Hassan A, Paridah MT, Zaidon A (2012) Oil palm biomass fibres and recent advancement in oil palm biomass fibres based hybrid biocomposites. Composites and their applications, INTECH Chapter 8, pp 187–220
26. Mwaikambo LY, Martuscelli E, Avella M (2000) Kapok/cotton fabric–polypropylene composites. Polym Test 19(8):905–918
27. Sapuan SM, Leenie A, Harimi M, Beng YK (2006) Mechanical properties of woven banana fibre reinforced epoxy composites. Mater Des 27(8):689–693
28. Bennet C, Rajini N, Jappes JW, Siva I, Sreenivasan VS, Amico SC (2015) Effect of the stacking sequence on vibrational behavior of Sansevieria cylindrica/coconut sheath polyester hybrid composites. J Reinf Plast Compos 34(4):293–306
29. Carmisciano S, De Rosa IM, Sarasini F, Tamburrano A, Valente M (2011) Basalt woven fiber reinforced vinylester composites: Flexural and electrical properties. Mater Des 32(1):337–342
30. Venkateshwaran N, ElayaPerumal A, Raj RA (2012) Mechanical and dynamic mechanical analysis of woven banana/epoxy composite. J Polym Environ 20(2):565–572

31. Mariatti M, Jannah M, Abu Bakar A, Khalil HA (2008) Properties of banana and pandanus woven fabric reinforced unsaturated polyester composites. J Compos Mater 42(9):931–941
32. Khan GA, Terano M, Gafur MA, Alam MS (2016) Studies on the mechanical properties of woven jute fabric reinforced poly (l-lactic acid) composites. J King Saud Univ-Eng Sci 28(1):69–74
33. Bassyouni M (2018) Dynamic mechanical properties and characterization of chemically treated sisal fiber-reinforced polypropylene biocomposites. J Reinf Plast Compos 37(23):1402–1417
34. Chee SS, Jawaid M, Sultan MTH, Alothman OY, Abdullah LC (2019) Thermomechanical and dynamic mechanical properties of bamboo/woven kenaf mat reinforced epoxy hybrid composites. Compos B Eng 163:165–174
35. Rajesh M, Pitchaimani J (2016) Dynamic mechanical analysis and free vibration behavior of intra-ply woven natural fiber hybrid polymer composite. J Reinf Plast Compos 35(3):228–242
36. Rajesh M, Sultan MTH, Uthayakumar M, Jayakrishna K, Shah AUM (2018) Dynamic behaviour of woven bio fiber composite. BioResources 13(1):1951–1960
37. Song YS, Lee JT, Ji DS, Kim MW, Lee SH, Youn JR (2012) Viscoelastic and thermal behavior of woven hemp fiber reinforced poly (lactic acid) composites. Compos B Eng 43(3):856–860
38. Gupta A, Raghavan J (2010) Creep of plain weave polymer matrix composites under on-axis and off-axis loading. Compos A Appl Sci Manuf 41(9):1289–1300
39. Jawaid M, Khalil HA, Alattas OS (2012) Woven hybrid biocomposites: dynamic mechanical and thermal properties. Compos A Appl Sci Manuf 43(2):288–293
40. Jawaid M, Khalil HA, Hassan A, Dungani R, Hadiyane A (2013) Effect of jute fibre loading on tensile and dynamic mechanical properties of oil palm epoxy composites. Compos B Eng 45(1):619–624
41. Boccarusso L, Carrino L, Durante M, Formisano A, Langella A, Minutolo FMC (2016) Hemp fabric/epoxy composites manufactured by infusion process: improvement of fire properties promoted by ammonium polyphosphate. Compos B Eng 89:117–126
42. Huang X, Netravali A (2007) Characterization of flax fiber reinforced soy protein resin based green composites modified with nano-clay particles. Comp Sci Technol 67(10):2005–2014
43. Tiber B, Balcıoğlu HE (2019) Flexural and fracture behavior of natural fiber knitted fabric reinforced composites. Polym Compos 40(1):217–228
44. Ashok RB, Srinivasa CV, Basavaraju B (2019) Dynamic mechanical properties of natural fiber composites—a review. Adv Compos Hybrid Mater 1–22
45. Rajesh M, Pitchaimani J (2017) Mechanical properties of natural fiber braided yarn woven composite: comparison with conventional yarn woven composite. J Bionic Eng 14(1):141–150
46. Rajesh M, Pitchaimani J (2017) Experimental investigation on buckling and free vibration behavior of woven natural fiber fabric composite under axial compression. Compos Struct 163:302–311
47. Rajesh M, Jeyaraj P, Rajini N (2016) Mechanical, dynamic mechanical and vibration behavior of nanoclay dispersed natural fiber hybrid intra-ply woven fabric composite. In: Nanoclay reinforced polymer composites. Springer, Singapore, pp 281–296
48. Soundhar A, Kandasamy J (2019) Mechanical, chemical and morphological analysis of crab shell/sisal natural fiber hybrid composites. J Nat Fibers 1–15
49. Ayranci C, Carey J (2008) 2D braided composites: a review for stiffness critical applications. Compos Struct 85(1):43–58
50. Peças P, Carvalho H, Salman H, Leite M (2018) Natural fibre composites and their applications: a review. J Compos Sci 2(4):66
51. Carus M, Eder A, Dammer L, Korte H, Scholz L, Essel R, Breitmayer E, Barth M (2015) Wood-Plastic Composites (WPC) and Natural Fibre Composites (NFC). Nova-Institute, Hürth, Germany, p 16
52. Partanen A, Carus M (2016) Wood and natural fiber composites current trend in consumer goods and automotive parts. Reinf Plast 60(3):170–173
53. Keskisaari A, Kärki T (2018) The use of waste materials in wood-plastic composites and their impact on the profitability of the product. Resour Conserv Recycl 134:257–261

54. Mohammed L, Ansari MN, Pua G, Jawaid M, Islam MS (2015) A review on natural fiber reinforced polymer composite and its applications. Int J Polym Sci 2015
55. Lertwattanaruk P, Suntijitto A (2015) Properties of natural fiber cement materials containing coconut coir and oil palm fibers for residential building applications. Constr Build Mater 94:664–669
56. Ticoalu A, Aravinthan T, Cardona F (2010) A review of current development in natural fiber composites for structural and infrastructure applications. In: Proceedings of the southern region engineering conference (SREC 2010). Engineers Australia, pp 113–117
57. Dweib MA, Hu B, O'donnell A, Shenton HW, Wool RP (2004) All natural composite sandwich beams for structural applications. Compos Struct 63(2):147–157
58. Sanjay MR, Arpitha GR, Naik LL, Gopalakrishna K, Yogesha B (2016) Applications of natural fibers and its composites: an overview. Nat. Resourc. 7(3):108–114
59. Väisänen T, Das O, Tomppo L (2017) A review on new bio-based constituents for natural fiber-polymer composites. J Clean Prod 149:582–596
60. Bhuvaneswari HB, Vinayaka DL, Ilangovan M, Reddy N (2017) Completely biodegradable banana fiber-wheat gluten composites for dielectric applications. J Mater Sci: Mater Electron 28(17):12383–12390
61. Huda MS, Drzal LT, Ray D, Mohanty AK, Mishra M (2008) Natural-fiber composites in the automotive sector. In: Properties and performance of natural-fibre composites. Woodhead Publishing, pp. 221–268
62. Monteiro SN, Lopes FPD, Ferreira AS, Nascimento DCO (2009) Natural-fiber polymer-matrix composites: cheaper, tougher, and environmentally friendly. JOM 61(1):17–22
63. Al-Oqla FM, Sapuan SM (2014) Natural fiber reinforced polymer composites in industrial applications: feasibility of date palm fibers for sustainable automotive industry. J Clean Prod 66:347–354
64. Bongarde US, Shinde VD (2014) Review on natural fiber reinforcement polymer composites. Int J Eng Sci Innov Technol 3(2):431–436
65. Taj S, Munawar MA, Khan S (2007) Natural fiber-reinforced polymer composites. Proc-Pakistan Acad Sci 44(2):129
66. Vaidya U (2011) Composites for automotive, truck and mass transit: materials, design, manufacturing. DEStech Publications, Inc.
67. Holbery J, Fifield L, Denslow K, Gutowska A, Simmons K (2005) Role of fiber adhesion in natural fiber composite processing for automotive applications

# Damage Characterization of Composite Stiffened Panel Subjected to Low Velocity Impact


**Sai Indira, D. Mallikarjuna Reddy, Jayakrishna Kandasamy, M. Rajesh, Vishesh Ranjan Kar, and M. T. H. Sultan**

**Abstract** Composite materials have become popular due to their properties like high specific strength and high stiffness to weight ratio. Composites are found extensive applications in automobile, aerospace, defense equipments and other critical components. Composite plates are predominantly used as alternative materials to regular material because of its properties. In order to provide even better strength and resistance to deformation, stiffeners are attached to the composite plates thereby increasing the bending stiffness to a large extent. These stiffened panels have found principle application in aircraft wings, ship hulls and bridge decks. In this particular work, the low velocity impact on composite panel has been studied. Numerical models of composite plates and stiffened panels are analyzed by finite element analysis using ABAQUS/Explicit. Further study has made with different oblique impact angles like 90°, 60°, 45° and 30° are simulated and analyzed. Different parameters such as displacement, contact force, energy absorbed were compared for composite panel with and without stiffeners. It was noted that stiffened panels offer more resistance to deformation and absorb more energy due to high stiffness.

**Keywords** Low velocity impact · Abaqus/explicit · Stiffened panel · Composite

S. Indira · D. Mallikarjuna Reddy (✉) · J. Kandasamy · M. Rajesh
Vellore Institute of Technology, Vellore 632014, Tamil Nadu, India
e-mail: dmreddy@vit.ac.in

V. R. Kar
National Institute of Technology Jamshedpur, Jamshedpur 831014, Jharkhand, India

M. T. H. Sultan
Department of Aerospace Engineering, Faculty of Engineering,
University Putra Malaysia, 43400 UPM Serdang, Selangor Darul Ehsan, Malaysia

© Springer Nature Singapore Pte Ltd. 2021

M. Jawaid et al. (eds.), *Structural Health Monitoring System for Synthetic, Hybrid and Natural Fiber Composites*, Composites Science and Technology,
https://doi.org/10.1007/978-981-15-8840-2_4

## 1 Introduction

The composite structures are being widely used in many manufacturing industries such as aircraft, wind mills, ships, automotive, sports, health care, bridges etc. The impact due to low velocity can generate a noteworthy damage and minimize the stiffness by over fifty percent [1–3]. It becomes very difficult to inspect damage in composite material. Composites are produced using various materials whose properties might or might not be homogeneous or isotropic [4]. Therefore, the utilization of composite material includes a wide selection of available materials such as fibers, reinforced concrete, metals, and fibers. However, it is primarily fiber reinforced composites that have been increasingly used for aerospace applications [5]. These composites generally consist of layers of unidirectional or bidirectional fibers of high specific modules for the high structural applications required, particularly in military aircraft, which are fortified together by matrix type of material [6]. Laminated composites have multiple benefits over other conventional materials like metals as high specific rigidity and strength, excellent corrosion resistance and anisotropic properties that can be tailored to strengthen the necessary requirements [7]. Certainly, the coupling between stretching, twisting and bending made available by selecting appropriate stacking sequence in composite laminate permits aero elastic tailored structures. Damage characterization is very important to achieve the safety of the structure [8, 9].

The stiffened panel is one of the most primary parts of airframe systems with low and higher intensity of loadings. These panels contain mainly two basic parts: Longitudinal as reinforcing members and skin. Stiffened panels with bonded stiffeners are widely used in aerospace and other eminent engineering applications [10] where the structural weight of the material and strength is the major concern. Stiffeners in a stiffened panel enable highly directional loads to be sustained and introduce multiple load paths that can protect against crack growth under tensile loads, compressive loads and damage. The major perk of the stiffeners is the improved bending stiffness of the structure loads and destabilizing of compressive loads. Besides the advantage of using them, the stiffened panels are designed using various techniques brings various advantages like reduction in usage of materials, improved performance and reduction in cost etc. Stiffened panel with application of composite material in particular due to its characteristics of both material and structural forms [11] has the tensile strength five to six times higher when compared with steel or aluminum, specific modulus about four times greater when compared with steel and aluminum.

Stiffened panels are widely classified as open type, box type or closed type [12]. Box type of stiffeners is more torsionally stiffer than open type. The stiffeners or stringers in the stiffened panel are attached perpendicularly to the composite panel [13]. The usage of these panels is increasing in structural applications due to high specific stiffness and good specific strength. The stiffeners in stiffened panels represent a small portion of the overall weight of a structure but have significant impact on structural stability and stiffness [14]. In order to understand stiffness and strength of the stiffened panel structure; different studies are done [15–17].

Impact damage is a major consideration of aircraft composite structure design and maintenance. Damage to airframe structure caused by low velocity impact is because of both operational as well as maintenance activities. There are usually few incidents of low velocity impact (LVI) damage in the operating environment and most can be attributed to birds hitting on aircraft and hailstone strikes. The major causes of LVI damage is due to improper handling and maintenance issues which include airframe part handling, transportation, storage and also accidental instrument drops [18]. LVI is a major safety concern as widespread damage may occur in the composite panel although visual inspection cannot identify it [19, 20]. In general panel without stiffeners tend to delaminate because of the flexibility to bending for low velocity impact loads. Charpy test, Izod test and drop weights are the three standard methods of tests for low velocity impact. Drop weight test unit simulate different real world impact conditions and gathers point by point performance data. The benefit of this test with regard to other tests is that it is possible to examine a wide range of test geometries so that complex components can be tested [21, 22].

## 2 Composite Damage Model

### *2.1 Failure Criteria*

In the composite laminates, the dynamic behavior is so complex, as there are many phenomena happen under impact loading during the failure of composite laminates. Some of the adverse effects are fiber breakage, large displacements and plastic deformations, delamination, and matrix cracking, when laminate is subject to impact load [23]. The popular Hashin's damage criterion is considered for the composite Laminate models to predict the damages. Johnson has also used the Hashin's damage criteria to predict the damage in composite plates/shell under impact. Some authors are worked on detection and localization of damages. The damage on composite plate is predicted by following Equations;

Fiber tension:

$$\left(\frac{\sigma_{11}}{X_{\mathrm{T}}}\right)^2 + r\left(\frac{\sigma_{12}}{S_{\mathrm{L}}}\right)^2 = 1, \quad 0 < r > 1 \tag{1}$$

Matrix tension:

$$\left(\frac{\sigma_{21}}{Y_{\mathrm{T}}}\right)^2 + \left(\frac{\sigma_{22}}{S_{\mathrm{L}}}\right)^2 = 1 \tag{2}$$

Fiber compression:

$$\left(\frac{\sigma_{11}}{X_C}\right)^2 = 1 \tag{3}$$

Matrix compression:

$$\left(\frac{\sigma_{22}}{2S_T}\right)^2 + \left[\left(\frac{Y_C}{2S_T}\right)^2 - 1\right]\left(\frac{\sigma_{22}}{Y_C}\right)^2 + \left(\frac{\sigma_{11}}{S_L}\right)^2 = 1 \tag{4}$$

where, $X_T$ is the tensile strength and $X_c$ is compressive strength in fiber direction, $Y_T$ and $Y_c$ tensile and compressive in matrix direction $S_T$ and $S_c$ are longitudinal and transverse shear strength and $r$ is the coefficient of contribution shear stress to tensile between the layer.

When composite laminate subjected to impact load, it undergoes fiber damage at the interface as well as bending moment of the panel. In case of pure-bending, tensile and compressive stresses exist. Actually bending phenomena also includes shear stress. In bending tensile and compressive stresses exist within the layer or fiber and shear stress exist between the two laminas. Tensile and compressive stress acts along the length of the fiber. But shear stress acts tangent to the surface of the layers. Composite materials are strong in tension and compression but weak in shear. Because epoxy holds the bond between two layers whose bonding strength is low for shear stress [24].

## 2.2 *Intra Ply Damage*

Intra ply damage is because of tensile failure of fibers when they are subjected to axial loading or breakage of fibers when they get ruptured between impactor and composite panel surface. When tensile stress in the fiber exceeds the tensile strength of the composite fiber, it breaks into pieces. The intra ply damage is results in fiber rupture. Micro buckling in fiber is caused due to compression forces however rupture of fibers is due to tensile forces. Fiber pull out happens when the bond between matrix and fiber is feeble. This causes the fiber to be drawn out of the matrix subsequently debonding mechanism occurs. If in case the bonding between matrix and fiber is firm then, there wouldn't be fiber debonding or fiber pull out [24] (Fig. 1).

## 2.3 *Inter Ply Damage*

The separation of two adjacent plies at the plies interface due to matrix weakening is called delamination. The inter ply damage in composite panel is called delamination,

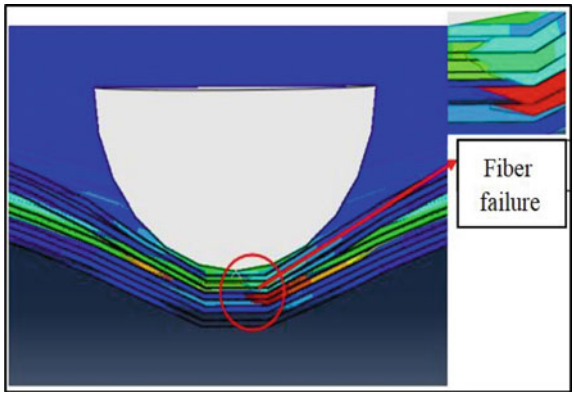


**Fig. 1** Fiber failure in panel

occurs where shear stress acts at the interface between two plies during bending. Delamination occurs in three modes as shown in Fig. 2. Opening mode, Shearing mode and tearing mode. When the impact load is applied on the composite panel, it undergoes bending. During bending top layers which are above the neutral layer are subjected to compression and bottom layers which are below the neutral layer are subjected to tensile. Due to strain differences in layers, shear stress is generated at the interface between the layers as shown in Fig. 2.

If the shear stress at the interface exceeds the shear bonding strength of the matrix, crack is initiated at the interface. The regions damaged at the ply, crack is generated and propagates which results in creating two new surfaces. This is inter ply failure and in the regions damaged at the ply, a crack is generated and grows as the load is increased. As the stiffness of the composite panels reduces, the delamination increases. This type of failure ceases when the impact energy is insufficient to trigger any further failure mechanism [25]. The energy used to create a unit amount of new surface by either deboning or by fiber pull out can be estimated theoretically are followed by,

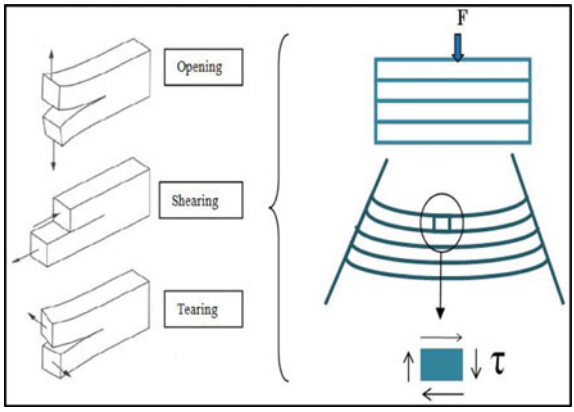


**Fig. 2** Modes of delamination and delamination mechanism

For pull out

$$\gamma = \frac{\sigma_{b2} L_c^2 \phi_2}{12L} \quad (L > L_c) \tag{5}$$

$$\gamma = \frac{\sigma_{b2} L_c^2 \phi_2}{12L_c} \quad (L > L_c)$$

For deboning

$$\gamma = \frac{\sigma_{b2} L_D^2 \phi_2}{4E_2} \tag{6}$$

where,

$\gamma$ = Fracture surface energy

$\sigma_{b2}$ = Tensile strength of fibers

$L$ = Length of the fibers

$L_c$ = critical length of fibers

$L_D$ = deboned length of the fibers

$\phi_2$ = volume fraction of the fiber

## 3 Methodology

Composite panel is modeled by Abaqus software. The nominal length and width of plate are 100 and 150 mm. The each layer nominal thickness of the plate is 0.3 mm. The mechanical properties of the material are defined inn Table 1. The stiffened composite is composed with five stiffeners. The orientation of fibers is $[+45°/0°/-45°/90]_{2S}$, the skin and stiffeners have layup of $[+45°/0°/-45°/90]_{2S}$ consists of 8 layers.

**Table 1** Glass fiber material properties

| Properties | Glass/epoxy |
|---|---|
| Density (kg/m$^3$) | 1000 |
| Elastic constants (GPa)<br>Poison's ratio | $E_1 = 152$, $E_2 = E_3 = 8.71$<br>$G_{12} = G_{13} = G_{23} = 3.35$<br>$\nu_{12} = \nu_{13} = \nu_{23} = 0.3$ |
| Strengths (MPa) | $X_t = 1930$, $X_c = 962$<br>$Y_t = 41.4$,$Y_c = 276$<br>$S_{12} = S_{13} = S_{23} = 82.1$ |

### *3.1 Modeling Strategy*

Modeling composite panel and stiffened panel are carried in ABAQUS software. The composite panel is modeled using 3D shell elements in ABAQUS. A total of 30,000 shell elements are used for composite panel and 31,800 shell elements are used for composite panel with stiffeners as shown in Fig. 3. Instead of brick elements, continuum elements are preferred as they allow three dimensional models and are also much better from computational point of view [26]. Composite stiffened panel consists with five I section stiffeners are placed at the bottom of the composite panel. Tie constraints is used for bottom surface of skin and stiffeners. All sides clamped boundary condition is used for analysis of both composite panels with and without stiffeners as shown in Fig. 4. The impactor is modeled as a 3D rigid body which consists mass of two kg.

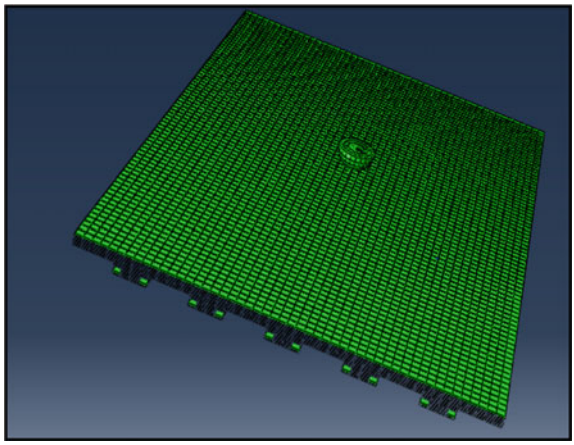

**Fig. 3** Meshed model for stiffened panel

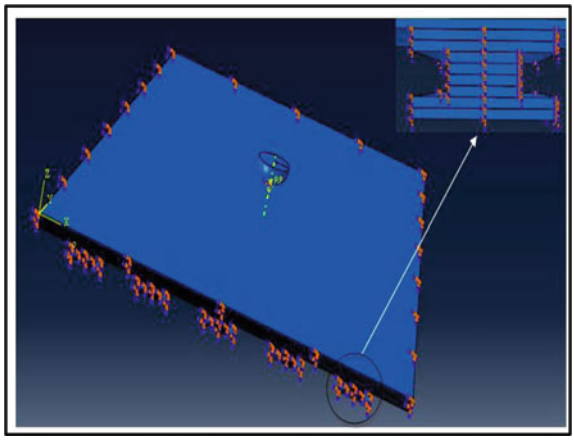

**Fig. 4** All sides clamped boundary condition for composite stiffened panel

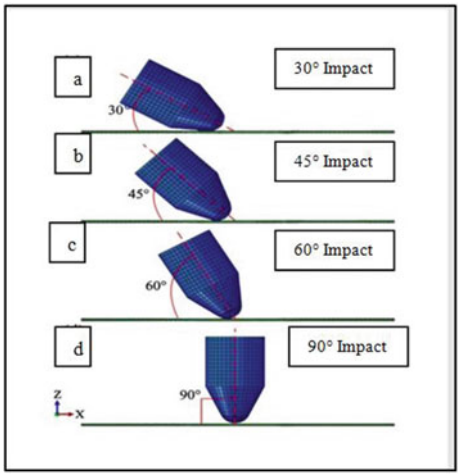


**Fig. 5** Different oblique impact views as **a** 30° impact angle **b** 45° impact angle **c** 60° impact angle and **d** 90° impact angle

Localized stiffener reductions will occur because of failure of elements individually in investigation and would cause intense distortions in some elements. To eliminate this, the damage parameters are confined to measure a maximum of 0.98 to make sure that the stiffness prevents the excessive distortion of elements [27]. The deletion of element technique is used in such a way that if any element fails due to tensile fiber failure, they are removed from the mesh [28] and 2200 rigid elements are used for discretization of impactor in the model. Hashin's fiber failure damage criteria is used for damage detection.

## *3.2 Oblique Low Velocity Impact*

Most of the cases in real life situations we observe oblique velocity impact. In Oblique impact, the impactor hits the target composite panel with different orientations. Normal velocity impact as discussed so far is one of the cases of oblique velocity impact, when the impactor makes a 90° angle with target surface [29]. Simulation of different impact angles including 90°, 60°, 45° and 30° with velocity 4 m/s is carried out to assess the influence of impact angles, damage behavior of composite panel and composite stiffened panel as shown in Fig. 5.

## *3.3 Material Properties*

Glass fiber material properties are assigned to the elements of composite panel with and without stiffeners. For intralaminar damage model, the fiber compressive and tensile failure mode values are taken as mentioned in following in Table 1.

## 4 Results and Discussion

In this paper, Simulations are performed using FE model in ABAQUS software for different velocities on composite panel. In this study particularly concentrated on maximum contact force, internal energy and deflection for panel with and without stiffeners, this study is more significance in damage initiation. The results of displacement versus time in the presence of consecutive plies of panels are plotted with fixed boundary condition for different velocities are presented in Fig. 6.

Figure 6 represents the deflection of the panel undergoes impact with different velocities for with and without stiffeners. It was observed that the deflection of composite panel without stiffeners is undergoes more deflection when compared with composite panel with stiffeners because composite panel with stiffeners has more resistance to deflect when compared with composite panel without stiffeners. It is also observed that the impact with 4 m/s has more deflection when compared with other velocities. It can be seen from Fig. 6 that deflections increase with increasing velocity of impactor for both panels respectively.

Figure 7 represents the internal energy absorbed by the panel undergoes impact with different velocities for with and without stiffeners. It is observed that the amount of internal absorbed by the panel is more with stiffeners compare to without stiffeners because stiffeners has the more toughness property. It can be seen from Fig. 7 that amount of internal energy absorbed by panels are increases with increasing velocity of impactor for both panels respectively.

Figure 8 presents the maximum contact force at the centre of the composite panel under impact with different velocities. The dynamic behavior of contact forces in low velocity impact loading is nonlinear. In Fig. 8, the contact forces histories are compared between composite panel with and without stiffeners for different velocities of impactor. It is seen that composite stiffened panel is offering more contact force

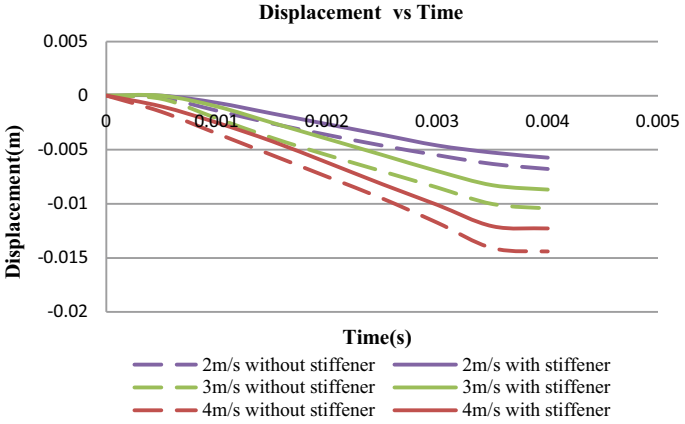


**Fig. 6** Displacement versus time graph for low velocity impact under different velocity

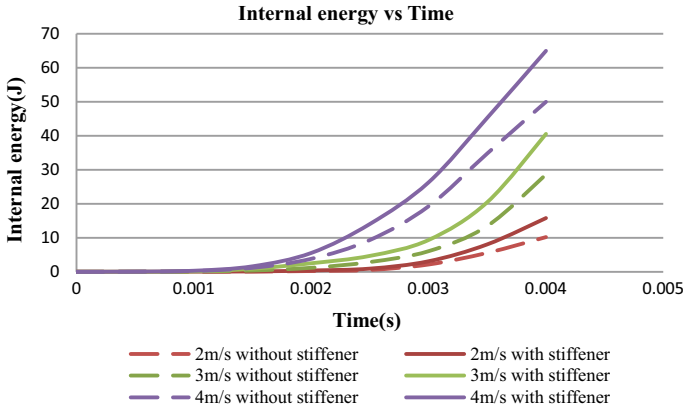


**Fig. 7** Internal energy versus time graph for low velocity impact under different velocity

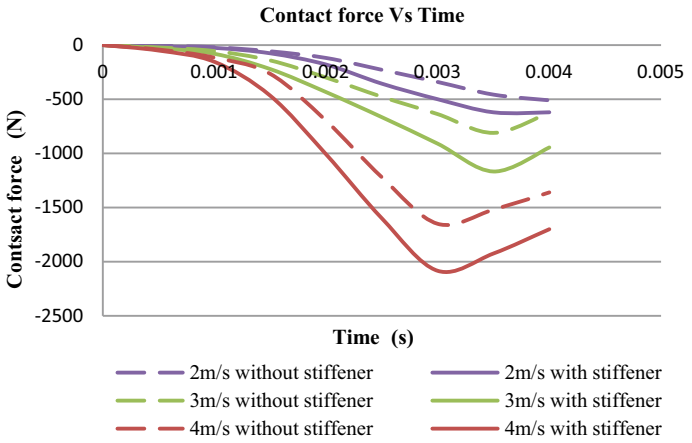


**Fig. 8** Contact force versus time graph for low velocity impact under different velocity

when compared with panel having without stiffeners. This is because of composite panel with stiffeners has more stiffness and it can give more resistance to contact forces. It is also observed that the impact with 4 m/s has more contact force when compared with other velocities.

## *4.1 Oblique Velocity Impact*

Simulation of different impact angles including 90°, 60°, 45° and 30° with same impact energy was carried out to assess the influence of impact angles, damage

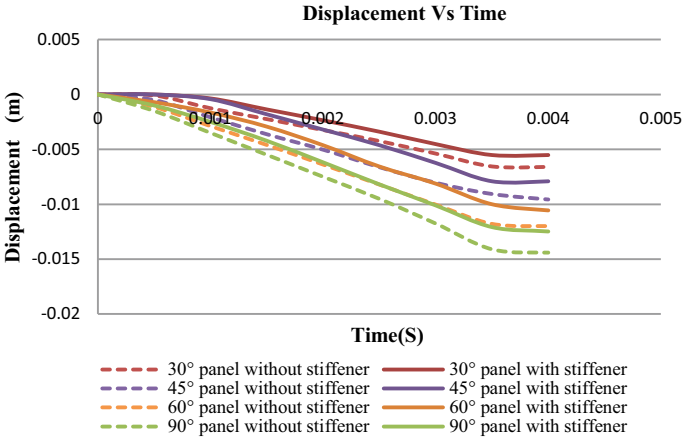


**Fig. 9** Displacement versus time graph for low velocity impact under different impact angles

behavior of composite panel and composite stiffened panel as shown in Fig. 6. The impactor hits the composite panel with an angle; velocity can be resolved into two components. One is normal to the composite panel surface and another component is tangent to the composite surface. Normal velocity component results into deflection and tangential component results into shear force. Shear force causes delamination in the composite panel.

In Fig. 9 the deflection is compared between composite panel and composite stiffened panel for different orientations of 30°, 45° and 60°. As it is observed in Fig. 9, the deflection of composite panel without stiffener is more when compared with composite panel with stiffener in oblique low velocity impact also. As the impact angle changes from 30° to 90° the deflection of the composite panel is increasing. As the impact angle increases normal component of the velocity increases which results in more deflection.

In Fig. 10, the Internal Energy is compared between composite panel and composite stiffened panel for different orientations of 30°, 45° and 60°. As it is observed in Fig. 7, Internal Energy Versus Time graph for normal velocity impact, the internal energy of composite panel is more when compared with composite stiffened panel in oblique velocity impact also. As the impact angle increases from 30° to 90° the internal energy of the composite panel is increasing.

In Fig. 11, the contact forces are compared between composite panel with and without stiffeners for different orientations of 30°, 45° and 60°. As it was observed in Fig. 8 Contact force Versus Time graph for normal velocity impact, the contact force of composite panel is more when compared with composite stiffened panel in oblique low velocity impact also. As the impact angle increases from 30° to 90°, the contact force of the composite panel is increasing. As the impact angle increases, normal component of the velocity increases which results in more contact force. Since the tangential velocity component results in delamination, as the impact angle

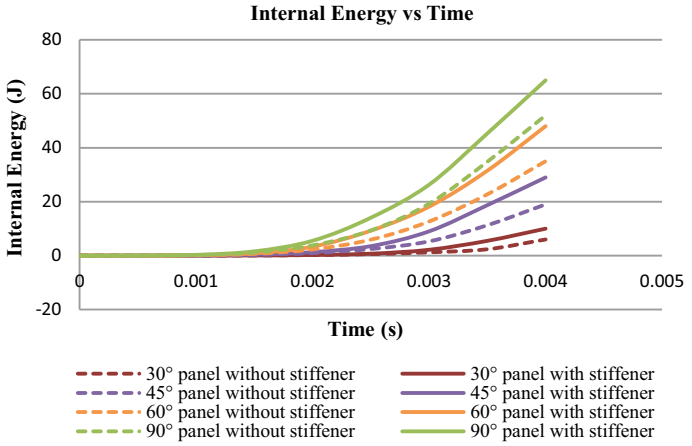


**Fig. 10** Internal energy versus time graph for different impact angles

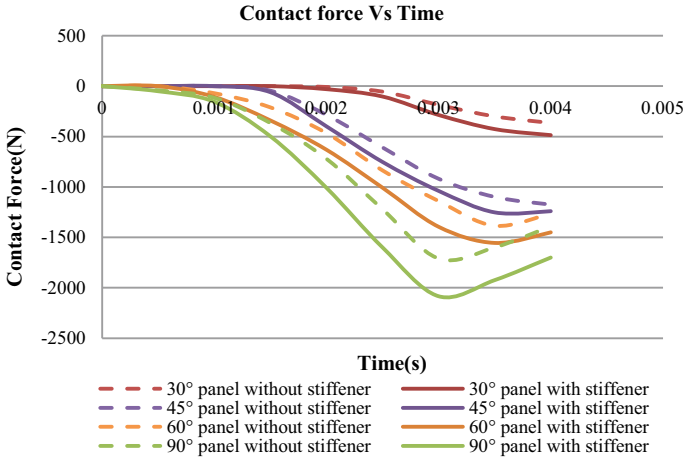


**Fig. 11** Contact force versus time graph for low velocity impact under different Impact angles

increases the delamination effect decreases. For low impact angles the shear velocity is more, delamination effect is also more when compared to high impact angles. When impact angle becomes 90°, shear velocity component becomes zero and it becomes normal velocity impact. So when impact angles are low then the delamination effect is predominant.

## 5 Conclusions

Comparative results are plotted for displacement, energy and contact force of panel with stiffener and without stiffener. Deflection in composite panel without stiffener is more when compared with composite panel with stiffener. Composite panel without stiffener can easily delaminate when compared with composite panel with stiffener. Composite panel with stiffener offers more stiffness during bending than composite panel without stiffener. So contact force in composite panel with stiffeners is more than composite panel without stiffeners. That energy absorption in composite panel with stiffeners is more than the composite panel without stiffeners. Finite element analysis is also done for oblique impact with 30°, 45°, 60°, and 90° angles. It is observed that as the angle of obliquity increase, the parameters like contact force, energy absorbed, deflection increases for both composite panel and composite stiffened panel and 90° impact is dangerous condition

**Acknowledgements** The project presented in this article is supported by and Engineering Research Board and Department of Science and Technology, Government of India (File Number: ECR/2017/000512).

## References

1. Cantwell WJ, Morton J (1978) The impact resistance of composite material—a review. Composites 22:347–362
2. Abrate S (1994) Impact on laminated composite materials: recent advances. Appl Mech Rev 47:517
3. Patil S, Mallikarjuna Reddy D, Reddy M (2018) Low velocity impact analysis on composite structures—a review. In: AIP conference proceedings, vol 1943, no 1. AIP Publishing
4. Campbell FC (2010) Introduction to composite materials; structural composite materials. ASM International
5. Jain HK, Upadhyay A (2009) Laminated composite stiffened panels: applications and behaviour. In: Civil engineering conference innovation without limit (CEC-09), 18–19 Sept 2009
6. Sang N, James T, Iannucci L (2016) Low, medium and high velocity impact on composites. In: 16th international conference on composite structures; ICCS 16
7. Ahmed A, Wei L (2015) The low-velocity impact damage resistance of the composite structures. Revised Adv Mater Sci 40:127–145
8. Mallikarjuna Reddy D, Jayaprakash G, Swarnamani S (2008) Detection and localization of damage in bridge model by spatial based wavelet approach. Int J Model 3:156–161
9. Kumar KS, Patil S, Mallikarjuna Reddy D (2018) Modeling and analysis of low velocity impact on composite plate with different ply orientations. In: International conference on innovation, engineering and entrepreneurship. Springer, Cham
10. Hoppmann WH, Baltimore M (1955) Bending of orthogonally stiffened plates. J Appl Mech 22:267–271
11. Faggiani A, Falzon BG (2010) Predicting low-velocity impact damage on a stiffened composite panel. Compos Part A 41:737–749
12. Pravallika K, Yugender M (2013) Structural evaluation of aircraft stiffened panel. ISSN: 2319-7064

13. Ahmadi H, Rahimi G (2018) Analytical and experimental investigation of transverse loading on grid stiffened composite panels. Compos Part B Eng 159:184
14. Zhu D (2004) Stiffened plates subjected to in-plane load and lateral pressure. Master's Thesis, ScholarBank@NUS Repository
15. Gal E, Levy R, Abramovich H, Pavsner P (2006) Buckling analysis of composite panels. Compos Struct J E 73:179–185
16. Lanzi L, Giavotto V (2006) Post-buckling optimization of composite stiffened panels: computations and experiments. Compos Struct J E 73:208–220
17. Zimmermann R, Klein H, Kling A (2006) Buckling and postbuckling of stringer stiffened fibre composite curved panels—tests and computations. Compos Struct J E 73:150–161
18. Mubarak Ali, Joshi SC, Sultan MTH (2017) Palliatives for low velocity impact damage in composite laminates. Adv Mater Sci Eng 2017 (Article ID 8761479)
19. Sun W, Guan Z, Li Z, Ouyang T, Jiang Y (2017) Modelling and simulating of the compressive behavior of T-stiffened composite panel subjected to stiffener impact. Compos Struct 168:47
20. Safri SNA, Sultan MTH, Yidris N, Mustapha F (2014) Low velocity and high velocity impact test on composite materials. ISSN (e): 2319 – 1813 ISSN (p): 2319 – 1805
21. Akula VMK (2015) Low velocity impact analysis of a stiffened composite panel. In: ASME 2015 pressure vessels and piping conference, PVP
22. Greenhalgh E, Bishop SM (1996) Characterisation of impact damage in skin-stringer composite structures. Compos Struct 36:187–207 (Elsevier Science Ltd.)
23. Hamamousse K, Serier Z, Poilane C (2019) Experimental and numerical studies on the low-velocity impact response of orthogrid epoxy panels reinforced with short plant fibers. Compos Struct 211:469–480
24. Richardson MOW, Wisheart MJ (1996) Review of low-velocity impact properties of composite materials. Compos Part A 27A:1123–1131
25. Nielsen LE, Landel RF. Mechanical properties of polymers and composites, second edition. CRC Press, New York (1993)
26. Kumar P (2009) Elements of fracture mechanics. Tata McGraw hill Education Private Limited, New Delhi
27. Sung N, Suh N (1979) Effect of fiber orientation on friction and wear of fiber reinforced polymeric composites. Wear 53(1):129–141
28. ABAQUS 6.7 Documentation (2007) Dessault systems
29. Li L, Sun L, Wang T, Kang N, Cao W (2019) Repeated low-velocity impact response and damage mechanism of glass fiber aluminium laminates. Aerosp Sci Technol 84:995–1010

# Natural Fibre for Prosthetic and Orthotic Applications—A Review


**Farah Syazwani Shahar, Mohamed Thariq Hameed Sultan, Ain Umaira Md Shah, and Syafiqah Nur Azrie Safri**

**Abstract** Prosthetics and Orthotics had significantly evolved since it was first used during the Egyptian Era around 5000 years ago. The materials used had advanced little by little with the increase of comfortability, cosmesis, and lighter in weight. The aim of this chapter is to review the natural fibres that has been used in the past decade for applications in Prosthetics and Orthotics. This chapter will consist of Introduction to Prosthetics and Orthotics devices, followed by the Ideal Specification for Materials used in Prosthetics and Orthotics, Types of Existing Natural Fibres used in Prosthetics and Orthotics, and finally Prosthetics and Orthotics Applications using Natural Fibres. The last section of this chapter will conclude the findings of this review chapter.

**Keywords** Applications · Natural fibre · Orthosis · Prosthesis

## 1 Introduction

This section was divided into two sub-sections where the first sub-section will be a brief introduction on prosthetics whereas the second sub-section will be on orthotics.

F. S. Shahar · M. T. H. Sultan (✉) · A. U. Md Shah
Department of Aerospace Engineering, Faculty of Engineering, Universiti Putra Malaysia, UPM Serdang 43400, Selangor Darul Ehsan, Malaysia
e-mail: thariq@upm.edu.my

M. T. H. Sultan · A. U. Md Shah · S. N. A. Safri
Laboratory of Biocomposite Technology, Institute of Tropical Forestry and Forest Products (INTROP), Universiti Putra Malaysia, UPM Serdang 43400, Selangor Darul Ehsan, Malaysia

M. T. H. Sultan
Aerospace Malaysia Innovation Centre (944751-A), Prime Minister's Department, MIGHT Partnership Hub, Jalan Impact, Cyberjaya 63000, Selangor Darul Ehsan, Malaysia

© Springer Nature Singapore Pte Ltd. 2021

M. Jawaid et al. (eds.), *Structural Health Monitoring System for Synthetic, Hybrid and Natural Fiber Composites*, Composites Science and Technology,
https://doi.org/10.1007/978-981-15-8840-2_5

## *1.1 Prosthetics Devices (Prosthesis)*

Prosthetics can be defined as an artificial replacement device which could help in regaining the function and appearance of the missing limb [1, 2]. Its main function was to provide the users the ability to perform daily tasks smoothly which previously may not be possible due to the missing limb. The amputations of a limb were usually caused by severe trauma, cancers, or diseases related to vascular complications [3].

The type of prosthesis indicated for a prosthetics user were mainly depended on the extent of the amputated limb and also which part was amputated [4]. Prosthesis and limb extremity amputations can be divided into two major parts which were the upper limbs and the lower limbs. Tables 1 and 2 shows the level amputation of upper extremity and lower extremity respectively whereas Figs. 1 and 2 shows an example of the upper limb prosthesis and the lower limb prosthesis respectively.

The upper limb prosthesis system can be divided into three categories which were the **passive system** [9], **body-powered system** [10], and **externally powered system** [11].

The **passive prosthesis system** which were also known as cosmetic prosthesis were usually used for as stabilizer. It was fabricated to look more natural but with the least functional abilities. This type of prosthesis were usually extremely lightweight but extremely expensive. Figure 3 shows an example of passive system prosthesis.

The **body powered prosthesis system** was a prosthesis which was controlled using cables. The generation of forces during body movements were transmitted into the cables which in return affect the joint operation. When compared to a passive prosthesis system, body powered prosthesis system were less expensive, a little heavier,

**Table 1** Level of upper extremity amputations [5]

| Amputation level | Body parts |
|---|---|
| Transcarpal | Fingers or partial area of the hand |
| Wrist disarticulation | From wrist joint to fingers |
| Transradial | From below the elbow to fingers |
| Elbow disarticulation | From elbow joint to fingers |
| Transhumeral | From above the elbow to fingers |
| Shoulder disarticulation | From shoulder joint to fingers |
| Interscapulothoracic | From above the shoulder to fingers |

**Table 2** Level of lower extremity amputations [6]

| Amputation level | Body parts |
|---|---|
| Foot | Toes or any part of the foot |
| Transtibial | From below the knee to the foot |
| Knee disarticulation | From knee joints to the foot |
| Transfemoral | From above the knee to the foot |
| Hip disarticulation | From hip joint to the foot |

**Fig. 1** Upper limb prosthesis [7]

**Fig. 2** Lower limb prosthesis [8]

and had highest durability. However, body powered prosthesis needed the most body movement for operation compared to other systems and had the least satisfactory of cosmetic appearance. Figure 4 shows an example of body powered prosthesis system.

**Fig. 3** Passive prosthesis system [12]

**Fig. 4** Body powered prosthesis system [13]

**External powered prosthesis system** worked by controlling electrical activity from the residual muscle at the amputated area via surface electrodes to enable the movement of the motorized prosthesis. This type of system can be further divided into three types which were myoelectrically controlled (uses muscle contractions signals to operate the prosthesis), switch controlled (uses small switch to activate the motors), and hybrid (uses both muscle strength and external power supply). External powered prosthesis system provides the most functional abilities, along better grip strength and cosmesis. However, the downside of this prosthesis was the weight and cost of

this prosthesis were the heaviest and the most expensive among all of the prosthesis system. Figure 5 shows an example of an external powered prosthesis system.

All prosthesis except passive prosthesis had several significant components which made a complete functional prosthesis. Table 3 shows the components available in complete prosthesis and their respective functions.

## *1.2 Orthotics Devices (Orthosis)*

Orthosis can be defined as an assist device which helps in controlling, correcting, or compensating the muscle strength due to deformity or trauma [2]. Unlike prosthesis which completely replaces the limbs, orthosis will only provide support or movement to the existing limbs. The function of an orthosis was similar to a prosthesis where it helps the users to do daily activities without any limitations or obstructions. The main difference between orthosis and prosthesis was that an orthosis supports the limbs whereas a prosthesis replaces the limbs.

Orthosis can be divided into three types of categorization which was regional [18], control system [19], and functional [18]. Figure 6 shows the categorization of orthosis.

Similar to prosthesis, **regional orthosis** were also divided into upper limb orthosis and lower limb orthosis with the addition of spinal orthosis. Figure 7 shows the regional types of orthosis available in the market.

The **upper limb orthosis** encases the region of the upper extremity of the limbs and can be categorized into four types which were Hand Orthosis, Wrist Orthosis, Elbow Orthosis, and Shoulder Orthosis.

**Hand orthosis**'s main objective was restoring the thumb's function for gripping and fingers' function for proper positioning during hand movements. Next, the **Wrist orthosis** designs were aimed to help in achieving an optimal Range of Motion (ROM). Meanwhile, **Elbow** orthosis focussed on the flexion of user's arm. Finally, the key component of **Shoulder orthosis** was its ability to positioned the limbs properly and provide critical support for shoulder stability.

The **lower limb orthosis** encases the region of the lower extremity of the limbs and were consist of Ankle-Foot Orthosis (AFO), Knee Orthosis (KO), Knee-Ankle-Foot Orthosis (KAFO), Hip-Knee-Ankle-Foot Orthosis (HKAFO), and Hip Orthosis (HO).

**AFO** controls the joint movement around the ankle region and supports the foot during gait movement. It was mostly used to fix the problems which were related to the foot to ground placement and provide foot clearance and heel contact. It was also used to restore the stability during the stance and swing phase of the gait movement, as well as compensating the weakness of the thigh muscle to avoid knee buckling due to weakness.

As for **KO**, it was beneficial to users who needs control of their knee only, not including the region around ankle and foot. It helps in controlling knee flexion due

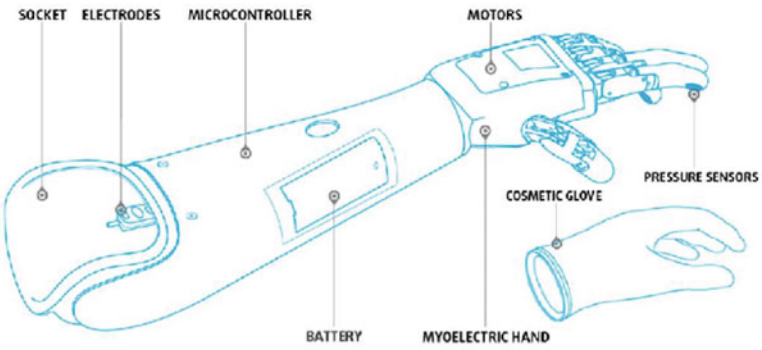


(a)

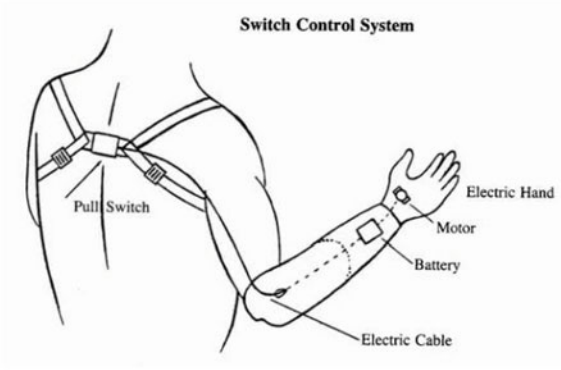


(b)

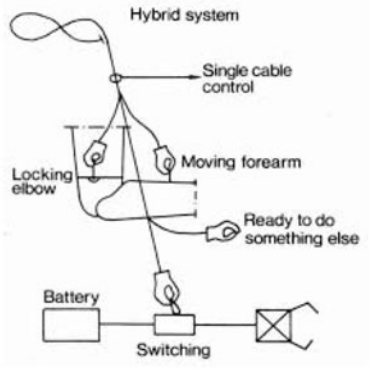


(c)

**Fig. 5** External powered prosthesis system; **a** myoelectrically controlled prosthesis [14]; **b** switch controlled prosthesis [15]; **c** hybrid prosthesis [16]

**Table 3** Components of prosthesis and their functions [17]

| Components | Functions |
|---|---|
| Sockets | The socket was designed with two layers where the inner layer acts as a cushion which contoured to the residual limb whereas the external layer gave length and shape for the device |
| Suspension system | The suspension system worked by securing the prosthesis to the residual limb. There were three types of harnesses:<br>– Figure of 8<br>– Chest strap<br>– Shoulder saddle |
| Control-cable system | The control system worked by helping in the operation of the limb movement. Usually used in external powered prosthesis system |
| Terminal device | This device was connected to the forearm socket which replaces the hand and enables hand movements such as grasp, flexing, and gripping |
| Components for interposing joints | This component provides angle orientation for the joints movement. There were three types of components which were needed based on the level of amputation:<br>– Wrist units<br>– Elbow units<br>– Shoulder units |

to muscle weakness, rotary instability, as well as anything that relates to angulation and instability of the knee.

The design of **KAFO** extends from the foot up to the thigh. This device was used to control motion and alignment of knee and ankle for stability or provide support for tibia, femur, or both. It also helps in relieving weight from the hip as well as stress in the leg.

**HO** encases the region around the hip area and supported with one thigh band to remain upright. It was commonly used to support hip and resist adduction as well as excessive flexion. The structure of the hip joint was made with features that could easily adjust flexion and extension stopper.

Finally, **HKAFO** was an extension from KAFO where, instead of only from foot to the thigh, HKAFO extends towards the hip. It helps in controlling the flexion or extension instability, abduction weakness, and rotational instability.

The **spinal orthosis** encases the region along the length of spine starting from the neck and ends at the lumbar region. It was mainly used to align skeletal structure, restrict motion, and prevent deformity progression. The spinal orthosis can be further divided into several categories which was Cervical Orthosis (CO), Cervicothoracic Orthosis (CTO), Halo Orthosis, Lumbosacral Orthosis (LSO), and Thoracolumbosacral Orthosis (TLSO).

**CO** encases the region around the head to the neck. It was used to restrict any movements of the head and neck, as well as limiting flexion, extension, rotation of the head and the cervical spine. It was basically a collar which wraps around the

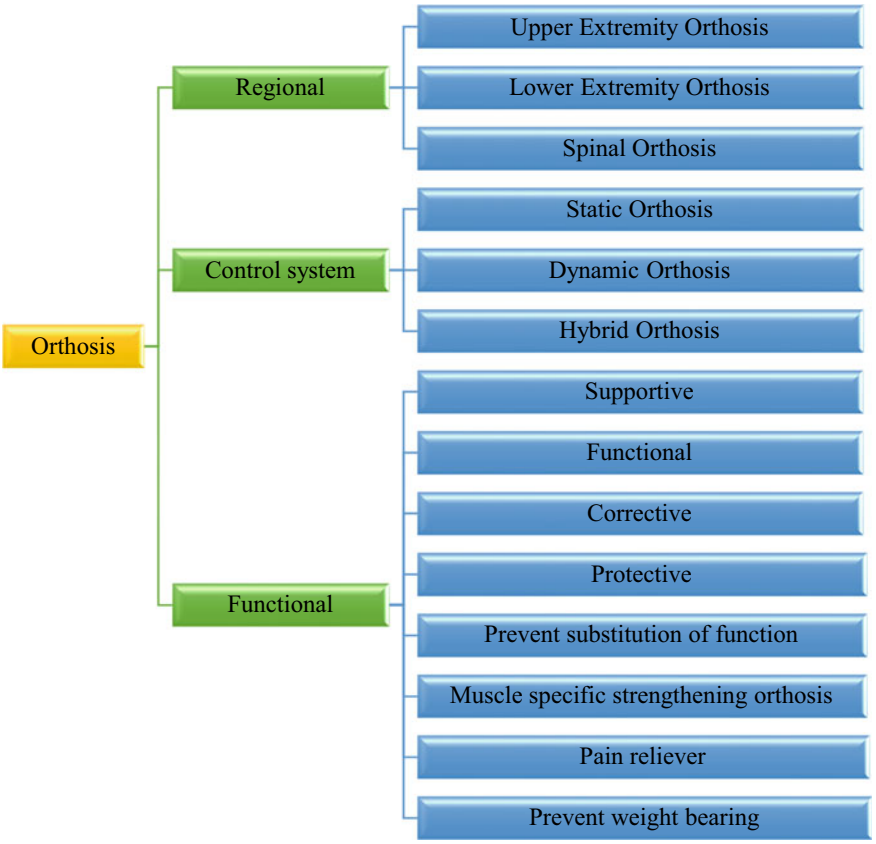


**Fig. 6** Orthosis categorization

neck and could be circumferentially adjustable. Depending on the type of CO used, the height adjustment may be included within the CO, could be made into single or multiple layered, as well as the variability in its firmness (soft or hard).

**CTO** encompassed the region from the upper cervical spine to the lower cervical spine. It had low restriction of motion on the upper cervical spine but the restriction becomes greater starting from the middle to the lower cervical spine. It was usually used to stabilise minimal fractures most suitable for bed patients due to the missing of posterior rods at the back of the patients.

**Halo Orthosis**, just like its name, appears like a halo which connected to the vest via the lateral bars. It provides flexion, extension, and rotational control of the cervical region. This orthosis had the greatest restriction of motions and stability compared to all cervical orthoses.

**LSO** extends from the sacrum to the inferior scapular angle of the spine. This orthosis limits flexion and extension of the body, as well as some rotation and side bending.

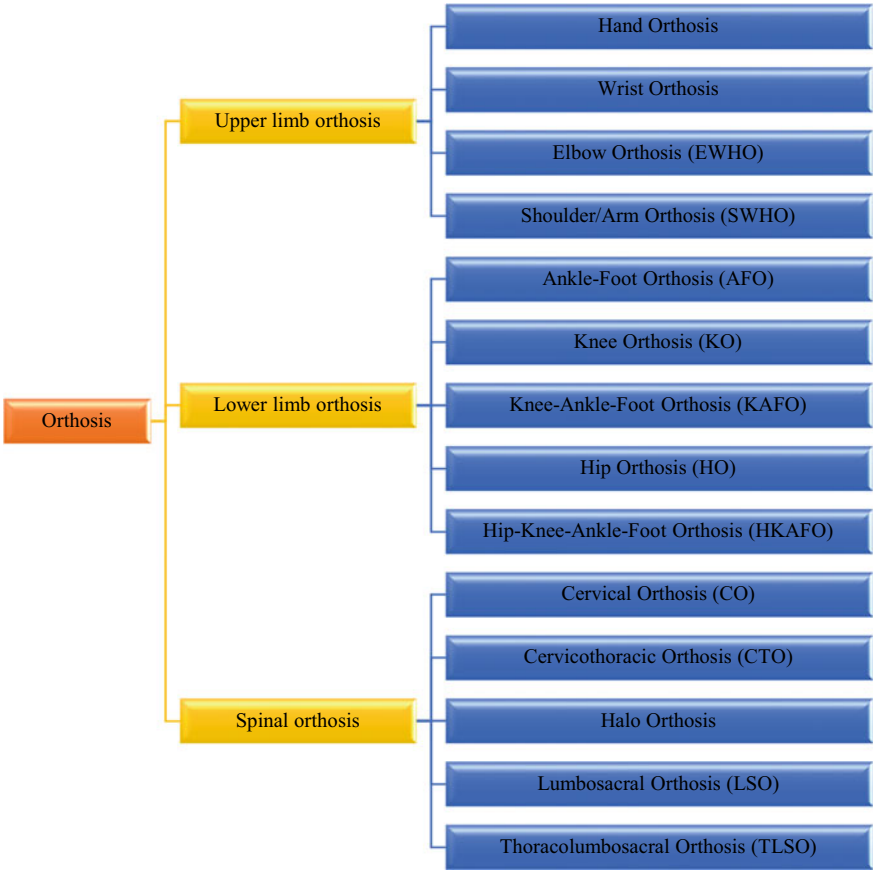


**Fig. 7** Types of orthosis based on anatomical region

Finally, the **TLSO** extends from the sacrum to above the inferior angle of scapula which was used for trunk's support and stability. It also helps in reducing weight on vertebral body.

The classification of orthosis could also be divided based on the type of **control system**. The three main type of control systems were static, dynamic, and hybrid. A **static orthosis** does not allow any movement, prevent deformity, and support the affected limbs. Meanwhile, a **dynamic orthosis** allows a certain range of motion and becomes a substitute for the loss of motor function. It helps in correcting an existing deformity by providing a controlled directional movement. It also helps in wound healing and fracture alignment.

As for **functional orthosis**, the design of the orthosis will be changing depending on the type of deformity or severity suffered by the users. Usually a functional orthosis will be combined with the regional orthosis and type of orthotic control system in order to achieve a specific or several criteria of a functional orthosis. As an example,

a user which suffered a fracture from the ankle-foot region will need a **supportive orthosis**. Thus, a static ankle-foot orthosis will be provided for the user.

## 2 Prosthetics and Orthotics Ideal Specification and Design Principles

This section will discuss on the ideal specification of prosthetics and orthotics devices and the underlying design principles for both type of devices.

### *2.1 Ideal Specification*

There were several ideal specifications that were needed to be fulfilled in order to create a prosthesis or orthosis. There were five main factors that could make an ideal prosthesis or orthosis which were function, comfort, cosmesis, fabrication, and economics [20].

The **function** factor was one of the main factor which affects the complete design of a prosthesis and orthosis. The design must fulfil the requirements needed by the users, whether they needed a hand prosthesis, hand orthosis, dynamic leg prosthesis or hybrid orthosis. Depending on the problems suffered by the users, different types of prosthesis or orthosis will be customized for them. The device must also be simple and could be easily learnt by the users, since a complicated device may need an unnecessary longer period of training which could become tedious.

The **comfort** factor also plays an important role to design an ideal prosthesis and orthosis. This is because, most users may stopped using their device completely which could hinder their healing time and obstructions in completing daily activities due to discomfort. The device must fit well on the users as well as able to easily put on and take off so that it would not unintentionally harm the users. In addition, a prosthesis and orthosis with low weight would not cause the users to expend too much energy to operate them and the users would feel as if the device were part of their bodies.

Another factor that should be taken into consideration was **cosmesis**. The prosthesis and orthosis must look like the original limb to help the users to blend in well within a society. Thus, it was important that both prosthesis and orthosis can be easily cleaned and maintained. Furthermore, in order to ensure a good hygiene, it was best for the device to be stain resistant.

The next factor was the **fabrication** aspects of an ideal prosthesis and orthosis. A good prosthesis and orthosis should have a fast fabrication method. In addition, the devices' parts and materials must be readily and widely available to ensure a continuous supply for repair and maintenance.

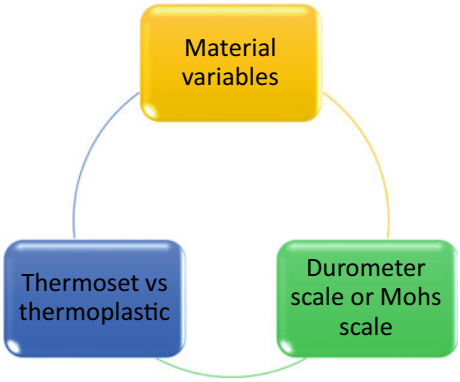


**Fig. 8** Design and structure consideration when choosing material for prosthetics and orthotics devices

Lastly, the **economics** factor in designing a prosthesis and orthosis must also be considered. The more affordable the device were available in the market, the higher the chances for the users to obtain the devices easily especially for users with poor income.

However, in order to achieve the specifications that were needed to make an ideal prosthesis and orthosis, researchers as well as P&O professionals usually considers the material aspects of the prosthesis and orthosis design. When choosing a material for prosthetics and orthotics devices, researchers and P&O professionals usually took into consideration of several factors as shown in Fig. 8.

The first factor, **material variables** affects the characteristics that were need in a certain type of prosthesis and orthosis. These variables will determine the characteristics of the end product such as flexibility, durability, corrosiveness, and much more. Table 4 show some of the material variables that were needed to be included into consideration before choosing a suitable material.

As mentioned in Hardness of the material variables previously, **durometer** was an instrument which was used to identify the hardness of materials such as polymers, elastomers and polymers [22]. It helps in determining the resistance of the materials towards permanent indentation. The most common measurement that has been used for prosthesis and orthosis were Shore D. Just like durometer, **Mohs scale** was also used to measure hardness of the materials. However, it is specifically used for minerals, gemstones, and metals [23].

Most prosthesis and orthosis were made from plastics. There were two type of plastics that can be used which was **thermosets and thermoplastics** [24]. Thermoset polymers were polymers that could not be reverse hardened and thus shaped permanently by curing from a liquid resin. Meanwhile, thermoplastic polymers were materials that could be hardened when it was heated and softened when it was cooled. This type of material enables the shaping of prosthesis and orthosis becomes much easier, thus resulting in its high demand in the market. Thermoset were generally cheaper compared to a thermoplastic, but it could not be remolded, reshaped, or recycled like thermoplastics.

**Table 4** Material variables affecting the decision in choosing a suitable material for prosthesis and orthosis [21]

| Material variables | Description |
|---|---|
| Strength | The material must be able to resist breaking under tension and compression, good yield strength, as well as the ability to sustain an applied load under impact |
| Durability | Prosthesis and Orthosis could withstand factors such as wear, pressure, or damage under any type of condition and time constraints |
| Stiffness | The loaded material must be able to resist deformation, bending, or compression. A stiff material means that it will be less flexible, thus causing the possibility of deformation becomes less likely to occur |
| Density | The device must be as light as possible while still retaining the strength, stiffness, and durability of the material |
| Hardness | This factor emphasised on the resistance towards permanent indentation of the material and determined by durometer (for rubbers, elastomers, and polymers) or Mohs scale (for metal) |
| Thickness | The thickness of the material were usually related to the weight and bulkiness of the device. The thicker the material, the heavier the device will be. It is especially important when dealing with leather. The thermoplastics used for prosthesis and orthosis also being sold in sheets with varying thickness |
| Corrosion resistance | The material must be able to resist chemical degradation especially when the device may have a direct contact with body fluids |
| Malleability | The material must be able to shaped easily without breaking especially materials such as metal which needs to be hammered, bent, pressed, or rolled into sheets |
| Lamination | When the different materials were glued together to form a single sheet, the characteristics of these materials could be blend together to produce a better functioning materials, namely composites |

## 2.2 *Design Principles*

The design of a prosthesis and orthosis followed several biomechanical principles, which were [25]:

i. **The three point pressure concept (Jordan's Principle)**—This principle states that the sum of forces created is equal to zero,

$$F_1 + F_2 = F_3 \tag{1}$$

where,
$F_1 + F_2$ = counter forces in opposing direction
$F_3$ = primary force acting on joints or stump

A single primary force will be located at the joint or stump area which reacted against two additional counter forces which were in opposing direction as shown

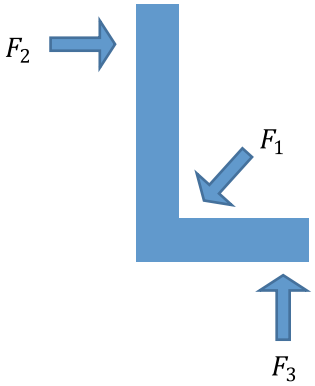


**Fig. 9** The three point pressure system

in Fig. 9. This principle could ensure stability during any types of movement control.

ii. **Total contact**—The greatest comfort could be achieved when the pressure distribution between device's interface and skin decreases as shown in Fig. 10. The higher the amount of surface area is in contact with the tissue, the lower the pressure distribution will be,

$$P = \frac{F}{A} \tag{2}$$

where,
$P$ = pressure distribution
$F$ = applied force
$A$ = surface area

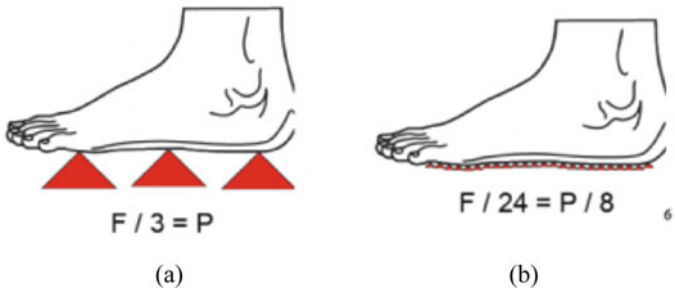


**Fig. 10** The total contact of an prosthesis and orthosis determines the comfortability of the device; **a** small surface area; **b** large surface area

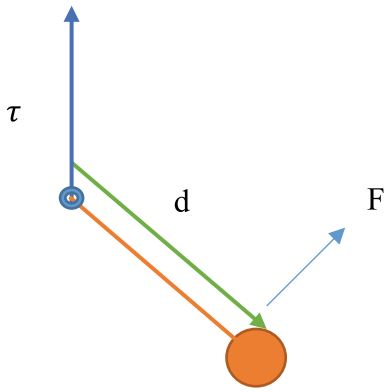


**Fig. 11** The principle of torque acting on an orthosis to help in partial weight relieving

iii. **The biomechanics of levers and forces for partial weight relieving**—The stability of the limbs movement highly depended on the rotational effect of the torque system,

$$\tau = F \times d \tag{3}$$

where,
$\tau$ = torque
$F$ = force applied
$d$ = moment arm distance from axis of rotation

The farther the point of force from the joint, the greater the moment of the arm, the smaller the magnitude of force required to produce a given torque at the joint. This principle could help in partial weight relieving during any type of movement control. Figure 11 shows an example of torque system acting on a prosthesis and orthosis.

## 3 Natural Fibres Used in Prosthetics and Orthotics and Its Applications

Currently, a lot of researchers were focussing on using natural fibers in several different fields in order to replace materials such as plastics and metals. The benefits of using natural materials were the renewability of the raw materials, the lightweight of the materials itself, and their ability to retain strength, stiffness, malleability, and durability while retaining its low weight [2, 26]. In addition, natural material were corrosive resistant and would not completely degrade if it was properly treated chemically.

The uses of natural materials has existed since the ancient Egyptian era where originally, instead of the fibers itself, they used the bark of a tree and shaped them into a prosthesis or orthosis [2].

The first material that has ever been discovered was **cork**, which was harvested from an oak tree. The cork main component was the waxy waterproof substance known as suberin which ensure its buoyancy, elasticity, and resistance towards fire [27]. The cork also has a honeycomb like structure which ensures its high strength and low weight properties. The honeycomb structure of the cork also ensures that it has high impact strength due to the cushioning effect formed from the structure as well as highly resilient and flexible. Thus ancient Egyptians made prosthesis or orthosis purely from corks and then wrapped with cartonnage to keep the limbs in place [2]. In the current era, Corks were usually combined with other types of material for better material properties.

Another type of natural material that was used was **Kenaf blends** [28]. Kenaf were one of the highest yield crop available around the Asian country. This raw material could yield around 6–10 tonnes of dry fiber within 6–8 months [26]. Kenaf materials were biodegradable and recyclable. The characteristics of Kenaf provides comfort and good shock absorption.

**Cotton fiber** was also one of the most famous material when it comes to absorbent materials [22]. This fiber was extracted from the capsules of the cotton plant and it was also resistant to tear. Table 5 shows current natural fiber materials and applications that has been researched.

It was obvious that there were a lot of wood and natural fiber materials that has been developed for prosthetics and orthotics applications. However, there were still limited numbers of prosthetics and orthotics applications that had applied natural fibers into the manufacturing of prosthesis and orthosis.

In prosthesis manufacturing and fabrication, natural fibers were mainly used in designing a socket, terminal devices, feet or the exoskeletal body. The socket is the part where the stump is inserted. The main concern for the design of a socket is that it has to be in total contact with the skin tissue. Usually, the socket of both upper extremity and lower extremity has a double wall framework where the inner wall were made from soft materials such as cotton whereas the outer wall was made from stronger but light materials such as Kenaf, or Cork. Figure 12 shows an example of natural fiber socket made from Kenaf fiber.

As for the prosthesis's body, the socket was connected to it either by exoskeletal construction or endoskeletal construction. Natural fibres were usually used to construct an exoskeletal body of the prosthesis. The exoskeletal body gains its structural strength from the outer laminated shell through the weight of the body was transmitted. The shell was made of resin or polymers over a filler material made from wood or natural fibres and the whole prosthesis was shaped into the appearance of the amputated limb. Figure 13 below shows the exoskeletal body of a prosthesis which was made from willow wood fiber.

Next, the feet were designed to have a high degree of cosmesis so that it will resemble completely like the original amputated limbs. It was usually made from

**Table 5** Current natural fiber materials and applications that has been researched

| Authors | Applications | Type of materials |
|---|---|---|
| JMS Plastics Supply Inc. [31] | Orthosis | Cork granules and nylon blend |
| | | Shredded cork and rubber blend |
| | | Cork granules and rubber blend |
| | | Shredded cork and Ethyl Vinyl Acetate (EVA) blend |
| JLFPro [32] | Orthotic insole | Wood and kenaf blend |
| | | Wool and kenaf blend |
| | | Cotton fiber |
| | | Wool |
| Becker [33] | Hip orthosis | Maple leaf |
| Campbell et al. [34] | Prosthetic sockets | Bamboo |
| | | Banana |
| | | Corn |
| | | Flax |
| | | Ramie |
| | | Seacell |
| | | Soya |
| Odusote et al. [35] | Prosthetic socket | Banana pseudo stem fiber reinforced epoxy composite |
| Kramer et al. [36] | Prosthesis and Orthosis | Bamboo reinforced composites |
| Irawan et al. [37] | Prosthetic socket | Ramie fiber reinforced epoxy composites |
| Irawan et al. [38] | Prosthetic shank | Rattan reinforced fiberglass and epoxy composites |
| Irawan et al. [39] | Prosthetic socket | banana fiber reinforced epoxy composites |
| Odusote and Kumar [40] | Prosthetic socket | Pineapple leaf fiber and epoxy composite |
| Widhata et al. [41] | Prosthetic socket | Water hyacinth composite |

**Fig. 12** Natural fiber socket [29]

**Fig. 13** Natural fiber exoskeletal body [30]

wood or natural fibers. Some examples of the applications were Solid Ankle Cushion Heel (SACH). Figure 14 shows an example of feet made from natural fiber.

In orthosis manufacturing and fabrication, depending on the requirement needed by the users, there were some orthosis were made completely from natural fibers. An example of application which could use natural fibers for fabrication was orthoplasty, orthopaedic insoles, and corset.

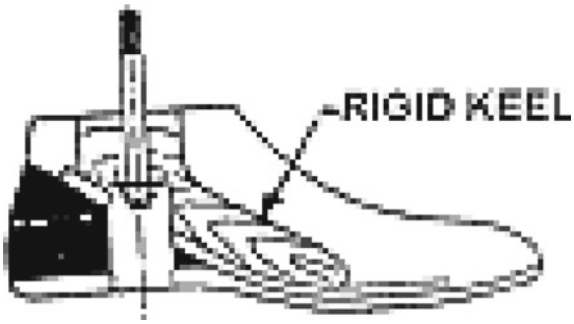


**Fig. 14** Solid ankle cushion heel (SACH) where the wooden keel provide mid-stance stability

## 4 Conclusions

At present, the orthotics and prosthetics field still keep on changing and evolving without any obstructions. With more and more advance technologies that comes out over the past several years, there are various design possibilities that can be explored and research especially when it comes to prosthesis and orthosis materials. From this review, it can be seen that there are still a limited research conducted on natural fibers in the orthotic and prosthetic field.

**Acknowledgements** The authors would like to thank Universiti Putra Malaysia for the financial support through the Geran Putra Berimpak, GPB 9668200. The authors would like to thank the Department of Aerospace Engineering, Faculty of Engineering, Universiti Putra Malaysia and Laboratory of Biocomposite Technology, Institute of Tropical Forestry and Forest Product (INTROP), Universiti Putra Malaysia (HICOE) for the close collaboration in this research.

## References

1. Arifin N, Hasbollah HR, Hanafi MH, Ibrahim AH, Wan Abdul Rahman WA, Che Aziz R (2017) Provision of prosthetic services following lower limb amputation in Malaysia. Malays J Med Sci 24(5):106–111
2. Shahar FS et al (2019) A review on the orthotics and prosthetics and the potential of kenaf composites as alternative materials for ankle-foot orthosis. J Mech Behav Biomed Mater 99:169–185
3. Bhuvaneswar CG, Epstein LA, Stern TA (2007) Reactions to amputation: recognition and treatment. Prim Care Companion J Clin Psychiatry 9(4):303–308
4. Smith DG (2004) General principles of amputation surgery. Atlas Amputations Limb Defic Surg Prosthet Rehabil Principles, pp 21–30
5. Ovadia SA, Askari M (2015) Upper extremity amputations and prosthetics. Semin Plast Surg 29(1):55–61
6. O'Keeffe B, Rout S (2019) Prosthetic rehabilitation in the lower limb. Indian J Plast Surg 52(1):134–144
7. Ottobock US (2020) Above-elbow prosthesis with DynamicArm. Available https://www.ottobockus.com/prosthetics/upper-limb-prosthetics/solution-overview/above-elbow-prosthesis-featuring-dynamicarm/. Accessed 17 May 2020 [Online]
8. Prosthetic Solution (2020) Lower limb prosthetics. Available https://prostheticsolutions.com.au/lower-limb/. Accessed 17 May 2020 [Online]
9. Maat B, Smit G, Plettenburg D, Breedveld P (2018) Passive prosthetic hands and tools: a literature review. Prosthet Orthot Int 42(1):66–74
10. Huinink LHB, Bouwsema H, Plettenburg DH, Van der Sluis CK, Bongers RM (2016) Learning to use a body-powered prosthesis: changes in functionality and kinematics. J Neuroeng Rehabil 13(1):1–12
11. Semasinghe CL, Ranaweera RKPS, Prasanna JLB, Kandamby HM, Madusanka DGK, Gopura RARC (2018) HyPro: a multi-DoF hybrid-powered transradial robotic prosthesis. J Robot 2018
12. Ottobock US (2020) Otto bock system hand-passive. Available https://shop.ottobock.us/Prosthetics/Upper-Limb-Prosthetics/Body-Powered-Systems/Ottobock-System-Hands/Otto-Bock-System-Hand–passive-/p/8K19. Accessed 17 May 2020 [Online]
13. Ottobock US (2020) Body-powered prosthetic solutions. Available https://www.ottobockus.com/prosthetics/upper-limb-prosthetics/solution-overview/body-powered-prosthetic-solutions/. Accessed 17 May 2020 [Online]

14. Calado A, Soares F, Matos D (2019) A review on commercially available anthropomorphic myoelectric prosthetic hands, pattern-recognition-based microcontrollers and sEMG sensors used for prosthetic control. In: 19th IEEE international conference on autonomous robot systems and competitions, ICARSC 2019
15. Switch Control System. Available http://www.oandplibrary.org/popup.asp?frmItemId=B157577C-D50F-4974-96BD-92AC74805FF6&frmType=image&frmId=3 [Online]
16. Ober JK (1982) Upper limb prosthetics for high level arm amputation. Prosthet Orthot Int 6(1):17–20
17. Abraham S (2013) A Study to assess the affectiveness of a self-instructional module on knowledge and attitude regarding prosthesis among family members between the age group of 18–50 yrs, of patients undergoing amputation at selected hospitals, Tumkur
18. Shroff G, Thakur D, Dhingra V, Baroli DS, Khatri D, Gautam RD (2016) Role of physiotherapy in the mobilization of patients with spinal cord injury undergoing human embryonic stem cells transplantation. Clin Transl Med 5(1)
19. Glasgow C, Tooth L, Fleming J (2008) Which splint? Dynamic versus static progressive splinting to mobilise stiff joints in the hand. Br J Hand Ther 13(4):104–110
20. Shankman GA, Manske RC (2014) Fundamental orthopedic management for the physical therapist assistant—E-book, 3rd edn. Elsevier Health Sciences
21. Kogler GF (2020) Materials and technology. Available https://musculoskeletalkey.com/materials-and-technology/. Accessed 17 May 2020 [Online]
22. Wong MS, Beygi BH, Zheng Y (2018) Materials for exoskeletal orthotic and prosthetic systems. Encycl Biomed Eng 1–3:352–367
23. Rothon PR, DeArmitt C (2017) Chapter 8—Fillers (including fiber reinforcements). In: Brydson's plastics materials, Eighth Edition, pp 169–204
24. Bîrcă A, Gherasim O, Grumezescu V, Grumezescu AM (2019) Chapter 1—Introduction in thermoplastic and thermosetting polymers. In: Materials for biomedical engineering: thermoset and thermoplastic polymers, vol 1–28
25. Physiopedia (2020) Biomechanics for cerebral palsy orthotics. Available https://www.physiopedia.com/Biomechanics_for_Cerebral_Palsy_Orthotics. Accessed 17 May 2020 [Online]
26. Shahar FS, Sultan MTH, Shah AUM, Safri SNA (2019) A short review on the extraction of kenaf fibers and the mechanical properties of kenaf powder composites. IOP Conf Ser Mater Sci Eng 670(1)
27. Pereira H (2015) The rationale behind cork properties: a review of structure and chemistry. BioResources 10(3):1–23
28. Nurhanisah MH, Saba N, Jawaid M, Paridah MT (2017) Design of prosthetic leg socket from kenaf fibre based composites. Green Energy Technol 9783319493817:127–141
29. Nurhanisah MH, Jawaid M, Ahmad Azmeer R, Paridah MT (2019) The AirCirc: design and development of a thermal management prototype device for below-knee prosthesis leg socket. Disabil Rehabil Assist Technol 14(5):513–520
30. Willow Wood (2020) WillowWood one transtibial system. Available https://www.willowwoodco.com/products-services/willowwood-one/willowwood-one-transtibial-system/. Accessed 17 May 2020 [Online]
31. JMS Plastics Supply Inc. (2020) Orthotic cork sheets. Available https://jmsplastics.com/product/orthotic-cork-sheets/. Accessed 17 May 2020 [Online]
32. JLFPro (2020) Innovation produits naturels. Available https://www.jlf-pro.com/en/ecocert. Accessed 17 May 2020 [Online]
33. Becker (2020) Maple leaf orthosis. Available https://www.beckerorthopedic.com/Product/PrefabricatedOrthoses/Hip/146. Accessed 17 May 2020 [Online]
34. Campbell AI, Sexton S, Schaschke CJ, Kinsman H, McLaughlin B, Boyle M (2012) Prosthetic limb sockets from plant-based composite materials. Prosthet Orthot Int 36(2):181–189
35. Odusote JK, Oyewo AT, Adebisi JA, Akande KA (2016) Mechanical properties of banana pseudo stem fibre reinforced epoxy composite as a replacement for transtibial prosthetic socket. J Assoc Prof Eng Trinidad Tobago 44(2):4–10

36. Kramer A, Sardo K, Slocumb W, Selvaduray G, Ph D (2015) Analysis of bamboo reinforced composites for use in orthotic and prosthetic application. American Academy of Orthotists & Prosthetists, p 2015
37. Irawan AP, Soemardi TP, Widjajalaksmi K, Reksoprodjo AHS (2011) Tensile and flexural strength of ramie fiber reinforced epoxy composites for socket prosthesis application. Int J Mech Mater Eng 6(1):46–50
38. Irawan AP, Daywin FJ, Fanando, Agustino T (2016) Mechanical characteristics of rattan reinforced fiberglass and epoxy composites for shank prosthesis application. Int J Eng Technol 8(3):1543–1550
39. Irawan AP, Sukania IW (2015) Tensile strength of banana fiber reinforced epoxy composites materials. Appl Mech Mater 776:260–263
40. Odusote J, Kumar V (2016) Mechanical properties of pineapple leaf fibre reinforced polymer composites for application as prosthetic socket. J Eng Technol 6(1):24–32
41. Widhata D, Ismail R, Sulardjaka (2019) Water Hyacinth (Eceng Gondok) as fibre reinforcement composite for prosthetics socket. IOP Conf Ser Mater Sci Eng 598(1)

# Experimental Characterization for Natural Fiber and Hybrid Composites


**M. Rajesh, Jayakrishna Kandasamy, D. Mallikarjuna Reddy, V. Mugeshkannan, and Vishesh Ranjan Kar**

**Abstract** Composite materials are more predominant in weight-sensitive applications in a different field such as Engineering, Medicine, Military applications due to its high impact strength, easy to manufacture the intricate part, high resistance against corrosion, deformation and high thermal stability. Thus, it makes them a good alternative for weight-sensitive applications compared to the traditionally used material. Though synthetic fiber-reinforced composite offers many advantages over conventional materials, it provides weak resistance for fire, more vulnerable to rays and oxidization, uncomfortable to human health. Thus, overcomes by replacing them with natural fiber for structural applications. The low elastic modulus of the natural fiber composite makes them not suitable for many practical applications. Researchers hybridized natural fiber with a smaller amount of synthetic fiber, and filler materials such as rice husk, wood powder, clay, CNT, etc. and enhanced the elastic modulus. Also, the addition of natural fiber in the matrix enhances the energy dissipating capability along with strength. In all mechanical design, strength and modulus of the material is the most important one which influences on material selection. A property of natural fiber composites always depending on a percentage of constitutes (cellulose, hemicellulose, and lignin), fiber distribution, fiber surface roughness, etc. The present study focuses on various characterization studies such as mechanical analysis, dynamic mechanical analysis, free vibration analysis, and stability analysis of natural fiber composites. Thus, it helps better understanding of factors affecting the strength, stiffness, and stability of natural fiber composite.

**Keywords** Fiber · Composite · Tensile strength · Filler · Stability · Dynamic mechanical analysis

M. Rajesh (✉) · J. Kandasamy · D. Mallikarjuna Reddy
Vellore Institute of Technology, Vellore 632014, Tamil Nadu, India
e-mail: rajesh261288@gmail.com

V. Mugeshkannan
PSG College of Technology, Coimbatore 641004, Tamil Nadu, India

V. R. Kar
National Institute of Technology Jamshedpur, Jamshedpur 831014, Jharkhand, India

© Springer Nature Singapore Pte Ltd. 2021

M. Jawaid et al. (eds.), *Structural Health Monitoring System for Synthetic, Hybrid and Natural Fiber Composites*, Composites Science and Technology,
https://doi.org/10.1007/978-981-15-8840-2_6

## 1 Introduction

Any applications enhance the performance without affecting its basics function is an important criterion. Material selection plays a vital role in that [1]. The primary purpose of the material selection is to reduce the bulk mass of the final weight of any structure or component without affecting its function and not to compensate for the strength, stiffness, stability, durability, carrion resistance, etc. [2]. In aerospace, marine, space, and automobile minimize the fuel consumption and enhance the operational performance, safety, reliability, and durability influenced by the type of material used for various parts [3]. During material selection for any practical applications, minor mistakes cause savior effects, and it makes questionable for safety.

A century ago, a large amount of conventional material had been used in engineering, aviation, marine, etc. Steel, Aluminum, and copper materials are commonly used in different engineering applications. The main advantages of conventional materials are easy availability, known processing techniques, high strength, elasticity, corrosion resistance, and low cost [4]. Though traditional materials offered considerable advantages, the main drawback is the production of conventional material on a massive level affects the environment seriously and directly impact human life and other specious. Hence, it is a compulsion to find good alternation to save a healthier environment [5].

Tremendous developments in the field of polymers make them into a good alternative for conventional material in the entire field due to easy preparation, manufacture [6]. However, polymer alone not enhancing strength, stability, and stiffness of the component or structure. To utilize the advantages of various polymers (thermo, thermoplastic, geo polymer and high temperature polymer), researchers are developing different types of filler, and reinforced materials which helps to enhances the safety, durability, stability, resistance to various chemical agents, resilience, low weight, dimensional stability, nonconductive, Nonmagnetic, Radar Transparent, impact Strength, Design Flexibility thermal properties, adhesive and coating compatibility and make them serve in the different environment (temperature, moisture, etc.) [7]. Glass, carbon, kevlar, and boron fibers are commonly used in a different matrix to enrich the strength, stiffness. Thus, it makes them a good alternative for diverse engineering applications over conventional materials [8].

Properties of composites are depended by the type of reinforcement, and its effect (distribution and orientation), amount of void, quality of the reinforcements. Other than reinforcement, interfacial bonding and load transfer at the interphase affects the properties of the composite seriously [9]. Thus can enhance by altering the adhesion properties of reinforcement by chemical or physical treatments [10]. Though synthetic fiber-reinforced composite offers many advantages over conventional materials, it offers weak resistance for fire, more sensitive to rays and oxidization, uncomfortable to human health. To overcome the problem associated with synthetic fiber, researchers used natural fiber for structural applications. The advantage of natural fiber composites over synthetic fiber composite is, the addition of natural fiber in the matrix enhances the energy dissipating capability along with strength.

Advantages associated with natural fibers such as excellent thermal properties, availability, and easy to fabricate them suitable replacement in the polymer matrix with comparable property for low and medium load structural applications [11]. Joshi et al. [12] found that the incorporation of natural fiber-enhanced fuel efficiency and reduced the final weight of the structure. Researchers have proven from their work, and natural fibers are more appropriate in the matrix. In general, structural application (door), home-based and packing applications, natural fiber composites are suitable.

Almost all mechanical design, elastic properties (Ultimate and yield strength) of materials influence their selection. A wealth of natural fiber composites always depending on a percentage of constitutes (cellulose, hemi-cellulose, and lignin), fiber distribution, fiber surface roughness, etc.

Any structural applications, strength, stiffness, and stability, along with higher energy dissipation, is an important one. To analyze the energy storing and dissipation behavior of the material dynamic mechanical analysis (DMA) will be employed. It helps to describe the storage modulus and loss factor of the composite materials under the dynamic load and thermal environment. It also reveals the factors affecting the modulus of the composite materials.

Similarly, dynamic properties of the material play a vital role in structural applications, which measured by vibration analysis. Though natural fiber having its advantages over synthetic composites, the disadvantage of natural fiber is its hydrophilic behavior which allows absorbing the moisture. Thus, it makes them mismatched in the matrix. Overcome the hydrophilic problem associated with natural fibers, and it is dipped in the chemical solution. Therefore, it helps to minimize the hydrophilic nature of fiber by removing more amount of hemicellulose from the fiber cell wall. However, the concentration of a chemical solution affects the fiber structural cell wall. Hence, it is essential to analyze the fiber surface before reinforcement in the polymer matrix. For that, scanning electron microscopic is used to examine the microstructure of natural fiber.

## 2 Factors Affecting Properties of Natural Fiber Composite

### 1. Types of Reinforcement and Matrix

Mechanical tests, DMA, and free vibration analysis are commonly used to analyze the properties of composites. Strength of the natural fibers calculated based on the percentage of cellulose and protein existing in the cell wall [13]. Harvesting time and extraction seriously affect on properties of natural fibers. It is observed that compared to fiber harvested by mechanically, manually harvested flax fiber has 20% higher strength [14, 15]. In general, higher moisture content affects the modulus of the composite. Other than moisture, the strength of natural fiber composites affects by fiber cross-section and interfacial strength [16]. Once achieve the reasonable interfacial bonding, fiber weight percentage influence on properties of composites.

Irrespective of reinforcement type, the stiffness of the composite is higher when fiber percentage falls between 40 and 55 wt%. The fiber aspect ratio affects the properties of composite reinforced with natural fiber seriously [17]. Short natural fiber with random distribution, the load can be transferred through the matrix to fiber due to shear at fiber/matrix [18]. Usually, under tensile load, tensile stress at the end of natural fiber becomes zero, whereas increasing along the length. Therefore, continuous natural fiber carries a more tensile load. Other than the selection of natural fiber, matrix selection contributes to properties of the natural fiber composites (NFC). Matrix fights against the hazard environment, transfer the load to fiber and fiber degradable.

## 2. Fiber distribution and its orientation

In the NFC, mechanical properties are depending alignment of fiber in the matrix to the loading direction [19–21]. Compared to synthetic fiber, it is difficult to achieve proper alignment in the high density resin [22, 23]. In the case of short fiber reinforcement, fiber weight percentage influence on mechanical properties of NFC. The mechanical property of short coir fiber-reinforced composite was analyzed by Monteiro et al. [24]. The weight percentage of coir fiber influenced much on the properties of composites. It revealed that 50 wt% of coir fiber makes composite rigid, whereas the addition of a higher amount of coir fiber in the matrix changes the rigidity of composite into flexible. Coir-polyester composite was used to fabricated by loading the fiber up to 15wt% and found that strength of the composite fall to 38 MPa [25]. Considerable availability of banana fiber forced the researcher to analyze the benefits of engineering applications. Many researchers tried the banana/epoxy composite for lightweight applications such as Helmet, car door, interior parts in automobiles, etc. [26, 27]. The research found that other than the fiber weight percentage of natural fiber, and its length influences the strength of the composites. Venkateshwaran et al. [28] found that 15 mm fiber length with 50 wt% improved the properties of banana/epoxy composites.

Similarly, jute fiber addition enriched the tensile, flexural, and dynamic properties of the epoxy composite [29]. Arenga pinnata fibers were reinforced with a different orientation, such as long fiber, short fiber is woven rowing in the epoxy by Sastra et al. [30]. Results revealed that woven rowing enriched the strength of the composites compared to long and short fiber orientation. Similar results have been observed for synthetic fiber composites. The study conducted by Brahim and Cheikh [31] revealed that Alfa fibre orientation influenced on the strength of the composite.

## 3. Effect of weaving pattern

To overcome the problem associated with fiber length and its orientation and distribution on properties of NFC, researchers used the advantages of the textile field. John and Thomas [32] propose weaving patterns, such as twill, basket, plain, and stain. Results revealed that the nature of yarn twist influences on the enhancement

of properties of the NFC. Higher fiber yarn twist helps to transfer the stress effectively under loading [33]. Banana fiber reinforcement enhanced the storage and loss modulus of banana/epoxy composite [34]. Results revealed that uniform stress distribution associated with plain weaving increased the storage modulus. Similarly, the storage modulus of epoxy composite enhanced by reinforcing hemp fiber with twill and plain form [35, 36]. Fiber orientation with 60° increased the damping behavior of composites. Rajesh and Pitchaimani [37] examined the DMA and dynamic behavior of NFC. They used a basket weaving style to prepare the conventional weaving, braided weaving, and knitting. Braiding composite enhanced the storage modulus of composite, whereas knitting increased the damping factor. Similarly, braided form reinforcement improved the tensile strength compared to composite prepared by the same wt% with random orientation. Maleque et al. [38] reinforced pseudo stem banana fiber into the epoxy matrix in woven form and found that the woven style enhanced the tensile strength. The reinforcement of banana fiber in the woven form minimizes the plastic deformation under static load, which is confirmed by SEM. Sapuan et al. [39] explained the advantage of woven banana fiber composite for householding applications. They developed the design detail of the telephone stand using epoxy composite and enhanced the properties of the telephone stand by reinforcing banana fiber in woven banana fiber. Features of NFC depends on resin viscosity, applied pressure, weave style, and surface modification. It is confirmed by Pothan et al. [40]. They found that type of fiber, and microvoid content influenced the mechanical properties of the composite. From the mechanical study, they found that higher fiber content enhanced the shear and impact properties of the composites. At the same time, increasing microvoid content decreasing the shear modulus of the composites. Other than weaving style, fiber alignment to loading and type of matrix, adhesion between fiber and matrix affects the properties of composite severely. For that, researchers alter the fiber surface with a chemical solution that removes the sufficient amount of the hemicellulose from the cell wall. Thus, it reduces the hydrophilic nature of the composites and enhancing the bonding.

## 4. Effect of Surface treatment

In general, the bonding strength of natural fiber and binder enhances by removing hemicellulose and lignin using chemical treatment [41]. Alkali surface modification removes hemicellulose and lignin from the cell wall of natural fiber effectively. Thus, it helps to increase the bonding strength. It is confirmed by Kabir et al. [42]. They carried out various chemical treatments to enhance the mechanical properties and observed that the concentration of NaOH influences on the removal of hemicellulose. Thus, it increased the bonding between hemp fiber and matrix. A similar study has been carried out on napier grass fiber by Reddy et al. [43] and found that 5% of NaOH surface modification enhanced the properties of composites.

Brgida et al. [44] improved the properties of composite by reinforcing chemically modified green coconut fiber in the matrix. They used NaOCl, NaOCl/NaOH, and $H_2O_2$ chemical solution and altered the properties of green coconut fiber and found that chemical treatments enhanced the features of the coconut composite. However, other than NaOCl solution, NaOCl/NaOH and $H_2O_2$ removed an only waxy layer of

fiber. In contrast, NaOCl removed the sufficient amount of hemicellulose and exposed more cellulose in the fiber cell wall. SEM and FT-IT analysis confirm it. SEM analysis revealed that fiber treated with NaOCl has no crack, whereas other solutions have more crack. However, compared to untreated composite surface-treated composite has minimum damage near the fiber and matrix. FT-IR analysis revealed a higher amount of cellulose present in the fiber cell wall for NaOCl treatment.

Similarly, Cao et al. [45] and Gassan and Bledzki [46] improved the strength and modulus of NFC using NaOH surface treatment. They found that treatment makes fiber surface rougher, which acts as a mechanical interlock in the matrix. Other than Alkali surface treatment, permanganate, benzoylation, and silane treatments alter the properties of NFC effectively. Sreenivasan et al. [47] found that a lower concentration of potassium permanganate enhanced the properties of composites. Henequen fiber was modified with a silane solution by Herrera-Franco and Valadez-Gonzlez [48]. Silane surface treatment increases fiber-matrix adhesion. Thus, enhanced the properties of composites. Rajesh and Jeyaraj Pitchaimani [49] found that surface treatment alters the features such as mechanical, dynamic mechanical, and vibration characteristics of composites. Benzoyl treatment enriched the impact and storage modulus of the composite, whereas untreated composite enhanced the damping factor of the composites. Thus, it is shown that surface treatment increased the fiber-matrix adhesion, which allows carrying more load and transfer stress effectively under loading. However, the surface treatment enhances the bonding strength between fiber-matrix and load carry behavior; single fiber alone cannot improve the properties of NFC. For that researcher used the hybridization of natural fiber with synthetic fiber, and different filler material to enhance the strength, stiffness, and stability of NFC for various applications.

## 5. Hybridization of natural fiber

The properties of the natural composite can be upgraded by the orientation of natural fiber in the matrix, surface treatment, hybridization, etc. Hybridization is the most effective method to improve the properties of NFC. Aji et al. [50] developed the resilience of pineapple leaf fibre/polyethylene (HDPE) composites. Hybridization of kenaf fiber with pineapple leaf fiber-enhanced properties of the composite. Similarly, hybridization of banana fiber with sisal-fiber enhanced the properties of polyester composite [51]. Properties of NFC can be improved by keeping woven natural fiber in layer form. Higher-strength natural fiber in the skin layer enhances the strength and modulus of the NFC. Venkateshwaran and ElayaPerumal [33] confirmed it. They compared the mechanical properties of hybrid composite by keeping banana as a skin layer (banana/jute/banana) and jute as a skin layer (jute/banana/jute). Mechanical investigation results revealed that banana woven fabric placed in the out layer enriched the mechanical strength and modulus of the composites. Jawaid et al. [29] increased the mechanical properties of oil palm composite by hybridizing jute woven fabric in the polymer composite. In another study, the effect of jute fiber addition in oil palm matrix on dynamic properties of a composite. They found that the hybridization of jute woven fabric improved the storage modulus of jute-oil palm composite and reduced the loss factor [52]. Kumar et al. [53] enhanced the dynamic properties

of woven coconut sheath-polyester composites by adding short banana fiber. Impact property of woven natural fiber composite has been increased by keeping two knitted natural fiber fabric as core layer [54]. Similarly, Muralidhar et al. [55] found that the flexural strength of the composite enhanced by placing knitted fabric as a skin layer. Bennet et al. [56] found that coconut sheath/sansevieria cylindrica/coconut sheath arrangement improved the properties of the polyester composite. Santulli et al. [57] used the intercalated and sandwich method to prepare the jute cloth/wool felts composite. They found that the manufacturing process of composite affects the properties of the composite seriously. Vani et al. [58] has used NaOH surface treatment and enhanced the natural frequency of the hybrid sisal and jute epoxy composite. Chemical treatment improved the bonding strength of the composite and natural frequency.

## 6. **Hybridization of natural fiber with Synthetic fiber**

In general, hybridization of natural fiber along with synthetic fiber enhances the properties of the NFC, hybridization of synthetic fiber enriches the modulus and strength drastically. Considerable variation in elastic modulus of synthetic fiber compared to natural fiber. Ahmed and Vijayarangan [59] carried out an experimental investigation and found that the addition of jute fiber enhanced the mechanical properties compared to neat polyester resin. In continuation, the hybridization of fiber with glass fiber mat improved the load carry behavior of the composite. Harish et al. [60] enhanced the tensile and flexural strength of the epoxy composite by hybridization of coir fiber with glass fiber. They improved the mechanical properties compared to coir-epoxy composite. Similarly, Ramesh et al. [61] found that hybridization of glass fiber with sisal and jute fiber-enriched the features of the composite. Thwe and Liao [62] compared the strength of bamboo—polypropylene composite enhanced by adding a small amount of glass fiber in the polypropylene matrix and found that 20 wt% glass fiber addition increased the tensile and flexural strength of the composites. Velmurugan and Manikandan [63] developed a sandwich composite by reinforcing palmyra fiber with glass fiber. Results revealed that when woven glass fabric act as a skin layer improved the properties of the sandwich composite. Idicula et al. [64] increased the free molecular movement of banana/epoxy composite by adding glass fiber in the epoxy matrix. Thus, it enhances the storage and loss modulus of the composite. It revealed that the hybridization of glass fiber in the NFC makes them rigid at higher temperature [65]. Similarly, Devi et al. [66] confirmed that the volume percentage of glass fiber in the NFC alters the dynamic properties. The addition of 0.2% glass fiber in the pineapple leaf fiber/polyester composite enhanced the dynamic properties of the NFC and reduced the free molecular movement under the thermal environment. Also, curing temperature affects the properties of the composite, which is confirmed by Goertzen et al. [67]. Khalili et al. [68] investigated the factors affecting the dynamic behavior of the composites. It is found that the parameter of the core material affects the dynamic properties of the sandwich NFC. Through NFC enhances the properties of the composite, stability is one of the critical factors in the engineering application.

High buckling load helps to them to carry more loads under axial compression. Buckling strength of NFC depends on a number of layers, weaving pattern, and bonding strength [69].

## 7. Hybridization of natural fiber with filler

Recently, researchers focused more on particle reinforcement to develop the biocomposites. Chandramohan and Kumar [70] developed the biocomposite by reinforcing coconut shell, walnut shells, and rice husk as powder form and carried out the mechanical study. Results revealed that the hybridization of the particle in the polymer enriched the properties of the composite compared to particle reinforced alone. To replace the traditional materials used for orthopedic applications Chandramohan and Marimuthu [71] developed bio natural fiber reinforced epoxy composite. Prakash and Viswanthan [72] analyzed the mechanical and thermal behavior of silane surface-treated kenaf fiber reinforced epoxy composite and enriched the properties of kenaf fiber composite by hybridization with sea-urchin spike fillers

Similarly, clay particle and glass spheres are commonly used to improve the strength and modulus of the NFC. Tensile and flexural properties of coir fiber composite was enhanced by hybridization of clay and glass sphere in the matrix and found that the addition of 4% and 8% clay and glass sphere enhanced the mechanical properties [73]. The addition of particles in the matrix increased the load transfer capacity for composites. Lignocellulose filler is used to improve the mechanical and thermal properties of the NFC. It helps to improve the strength, stiffness [74]. Fundamental natural frequency of the chopped strand mat- vinyl ester composite by adding montmorillonite clay [75]. Rajini et al. [76] hybridized coconut sheath/nanoclay. They found that hybridization enhanced the natural frequency of the NFC. Redmud is used as filler material to increase the natural frequency of the banana-polyester composite. They observed that the addition of redmud enhanced dynamic properties [77]. It is due to the addition of filler enhanced the load carry behavior and modulus of the composite. Similarly, the natural frequency of the jute-polyester composite increased by adding nanoclay [78]. CNT and sepiolite nanoclay has been used to improve the flame retardancy of bio-based polylactic acid [79]. Flammability performance has been performed using a microcalorimeter.

## 8. Effect of Moisture

The main drawback of the NFC is moisture absorbing behavior of the natural fiber weakens the bonding strength between fiber and matrix, which affects the load carry behavior of the NFC. Though the hydrophilic nature of natural fibers is reinforced in the hydrophobic matrixes such as polyester, epoxy, polypropylene, etc., strength and modulus of NFC composites reduced due to the experience of moisture in the environment and submersion of those NFCs in the aquatic environment over a considerable time [80, 81]. To improve the resistance against water absorption, coupling agents have been employed. Thus, it helps to enhance the strength of NFCs. Natural fiber distribution in the matrix also influences on moisture observation. When natural fibers are used as short form and random distribution, than natural fiber aligned parallel to

loading increases the moisture intake. Non-alignment of natural fiber in the matrix increases the porosity. Thus, it increases moisture observation. Also, the porosity of the NFCs depending on the amount of natural fiber present in the matrix.

## 3 Conclusion

Replacement of natural fiber composite for traditional material for structural applications brings in weight saving. Thus, it helps to save the environment and mineral sources. Type of fiber, and its orientation, weaving pattern, porosity, chemical treatment, type of filler affecting the strength and modulus of the NFCs. It has been debated seriously in this chapter. Experimental characterization such as mechanical analysis, dynamic mechanical analysis, free vibration analysis, stability analysis, and scanning electron microscopic analysis employed to studies the strength, stiffness of the natural fiber reinforced composites (NFC) has been reviewed. Investigation revealed that the addition of natural fiber enhances strength and elastic modulus and increases the energy dissipating properties of the NFCs. It is not found in conventional material such as steel, Aluminum, etc.

## References

1. Sapuan SM (2001) A knowledge-based system for materials selection in mechanical engineering design. Mater Des 22(8):687–695
2. Browning TR, Heath RD (2009) Reconceptualizing the effects of lean on production costs with evidence from the F-22 program. J Oper Manage 27(1):23–44
3. Jayakrishna K, Kar VR, Sultan MT, Rajesh M (2018) Materials selection for aerospace components. In: Sustainable composites for aerospace applications, pp 1–18
4. Smith RJ, Lewi GJ, Yates DH (2001) Development and application of nickel alloys in aerospace engineering. Aircr Eng Aerosp Technol 73(2):138–147
5. Sawyer C (2003) Framing the question—on cars—automobile body-on frame construction method. Automotive design & production. Focus Books, Sydney
6. Rajesh M, Pitchaimani J (2017) Mechanical and dynamic mechanical behaviour of novel glass—natural fibre intra-ply woven polyester composites. Sādhanā 42(7):1215–1223
7. Landel RF, Nielsen LE (1993) Mechanical properties of polymers and composites. CRC Press, New York
8. Fu SY, Lauke B, Mäder E, Yue CY, Hu X (2000) Tensile properties of short-glass-fiber- and short-carbon-fiber-reinforced polypropylene composites. Compos A Appl Sci Manuf 31(10):1117–1125
9. El-Wazery MS, EL-Elamy MI, Zoalfakar SH (2017) Mechanical properties of glass fiber reinforced polyester composites. Int J Appl Sci Eng 14(3):121–131
10. Varga C, Miskolczi N, Bartha L, Lipóczi G (2010) Improving the mechanical properties of glass-fibre-reinforced polyester composites by modification of fibre surface. Mater Des 31(1):185–193
11. Vimalanathan P, Venkateshwaran N, Srinivasan SP, Santhanam V, Rajesh M (2018) Impact of surface adaptation and Acacia nilotica biofiller on static and dynamic properties of sisal fiber composite. Int J Polym Anal Charact 23(2):99–112

12. Joshi SV, Drzal LT, Mohanty AK, Arora S (2004) Are natural fiber composites environmentally superior to glass fiber reinforced composites? Compos A Appl Sci Manuf 35(3):371–376
13. Pickering KL, Efendy MA, Le TM (2016) A review of recent developments in natural fibre composites and their mechanical performance. Compos A Appl Sci Manuf 1(83):98–112
14. Bos HL, Van Den Oever MJ, Peters OC (2002) Tensile and compressive properties of flax fibres for natural fibre reinforced composites. J Mater Sci 37(8):1683–1692
15. Pickering KL, Beckermann GW, Alam SN, Foreman NJ (2007) Optimising industrial hemp fibre for composites. Compos A Appl Sci Manuf 38(2):461–468
16. Madsen B, Lilholt H (2003) Physical and mechanical properties of unidirectional plant fibre composites—an evaluation of the influence of porosity. Compos Sci Technol 63(9):1265–1272
17. Shah DU, Schubel PJ, Licence P, Clifford MJ (2012) Determining the minimum, critical and maximum fibre content for twisted yarn reinforced plant fibre composites. Compos Sci Technol 72(15):1909–1917
18. Matthews FL, Rawlings RD (1999) Composite materials: engineering and science. CRC Press, New York
19. Ben Amor I, Rekik H, Kaddami H, Raihane M, Arous M, Kallel A (2010) Effect of palm tree fiber orientation on electrical properties of palm tree fiber-reinforced polyester composites. J Compos Mater 44(13):1553–1568
20. Herrera-Franco P, Valadez-Gonzalez A (2005) A study of the mechanical properties of short natural-fiber reinforced composites. Compos B Eng 36(8):597–608
21. Norman DA, Robertson RE (2003) The effect of fiber orientation on the toughening of short fiber-reinforced polymers. J Appl Polym Sci 90(10):2740–2751
22. Lee SH, Wang S (2006) Biodegradable polymers/bamboo fiber biocomposite with bio-based coupling agent. Compos A Appl Sci Manuf 37(1):80–91
23. Essabir H, El Achaby M, Bouhfid R, Qaiss A (2015) Morphological, structural, thermal and tensile properties of high density polyethylene composites reinforced with treated argan nut shell particles. J Bionic Eng 12(1):129–141
24. Monteiro SN, Terrones LA, D'almeida JR (2008) Mechanical performance of coir fiber/polyester composites. Polym Testing 27(5):591–595
25. Satyanarayana KG, Sukumaran K, Kulkarni AG, Pillai SG, Rohatgi PK (1986) Fabrication and properties of natural fibre-reinforced polyester composites. Composites 17(4):329–333
26. Kulkarni AG, Satyanarayana KG, Rohatgi PK, Vijayan K (1983) Mechanical properties of banana fibres (*Musa sepientum*). J Mater Sci 18(8):2290–2296
27. Jústiz-Smith NG, Virgo GJ, Buchanan VE (2008) Potential of Jamaican banana, coconut coir and bagasse fibres as composite materials. Mater Charact 59(9):1273–1278
28. Venkateshwaran N, ElayaPerumal A, Alavudeen A, Thiruchitrambalam M (2011) Mechanical and water absorption behaviour of banana/sisal reinforced hybrid composites. Mater Des 32(7):4017–4021
29. Jawaid M, Khalil HA, Hassan A, Dungani R, Hadiyane A (2013) Effect of jute fibre loading on tensile and dynamic mechanical properties of oil palm epoxy composites. Compos B Eng 45(1):619–624
30. Sastra HY, Siregar JP, Sapuan S, Hamdan MM (2006) Tensile properties of *Arenga pinnata* fiber-reinforced epoxy composites. Polym Plast Technol Eng 45(1):149–155
31. Brahim SB, Cheikh RB (2007) Influence of fibre orientation and volume fraction on the tensile properties of unidirectional Alfa-polyester composite. Compos Sci Technol 67(1):140–147
32. John MJ, Thomas S (2008) Biofibres and biocomposites. Carbohyd Polym 71(3):343–364
33. Venkateshwaran N, ElayaPerumal A (2012) Mechanical and water absorption properties of woven jute/banana hybrid composites. Fibers Polym 13(7):907–914
34. Venkateshwaran N, ElayaPerumal A, Raj RA (2012) Mechanical and dynamic mechanical analysis of woven banana/epoxy composite. J Polym Environ 20(2):565–572
35. Song YS, Lee JT, Ji DS, Kim MW, Lee SH, Youn JR (2012) Viscoelastic and thermal behavior of woven hemp fiber reinforced poly (lactic acid) composites. Compos B Eng 43(3):856–860
36. Rajesh M, Pitchaimani J (2018) Dynamic mechanical and free vibration behavior of natural fiber braided fabric composite: comparison with conventional and knitted fabric composites. Polym Compos 39(7):2479–2489

37. Rajesh M, Pitchaimani J (2017) Mechanical properties of natural fiber braided yarn woven composite: comparison with conventional yarn woven composite. J Bionic Eng 14(1):141–150
38. Maleque MA, Belal FY, Sapuan SM (2007) Mechanical properties study of pseudo-stem banana fiber reinforced epoxy composite. Arab J Sci Eng 32(2B):359–364
39. Sapuan SM, Maleque MA (2005) Design and fabrication of natural woven fabric reinforced epoxy composite for household telephone stand. Mater Des 26(1):65–71
40. Pothan LA, Mai YW, Thomas S, Li RK (2008) Tensile and flexural behavior of sisal fabric/polyester textile composites prepared by resin transfer molding technique. J Reinf Plast Compos 27(16–17):1847–1866
41. Shah H, Srinivasulu B, Shit S (2012) The effect of surface treatment on the properties of woven banana fabric based unsaturated polyester resin composites. Int J Sci Eng Technol 1:86–90
42. Kabir MM, Wang H, Lau KT, Cardona F (2013) Effects of chemical treatments on hemp fibre structure. Appl Surf Sci 1(276):13–23
43. Reddy KO, Maheswari CU, Shukla M, Rajulu AV (2012) Chemical composition and structural characterization of Napier grass fibers. Mater Lett 67(1):35–38
44. Brígida AI, Calado VM, Gonçalves LR, Coelho MA (2010) Effect of chemical treatments on properties of green coconut fiber. Carbohyd Polym 79(4):832–838
45. Cao Y, Shibata S, Fukumoto I (2006) Mechanical properties of biodegradable composites reinforced with bagasse fibre before and after alkali treatments. Compos A Appl Sci Manuf 37(3):423–429
46. Gassan J, Bledzki AK (1999) Possibilities for improving the mechanical properties of jute/epoxy composites by alkali treatment of fibres. Compos Sci Technol 59(9):1303–1309
47. Sreenivasan VS, Ravindran D, Manikandan V, Narayanasamy R (2012) Influence of fibre treatments on mechanical properties of short *Sansevieria cylindrica*/polyester composites. Mater Des 1(37):111–121
48. Herrera-Franco PJ, Valadez-Gonzalez A (2004) Mechanical properties of continuous natural fibre-reinforced polymer composites. Compos A Appl Sci Manuf 35(3):339–345
49. Rajesh M, Pitchaimani J (2017) Mechanical characterization of natural fiber intra-ply fabric polymer composites: influence of chemical modifications. J Reinf Plast Compos 36(22):1651–1664
50. Aji IS, Zainudin ES, Abdan K, Sapuan SM, Khairul MD (2013) Mechanical properties and water absorption behavior of hybridized kenaf/pineapple leaf fibre-reinforced high-density polyethylene composite. J Compos Mater 47(8):979–990
51. Idicula M, Joseph K, Thomas S (2010) Mechanical performance of short banana/sisal hybrid fiber reinforced polyester composites. J Reinf Plast Compos 29(1):12–29
52. Jawaid M, Abdul Khalil HPS, Alattas OS (2012) Woven hybrid biocomposites: dynamic mechanical and thermal properties. Compos A Appl Sci Manuf 43(2):288–293
53. Kumar KS, Siva I, Jeyaraj P, Jappes JW, Amico SC, Rajini N (2014) Synergy of fiber length and content on free vibration and damping behavior of natural fiber reinforced polyester composite beams. Mater Des (1980–2015) 56:379–386
54. Ye L, Mai YW, Su Z (eds) (2004) Composite technologies for 2020: proceedings of the fourth Asian-Australasian Conference on Composite Materials (ACCM 4). Woodhead Publishing, Cambridge
55. Muralidhar BA, Giridev VR, Raghunathan K (2012) Flexural and impact properties of flax woven, knitted and sequentially stacked knitted/woven preform reinforced epoxy composites. J Reinf Plast Compos 31(6):379–388
56. Bennet C, Rajini N, Jappes JW, Siva I, Sreenivasan VS, Amico SC (2015) Effect of the stacking sequence on vibrational behavior of *Sansevieria cylindrica*/coconut sheath polyester hybrid composites. J Reinf Plast Compos 34(4):293–306
57. Santulli C, Sarasini F, Tirillò J, Valente T, Valente M, Caruso AP, Infantino M, Nisini E, Minak G (2013) Mechanical behaviour of jute cloth/wool felts hybrid laminates. Mater Des 1(50):309–321
58. Vani M A, Maheeja B, Reddy P (2016) Modal analysis of hybrid sisal/jute natural fiber polymer composite beam. Int J Res Eng Technol 5(3):1–5

59. Ahmed KS, Vijayarangan S (2008) Tensile, flexural and interlaminar shear properties of woven jute and jute-glass fabric reinforced polyester composites. J Mater Process Technol 207(1–3):330–335
60. Harish S, Michael DP, Bensely A, Lal DM, Rajadurai A (2009) Mechanical property evaluation of natural fiber coir composite. Mater Charact 60(1):44–49
61. Ramesh M, Palanikumar K, Reddy KH (2013) Mechanical property evaluation of sisal–jute–glass fiber reinforced polyester composites. Compos B Eng 1(48):1–9
62. Thwe MM, Liao K (2002) Effects of environmental aging on the mechanical properties of bamboo–glass fiber reinforced polymer matrix hybrid composites. Compos A Appl Sci Manuf 33(1):43–52
63. Velmurugan R, Manikandan V (2007) Mechanical properties of palmyra/glass fiber hybrid composites. Compos A Appl Sci Manuf 38(10):2216–2226
64. Idicula M, Malhotra S, Joseph K, Thomas S (2005) Dynamic mechanical analysis of randomly oriented intimately mixed short banana–sisal hybrid fibre reinforced polyester composites. Compos Sci Technol 65(78):1077–1087
65. Jeyaraj P, Ganesan N, Padmanabhan C (2009) Vibration and acoustic response of a composite plate with inherent material damping in a thermal environment. J Sound Vib 320(1–2):322–338
66. Devi LU, Bhagawan SS, Thomas S (2010) Dynamic mechanical analysis of pineapple leaf/glass hybrid fiber reinforced polyester composites. Polym Compos 31(6):956–965
67. Goertzen WK, Kessler MR (2007) Dynamic mechanical analysis of carbon/epoxy composites for structural pipeline repair. Compos B Eng 38(1):1–9
68. Khalili SM, Nemati N, Malekzadeh K, Damanpack AR (2010) Free vibration analysis of sandwich beams using improved dynamic stiffness method. Compos Struct 92(2):387–394
69. Rajesh M, Pitchaimani J (2017) Experimental investigation on buckling and free vibration behavior of woven natural fiber fabric composite under axial compression. Compos Struct 1(163):302–311
70. Chandramohan D, Kumar AJ (2017) Experimental data on the properties of natural fiber particle reinforced polymer composite material. Data Brief 1(13):460–468
71. Chandramohan D, Marimuthu K (2011) Natural fiber particle reinforced composite material for bone implant. Eur J Sci Res 54(3):384–406
72. Prakash VA, Viswanthan R (2019) Fabrication and characterization of echinoidea spike particles and kenaf natural fibre-reinforced Azadirachta-Indica blended epoxy multi-hybrid bio composite. Compos A Appl Sci Manuf 1(118):317–326
73. Muthu J, Priscilla J, Odeshi A, Kuppen N (2018) Characterisation of coir fibre hybrid composites reinforced with clay particles and glass spheres. J Compos Mater 52(5):593–607
74. Prasad V, Joseph MA, Sekar K (2018) Investigation of mechanical, thermal and water absorption properties of flax fibre reinforced epoxy composite with nano $TiO_2$ addition. Compos A Appl Sci Manuf 1(115):360–370
75. Chandradass J, Kumar MR, Velmurugan R (2007) Effect of nanoclay addition on vibration properties of glass fibre reinforced vinyl ester composites. Mater Lett 61(22):4385–4388
76. Rajini N, Jappes JW, Rajakarunakaran S, Jeyaraj P (2013) Dynamic mechanical analysis and free vibration behavior in chemical modifications of coconut sheath/nano-clay reinforced hybrid polyester composite. J Compos Mater 47(24):3105–3121
77. Uthayakumar M, Manikandan V, Rajini N, Jeyaraj P et al (2014) Influence of redmud on the mechanical, damping and chemical resistance properties of banana/polyester hybrid composites. Mater Des 64:270–279
78. Arulmurugan S, Venkateshwaran N (2016) Vibration analysis of nanoclay filled natural fiber composites. Polym Polym Compos 24(7):507–516
79. Akbari A, Majumder M, Tehrani A (2015) Polylactic acid (PLA) carbon nanotube nanocomposites. In: Handbook of polymer nanocomposites. Processing, performance and application. Springer, Berlin, pp 283–297

80. Hargitai H, Rácz I, Anandjiwala RD (2008) Development of hemp fiber reinforced polypropylene composites. J Thermoplast Compos Mater 21(2):165–174
81. Bledzki AK, Jaszkiewicz A, Scherzer D (2009) Mechanical properties of PLA composites with man-made cellulose and abaca fibres. Compos A Appl Sci Manuf 40(4):404–412

# Numerical Simulation Techniques for Damage Response Analysis of Composite Structures


**Shirsendu Sikdar, Wim Van Paepegem, Wiesław Ostachowiczc, and Mathias Kersemans**

**Abstract** Structural health monitoring (SHM) of composite structures plays an important role in nondestructive evaluation of safety-critical engineering applications. Elastic wave propagation based SHM techniques have proven their potential in effective assessment of structural discontinuities and damages. Numerical simulations play a significant role in development of robust SHM strategies for such composite structures. These simulations are experimentally validated for selected baseline cases and then applied to solve a panoptic range of plausible study cases, such as—variable operating conditions, increasing structural complexities, damage size and damage shapes. Thus, the numerical simulations can significantly help in reducing rigorous laboratory experimentations, saving time and cost. This chapter is mainly focused on the guided wave propagation and acoustic emission-based damage response analysis in fiber (graphite/glass/natural) reinforced composite structures used in the automotive, marine, wind-energy and aerospace industries. Based on the problem-solving efficiency and popularity, the spectral element and finite element method based numerical simulation technics are explicitly selected to be discussed here.

**Keywords** Composite structure · Damage · Guided wave propagation · Numerical simulation, acoustic emission · Acoustic emission · Structural health monitoring (SHM) · Piezoelectric transducer (PZT)

S. Sikdar (✉) · W. Van Paepegem · M. Kersemans
Mechanics of Materials and Structures (UGent-MMS), Department of Materials, Textiles and Chemical Engineering (MaTCh), Ghent University, Technologiepark-Zwijnaarde 46, 9052 Zwijnaarde, Belgium
e-mail: Shirsendu.Sikdar@UGent.be

W. Ostachowiczc
Institute of Fluid-Flow Machinery, Polish Academy of Sciences, 14, Fiszera Street, 80-231 Gdansk, Poland

© Springer Nature Singapore Pte Ltd. 2021

M. Jawaid et al. (eds.), *Structural Health Monitoring System for Synthetic, Hybrid and Natural Fiber Composites*, Composites Science and Technology,
https://doi.org/10.1007/978-981-15-8840-2_7

## 1 Introduction

Lightweight fiber-reinforced composite structures (laminates and sandwiches) are of huge demand in automotive, aviation, marine and wind energy industries, due to their construction flexibilities, high in-plane strengths, high stiffness/weight ratios and damping capacities [1–5]. But, variable loading conditions (such as—abrasion, impact, fatigue) and hazardous ambient conditions (such as—moisture-content variation, temperature fluctuations) can eventually generates various types of damage (debond, delamination, fibre-cracking, localized inhomogeneity, breathing-cracks, amongst others) in these structures, and may grow further leading to a sudden failure of the structure while in service [6–11]. Therefore, development of nondestructive robust structural health monitoring (SHM) strategies are needed to identify the damage symptoms in advance. Some nondestructive evaluation techniques are proposed that uses the acoustic emission (AE), guided wave (GW) propagation, infrared-thermography, laser-vibrometry, X-ray computed tomography, ultrasonic goniometric-immersion methods for the inspection of composite structures [12–14]. The ultrasonic GW propagation and AE based SHM methods are popularly used for damage identification in composite structures [15–21].

Ultrasonic GW are elastic waves (e.g., Rayleigh wave, Lamb wave) that generate various wave modes while propagating in the structure. These SHM methods have the potential to detect minor structural defects in composite structures [6, 22–25]. The major advantages of these SHM methods are the capacity of GWs to penetrate hidden layers in the structures and the potential of large area inspection [26, 27].

AE is a sudden release of strain energy in the form of elastic waves that emitted due to the extension and initiation of damages in structures. These SHM techniques offer large-area inspection with limited instrumentation and give a clear idea about structural damage propagation and/or initiation events [21]. In these SHM techniques, the AE sensors register the wave motion owing to the damage in the materials and converts them to waveforms. Analysis of these waveforms can help to understand the intensity and the nature of damage. This technique has in-service monitoring potential without any external supplied excitations [28].

Numerical simulation of AE and GW propagation and their interaction with different types of damages in composite structures plays a vital role for the development of SHM strategies by giving the scope of exploring several possible case-studies without conducting physical experiments that significantly saves time and cost. The finite element simulations of GW propagation and AE in composites have established their capability to replicate the physical experiments for a wide range of study cases. In Patera [29], the spectral element simulation technique has introduced that flexibility and coalesces of finite element method with fast-convergences. Willberg [30] presented a study on the vantages of higher-order finite element method-based simulation techniques for the solution of elastodynamic problems. In these finite element simulations, a relatively finer discretization (min. 15 nodes per wavelength) is recommended. Whereas, the spectral element simulations can handle a relatively coarse discretization (min. 8 nodes per wavelength). The spectral element simulation

also offers the capacity to efficiently simulate the GW propagation in composites [27, 31–33]. This chapter presents some experimentally validated numerical simulations of AE and GW propagation in damaged composite structures.

## 2 Numerical Simulation Using Finite Element Method

Finite element simulations of damage induced AE and GW propagation and their interaction with damages in composite structures are presented by many researchers [3, 5, 7, 9]. These numerical simulations are usually carried out using popular finite element software, such as—Abaqus, ANSYS, COMSOL Multiphysics, LS-DYNA, Nastran, amongst others. Some experimentally validated simulation cases using Abaqus are described here.

### *2.1 Numerical Simulation of AE in Composites*

Numerical simulation of damage-induced acoustic emission in a stiffened composite panel (SCP) can be carried out using the in Abaqus explicit analysis code. The SCP (500 mm × 500 mm × 2 mm) is made of carbon fibre composite laminate (CFCL) and it consists of 4-nos. of 500 mm long L-shaped (30 mm × 30 mm) stiffeners those bonded to the baseplate with epoxy adhesive, as presented in Fig. 1.

The three-dimensional (3D) SCP was modelled using 8-noded linear brick C3D8R elements of size (1 × 1 × 0.25) mm for the CFCL and (1 × 1 × 0.01) mm for the adhesive. Fixed boundary conditions (zero displacements and rotations) are assigned to the edges of the SCP. The assumed material properties of the CFCL and epoxy adhesive are given in Table 1.

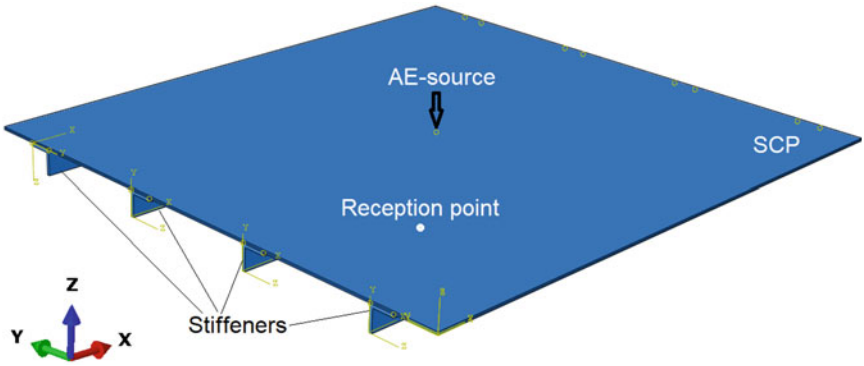


**Fig. 1** Numerical model of the stiffened composite panel

**Table 1** Material properties of stiffened composite panel

| Material | $E_{11}$ (GPa) | $E_{22}$ (GPa) | $E_{33}$ (GPa) | $G_{12}$ (GPa) | $G_{23}$ (GPa) | $G_{13}$ (GPa) | $\nu_{12}$ | $\nu_{13}$ | $\nu_{23}$ | $\rho$ (kg/m$^3$) |
|---|---|---|---|---|---|---|---|---|---|---|
| CFCL | 76.02 | 76.02 | 9.85 | 3.77 | 3.35 | 3.35 | 0.03 | 0.36 | 0.36 | 1560 |
| Adhesive | 4.052 | 4.052 | 4.052 | 1.447 | 1.447 | 1.447 | 0.40 | 0.40 | 0.40 | 1100 |

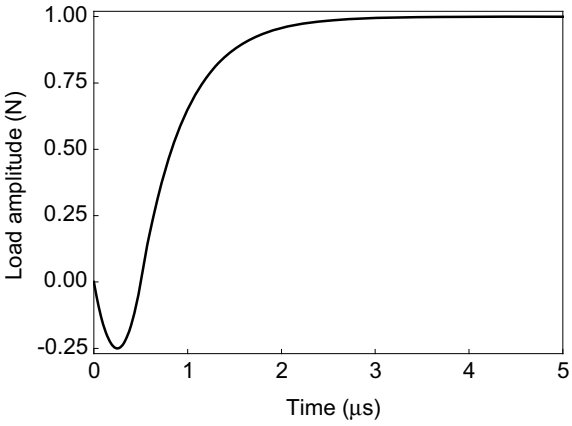


**Fig. 2** Artificial AE-source for the simulation of acoustic emission in SCP

Selection of a proper loading-source is a vital component for simulation of AE in composite structures [34–36]. The cosine bell-function can be used for the simulation of artificial AE source that resembles a crack-like damage initiation in the structure [35]. The AE-source located at a point is described as

$$P(x_1, x_2, t) = p(t)\delta(x_1), \delta(x_2) \tag{1}$$

$$p(t) = \begin{cases} \frac{t(t-\tau)}{\tau^2}, & 0<t<\tau \\ 1-e^{-2.1(t-\tau)}, & t<\tau \end{cases} \tag{2}$$

where '$p(t)$' is the forcing-function, time-variable $t = 0 \rightarrow \tau$ and '$\tau$' represents rise-time of load and the AE source is a graphically represented in Fig. 2. In all simulation, a stable time-step of 1e−7 is considered.

The numerical AE signal collected at the 180 mm distant reception point (Fig. 1) from the applied AE source location is presented in Fig. 3. The waveform plot of a typical AE signal in Fig. 4 shows the generation and propagation of the AE signal in SCP.

## *2.2 Numerical Simulation of GW Propagation in Composites*

Finite element simulation of ultrasonic GW propagation in an adhesively bonded composite structure with hidden disbond (bond failure) is described here. The simulation in Abaqus is carried using 0.5 mm thick and 10 mm diameter circular piezoelectric wafer transducer (PWTs) for GW signal actuation and reception in a bonded composite panel (BCP). The 7 mm thick BCP is made of two woven CFCL (300 mm × 300 mm × 3.5 mm) bonded with epoxy adhesive. An 8 mm dia. zero-volume

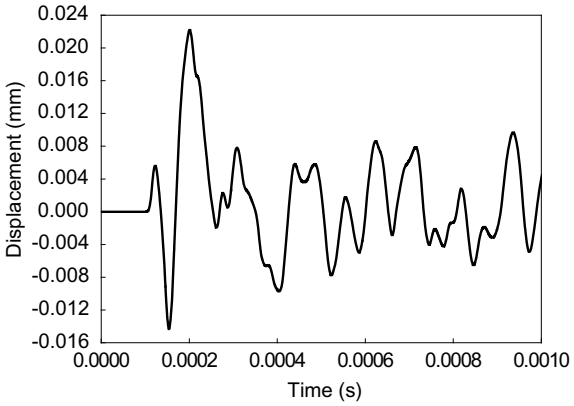


**Fig. 3** AE signal registered at the reception point (Fig. 1)

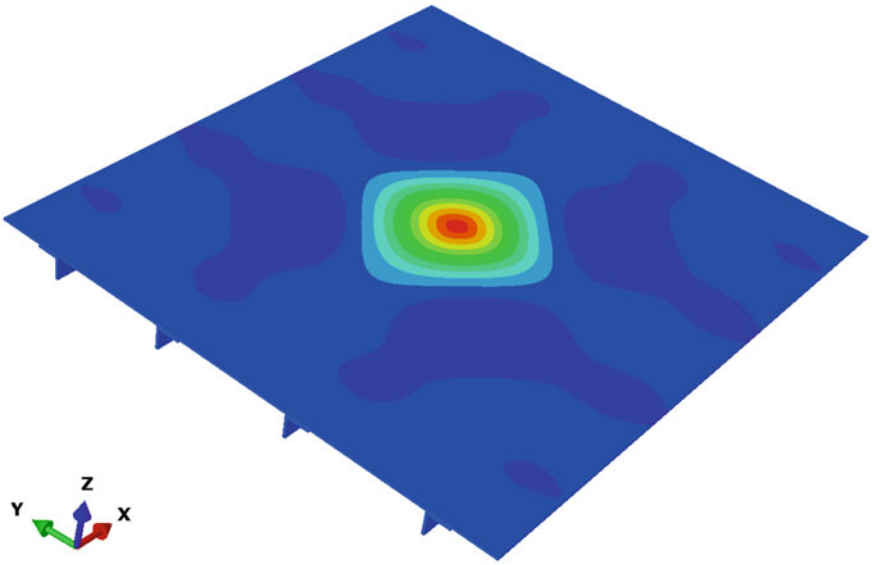


**Fig. 4** Waveform of the AE signals in the SCP

disbond region was modelled in the BCP by undying the adhesive-to-top CFCL nodes at the adhesive layer, as shown in Fig. 5.

Numerical simulation of GW propagation in composites using actuator-sensor PWTs required the implicit and explicit solvers. In Abaqus, the implicit analysis solver is not effective to handle the transient analysis of elastic wave propagation in complex composite structures. Whereas, the explicit code can efficiently handle the GW propagation in such composites but, it has no provision for piezoelectric elements which is available in the implicit solver [37]. Therefore, GW in BCP is

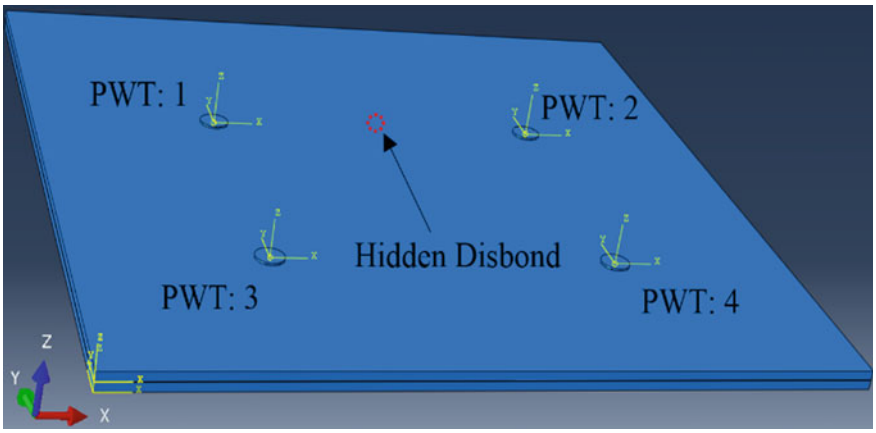


**Fig. 5** Numerical model of the sample panel in Abaqus

modeled in explicit analysis solver and PWTs are modeled in the implicit analysis solver. The 'standard explicit co-simulation' is assigned to link the implicit and explicit analysis of wave propagation in BCP [37, 38].

In explicit modeling, the C3D8R elements are used and the layer-wise element sizes for CFCL and adhesive are considered as (0.5 × 0.5 × 0.25) mm and (0.5 × 0.5 × 0.01) mm, respectively. Whereas, in the implicit solver the PWTs (actuator/sensor) are modeled with the standard C3D8E linear piezoelectric brick elements (8-nodes, 6-degrees of freedom at each node) are selected. The C3D8E elements are capable to handle the electro-mechanical coupling of the PWTs, where the 'voltage' is assigned as an additional degree of freedom in those coupling elements. A preselected input of 150 kHz 5-cycle sine wave signal in Hanning-window described in Fig. 6 is applied

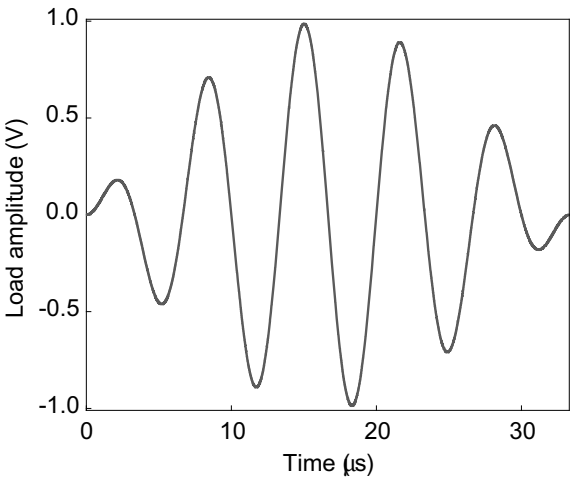


**Fig. 6** Input signal for the actuator PWTs in the BCP

to the front-surface nodes of the actuators (PWT: 1 and PWT: 3), and zero voltage is assigned to the back-surface nodes of the actuators as well as sensors (PWT: 2 and PWT: 4) for grounding operation.

The output signal (in terms of voltage) is registered at the front-surfaces of sensors (PWT 2 and PWT 4). The PWT (NCE51) properties are assumed as:

$$[\varepsilon] = \begin{bmatrix} 1.72 & 0 & 0 \\ & 1.72 & 0 \\ \text{Symmetry} & & 1.68 \end{bmatrix} \times 10^{-8}\,\text{C/Vm},$$

$$[e] = \begin{bmatrix} 0 & 0 & 0 & 0 & 13.7 & 0 \\ 0 & 0 & 0 & 13.7 & 0 & 0 \\ -6.06 & -6.06 & 17.2 & 0 & 0 & 0 \end{bmatrix} \text{C/m}^2,$$

$$[c] = \begin{bmatrix} 13.4 & 8.89 & 9.09 & 0 & 0 & 0 \\ & 13.4 & 9.09 & 0 & 0 & 0 \\ & & 12.1 & 0 & 0 & 0 \\ & & & 2.05 & 0 & 0 \\ & & & & 2.05 & 0 \\ & & \text{Symmetry} & & & 2.24 \end{bmatrix} \times 10^{10}\,\text{N/m}^2$$

where $[\varepsilon]$ represents piezoelectric permittivity-matrix, $[e]$ represents piezoelectric stress-matrix, $[c]$ is the tensor of mechanical-stiffness, and the piezoelectric material mass-density '$\rho$' is 7650 kg/m$^3$. In the simulation, the time-step was considered as $\leq$1e$-$7 (less than the minimum distance of any node-to-node connection/the maximum achievable velocity of the GW mode).

In the numerical simulation, the PWT#1 is actuated with the input signal and the propagated signal is collected at PWT#2 to get the without-disbond signal corresponding to the PWT actuator-sensor path#1-2. Similarly, PWT#3 is actuated and the signal at PWT#4 is registered to get the with-disbond signal from PWT actuator-sensor path#3-4. A comparison of those without-disbond signal and with disbond signal is shown in Fig. 7. The numerically obtained waveform plot in Fig. 8 indicates the disbond influence on the propagating GW signals in BCP.

## 3 Numerical Simulation Using Spectral Element Method

The spectral element simulation also offers the potential to solve the ultrasonic GW propagation problems in composites [31, 32]. A time-domain spectral element simulation of GW propagation in the sample BCP is carried out in MATLAB using 100 kHz 5-cycle tone-burst sine wave, as presented in Fig. 9.

This spectral element analysis technique has some similarities with the finite element method (Sect. 2.2) except in the node distributions and in the approximation functions those resembles the changes in displacements calculated during the

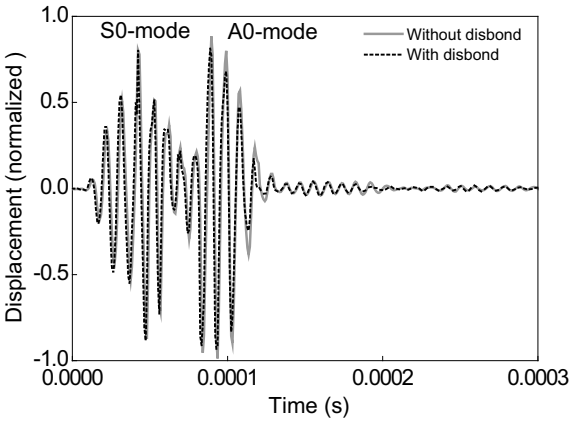


**Fig. 7** Comparison of GW signals corresponding to the without and with disbond paths

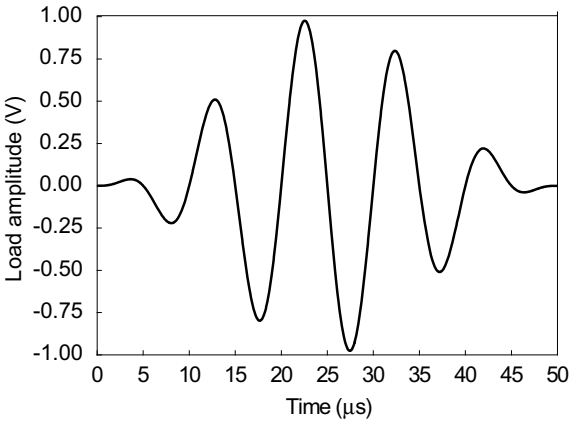


**Fig. 8** Waveform plot shows the disbond effect in the propagated GWs in the BCP

simulation. The nodes are non–uniformly distributed in spectral elements and their locations can be obtained by evaluating the roots (real values) of '$\xi_i$' as

$$\left.\begin{aligned}\left\{\left(1-\xi^2\right)U'_{a-1}(\xi)\right\}=0\\ \left\{\left(1-\eta^2\right)U'_{b-1}(\eta)\right\}=0\\ \left\{\left(1-\varsigma^2\right)U'_{c-1}(\varsigma)\right\}=0\end{aligned}\right\rangle \tag{3}$$

where the *Legendre polynomials are represented as* $\xi$, $\eta$, $\zeta$, $\epsilon$ $[-1; 1]$, $U_{a-1}$, $U_{b-1}$, $U_{c-1}$; the number of nodes along $\xi$, $\eta$, $\zeta$ directions are represented as *a, b, c* and the first-derivatives are indicated with '′'. The shape function (3D) is formulated by using the tensor product of 1D shape functions with Lagrange polynomials $N_j(\xi)$, $N_k(\eta)$,

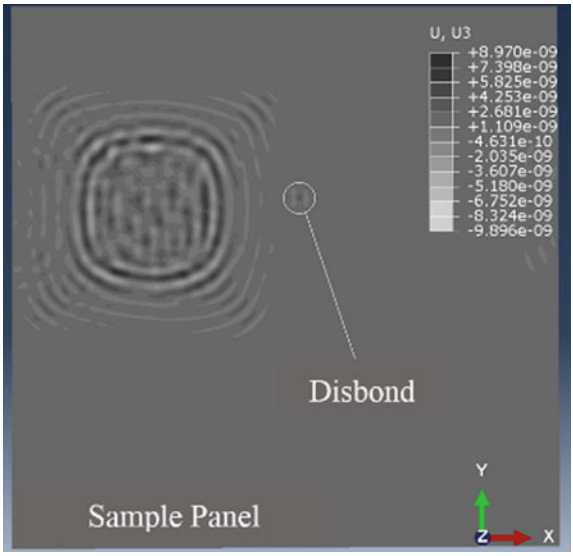


**Fig. 9** Input signal for the actuator PWTs in the BCP

$N_l(\varsigma)$ of degree $(a-1)$, $(b-1)$, $(c-1)$ as described in Fig. 10. The polynomials are represented as:

$$N_p(\xi, \eta, \varsigma) = N_j(\xi) N_k(\eta) N_l(\varsigma) \tag{4}$$

in which, $j = 1 \rightarrow a, k = 1 \rightarrow b \text{and} l = 1 \rightarrow c$.

The *Gauss Lobato Legendre* (GLL) integration technique is applied to compute the element matrices, where these integration points coincide with selected number of spectral nodes. The quadrature of GLL is a product of one-dimentional quadrature with weights of $p_j$, $p_k$, $p_l$ as

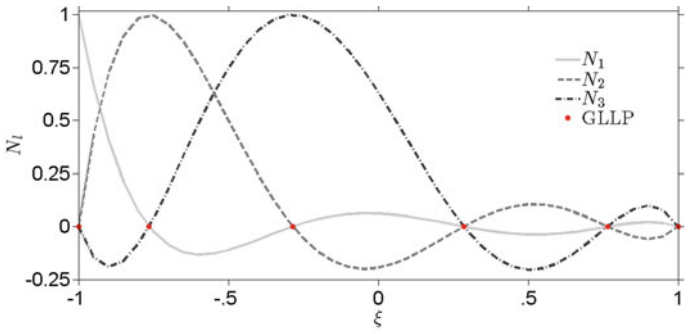


**Fig. 10** Graphical presentation of the shape functions ($N_i(\xi)$)

$$\left.\begin{aligned} p_j &= \frac{2}{a(a-1)\left(U_{a-1}(\xi_j)\right)^2} \\ p_k &= \frac{2}{b(b-1)\left(U_{b-1}(\eta_k)\right)^2} \\ p_l &= \frac{2}{c(c-1)\left(U_{c-1}(\varsigma_l)\right)^2} \end{aligned}\right\rangle \tag{5}$$

Constitutive equation for the linear-piezoelectric materials can be represented as per Giurgiutiu and Lyshevski [39]

$$\begin{Bmatrix} \sigma \\ D \end{Bmatrix} = \begin{bmatrix} B^F & -e^T \\ e & \varepsilon^X \end{bmatrix} \begin{Bmatrix} X \\ f \end{Bmatrix} \tag{6}$$

where the tensors '$\varepsilon^X$' represents *dielectric* components, '$B^F$' represents elastic components, '$e$' represents *piezoelectric* components, '$F$' is corresponding to the electrical-field constants, '$D$' is corresponding to the electrical-displacements, '$\sigma$' is the stress and '$X$' is corresponding to the strains. The initial electric-fields, initial strains and transpose matrix are represented by the superscripts '$F$', '$X$' and '$T$', respectively. The elementary governing equation of motion can be defined as:

$$\begin{bmatrix} m^e_{uu} & 0 \\ 0 & 0 \end{bmatrix} \begin{Bmatrix} \ddot{u}^e \\ \ddot{\varphi}^e \end{Bmatrix} + \begin{bmatrix} c^e_{uu} & 0 \\ 0 & 0 \end{bmatrix} \begin{Bmatrix} \dot{u}^e \\ \dot{\varphi}^e \end{Bmatrix} + \begin{bmatrix} k^e_{uu} & k^e_{u\varphi} \\ k_{u\varphi}{}^{eT} & k^e_{\varphi\varphi} \end{bmatrix} \begin{Bmatrix} u^e \\ \varphi^e \end{Bmatrix} = \begin{Bmatrix} F^e \\ G^e \end{Bmatrix} \tag{7}$$

where '$m^e_{uu}$' represents structural mass-matrix, '$k^e_{uu}$' represents stiffness-matrix, '$c^e_{uu}$' represents damping-matrix, '$k^e_{\varphi\varphi}$' represents dielectric permittivity-matrix, '$k^e_{u\varphi}$' is piezoelectric coupling-matrix, '$\varphi^e$' is electric potential vector, '$u^e$' is nodal displacement-vector, '$F^e$' is the external force-vector, '$G^e$' represents the applied charge vector, and $c^e_{uu}$ is defined based on the *damping model* by *Rayleigh in* [31] as

$$c^e_{uu} = \mu_m m^e_{uu} + \lambda_k k^e_{uu} \tag{8}$$

where '$\lambda_k$' is the coefficient of stiffness proportionality and '$\mu_m$' is the mass-proportionality coefficients. The computation time is reduced by applying a central-difference scheme to solve Eq. (7).

A numerical model of PWT-induced GW propagation in BCP is presented in Fig. 11. The assumed material properties of BCP is given in Table 1. The PWT properties are selected as per the manufacturer's (*Noliac NCE51*) data (Sect. 2.2). In the simulation, the BCP and PWTs are modeled with 108 noded 3D spectral elements (36 in-plane nodes and 3-through thickness nodes), as schematically represented in Fig. 12. Each PWT element nodes has three displacement DOFs with one additional DOF (i.e. electric-voltage).

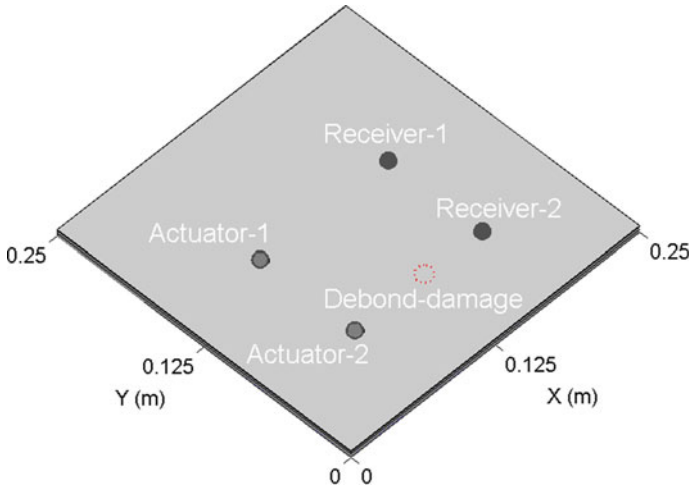


**Fig. 11** Numerical model of BCP with PWTs

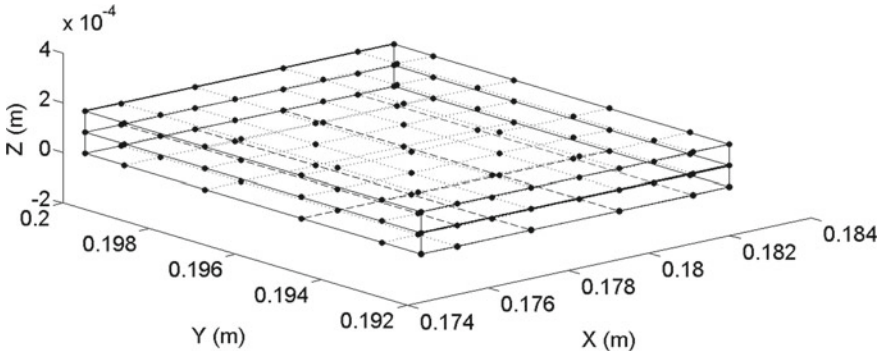


**Fig. 12** Schematic of node distribution in the 3D spectral element

In each layer, there are 3500 number of in-plane elements and 24 number of elements in PWTs are connected to the front-layer of the BCP. The contact effect is not considered in simulation and a debond region of 8 mm diameter is modeled by demerging the adjoining nodes at the bond-layer (Fig. 12). The simulation was carried out in MATLAB and the time-step of calculation was selected as 1e−7. A comparison between the without-debond (signal corresponding to Actuator-1–Receiver-1) and with-debond (signal corresponding to Actuator-2–Receiver-2) is presented in Fig. 13 and a waveform plot is shown in Fig. 14 that shows the debond influence on the propagated GWs.

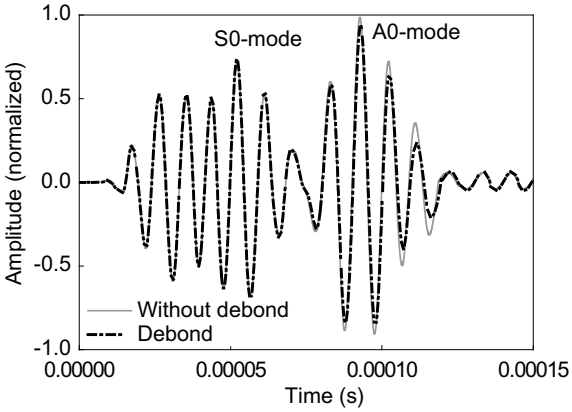


**Fig. 13** Comparison of without debond and debond-influenced signals

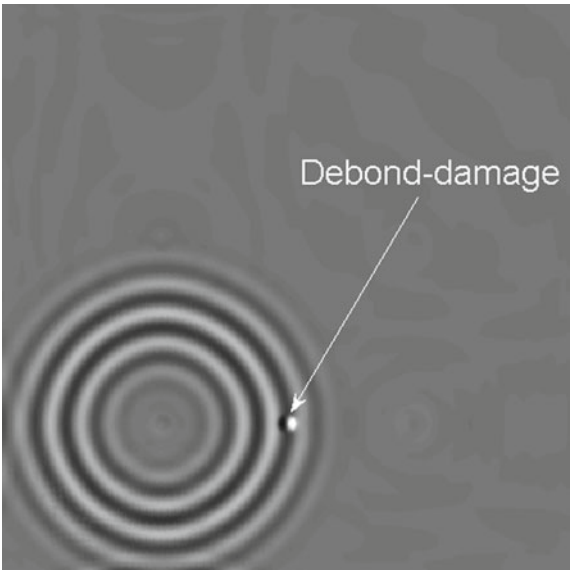


**Fig. 14** Waveform plot from the simulation of BCP model indicates debond effect on the propagated GWs

## 4 Conclusions

This study is an effort to provide insights on the numerical simulation techniques for damage-induced AE as well as the PWT-induced GW propagation and interactions with damages in composite structures. It evident that the numerical simulations can give the insights about the damages in composites and can significantly contribute to the development of robust SHM strategies that use the AE and/or GW propagation-based nondestructive evaluation techniques. The finite element simulation of AE in a composite structure is quite straightforward and requires a proper artificial AE-source function to replicate the damage-source. This simulation technic can be used

for the solution of a wide range of laboratory-scale AE problems. This method is also suitable for simulation of ultrasonic GW propagation in composites with hidden damages (such as debond/disbond), using PWTs (actuators/sensors). The spectral element method-based simulation technique can be applied for fast and efficient simulation of elastic waves and damage response estimation in composite structures. It is expected that the given information will help the readers to understand the numerical simulation techniques and their applicability for different types of damage response analysis for composite structures.

**Acknowledgements** The wish to acknowledge the support from the Polish National Science Centre (NCN) Poland under agreement no. UMO.2018/29/B/ST8/02904 and the Research Foundation-Flanders (FWO) Belgium under agreement no. FWO.3E0.2019.0102.01.

## References

1. Peters ST (1998) Handbook of composites. Chapman and Hall, Boca Raton, FL
2. Gay D, Hoa SV, Tsai SN (2003) Composite materials: design and application. CRC, New York
3. Sikdar S, Banerjee S (2017) Structural health monitoring of advanced composites using guided waves. LAP LAMBERT Academic Publishing, Saarbrücken
4. Safri SN, Sultan MT, Jawaid M, Jayakrishna K (2017) Impact behaviour of hybrid composites for structural applications: a review. Compos B Eng 133:112–121
5. Giurgiutiu V, Zagrai AN, Bao JJ (2002) Piezoelectric wafer embedded active sensors for aging aircraft structural health monitoring. Struct Health Monit 1:41–61
6. Hay TR, Wei L, Rose JL (2003) Rapid inspection of composite skin-honeycomb core structures with ultrasonic guided waves. J Compos Mater 37(10):929–939
7. Sikdar S, Kudela P, Radzieński M, Kundu A, Ostachowicz W (2018) Online detection of barely visible low-speed impact damage in 3D-core sandwich composite structure. Compos Struct 185:646–655
8. Maslov KI, Kundu T (1996) Selection of lamb modes for detecting internal defects in laminated composites. Ultrasonics 35:141–150
9. Mitra M, Gopalakrishnan S (2016) Guided wave based structural health monitoring: a review. Smart Mater Struct 25(5):053001
10. Wandowski T, Malinowski PH, Ostachowicz WM (2016) Circular sensing networks for guided waves based structural health monitoring. Mech Syst Signal Process 66:248–267
11. Yang B, Xuan FZ, Xiang Y, Li D, Zhu W, Tang X, Xu J, Yang K, Luo C (2017) Lamb wave-based structural health monitoring on composite bolted joints under tensile load. Materials 10(6):652
12. Li Y, Yang ZW, Zhu JT, Ming AB, Zhang W, Zhang JY (2016) Investigation on the damage evolution in the impacted composite material based on active infrared thermography. NDT&E Int 83:114–122
13. Castellano A, Fraddosio A, Piccioni MD (2017) Ultrasonic goniometric immersion tests for the characterization of fatigue post-LVI damage induced anisotropy superimposed to the constitutive anisotropy of polymer composites. Compos B Eng 116:122–136
14. Jespersen KM, Zangenberg J, Lowe T, Withers PJ, Mikkelsen LP (2016) Fatigue damage assessment of uni-directional non-crimp fabric reinforced polyester composite using X-ray computed tomography. Compos Sci Technol 136:94–103

15. Prosser WH (1996) Advanced AE techniques in composite materials research. J Acoust Emission 14:1–11
16. Wevers M (1997) Listening to the sound of materials: acoustic emission for the analysis of material behavior. NDT&E Int 30:99–106
17. Giordano M, Calabro A, Exposito C, D'Amore A, Nicolais L (1998) An acoustic-emission characterization of the failure modes in polymer composite materials. Compos Sci Technol 58:1923–1928
18. Green ER (1998) Acoustic emission in composite laminates. J Nondestr Eval 17:117–127
19. Bussiba A, Kupiec M, Ifergane S, Piat R, Bohlke T (2008) Damage evolution and fracture events sequence in various composites by acoustic emission technique. Compos Sci Technol l68:1144–1155
20. Unnthorsson R, Runarson TP, Jonsson MJ (2008) Acoustic emission based failure criterion for CFRP. Int J Fatigue 30:11–20
21. Wevers M, Lambrighs K (2009) Applications of acoustic emission for SHM: a review. Encyclopedia of structural health monitoring. Wiley, New York
22. Mustapha S, Ye L (2015) Propagation behaviour of guided waves in tapered sandwich structures and debonding identification using time reversal. Wave Motion 57:154–170
23. Pieczonka L, Ukowski P, Klepka A, Staszewski WJ, Uhl T, Aymerich F (2014) Impact damage detection in light composite sandwich panels using piezo-based nonlinear vibro-acoustic modulations. Smart Mater Struct 23(10):105021
24. Luchinsky DG, Hafiychuk V, Smelyanskiy VN, Kessler S, Walker J, Miller J, Watson M (2013) Modeling wave propagation and scattering from impact damage for structural health monitoring of composite sandwich plates. Struct Health Monit 12(3):296–308
25. He F, Zhou Z, Feng Z (2008) Research on an inspection method for de-bond defects in aluminum skin-honeycomb core sandwich structure with guided waves. In: 17th world conference on nondestructive testing
26. Lowe MJ, Challis RE, Chan CW (2000) The transmission of Lamb waves across adhesively bonded lap joints. J Acoust Soc Am 107(3):1333–1345
27. Ostachowicz W, Kudela P, Krawczuk M, Zak A (2011) Guided waves in structures for SHM: the time-domain spectral element method. Wiley, New York
28. Ono K, Gallego A (2012) Research and application of AE on advanced composite. J Acoust Emission 180–229
29. Patera AT (1984) A spectral element method for fluid dynamics: laminar flow in a channel expansion. J Comput Phys 54(3):468–488
30. Willberg C, Duczek S, Perez JV, Schmicker D, Gabbert U (2012) Comparison of different higher order finite element schemes for the simulation of Lamb waves. Comput Methods Appl Mech Eng 241:246–261
31. Kudela P, Żak A, Krawczuk M, Ostachowicz W (2007) Modelling of wave propagation in composite plates using the time domain spectral element method. J Sound Vib 302(4–5):728–745
32. Kudela P (2016) Parallel implementation of spectral element method for Lamb wave propagation modeling. Int J Numer Meth Eng 106(6):413–429
33. Ha S, Chang FK (2009) Optimizing a spectral element for modeling PZT-induced Lamb wave propagation in thin plates. Smart Mater Struct 19(1):015015
34. Sause MG (2011) Investigation of pencil-lead breaks as acoustic emission sources. J Acoust Emission 29
35. Mal AK, Banerjee S (2004) Guided acoustic emission waves in a thick composite plate. In Health monitoring and smart nondestructive evaluation of structural and biological systems III. Int Soc Opt Photon 5394:42–53
36. Banerjee S, Mal AK (2005) Acoustic emission waveform simulation in multilayered composites. J Strain Anal Eng Des 40(1):25–32
37. Soorgee MH, Lissenden CJ, Rose JL, Yousefi-Koma A (2013) Planar guided waves for SHM of plate structures using piezoelectric fiber transducers. AIP Conf Proc 1511:254–261

38. Sikdar S, Banerjee S (2016) Identification of disbond and high density core region in a honeycomb composite sandwich structure using ultrasonic guided waves. Compos Struct 152:568–578
39. Giurgiutiu V, Lyshevski SE (2016) Micro mechatronics: modeling, analysis, and design with MATLAB. CRC Press, New York

# Modeling of Damage Evaluation and Failure of Laminated Composite Materials


**Fatima-Zahra Semlali Aouragh Hassani, Rachid Bouhfid, and Abouelkacem Qaiss**

**Abstract** Like conventional materials, laminated composite materials lose much of their structural integrity when damaged. The objective of this chapter is to present the different types of damage that can develop in a laminated composite structure. The heterogeneity and the anisotropy of these materials make their mechanisms of damage numerous and complex. The evolution of the damage depends on the nature of the initial rupture mechanisms and their progression but also on the possible interactions between them. In other words, the final failure of a composite often results from a combination of several damage modes capable of interacting with each other. Many parameters are involved such as: the load nature, the reinforcement architecture, the faults presence, the quality of the matrix and of the fiber/matrix interface. To understand the main damage mechanisms that occur within a laminated material, we will present a bibliographic study on the damage evolution in unidirectional and woven folds, followed by a description of the methods used to model damage and failure of laminated composite materials.

**Keywords** Laminated composites · Mechanical behavior · Thermoplastics · Thermosetting · Damage mechanisms · Failure mechanisms; modeling

## 1 Introduction

In recent years, composite materials have been used more and more in different industrial sectors: automotive, aeronautics, building, etc. [1–3]. In addition to their very good mechanical characteristics, they have the advantage of being much lighter than metallic materials and greater absorption of specific energy, that is to say, the energy

F.-Z. Semlali Aouragh Hassani · R. Bouhfid · A. Qaiss (✉)
Composites and Nanocomposites Center, Moroccan Foundation for Advanced Science, Innovation and Research (MAScIR), Rabat, Morocco
e-mail: a.qaiss@mascir.com

F.-Z. Semlali Aouragh Hassani
Mechanics of Materials Laboratory, Faculty of Science, Mohammed V-Rabat, University, Rabat, Marocco

© Springer Nature Singapore Pte Ltd. 2021

M. Jawaid et al. (eds.), *Structural Health Monitoring System for Synthetic, Hybrid and Natural Fiber Composites*, Composites Science and Technology,
https://doi.org/10.1007/978-981-15-8840-2_8

absorbed by mass [1–3]. However, more recently, a new type of composite material, with a laminated architecture, has attracted increasing interest from manufacturers. Indeed, one of the major advantages of laminate composites is the ability to orient the fibers of each ply in order to orient the high-performance mechanical properties allowing it to withstand the stresses imposed. In addition, they allow complex structures to be produced in a limited number of operations, which reduces manufacturing costs [3–5].

Like conventional materials, laminated composite materials lose much of their structural integrity when damaged; therefore, their mechanical behavior must be clearly described. In general, the fibers are the main constituent supporting the load [6, 7]. The surrounding matrix maintains fibers in the desired location and orientation. The matrix acts as a charge transfer medium between the fibers and protects them from environmental damage. Consequently, failure in composite materials begins in the matrix, which is generally of a fragile nature; while the fibers can remain intact. These last forms a bridging on the surface of the micro-cracked matrix, delaying or probably preventing the future progression of the cracking of the matrix. The further loading ultimately leads to crack propagation and then the breaking of the fibers, hence the ruin of the material [6–8].

The composite materials failure can be classified as interlaminar and intralaminar rupture. Interlaminar rupture is generally produced in the form of delamination. The latter has been the subject of several studies. The intralaminar rupture (mode I), also known as the translaminar rupture, which is generally characterized by a fissure manifestly propagating parallel to the fibers along the thickness, has so far not found a large extension in Literature. Due to their anisotropic nature it is difficult to fully predict their mechanical characteristics and behavior, particularly if they are produced with complicated architectures, as in the case of woven reinforcements [6, 9].

The tensile strength of notched composite materials strongly depends on the direction of the load. For example, the breaking strength of a unidirectional composite material is maximum when this breaking strength is measured for a crack perpendicular to the longitudinal direction of the fibers. At any other stress position, this resistance decreases. The minimum value is obtained when the crack is aligned with the longitudinal direction [6, 9].

The translaminar fracture properties of cracked laminates are not characterized as in the case of intralaminar rupture. As a result, this work is part of the ongoing effort to build on the results established in the area of laminated composite materials. When, a notched laminate is loaded in tension, a damage zone forms at the bottom of the notch [6, 10]. As the load increases, stress concentrations appear at the bottom of the crack and microcracks appear, signaling an unfavorable situation that the material will undergo. Once the critical load is reached, the crack propagates catastrophically. The path traveled by the crack, as well as the damage mechanisms observed during the rupture process are often complex, especially if the layers of the laminated material are arranged in various orientations. Fortunately, the symmetry and geometry of the specimen reduce the number of possible cases of damage [6, 10].

This chapter mainly deals with the study of the mechanical behavior of cracked laminated materials, and then illustrates the main damage mechanisms of a composite

structure. Analysis of the initiation and the propagation of failure in cracked laminated composites with fabric reinforcement at different ply configurations are discussed depending on the orientation and location of the laminate plies. After a few reminders of the theory of linear failure mechanics, we then describe the methods used to model the damage and failure of laminated composite materials.

## 2 A Laminated Composite

A set of several identical folds or monolayers arranged in the same way constitutes a layer. We call laminate what results from the superposition of several of these layers or folds of unidirectional sheets, fabrics or mats, with orientations specific to each fold: this is the draping operation (Fig. 1). There are different types of laminates. Monolithics consist only of fiber/resin composite plies; sandwiches consist of two monolithic layers called skins, separated by a foam or honeycomb core. A monolithic laminate consists of several folds, the direction of which is offset in each layer. When the fibers are all in the same direction, the fold is said to be unidirectional; when the fibers are in the form of fabric, the ply is said to be woven, it comprises fibers in two directions called warp direction and weft direction. If there are as many fibers in the warp and weft directions, the ply is said to be balanced woven. In Fig. 1 a presentation of a laminate is given [11–14].

The laminated materials have several basic constituents, generally a matrix and reinforcements, the association of which enables exceptional performances to be achieved.

The essential role of the matrix is to ensure the cohesion of the assembly and to protect the reinforcement from external aggressions such as humidity or corrosion. From the mechanical point of view, the matrix transmits the stresses towards the reinforcements and must therefore have good compatibility with the latter [4].

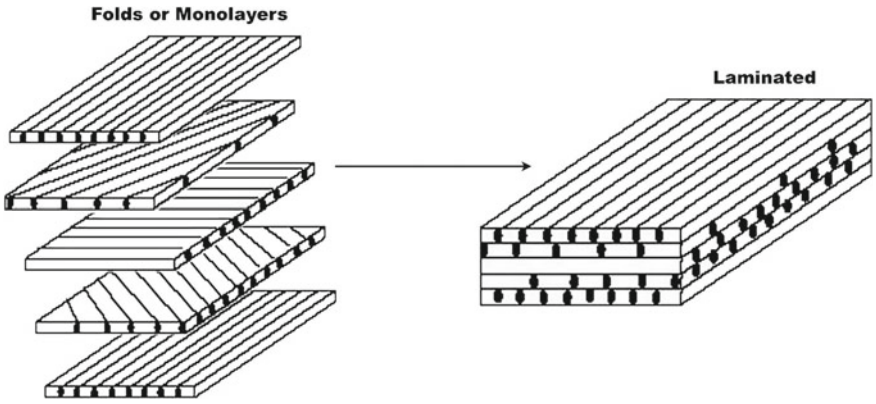


**Fig. 1** Constitution of a laminate

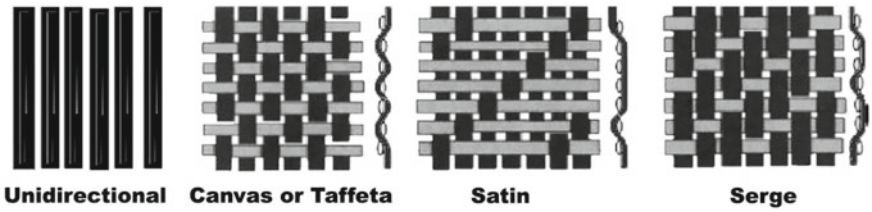


**Fig. 2** Examples of flat weaving frames

For laminates, we generally distinguish:

- Composites with an organic matrix (such as thermoplastic or thermosetting polymer resins), which today constitute the vast majority of industrial composites;
- Mineral matrix composites (Ceramics, carbon), often reserved for high temperature applications.

The reinforcements are in this case in the form of long fibers which give the composite major mechanical properties (rigidity, resistance to rupture, to fatigue, to impact, etc.). The nature of the reinforcements is chosen according to the intended application, both in terms of the material used (minerals such as carbon or glass, organic such as Kevlar) and in terms of their structure [15]. For this second aspect, the fibers consist of fibers or filaments assembled to form wicks which are then combined to form different forms of reinforcement: unidirectional sheets, fabrics. Composites with woven reinforcement (flat or multidirectional) are among the most used due to a lower risk of cracks and easy handling. Some examples of flat weaving reinforcements are shown in Fig. 2.

From the point of view of the final architecture, the layering technique makes it possible to design thin structural parts capable of withstanding complex and significant forces. The monolithic laminates are produced in successive layers formed of composite fiber/matrix plies which may have various orientations. Given the properties of the fibers, their orientation and the stacking of the strata, these materials therefore generally exhibit an anisotropic initial behavior [15].

## *2.1 Standardized Orientations*

One indicates the laminates by the orientation of the fibers of each fold compared to an arbitrary global reference mark (x, y, z), the axis x corresponding most often to the direction of the loading. A fold oriented at 0° has fibers oriented along the x axis and a fold oriented at 90° fibers along y. Any laminate of N folds is thus designated by the N-tuplet of the orientations of its folds in the direction of increasing z. To condense the writing, we note in index form the number of adjacent folds of the same orientation as well as the number of repetitions of the same sequence of folds. The index "s" corresponds to a symmetrical laminate for which only half of the

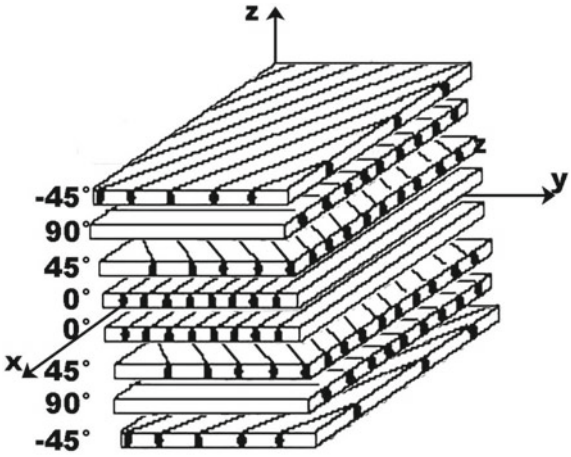


**Fig. 3** Example of quasi-isotropic symmetric stacking $[-45/90/45/0]_s$

stack is given, from the surface to the mirror plane of symmetry. Figure 3 shows the example of a symmetric stack $[-45/90/45/0]_S$ [15].

## *2.2 Why Mirror Symmetry?*

During the constitution of the laminated part, the successive plies impregnated with resin are draped at room temperature, then placed in an oven for polymerization. In the composite thus created when hot, the overall expansion of the part, of thermal origin, takes place without any overall variation in its shape by warping or warping. By cons, during cooling, the folds tend to contract differently in the direction of the fibers or in the cross direction. From there, the appearance of the constraints of thermal origin [15, 16].

When mirror symmetry is achieved, it causes these constraints to be symmetrical, and thus prevents the appearance of overall deformations of the part: warping, warping, as illustrated in the diagram in Fig. 4.

## *2.3 Positive and Negative Angles*

When layers are oriented at equal angles in absolute values, but opposite signs, the signs + or − are used. The convention for positive or negative angles depends on the system of axes chosen: an inversion may appear depending on the choice made (Fig. 5) [15].

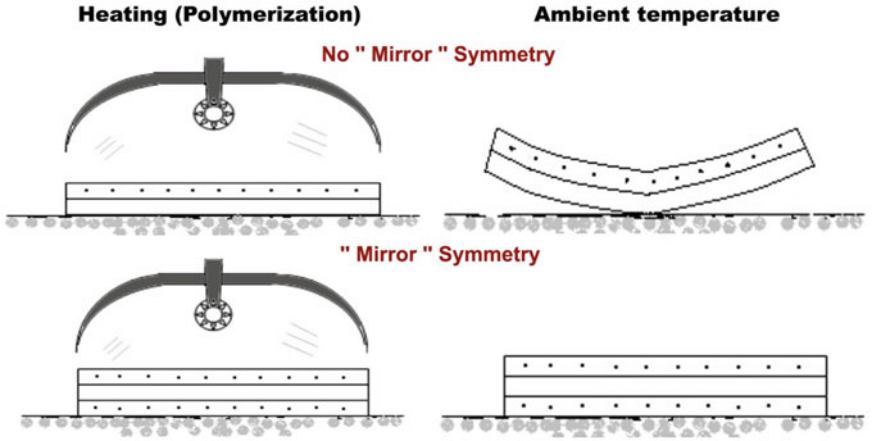


**Fig. 4** Diagram of the mirror effect on the stratification

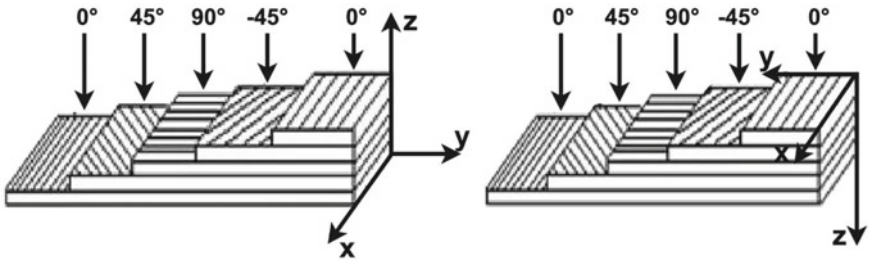


**Fig. 5** Orientation sign designation

## *2.4 Main Classes of Laminates*

The most tested laminate classes are shown in Fig. 6 [15].

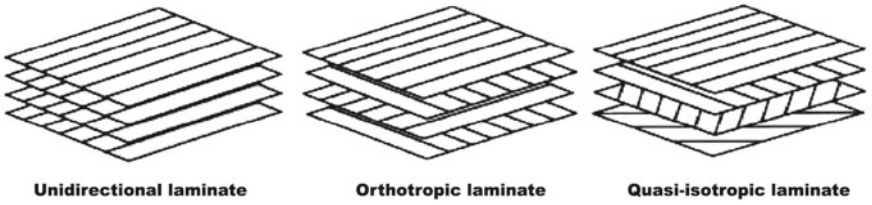


**Fig. 6** Diagram of the most suitable laminates

## 3 Mechanical Behavior of Laminated Composite in Static

The elastic mechanical behavior of a laminated structure is generally analyzed by the theory of laminated plates. This theory uses the same assumptions as the general theory of plates which are, in a scheme of first degrees, associated with the names of Reissner/Mindlin and Kirchhoff/Love. Kirchhoff–Love theory is historically one of the first two-dimensional approaches to bending elastic plates. It is based on the assumption of conservation of the normals while neglecting the transverse shearing. This theory is applied in the case of thin composite plates. The rigid displacements of the line segments orthogonal to the mean plane of the laminate in the case of the Kirchhoff model [17] are given by:

$$\begin{cases} u(x, y, z) = u_0(x, y) - z\frac{\partial w_0}{\partial x}(x, y) \\ v(x, y, z) = v_0(x, y) - z\frac{\partial w_0}{\partial y}(x, y) \\ w(x, y, z) = w_0(x, y) \end{cases} \tag{1}$$

Which gives for the deformations in laminate the plane:

$$\varepsilon = \begin{pmatrix} \varepsilon_x \\ \varepsilon_y \\ \varepsilon_z \end{pmatrix} = \begin{bmatrix} \partial u_0/\partial x \\ \partial v_0/\partial y \\ \partial u_0/\partial y + \partial u_0/\partial x \end{bmatrix} + z \begin{bmatrix} -\partial^2 w_0/\partial^2 x \\ -\partial^2 w_0/\partial^2 y \\ -2\partial^2 w_0/\partial x \partial y \end{bmatrix} \tag{2}$$

$$\varepsilon = \varepsilon^0 + zk = \begin{bmatrix} \varepsilon^0_{xx} \\ \varepsilon^0_{yy} \\ \varepsilon^0_{xy} \end{bmatrix} + z \begin{bmatrix} k_x \\ k_y \\ k_{xy} \end{bmatrix} \tag{3}$$

where, one distinguishes the deformations in membrane and the curvatures. In each fold "i" the law of behavior is written:

$$\sigma^i = \begin{bmatrix} x \\ y \\ \tau_{xy} \end{bmatrix} = Q^i \varepsilon^i = Q^i(\varepsilon_0 + zk) \tag{4}$$

where, $Q^i$ is the stiffness matrix of a laminate layer, the terms of which are presented in [17].

We define for the laminates the generalized forces by integration of the constraints in the thickness of the laminate:

$$N = \int_{-h/2}^{h/2} \sigma dz \tag{5}$$

$$M = \int_{-h/2}^{h/2} z\sigma\, dz \tag{6}$$

The constitutive equation of a laminated plate makes it possible to express the resultants and the moments as a function of the membrane deformations and the curvatures. It is written:

$$\begin{bmatrix} N_x \\ N_y \\ N_{xy} \\ M_x \\ M_y \\ M_{xy} \end{bmatrix} = \begin{bmatrix} A_{11} & A_{12} & A_{16} & B_{11} & B_{12} & B_{16} \\ A_{12} & A_{22} & A_{26} & B_{12} & B_{22} & B_{26} \\ A_{16} & A_{26} & A_{66} & B_{16} & B_{26} & B_{66} \\ B_{11} & B_{12} & B_{16} & D_{11} & D_{12} & D_{16} \\ B_{12} & B_{22} & B_{26} & D_{12} & D_{22} & D_{26} \\ B_{16} & B_{26} & B_{66} & D_{16} & D_{26} & D_{66} \end{bmatrix} \begin{bmatrix} \varepsilon_{xx}^0 \\ \varepsilon_{yy}^0 \\ \gamma_{xy}^0 \\ k_x \\ k_y \\ k_{xy} \end{bmatrix} \tag{7}$$

The Coefficients of this matrix are given in [17].

The components $N_X$, $N_Y$ and $N_{XY}$ are the results respectively of the normal stresses and the shear stresses in the plane (X, Y). They are shown symbolically in Fig. 7. The components $M_X$ and $M_Y$ are the bending moments in the X and Y directions, respectively and $M_{XY}$ is the torsional moment. These components are shown diagrammatically in Fig. 7 [17].

The behavior of the laminated composites is then defined by the calculation of the coefficients $A_{ij}$, $B_{ij}$ and $D_{ij}$. One obtains, starting from the boundary conditions on the laminate and the constitutive law, the state of stresses and deformations in each fold by inverse computation. It is also possible to go back to the stresses and deformations in the matrix and the fibers by models of homogenization and localization. However, this step is seldom used in a design office because the models are either too simplistic or very precise but complicated to handle [17].

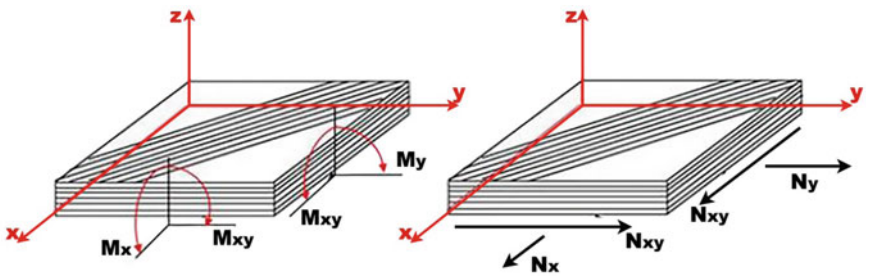


**Fig. 7** Laminate loading mode

## 4 Damage Mechanisms

Damage refers to the phenomena of creating new surfaces within a material under the effect of a stress. Krajcinovic [7] defines damage as an increase in the size or number of cracks. This generates a reduction in the mechanical characteristics of the system which leads to its ruin. Damage is a complex problem in laminate composites because it varies depending on the stack and the thickness of the plies where the defects are not stressed in the same way. When laminate composites are subjected to mechanical stress, different types of damage appear and develop.

### *4.1 The Failure Mechanisms of Laminated Composite with Long Fiber Reinforcement*

Failure of composite laminates can occur in a number of very complex ways. The failure modes depend on the stratification and the direction of the loading in relation to the orientation of the fibers.

The description of the rupture at the fold scale is, on the other hand, relatively effective for the classification of the rupture mechanisms. Laminates with long fiber reinforcement have three types of rupture: intralaminar rupture, interlaminar rupture, and translaminar rupture [9, 18]. These three rupture mechanisms (Fig. 8) define the rupture plane in relation to the constituents of the material. The intralaminar rupture is located inside a fold while the interlaminar rupture describes a rupture between two adjacent folds. The translaminar rupture is oriented transversely to the orientation of fibers in the damaged fold. With this convention, the ruptures of laminates with long fiber reinforcement can be described in terms of the failure mechanisms at the fold scale, identifiable by microscopic observations on the rupture surfaces [9, 15].


**Fig. 8** Failure mechanisms in 0/90/0 laminate

### 4.1.1 Intralaminar Failure

The intralaminar rupture is mainly due to the low resistance of the matrix and the adhesion between the matrix and the fibers. It is caused by stresses in the plane of the laminate. A crease deteriorates due to the resulting tensile stress in the direction normal to the fibers. This type of rupture is therefore commonly called "transverse cracking". Normally this cracking of the matrix occurs well before the fiber breakage. In multidirectional laminates, transverse cracking occurs, in general, successively from the weakest fold to the most resistant [9].

### 4.1.2 Interlaminar Failure

Interlaminar rupture occurs in the interface between two folds of a laminate. The rupture surface generally shows the rupture of the matrix and the fiber/matrix decohesion. These mechanisms involve little fiber breakage. As for metallic materials, the rupture can be in mode I (opening), mode II (right sliding), mode III (screw sliding), or a combination of the three modes. Although mode III is less studied, a large number of studies describe the separation mechanisms in mode I and mode II (Fig. 9) [18, 19]. The characteristics of the rupture surface depend on the types of

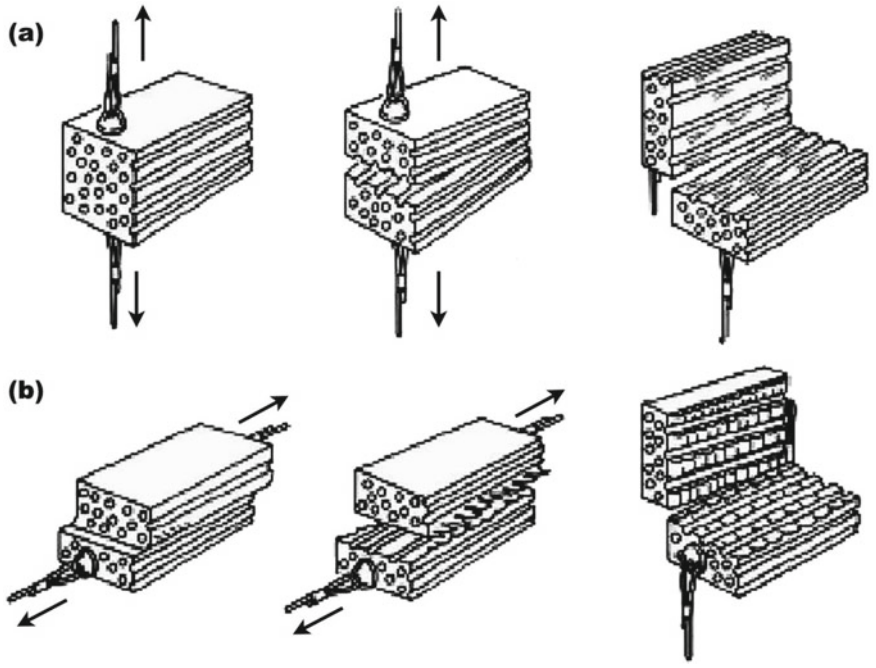


**Fig. 9** Diagram of the interlaminar rupture, **a** Mode I tensile, **b** Mode II shear

polymer used. For most thermosetting matrices, the rupture is of the fragile type. The fracture surface has a relatively flat plane with few marks of material deformation. In the case of mode I, the rupture plane is parallel to the fiber plane. The rupture facies has a relatively flat surface of the matrix containing "river marks". During the rupture process, these microcracks unite. A multitude of small tabs are formed on one of the rupture surfaces. On the opposite surface, the resin has small concave zones corresponding to the tabs of the first surface. Several terms have been used to describe these facies of rupture. The most commonly used terms are "hackles", which describe the tabs, and "scallops", which describe the concave areas. The failure facies of thermoplastic matrix composites are notably different from those of thermosetting matrix composites previously discussed. The surfaces of the two modes have "spikes" caused by the significant plastic deformation of the matrix. The main difference between the two modes is the orientation of the "spikes". For mode I, they point randomly in different directions. The ridges and valleys are due to the grubbing up of fibers. For failure in mode II, the tips are oriented parallel to the direction of propagation. There is no indication of the presence of hackles and scallops as in thermosetting matrices [9, 19, 20].

### 4.1.3 Translaminar Failure

Translaminar rupture concerns fiber rupture. The breaking surfaces are therefore generally marked by the rough morphology of the ends of the fibers. Indeed, the breaking stress of fibers is greater than that of all the other constituents of a composite laminate. As a result, this failure mechanism often results in total failure of the laminate. Translaminar rupture can be separated into two modes according to the loadings: rupture by traction and micro-buckling by compression. The rupture can be caused by an individual mode or a combination of the two modes [10].

#### Translaminar Failure in Tensile

Fragile fiber breakage is the primary mechanism, with breakage of the surrounding matrix considered secondary. The fibers typically break in bundles; the fibers in each pack have a common rupture plane. Different ruptures planes are then joined by the fiber/matrix decohesion and by the shear rupture of the matrix [9, 10].

#### Translaminar Failure in Compression

Compression micro-buckling is the main mechanism for this type of failure. The individual fibers flare locally to the point where instability is maximum. The bend of each fiber causes two ruptures separated by a distance of 5–10 times the diameter of the fiber [9, 10].

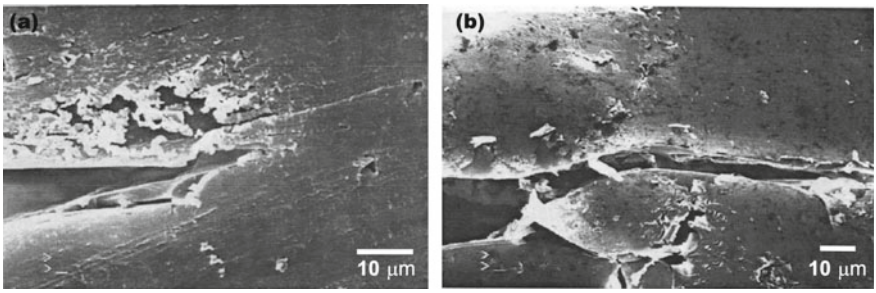


**Fig. 10** **a** Micro-cracks in the matrix, **b** Coalescence of micro-cracks in the matrix

The rupture surface is much flatter than that of the tensile rupture. The considerable damage after rupture is due to the relative movement between the two rupture surfaces in contact [9, 10].

## *4.2 The Damage Mechanisms in Laminated Composite*

The heterogeneity and anisotropy of composite materials make their damage mechanisms numerous and complex. These damages can appear very early in the life of a structure and constitute zones of initiation of macroscopic rupture strongly prejudicial to its integrity. We now propose to highlight these different elementary mechanisms leading to the creation of decohesion surfaces within laminate composites [21].

### 4.2.1 Matrix Microcracking

This mechanism intervenes in the first place due to a weak deformation at break of the fragile matrix and constitutes one of their predominant degradation mechanisms [8, 21, 22]. Matrix cracks are generally initiated in stress concentration zones such as the heterogeneities of the material (porosities, inclusions, etc.) [23]. Then, they propagate according to the orientation of the load, in particular perpendicular to the axis of traction (Fig. 10a) [8, 23]. The subsequent increase in the applied load leads to the coalescence of micro-cracks (Fig. 10b) [8, 23].

### 4.2.2 Fiber-Matrix Decohesion

The fiber-matrix interface is the weakest point inside the folds. At the level of the latter, initial defects exist [21]. These are detachments that can result from poor impregnation of the fibers by the resin. These adhesion breaks, generally induced by local shear stresses, propagate along the fibers until they form transverse cracks

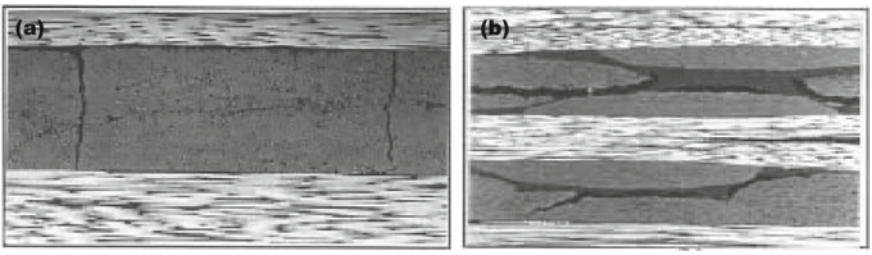


**Fig. 11** **a** Transverse cracking, **b** Longitudinal cracks

(crossing the entire fold, Fig. 11a) in the case of unidirectional laminates or longitudinal (Fig. 11b) in the plane of the folds in the case of woven composites [21]. Under these conditions, the cohesion between fiber and matrix is locally no longer ensured, which leads, during the application of the load, to defibering without cracking of the matrix (loosening). Two damage mechanisms can cause rupture initiation: initiation due to matrix micro-cracking and initiation due to decohesion of the fiber/matrix interface [21].

### 4.2.3 Fiber Breakage

First, it should be emphasized that there is no intrinsic resistance of fibers but a statistical distribution of their breaking properties. Fibers are very sensitive to defects and their resistance depends on the volume of material used [9, 21].

Irwin's relationship illustrates this dependence. The maximum normal stress ($\sigma_{max}$) that the fiber can withstand being a function of the stress applied to $\sigma$ and the geometry of the defect (length x and radius $\rho$ at the crack front):

$$\sigma_{max} = 2\sigma_a[x/\rho]^{1/2}. \tag{8}$$

If fiber breakage can occur as a continuation of the fiber-matrix decohesions (Fig. 12), fiber rupture often occurs, by definition of reinforcement, at an advanced stage of structural damage and in a brutal manner (behavior brittle). They mainly occur within the least disoriented folds in relation to the direction of the stress for which the fibers take up the most effort [9, 21].

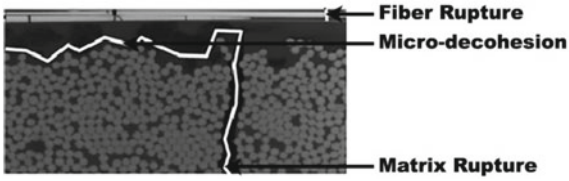


**Fig. 12** Fiber-matrix decohesion and fiber breakage

### 4.2.4 Delamination

One of the major advantages of composite laminates with long fiber reinforcement is the ability to orient the fibers of each ply in order to have the properties, often resistance and rigidity, suitable for loading in the intended directions. For example, a laminated plate can have a tensile stiffness in one direction twice that in another direction [14, 21, 22]. Despite excellent planar properties, laminates present a problem specific to the materials produced by lamination: interlaminar rupture. This rupture mechanism is characterized by detachment or decohesion between the plies of the laminate. It is commonly called "delamination" (Fig. 13).

If the three mechanisms presented above (matrix microcracking, fiber-matrix decohesion and fiber breakage) can be considered as diffuse within the fold, delamination or inter-fold decohesion corresponds on the other hand to macroscopic degradation in since it is visible to the naked eye. This detachment generally begins in areas with strong stress gradients such as the free edges of the structure, or near macroscopic defects to progress then by separating the layers. The porosities generated within the preform by the stacking of the layers obviously constitute aggravating factors for this phenomenon [14, 21, 22].

## *4.3 Development of Failure Mechanisms and Processes*

Figure 14 summarizes the degradation mechanisms presented above and their corresponding scales. Besides the nature of the applied stress (static/dynamic, direction, speed, …), these mechanisms are strongly conditioned in their types (evolution and kinetics) by the following parameters [6, 21]:

- The nature and properties of the constituents (in particular their own method of damage),
- Their geometric arrangement (proportion, shape and orientation in each fold, stacking sequence),
- The interaction between the different phases (types of interfaces in particular),
- The manufacturing process (initial porosity, residual stresses).

**Fig. 13** Delamination of laminated composite

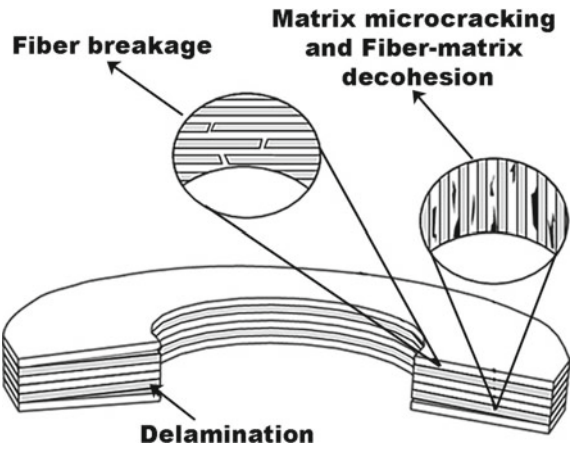


**Fig. 14** Damage mechanisms in laminates

## 5 Failure of Materials

When a part is subjected to stresses of various origins, there are limits, in constraints or deformations, which it must not exceed, under penalty of damaging the material and causing it to rupture. Depending on whether one is interested in the degradation of the material from a micro-mechanical or macro-mechanical point of view, two approaches can be used [24]:

- **The mechanics of damage** propose to continuously describe the progressive degradation of the material due to the appearance, growth, and then to the coalescence of micro-cracks or micro-cavities present in the material.
- **The failure mechanics** aims at studying the mechanical behavior of a material in the presence of macroscopic cracks. This amounts in particular to determining the field of stresses and deformations in the vicinity of the tip of a crack. The study of these mechanical fields then making it possible to judge the stability or not of a crack. It is also possible, as we will see later, to approach the fracture mechanics through an energy study of the cracked solid.

### *5.1 Failure Modes*

Cracking is manifested by the irreversible separation of a continuous medium into two parts, called the lips of the crack, which introduces a discontinuity in the direction of movement. According to Irwin [24], one can distinguish three modes of solicitations represented by Fig. 15. These three modes are each defined by the movement of the two surfaces of the crack one compared to the other. The possible movements of the lips of each crack are combinations of three independent modes [9, 24]:

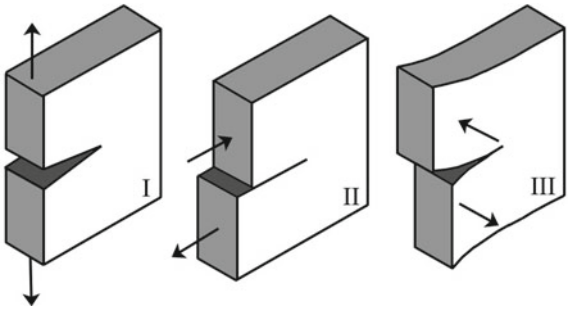


**Fig. 15** Failure modes

- **Mode I**: said mode by opening (or cleavage), corresponds to a relative spacing of the two surfaces of the crack by the angular opening of these;
- **Mode II**: said plane shear;
- **Mode III**: said anti-plane shearing, and corresponds to a transverse sliding of the two surfaces of the crack, in opposite directions, but this time in a direction parallel to the front of the crack.

Of the three types of stress, mode I is considered to be the most severe, and it is for this reason that most studies of the fracture mechanics have been carried out using this mode; however, once initiated and for mixed stresses or complex geometries, the crack tends to fork, and therefore rarely remains rectilinear (2D) or plane (3D).

## *5.2 Linear and Nonlinear Failure Mechanics*

The failure mechanics proposes to describe the stages of initiation and propagation of the cracking. According to the behavior of the material during the propagation of a crack, one can be confronted with two types of rupture [9, 19]:

- **Fragile rupture**, in the absence of significant plastic deformation (linear mechanical failure);
- **Ductile failure**, in the presence of significant plastic deformation (non-linear mechanical failure). In this case, depending on the extent of the plastic zone at the crack tip, we differentiate the case of confined plasticity from that of extended plasticity.

## *5.3 Theory of Failure Mechanics*

### 5.3.1 Griffith's Approach

The idea that small structures generally show higher resistances than larger ones was taken up by Griffith in the 1920s who studied the phenomena of glass rupture

[25]. He made the claims that each body contains a distribution of imperfections or flaws and that rupture occurs at the largest of these. Larger bodies are more likely to contain larger flaws and will thus fail at lower stresses. Through these claims he presented the fundamental notions of the science of fracture mechanics. However, it can be noted that new theories always have precursors. For example, in 1913, Inglis [26] studied the forces applied near the edge of an elliptical notch. In the case where the relative size of the minor axis to the main axis is very small, the ellipse would appear because a straight crack and a small increase in the force applied at the end would be enough to start a tear in the material. In addition, he noted that the increase in length exaggerates the large stress and the crack continues to propagate in the characteristic manner of the cracks [26].

Griffith [25] assumed that failure is an energy absorbing process and that in order to propagate a crack, the material must be supplied with the necessary energy corresponding to the increase in the area of crack. It follows that the crack instability that occurs when the energy stored at the time of propagation exceeds the energy necessary for the creation of new surfaces. If one considers a purely elastic solid of uniform thickness B, containing an elliptical crack of length "2a" subjected to a field of axial stress "σ". According to Griffith [25], the net change in the potential energy of the solid (Fig. 16):

$$W_p = \frac{\Pi a^2 \sigma^2 B}{E'} \tag{9}$$

with: $E' = E/(1 - \nu^2)$ or $E' = E$ respectively for the case of plane deformation and plane stress. Here, E is the Young's modulus and $\nu$ the poison coefficient.

The energy for creating a new surface is written (Fig. 16):

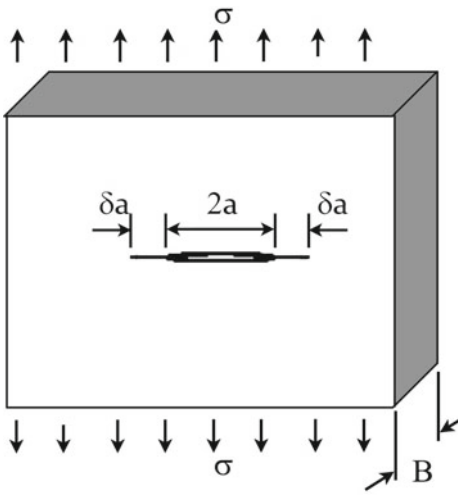


**Fig. 16** Diagram of a solid containing an elliptical crack "2a"

$$W_s = 4aB\gamma_s \tag{10}$$

where, $\gamma$ is the surface energy of rupture per unit of area. The total energy of the system is then given by:

$$U = W_p + W_s = \frac{\Pi a^2 \sigma^2 B}{E'} + 4aB\gamma_s \tag{9}$$

Griffith [25] noted that the critical state for the beginning of the crack progression is:

$$\frac{dU}{dA} = \frac{dW_p}{dA} + \frac{dW_s}{dA} = -\frac{\Pi a \sigma^2 B}{E'} + 2\gamma_s \tag{10}$$

where A = 2aB is the broken surface and dA denotes the increment of increase in the crack. Note that the area of two broken surfaces is 2A. The critical stress for triggering a rupture is:

$$\sigma_f = \sqrt{\frac{2E'\gamma_s}{\Pi a}} \tag{11}$$

As the second derivative of $d^2U/da^2$ is negative, the above state of equilibrium (Eq. 11), causes an unstable crack propagation. In addition, the materials considered by Griffith [25] in this theory are inorganic glasses, which gave cracks almost perfectly fragile because the energy necessary to create new surfaces equals the external energy.

For most materials this does not apply since the forces induced at the bottom of the crack cause large deformations and flow, which result in much more energy being absorbed. Orowan [27] and Irwin [24] studied, independently, the damage of steel test-tube; these authors declared that the dissipation was confined to the small areas at the bottom of the crack. This means that Eq. 9 could still be used, but a dissipation of plastic energy must be considered. The resulting expression for the rupture trigger is:

$$\sigma_f = \sqrt{\frac{2E'(\gamma_s + \gamma_p)}{\Pi a}} \tag{11}$$

Here $\gamma_p$ is the plastic energy per unit area of the surface created. Note that $\gamma_p$ is much larger than $\gamma_s$. The criterion for increasing the crack can be expressed as follows: the energy release rate G must be greater than the critical work $G_{lc}$ which is required to create a new failure surface.

Irwin [24] extended the theory of A.A. Griffith using the method of Westergaard [28], developed in 1939. Thus, Eq. 11 can be rewritten in the form:

$$\sigma_f = \frac{K}{\sqrt{\Pi a}} \tag{12}$$

In Eq. 12, K is called the stress intensity factor. The K notation is said to come from J.A. Kies, a colleague of G.R. Irwin at the US Naval Research Laboratory.

### 5.3.2 Energy Release Rate

Definition of G and R

Suppose that the body in Fig. 15 is subjected to a loading which leads to the progression of crack. A change in the energy balance occurs irreversibly during the progress of the crack. Specific energy is required to propagate the crack beyond the dA increment. We can define R as a breaking strength:

$$R = \frac{dW_s}{dA} \tag{13}$$

It is necessary to consider the change of energy of the system due to the increment of fracture of crack arising from the changes of external work and internal energy. This is defined as G, the energy release rate. Let us consider an elastic body of uniform thickness B containing a crack of length subjected to an external force ($F_{ext}$) related to a displacement u. The total mechanical energy of the broken body $W_p$ is:

$$W_p = \phi - W_F \tag{14}$$

Here: Φ: is the stored elastic strain energy; $W_F$: is the external work carried out by external forces.

In 1956, Irwin [24] proposed to approach the characterization of the driving force for rupture in cracked elastic bodies. He presented the energy release rate G defined as follows:

$$G = \frac{dW_p}{dA} \tag{15}$$

where A = 2aB is the broken surface and dA denotes the increment of increase in the crack.

Evaluation of G

Let us consider two simple situations, the first test is under imposed force in which, the loads applied on the surfaces of the solid remain constant during the increase in crack. The Clapeyron theorem of linear elasto-static states allows in summary to

say that, the work established by the applied charges is equal to twice the energy of elastic deformation, $W_F = 2\Phi$, thus Eq. 15 will be in this case:

$$W_p = -\phi \tag{16}$$

The second case is that of an imposed displacement test. In this case, the surfaces of the outline of the solid, on which the loads are applied, are supposed to remain stationary during the increase in crack. If the forces of the solid body are ignored, the work deduced by the applied loads disappears, so Eq. 15 is written:

$$W_p = \phi \tag{17}$$

Contrary to this last case, in the test with imposed displacement, the energy necessary for the increase in crack is not caused by the elastic energy specific to the body, but, by the forces of the external loads applied to the solid, the elastic deformation energy of the solid has increased. So the term energy release rate, in this case, is not appropriate.

Linear Elastic Mechanics of Rupture (MLER)

The fracture mechanics studies the behavior of cracked bodies. It makes it possible to assess and predict the breaking stress of materials containing defects. For a linear elastic behavior, the MLER is applied. For a material containing a crack, subjected to an axial stress field, Griffith [25], limits the energy necessary to reform a crack with the only thermodynamic energy. On the other hand, the analysis of Irwin [24] is more general. It takes into account all the mechanisms which intervene in the propagation of crack. From the relations of Westergaard [28], it introduces a factor which makes it possible to describe the singular stress fields at any distance "r" from the crack tip, with "r" much less than the length of crack "a". At a point M close to the crack (Fig. 17a), the stresses $\sigma_{ij}$ identified by the polar coordinates (r, θ), are given by the relation:

$$\sigma_{ij} = \frac{K_r}{\sqrt{2\Pi r}} f_{ij}(\theta) \tag{18}$$

with: $K_R$: stress intensity factor according to failure mode I; r: distance between point M and the crack tip; $f_{ij}$: angle function, between OX and OM.

For a small distance "r", the value of the stress $\sigma_y$ exceeds that of the flow stress, this shows that a plastic deformation takes place at the end of the crack and even if the state of deformation is plane. The stresses at the end of the crack are thus limited to finite values (Fig. 17b). Ultimately we have:

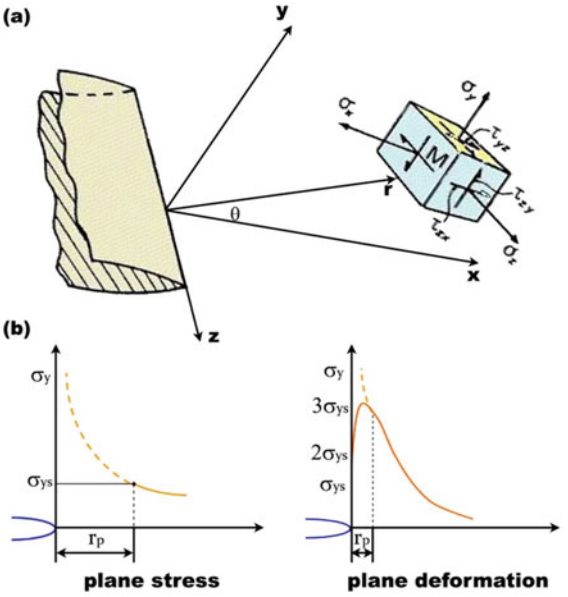


**Fig. 17** **a** Coordinate system around the crack tip, **b** Approximate distribution of the stress $\sigma_y$

$$\sigma_y = \frac{K_r}{\sqrt{2\Pi r_p}} = \sigma_{ys} \tag{19}$$

with: $\sigma_{ys}$ the flow stress with respect to the y axis.

$K_R$ represents the stress intensity factor in mode I. It simultaneously describes the effect of the applied stress, perpendicular to the plane of the crack propagation, at infinity and the effect of the crack length "a". For this case, $K_R$ is expressed by:

$$K_R = \sigma\sqrt{\Pi a} \tag{20}$$

The shape of the plastic zone $2(r_p/a)$ is therefore proportional to $(\sigma/\sigma_{ys})^2$. If this zone is very small or generally limited in shape, compared to the dimensions of the crack and the structure, it is possible to extend the theory of elastic linear mechanics by using the effective length of the crack $\sigma_{eff}$, given by the correction of Irwin [29]:

$$\sigma_{eff} = a + r_p \tag{21}$$

As the plastic zone developed at the end of the crack depends on the type of stress, it is proportional to the ratio $(K_R/\sigma_{ys})^2$ at a coefficient near β. The latter depends on the stress state existing in this region:

$$r_p = \beta\left[\frac{K_R}{\sigma_{ys}}\right]^2 \tag{22}$$

Irwin's model considers that the plastic zone is circular (Fig. 17b) of radius $r_p$. The coefficient β is therefore equal to (1/2Π) (Eq. 19).

On the free surface of the crack tip, the plane deformation state does not exist because the stress $\sigma_x$, is zero; the stress $\sigma_y$, starting from a value equal to $\sigma_{ys}$, rises to a value x y three times greater at a distance close to the end of the crack (Fig. 17b). In this area, Irwin has shown that the stress $\sigma_y$ is less than $3\sigma_{ys}$ and is rather equal to $\sqrt{2\sqrt{2}}\sigma_{ys} \approx 1.68\sigma_{ys}$.

Finally:

$$\begin{cases} r_p = \frac{1}{2\Pi}\left[\frac{K_I}{\sigma_y}\right]^2 & \text{(plane stress)} \\ r_p = \frac{1}{6\Pi}\left[\frac{K_I}{\sigma_y}\right]^2 & \text{(plane deformation)} \end{cases} \tag{23}$$

### 5.3.3 Stress Intensity Factor

The American society for materials testing (ASTM) under the standard E399 [30], offers a possibility to determine the factor ($K_{IC}$). This is done using a variety of fatigue-cracked test pieces. The standard (ASTM) proposes the use of the Compact Tensile test piece "Compact Tension" (CT) (Fig. 18a) or the cracked three-point bend test piece (SENB) (Fig. 18b) [9, 10].

The main relation of the factor $K_R$, for a cracked test-piece of finite dimensions and requested by a uniaxial stress in mode I, is as follows:

$$K_R = Y\sigma\sqrt{a} \tag{24}$$

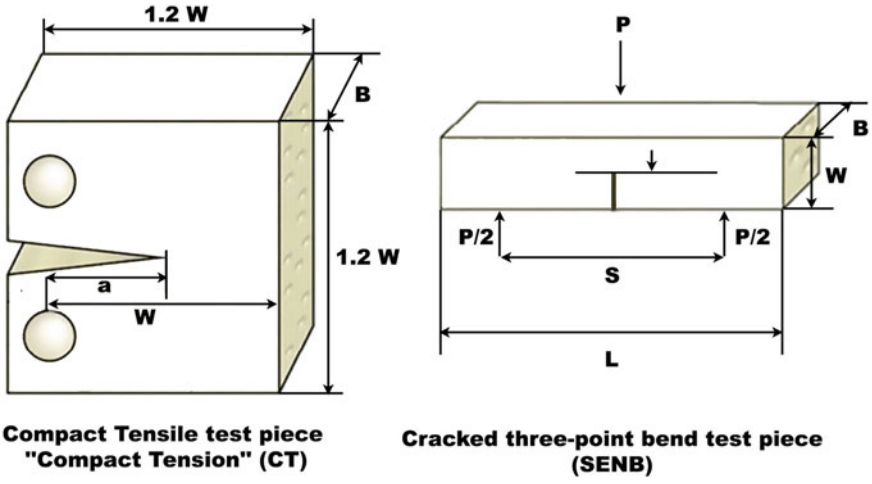


**Fig. 18** Test piece proposed by ASTM in mode I

The parameter Y is a geometry correction factor, often represented as a function of the a/W ratio (length of the crack across the width of the test piece). In the case of fragile materials, when the applied stress is increased, the sudden rupture occurs at the moment when $K_R$ reaches a critical value $K_{IC}$. So at the time of the rupture, we have:

$$K_{IC} = Y\sigma_F\sqrt{a_c} \tag{25}$$

with: $a_c$: is the critical fault size; $\sigma_F$: is the value of the tensile strength of the test piece.

### 5.3.4 Equivalence Between $G_R$ and $K_R$

Irwin [29] has shown that $K_R$ is related to $G_R$. This relationship is given by:

$$G_R = \frac{{K_R}^2}{E} f(\nu) \tag{26}$$

with: E: is Young's modulus; $f(\nu) = 1$ in plane stress (thin plate); $f(\nu) = (1 + \nu^2)$ in plane strain (thick plate).

Unlike A.A. Griffith, G.R. Irwin does not limit the term "G" to the sole thermodynamic energy of the surface but extends it to all the mechanisms which can contribute to the extension of the crack (micro-cracking, plasticity….) [9, 10].

## 6 Conclusion

Composite materials are one of the most crucial aspects of current and future engineering technologies. Thanks to their excellent mechanical properties, they find their applications in a multitude of fields as diverse as the mechanical industry. In this chapter, the mechanical behavior of laminate composites and their resulting damage modes in the impact loading scenario were discussed. During service life, composites are often subject to loading conditions of different impacts that trigger various damage mechanisms depending on the extent of the impact. Laminate composites subjected to various impacts at low speed often absorb contact energy by cracking and delamination between fiber/matrix. However, these deterioration modes do not lead to the ultimate failure of a composite structure; nevertheless it considerably reduces its carrying capacity. Laminate composites are often exposed to varying degrees of impact loading rates, to which their responses may be significantly different. At low impact load, cracking and delamination of the matrix are often the dominant modes, while at high impact load, composite structures can rupture by undergoing fiber cracking and total failure of the composite. Typical damage to the impacted

composite laminate includes both intra-laminar and inter-laminar damage mechanisms. The first mentioned often occur within the single layer in the form of fiber fracture, cracking of the matrix or plasticity and separation between the fibers and matrix. The inter-laminar damage represented by delamination occurs between adjacent layers inside the composite laminate. Fiber breakage occurs much later than matrix damage and delamination when the impact energy reaches a high level. Fiber failure often occurs around the impactor (contact area) or on the opposite side of the laminate, due to extremely high local stresses and the effect of impact or high bending stresses.

## References

1. Ouarhim W, Semlali Aouragh Hassani F, Qaiss A, Bouhfid R (2019) Rheology of polymer nanocomposites. In: Rheology of polymer blends and nanocomposites theory, modelling and applications, pp 73–96
2. Semlali Aouragh Hassani F et al (2019) Mechanical properties prediction of polypropylene/short coir fibers composites using a self-consistent approach. Polym Compos 40(5):1919–1929.
3. Banakar P, Shivananda HK, Niranjan HB (2012) Influence of fiber orientation and thickness on tensile properties of laminated polymer composites. Int J Pure Appl Sci Technol 9(1):61–68
4. Abdussalam SR, Ayari ML (1998) Experimental study of fracture toughness and energy in composite materials. Mech Compos Mater 34(3):235–242
5. Huda MS, Drzal LT, Mohanty AK, Misra M (2008) Effect of fiber surface-treatments on the properties of laminated biocomposites from poly(lactic acid) (PLA) and kenaf fibers. Compos Sci Technol 68(2):424–432
6. Ladevèze P, Allix O, Deü JF, Lévêque D (2000) A mesomodel for localisation and damage computation in laminates. Comput Methods Appl Mech Eng 183(1–2):105–122
7. Krajcinovic D (2000) Damage mechanics: accomplishments, trends and needs. Int J Solids Struct 37(1–2):267–277
8. Baste S (2001) Inelastic behaviour of ceramic-matrix composites. Compos Sci Technol 61(15):2285–2297
9. Falzon BG, Apruzzese P (2011) Numerical analysis of intralaminar failure mechanisms in composite structures. Part I: FE implementation. Compos Struct 93(2):1039–1046
10. Laffan MJ, Pinho ST, Robinson P, McMillan AJ (2012) Translaminar fracture toughness testing of composites: a review. Polym Test 31(3):481–489
11. Berthelot JM (1992) Matériaux composites: comportement mecanique et analyse des structures, Paris, édition MASSON, 2ème édition
12. Gay D (1997) Matériaux composites, Paris, édition HERMES, 4ème édition
13. Weiss CBJ (1983) Les matériaux composites: calculs, Essais et contrôles, conception, Paris, édition de L'USINE
14. Jones RM (1999) Mechanics of composite materials, USA, TAYLOR & FRANCIS, 2ème édition.
15. Gay D, Hoa SV, Tsai SW (2003) Composite materials design and applications. CRC Press LLC
16. Semlali Aouragh Hassani F, Ouarhim W, Zari N, Bouhfid R, Qaiss A (2019) Natural fiber-based biocomposites. In: Biodegradable composites materials, manufacturing and engineering, pp 49–79
17. Berthelot J-M (2010) Mécanismes de rupture et endommagement des materiaux composites. Mécanique des Matériaux Struct Compos, 224–260

18. Smith BW (1993) Fractography for continuous fiber composites, engineered materials handbook-volume 1: composites. ASM International, Ohio, USA. ISBN 0871702797 (v.1), pp 786–793
19. Goyal VK, Jaunky NR, Johnson ER, Ambur DR (2004) Intralaminar and interlaminar progressive failure analyses of composite panels with circular cutouts. Compos Struct 64(1):91–105
20. Reeder JR (1992) An evaluation of mixed-mode delamination failure criteria. Langley research center, Virginia, N°NASA-TM-104210, pp 1–49
21. Talreja R (1981) Fatigue of composite materials: damage mechanisms and fatigue-life diagrams. Proc R Soc Lond Ser A Math Phys Sci **378**(1775):461–475
22. Berthelot JM (2003) Transverse cracking and delamination in cross-ply glass-fiber and carbon-fiber reinforced plastic laminates: Static and fatigue loading. Appl Mech Rev 56(1):111–147
23. Park JM, Kim DS, Kim SR (2003) Interfacial properties and microfailure degradation mechanisms of bioabsorbable fibers/poly-L-lactide composites using micromechanical test and nondestructive acoustic emission. Compos Sci Technol 63(3–4):403–419
24. Irwin GR (1957) Analysis of stresses and strains near the end of crack traversing a plate. J Appl Mech 24(3):361–364
25. Griffith AA (1920) The phenomena of rupture and flow in solids. Philos Trans R Soc Lond 221:163–198
26. Inglis CE (1913) Stresses in a plate due to the presence of cracks and sharp corners. Trans Inst Nav Arch Lond **55**:219–230
27. Orowan E (1955) Energy criteria of fracture. Weld J 34(3):157–160
28. Westergaard HM (1939) Bearing pressure and cracks. J Appl Mech 6(2):49–53
29. Irwin GR (1960) Plastic zone new a crack and fracture toughness. In: Proceedings of the 7th Sagamore Conference, p 63
30. Srawley JE (1976) Wide range stress intensity factor expressions for ASTM E 399 standard fracture toughness specimens. Int J Fract 12(6):475–476

# Review of Fatigue Responses of Fiber-Reinforced Polymer (FRP) Composite


**M. K. R. Hashim, M. S. Abdul Majid, and M. J. M. Ridzuan**

**Abstract** The engineering structures were subjected to cyclic loading which lead to fatigue failure that affecting the service-life. Carbon fibre reinforced plastics (CFRP) is an advance man-made material with outstanding mechanical properties and thus show potential to replace non-fibrous materials. Besides a good strength-to-weight properties, CFRP are corrosion resistant materials. Abundant of studies were discussing about response of CFRP to cyclic loading, thus this article aims to review general information on the fatigue of CFRP. The review subjected to damage mechanics and factors tolerant to fatigue of CFRP. The factors focus in particular on effect of types fiber and matrix, fiber volume fractions, fiber orientation, stress ratio and mean stress and lastly on hysteresis and frequency.

**Keywords** Fatigue · Composite · Fiber-reinforeced polymer · Damage machanism · Orientation

## 1 Introduction

Fibre-reinforced polymer (FRP) composite materials are broadly utilised in structural applications due to their high specific strength and stiffness besides its is anisotropic and inhomogeneous in nature. Their uniqueness allows them to replace conventional metal alloys in various structural applications (e.g., automotive, automation, aerospace, marine industries and etc.). The mechanical behaviour of FRP materials mainly depends on the properties of its constituent elements likes the matrix/ fiber strength and modulus, force interface between matrix/fiber and chemical stability [16]. Most of structures are frequently subjected to fluctuate and cyclic load like

M. K. R. Hashim · M. S. Abdul Majid (✉)
School of Manufacturing Engineering, Universiti Malaysia Perlis, Pauh Putra Campus, Arau, Perlis, Malaysia
e-mail: shukry@unimap.edu.my

M. S. Abdul Majid · M. J. M. Ridzuan
School of Mechatronic Engineering, Universiti Malaysia Perlis, Pauh Putra Campus, Arau, Perlis, Malaysia

© Springer Nature Singapore Pte Ltd. 2021

M. Jawaid et al. (eds.), *Structural Health Monitoring System for Synthetic, Hybrid and Natural Fiber Composites*, Composites Science and Technology,
https://doi.org/10.1007/978-981-15-8840-2_9

vibration, this situation contribute to material face the fatigue failure. Fatigue failure is among of major problem encountered by the structural components. Fatigue failure is affecting the composites's mechanical properties by fibre breakage, cracking of matrix, debonding of fibre and matrix, and also lead to delaminate between the ply layers.

An FRP composite is an advance human-made material consist of a polymer that is reinforced by fibre. The manufacturing process is to produce a bulk material with better properties than the constituent based materials. The processes involve various phase materials by mixing reinforcing fibres (human-made or natural) either with or without fillers to polymer matrix–resins. Fibre is a main element in FRP composites where its mechanical properties (stiffness, strength, and toughness) highly contribute to mechanical properties of FRP composite. The mechanical properties of FRP composites can be varying depend on the fibre volume fraction ($V_f$) of the composite. The increase of the fibre volume fraction lead to better the mechanical properties of FRP composites [45] at between 30 and 70% based on previous studies [9, 10]. Laminate orientation another factor contributes to mechanical properties of the composite. There are many studies on fibre orientation with angles 0°, 45°, and 90° for uni-directional and multi-directional laminates [9, 10]. Specific properties of the composite can be improved by mix filler materials such as hydrated alumina, calcium carbonate or clay beside for lower its cost. The matrix of FRPs can be classified into two type resins which are thermosetting and thermoplastics. Epoxy resins (thermosetting matrices) are widely used as the matrix material in FRP composites, which has crossed linked bonding [20].

The stress ratio (R) is one of an important parameter that contributes to fatigue response. Sturgeon [41] and Branco et al. [8] described the fatigue strength of the composite reduce along with development of the stress ratio. Fatigue failure criterion based on the input strain energy for fibre-reinforced materials [37]. Most previous studies involve analysing the fatigue behaviour of composite laminates with stress ratio at range between −1 and 1 [29, 32, 37]. The fatigue loads type can also be classified base the stress ratio as Compression—Compression ($1 < R < \infty$), Tension–Compression ($-\infty < R < 0$), and Tension–Tension ($0 \leq R \leq 1$).

Geometric discontinuities (e.g., sharp corners or holes) at components made of FRP composites can develop the local intensity of stress/strain. A study by Curtis [13] identified that short fatigue life was affected by stress concentration (produced by holes). Hyakutake et al. [22] observed a slight effect of the fatigue life of a glass fibre/ epoxy laminate for the notch-root radius.

In many engineering materials, fatigue failure observed was affected by frequency response. The internal heating of the composite during fatigue depends on the test frequency magnitude. During the fatigue test, the temperature was continuously developed on the specimens with the number of fatigue cycles increase and getting worst close to final fracture [36]. The fatigue life of composite decrease along with increase frequency of the fatigue load and lead to increase internal heating of the composite.

Due to prolonged exposure of the composite components to fatigue loads under various environmental condition, internal damages develops in the composites such as matrix cracks delamination, and disbands [38, 40, 42]. Present of internal damages in composite cause reducing the ability of the static load carrying by the composite. Consequently, under cyclic fatigue loads, the damages propagate sub-critically.

## 2 Damage Mechanism

It is intrinsically difficult to describe the damage mechanism of fatigue in an FRP composite. There are stages of fatigue life identified by Reifsnider et al. [39]. Commonly, the fatigue damage mechanisms of fibre composites are started by cracking of matrix, debonding of fibre-matrix, breakage of fibre, delamination of fibre layers, and end up failure of component. Vasiukov et al. [43] described that the damage mechanism is a non directly proportional to a series of cycles. The rapid damage propagation is recorded at the beginning and the end of the cyclic loading for the composite with no stress concentrations [6, 34]. Usually, in the middle of the stage, damage growth is linearly progressive [18]. Figure 1 shows the fatigue life of unidirectional composite materials with can be categorize into three stages of failure damage initiation and growth process. Stage I is started at a local micro-defect by debonding of the matrix-fibre interface of the matrix material. The local micro-defect such as voids contains, resin-rich regions or misaligned fibres. Stage II is an almost linear process in nature which starts delamination of composites materials. Stage III is a continuity stages previous where fibre breakage occurs.

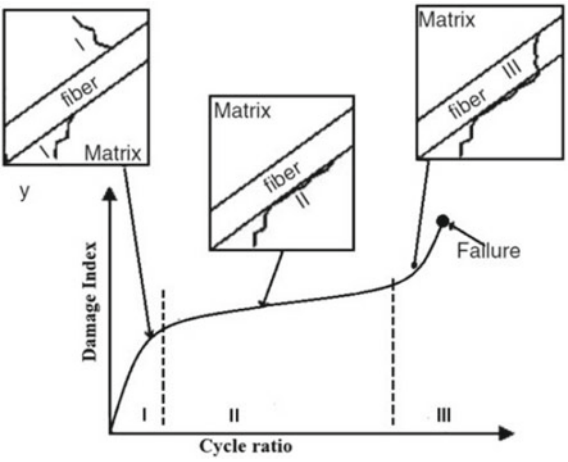


**Fig. 1** The damage mechanism of unidirectional composite [39]

## 3 Effect of Fibre and Matrix

Fibres are the main factor that contributes to fatigue behaviour because of their roles as the primary load bearers in the composite structures. Usually, 30 to 70% of the composites volume are occupied by the fibre in the form of chopped, stitched, woven, and braided. There are numbers of past studies on the effect of fibre properties on the advanced polymer matrix composite, especially on the glass fibre, carbon fibre, and aramid fibre. In term of cost, carbon fibre being the most expensive compare to the rest, while the least expensive is glass fibre. There are numerous types of glass fibres available in the market which originally come out from some classic glass fibres (E-glass, C-glass, S-glass, and ECR-glass fibre). E-glass composites have a poor fatigue performance than S-glass composites at same matrices due to S-glass fibres have the best mechanical strength and stiffness compare to the other glass fibres [7]. The glass fibre reacts differently under a corrosive environment [30]. Jones et al. [23] reported the relationship of the Carbon FRPs (CFRPs) composites on fatigue behaviour. Based on Fig. 2, the S-N curve is steeper for the low modulus CFRP compare to the high modulus CFRP, which has a better fatigue performance. Curtis [14] studied on fatigue behaviour of Carbon FRPs (CFRPs), Glass FRPs (GFRPs) and Kevlar FRPs (KFRPs). Figure 3 shows the S-N fatigue curves for three unidirectional composites which GFRPs show more severe drop down in its fatigue strength compare to CFRPs. Kevlar fibre has characteristics of fatigue sensitive cause more complex fatigue behaviour than that carbon and glass fiber [14].

The matrix resin is crucial element for prediction strength of the fatigue for fibre reinforced composites which is contribute by the resin's properties [35]. Usually, crack was started at the matrix region lead formation of a fatigue failure. Previous studies have proven the thermosetting resins have poor properties than the thermoplastic resins in term of toughness and ductility [3, 11, 12]. Thus, thermoplastic resins exhibit longer fatigue life significantly with higher interlaminar fracture toughness against delamination [19]. Boller (Jones et al. [23]) found that laminates of epoxy matrix composites with E-glass fabric have a better fatigue behaviour compare to laminates of polyester, phenolic and silicone, as shown in Fig. 4. The effectiveness

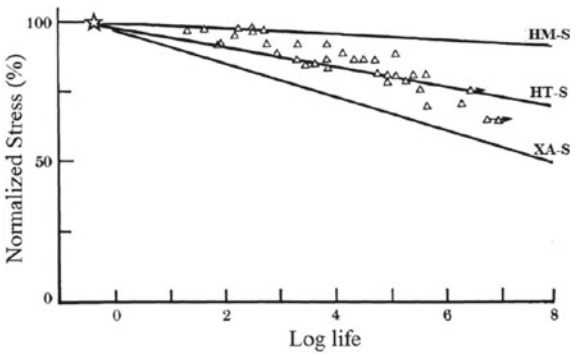


**Fig. 2** S-N curves for different unidirectional CFRPs [23]

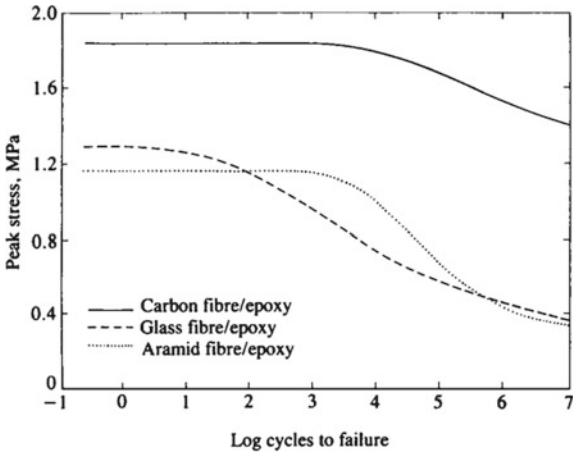


**Fig. 3** S-N fatigue curves for unidirectional composite materials [14]

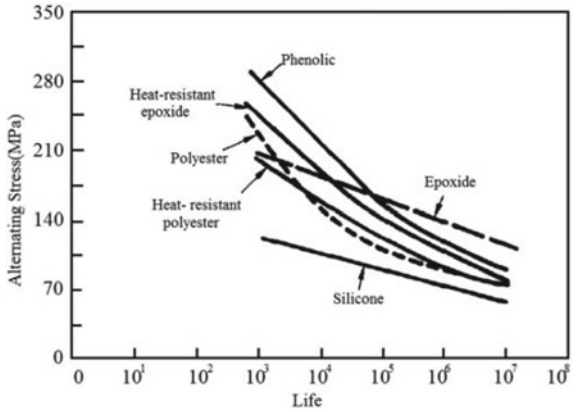


**Fig. 4** S-N curves for E-glass fibre composites [23]

of the stress transfer reduce due to the fibre–matrix with a weaker interface allow the cracks from propagating through the matrix and leading to the fracture toughness [46]. The mixing of nanoparticles likes rubber particles in the matrix material improve tensile strength and impact strength which can increase the resistance to crack growth in the matrix material [31].

Newaz [33] analyzed the fatigue behaviour of E-glass/vinyl ester and E-glass/epoxy unidirectional composites with 48% and 50% volume of fibre for, respectively. Both of them have similar mechanisms of fatigue damage either at high or low deflection levels under flexural loading. The difference between them was identified where E-glass/epoxy specimen late attained the similar damage stage as E-glass/vinyl ester in the specimen due to slow accumulation of multiple cracking. Manjunatha et al. [27] studied respond of the the hybrid epoxy polymer and neat epoxy polymer with silica and nanoparticles carboxyl-terminated butadiene-acrylonitrile (CTBN) rubber microparticles to the tensile fatigue behaviour. The test was run at frequency

of 1–3 Hz with stress ratio of 0.1 in order to reduce the effect of thermal to fatigue life. Based on the studied, cyclic fatigue life of a the hybrid epoxy polymer/hybrid GRPF composite composite was about six to ten times higher than neat-epoxy polymer/GFRP—neat epoxy matrix due to hybrid epoxy polymers has lower crack growth rates.

Wu et al. [44] investigated the fatigue performance hybrid epoxy matrix composite specimens of different layers of two different materials of carbon, glass, basalt, and polyparaphenylenl benzobisoxazole (PBO) fibre. The two different combination layers with ratio of 1:1 with 50% nominal fibre volume fraction for preparing hybrid composite specimens. The CFRP/PBOFRP composites show the best fatigue performance than the rest combination. The BFRP composite obviously less fatigue resistance compared to the CFRP/BFRP hybrid.

## *3.1 Effect of Fibre Volume Fractions*

The quantity of fibre present in composite materials can be expressed by volume fraction ($V_f$). The fibre volume fraction is a ratio of the fibres relative proportion to the laminate's matrix. Generally, the fibre volume fraction contribute nearly most of the properties of the material of the laminate. The higher fibre content proportionally contributes to higher strength, stiffness, and the load-carrying capacity of the composite. However, the ultimate strength of the composite decreases when the fibre volume fraction is adequately high. When the fibre content increases, the amount of matrix decreases in the composite. The optimum value for the fibre volume fraction is 45 to 60% while exceeding the limit causes strength to reduce due to the lack of sufficient resin to transfer the load to the fibres effectively.

Brunbauer and Pinter [9] studied a fatigue behaviour of unidirectional carbon/epoxy composite with fibre orientations of 0, 45, and 90% fibre at a volume fraction of 30 and 55%. Based on the finding, the nominal stress was increasing of 40 in 90% unidirectional laminate for in fibre volume fraction from 30 to 55% as shown in Fig. 5. The matrix cracking and fibre-matrix debonding were recorded as the main damage mode for low fibre fraction composites. For in high fibre fraction composites, the damage mode was fibre pullout. The higher fibre volume fraction was contributed in higher fatigue strength for 45% unidirectional composite.

Abd Allah et al. [1] analysed the fatigue behaviour of GRP rods with various fibre volume fractions for no mean stress. The samples were fabricated by a method of modified. The specimens reached nearly quarter of the initial specimen stiffness at starting phase of the fatigue test cause by effect of machining process which fibre at the surface was cut. The surface show shear crack at surface flaws in glass fibres and the waist of the sample.

Mini et al. [28] studied the fatigue behaviour of glass/epoxy composite (volume fractions of range 34–57%) with frequencies loading at range 7 and 9 Hz. The stress ratio was set at (R) = –1. Based on the study, low fibre volume fraction lost its stiffness slowly owning to matrix cracking and attained a constant value upon an

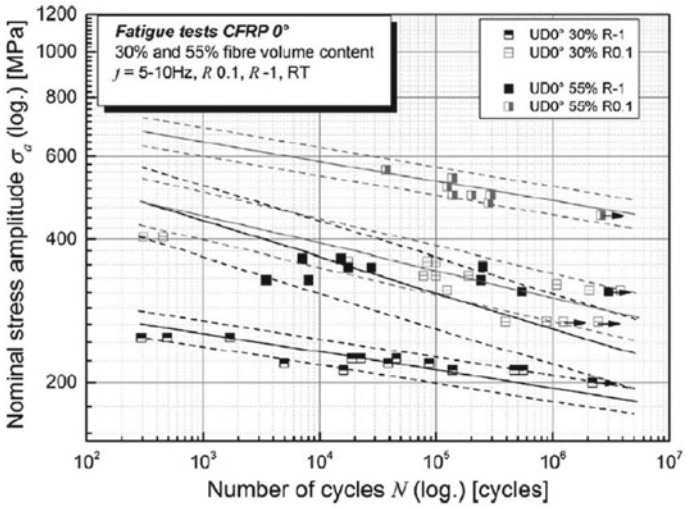


**Fig. 5** Fatigue life of two different fibre volume fraction [9]

increase in loading cycles. While rapid decrement occurred in stiffness of composite having higher fibre volume fraction. It is concluded that fibre cracking is contributing to the reduction of stiffness.

Belmonte et al. [4] studied the effect of the fibre volume fraction of fibre-reinforced polyamide (PA66) specimens (0, 15, 25, 35, and 50%) concerning damage mechanisms in a notched sample. Based on FESEM images, crack initiated near the vicinity of the notch are of the sample. As conclusion, the fatigue strength contribute to crack initiation and final failure of the composite are enhanced with the increase in fibre volume fraction. The relative contribution of the fibre volume fraction increases with increasing the crack propagation to the total lifetime.

## *3.2 Effect of Fibre Orientation*

Besides fibre type and volume fraction, fibre orientation is also other critical character affecting the mechanical properties of fibre reinforced composites. Kadi and Ellyin [24] analysed the fatigue behaviour of unidirectional glass fibre/epoxy composite laminates with fibre orientations; 0°,19°, 45°, 71° and 90°. The laminates were tested under both positive and negative stress ratios at range R = 0.5, 0, and −1 for T-T and T-C fatigue tests. Based on results as shown in Fig. 6, the strength of laminate depends on the fibre orientation which the increase of fibre orientation and the strength is decreased.

Kawai et al. [25] studied the effect of nine different fibre orientation angles having 64% fibre volume on the fatigue behaviour of unidirectional T800H/ Epoxy

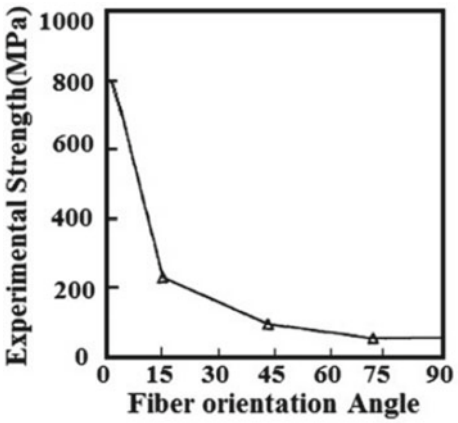


**Fig. 6** Variation of monotonic strength with fibre orientation angle [24]

composite. Figure 7 shows the unidirectional T800H/Epoxy subjected to tensile fatigue under macroscopic failure morphology analysis. The results showed for fibre orientation 0°; the failure was started with parallel splitting arises followed by prolonged to end tap section before pull-out. The ruptured patterns show in a single cross-section parallel to fibre with thickness direction for orientation angles ($0° < \theta < 90°$).

Bernasconi et al. [5] studied T-T axial fatigue tests on short the glass-fibre-reinforced polyamide-6 composite with orientations 0°, 30°, 60° and 90°. The water jet cutting was used to cut the specimens. Referring to Fig. 8, the fatigue strength decrease with the increase in the orientation angle of the samples. The slope of the S-N curve is inversely proportional to the number of cycles.

Figure 9 shows the fatigue life curves (S-N) of GFRP. There are three laminate orientation of 0°, ±45°, and 0°±45° had been tested at three different stress ratios (R) of −0.2, 0.1, and 0.5 based on Huh et al. [21]. The angle of fibre orientation is completely inversely proportional stiffness of the composite.

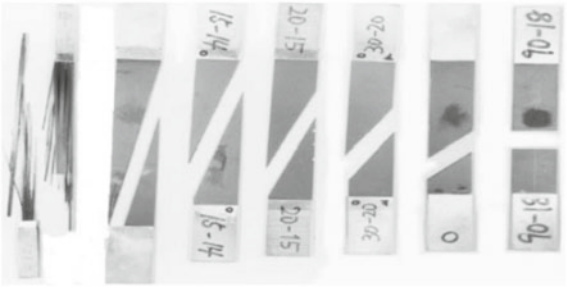

**Fig. 7** Fatigue of tensile coupon specimens at room temperature [25]

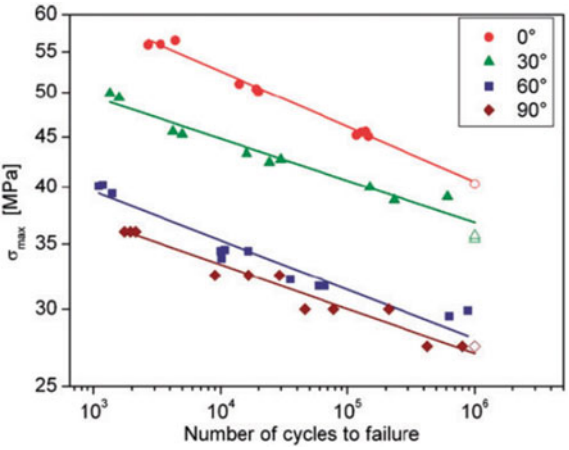


**Fig. 8** S-N curves for different specimens [5]

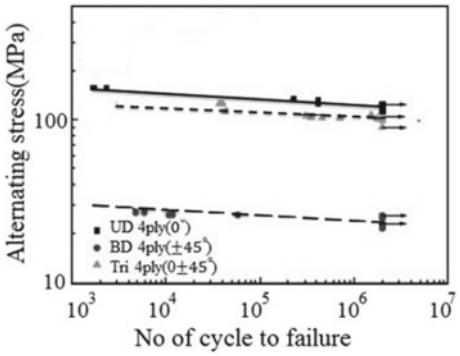


**Fig. 9** S-N curves for composite with different laminates [21]

## *3.3 Effect of Stress Ratio and Mean Stress*

Mean stress and stress ratio are essential parameters in the prediction of fatigue life. Mean stress present average value of maximum stress ($\theta_{max}$) and minimum stress ($\theta_{min}$) while stress ratio (R) is the ratio of the minimum stress ($\theta_{min}$) to the maximum stress ($\theta_{max}$).

The fatigue loading decides by the stress ratio (R) which $-\infty < R < 0$ represents T-C mode, $0<R<1$ represents T-T mode and $1 < R < \infty$ represents C-C mode. Kadi and Ellyin [24] studied thestress ratio (R) subjected to off-axis tensile loading on the fatigue behaviour of unidirectional fibre glass-epoxy specimens. The specimens were subjected to a number of cyclic off-axis tensile loading with stress ratios $R = -1, 0$ and 0.5. Based on their findings, the stress ratio (R) increases cause fatigue rate strength decreases which the slope of the S-log N line for $R = 0.5$ is considerably smaller than that for $R = 0$.

Nasr et al. [32] analyzed the fatigue behaviour of GFRPs samples effect by torsional mean stress on at two fibre orientations $[\pm 45°]_{2s}$ and $[0°, 90°]_{2s}$ with volume fraction ranging from 55 to 65%. The specimens were tested under stress ratios (R) of range between −1 and 0 for five negative with an increment of 0.25. There is only little different strength for different volume fractions specimens which not sufficient to in failure mechanisms. The higher fatigue strength was recorded by samples with $[\pm 45°]_{2s}$ fibre orientation than the sample with $[0°, 90°]_{2s}$ at all stress ratios due to the local stress component. The $[\pm 45°]_{2s}$ samples were subjected to T-C local stress component while $[0°, 90°]_{2s}$ samples subjected to pure local shear stress.

Mortazavian and Fatemi [29] studied the fatigue behaviour of two small glass fibre reinforced thermoplastic composites polyamide-6 (PA6)) and (polybutylene terephthalate (PBT) which effect of mean stress. The samples with different fibre orientations were tested on the various ratios (R= −1, 0.1, and 0.3). Based on the results in Fig. 10 for both longitudinal and transverse directions, significant reducing in fatigue strength under R = 0.1 compared to R = −1.

Based on the study, the mean stresses effect obviously at the low cycle fatigue (LCF) failure compared to the high cycle fatigue (HCF) failure. This situation may arise due to the increased dependency of the maximum stress in this life reign to fatigue life.

Mallick and Zhou [26] studied the effect the HCF strength of short E-glass fibre-reinforced polyamide-6,6 composite on mean stress. Figure 11 shown fatigue performed of GF/PA-6,6 composite at different mean stress. The curve establishes the fatigue strength increased while the stress amplitude decreased as the stress ratio increases. The fatigue strength decreased with increasing mean stress ratio.

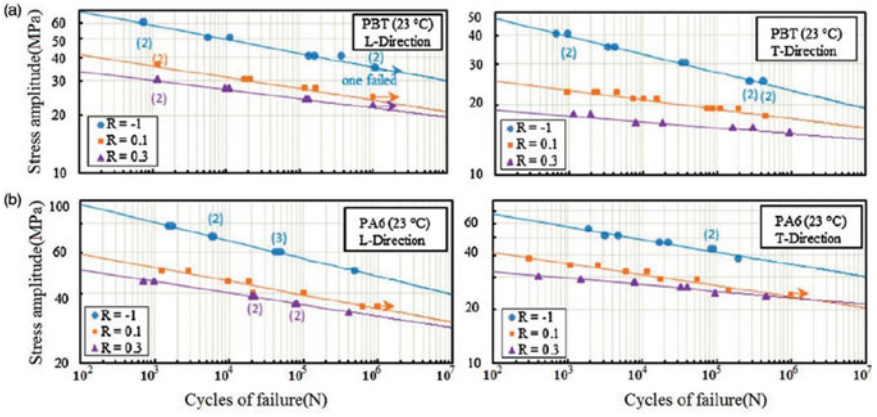


**Fig. 10** The fatigue behaviour of **a** PBTand **b** PA6 in the longitudinal and transverse [29]

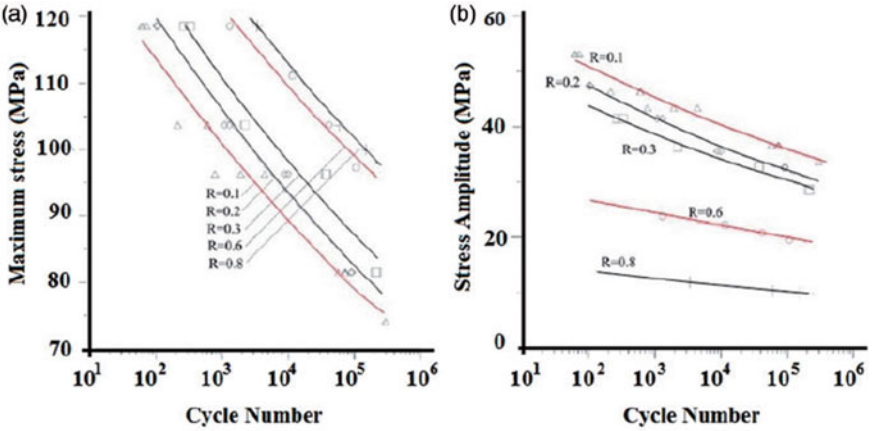


**Fig. 11** S-N plots **a** $\sigma_{max}$ versus N and **b** $\sigma_a$ versus N for short E-glass fibre-reinforced polyamide [26]

## *3.4 Effect of Hysteresis and Frequency*

The loading frequency contributes to hysteresis heating or self-heating of the specimen. The loading frequency affect the strain rate of FRP composite, which significant effecting on the fatigue life. Naturally, the matrix polymers in the form of viscoelastic, at high-frequency composites will achieve glass transition temperature (Tg) for matrix polymers. The polymer composite starts to transform from glassy brittle material into a soft rubbery material. The polypropylene/glass fibre thermoplastic composites with the fibre volume fraction of 0.338 were analysed the effect of frequency on the fatigue behaviour by Ferreira et al. [17]. Under fatigue test at stress ratio, 0 and 0.25 influence of frequency on fatigue strength of unnotched sample was negligible within the range 2–10 Hz.

Barron et al. [2] studied on fatigue behaviour of a carbon fibre/epoxy matrix composite at various the loading frequency (5, 10, and 20 Hz) and different stress. The three specimens with difference orientations were tested on TTF. Results indicate in Table 1 shown the fatigue behaviour of CFRP composite influence by frequency significantly. Both angle-ply and cross-ply laminates show fatigue results highly

**Table 1** Summary of the effects of frequency on fatigue behaviour of carbon fibre-reinforced polymer composites [2]

| Composite | Unidirectional | Cross-ply | | Angle-ply | |
|---|---|---|---|---|---|
| Increased frequency | Too | 5–10 Hz | 10–20 Hz | 5–10 Hz | 10–20 Hz |
| Fatigue life | Much | Decrease | Increase | Increase | Decrease |
| Max. strain | Scatter | Increase | Decrease | Decrease | Increase |
| Sample temperature | | Increase | Increase | Increase | Increase |

depending on dynamic mechanical response while the unidirectional laminates were indeterminate due to a large amount of scattering in the S-N curve.

Flore et al. (Eftekhari and Fatemi [15]) studied the very high cycle fatigue (VHCF) regime on the fatigue behaviour of GFRPs. The conventional methods were replaced by Ultrasonic fatigue testing (UFT) with capability to reduce the testing time up to factor of 100. The results of the conventional fatigue tests are equated with the results of the UTF. Based on both tests, stiffness loss and plasticity has a small difference in the fibre direction. The S-N curve becomes flattered in the section of $10^8$–$10^{10}$ fatigue cycles cause The fatigue limit cannot be determined.

## 4 Summary

Composites have gained considerable popularity over the last five decades due to unique materials behaviour likes higher stiffness, higher strength, improved fatigue behaviour, tailored and corrosion resistance. The fatigue behaviour of composite materials is complex which initiated by fibre breakage, matrix cracking, fibre-matrix debonding, delamination and fully fracture. The fatigue performance of composites is influenced by the composite system itself. Particularly influential parameters include; fibre and matrix properties, lay-up sequence, residual stresses due to the manufacturing process or due to discontinuities and the maximum to minimum ratio of stress endured by the material, ply orientation, the fibre/matrix fractions, and environmental conditions affecting the composite components.

## References

1. Allah MHA, Abdin EM, Selmy AI, Khashaba UA (1996) Effect of fibre volume fraction on the fatigue behaviour of GRP pultruded rod composites. Compos Sci Technol 56(1):23–29. https://doi.org/10.1016/0266-3538(95)00125-5
2. Barron V, Buggy M, McKenna NH (2001) Frequency effects on the fatigue behaviour on carbon fibre reinforced polymer laminates. J Mater Sci 36(7):1755–1761. https://doi.org/10.1023/A:1017576725885
3. Bathias C (1991) Fracture and fatigue of high performance composite materials: mechanisms and prediction. Eng Fract Mech 40(4):757–783. https://doi.org/10.1016/0013-7944(91)90234-R
4. Belmonte E, Monte M, De Hoffmann C-J, Quaresimin M (2017) Damage initiation and evolution in short fiber reinforced polyamide under fatigue loading: influence of fiber volume fraction. Compos Part B Eng 113:331–341. https://doi.org/10.1016/j.compositesb.2017.01.023
5. Bernasconi A, Davoli P, Basile A, Filippi A (2007) Effect of fibre orientation on the fatigue behaviour of a short glass fibre reinforced polyamide-6. Int J Fatigue 29(2):199–208. https://doi.org/10.1016/j.ijfatigue.2006.04.001
6. Bizeul M, Bouvet C, Barrau JJ, Cuenca R (2011) Fatigue crack growth in thin notched woven glass composites under tensile loading. Part I: experimental. Compos Sci Technol 71(3):289–296. https://doi.org/10.1016/j.compscitech.2010.11.019

7. Boller KH (1969) Fatigue fundamentals for composite materials. In Yurenka S (ed) Composite materials: testing and design, pp 217–235. https://doi.org/10.1520/STP49819S
8. Branco CM, Ferreira JM, Richardson MOW, Fael P (1992) Fatigue behaviour of a phenolic matrix composite. Int J Fatigue 14(6):367–376. https://doi.org/10.1016/0142-1123(92)90224-Z
9. Brunbauer J, Pinter G (2015) Effects of mean stress and fibre volume content on the fatigue-induced damage mechanisms in CFRP. Int J Fatigue 75:28–38. https://doi.org/10.1016/j.ijfatigue.2015.01.014
10. Brunbauer J, Stadler H, Pinter G (2015) Mechanical properties, fatigue damage and microstructure of carbon/epoxy laminates depending on fibre volume content. Int J Fatigue 70:85–92. https://doi.org/10.1016/j.ijfatigue.2014.08.007
11. Bureau M, Denault J (2000) Fatigue behavior of continuous glass fiber composites: effect of the matrix nature. Polym Compos 21:636–644. https://doi.org/10.1002/pc.10219
12. Caprino G, D'Amore A (1998) Flexural fatigue behaviour of random continuous-fibre-reinforced thermoplastic composites. Compos Sci Technol 58(6):957–965. https://doi.org/10.1016/S0266-3538(97)00221-2
13. Curtis PT (1987) A review of the fatigue of composite materials. Technical Report 87031, Royal aircraft establishment
14. Curtis PT (1989) The fatigue behaviour of fibrous composite materials. J Strain Anal Eng Design 24(4):235–244
15. Eftekhari M, Fatemi A (2016) On the strengthening effect of increasing cycling frequency on fatigue behavior of some polymers and their composites: experiments and modeling. Int J Fatigue 87:153–166. https://doi.org/10.1016/j.ijfatigue.2016.01.014
16. Erden S, Sever K, Seki Y, Sarikanat M (2010) Enhancement of the mechanical properties of glass/polyester composites via matrix modification glass/polyester composite siloxane matrix modification. Fibers Polym 11(5):732–737. https://doi.org/10.1007/s12221-010-0732-2
17. Ferreira JAM, Costa JDM, Richardson MOW (1997) Effect of notch and test conditions on the fatigue of a glass-fibre-reinforced polypropylene composite. Compos Sci Technol 57(9):1243–1248. https://doi.org/10.1016/S0266-3538(97)00052-3
18. Harris B (2003) Fatigue in composites: science and technology of the fatigue response of fibre-reinforced plastics
19. Hojo M, Matsuda S, Tanaka M, Shojiro O, Murakami A (2006) Mode I delamination fatigue properties of interlayer-toughened CF/epoxy laminates. Compos Sci Technol 66:665–675. https://doi.org/10.1016/j.compscitech.2005.07.038
20. Hollaway LC (2010) A review of the present and future utilisation of FRP composites in the civil infrastructure with reference to their important in-service properties. Construct Build Mater 24(12):2419–2445. https://doi.org/10.1016/j.conbuildmat.2010.04.062
21. Huh Y-H, Lee J-H, Kim D-J, Lee Y-S (2012) Effect of stress ratio on fatigue life of GFRP composites for WT blade. J Mech Sci Technol 26(7):2117–2120. https://doi.org/10.1007/s12206-012-0526-0
22. Hyakutake H, Hagio T, Yamamoto T (1993) Fatigue failure criterion for notched FRP plates. JSME Int J Ser A Mech Mater Eng 36(2):215–219. https://doi.org/10.1299/jsmea1993.36.2_215
23. Jones CJ, Dickson RF, Adam T, Reiter H, Harris B, Kelly A (1984) The environmental fatigue behaviour of reinforced plastics. Proc R Soc London A Math Phys Sci 396(1811):315–338. https://doi.org/10.1098/rspa.1984.0125
24. Kadi El, H, Ellyin F (1994) Effect of stress ratio on the fatigue of unidirectional glass fibre/epoxy composite laminae. Composites 25(10):917–924. https://doi.org/10.1016/0010-4361(94)90107-4
25. Kawai M, Yajima S, Hachinohe A, Takano Y (2001) Off-axis fatigue behavior of unidirectional carbon fiber-reinforced composites at room and high temperatures. J Compos Mater 35(7):545–576. https://doi.org/10.1177/002199801772662073

26. Mallick PK, Zhou Y (2004) Effect of mean stress on the stress-controlled fatigue of a short E-glass fiber reinforced polyamide-6,6. Int J Fatigue 26(9):941–946. https://doi.org/10.1016/j.ijfatigue.2004.02.003
27. Manjunatha C, Sprenger S, Taylor A, Kinloch A (2010) The tensile fatigue behavior of a glass-fiber reinforced plastic composite using a hybrid-toughened epoxy matrix. J Compos Mater 44:2095–2109. https://doi.org/10.1177/0021998309360943
28. Mini KM, Lakshmanan M, Mathew L, Mukundan M (2012) Effect of fibre volume fraction on fatigue behaviour of glass fibre reinforced composite. Fatigue Fract Eng Mater Struct 35(12):1160–1166. https://doi.org/10.1111/j.1460-2695.2012.01709.x
29. Mortazavian V, Fatemi A (2015) Effects of mean stress and stress concentration on fatigue behavior of short fiber reinforced polymer composites. Fatigue Fract Eng Mater Struct 39. https://doi.org/10.1111/ffe.12341
30. Myers T, Kytomaa H, Smith TR (2007) Environmental stress-corrosion cracking of fiberglass: lessons learned from failures in the chemical industry. J Hazard Mater 142:695–704. https://doi.org/10.1016/j.jhazmat.2006.06.132
31. Nagalingam R, Sundaram S, Stanly B, Retnam J (2010) Effect of nanoparticles on tensile, impact and fatigue properties of fibre reinforced plastics. Bull Mater Sci 33(5):525–528. https://doi.org/10.1007/s12034-010-0080-2
32. Nasr M, Abouelwafa M, Gomaa A, Hamdy A, Morsi E (2005) The effect of mean stress on the fatigue behavior of woven-roving glass fiber-reinforced polyester subjected to torsional moments. J Eng Mater Technol Trans ASME 127. https://doi.org/10.1115/1.1925285
33. Newaz GM (1985) Influence of matrix material on flexural fatigue performance of unidirectional composites. Compos Sci Technol 24(3):199–214. https://doi.org/10.1016/0266-3538(85)90073-9
34. Nixon-Pearson OJ, Hallett SR, Withers PJ, Rouse J (2013) Damage development in open-hole composite specimens in fatigue. Part 1: experimental investigation. Compos Struct 106:882–889. https://doi.org/10.1016/j.compstruct.2013.05.033
35. Owen MJ, Howe RJ (1972) The accumulation of damage in a glass-reinforced plastic under tensile and fatigue loading. J Phys D Appl Phys 5(9):1637–1649. https://doi.org/10.1088/0022-3727/5/9/319
36. Pink E, Campbell JD (1974) Deformation characteristics of reinforced epoxy resin. J Mater Sci 9(4):658–664. https://doi.org/10.1007/BF02387541
37. Rahman S, Abdul Majid MS, Mohd Jamir MR, Basaruddin K, Peng T (2017) Effect of stress ratio on the fatigue behaviour of glass/epoxy composite. J Phys Conf Ser 908:12030. https://doi.org/10.1088/1742-6596/908/1/012030
38. Reifsnider KL, Jamison R (1982) Fracture of fatigue-loaded composite laminates. Int J Fatigue 4(4):187–197. https://doi.org/10.1016/0142-1123(82)90001-9
39. Reifsnider KL, Schulte K, Duke JC (1983) Long-term fatigue behavior of composite materials. In Brien TKO (ed) Long-term behavior of composites, pp 136–159. https://doi.org/10.1520/STP31820S
40. Stinchcomb WW, Bakis CE (1991) Fatigue behavior of composite laminates. In Reifsnider KL (ed) Fatigue of composite materials, pp 105–180. https://doi.org/10.1016/B978-0-444-70507-5.50008-1
41. Sturgeon JB (1977) Fatigue of multi-directional carbon fibre-reinforced plastics. Composites 8(4):221–226. https://doi.org/10.1016/0010-4361(77)90106-9
42. Talreja R (1999) Damage mechanics and fatigue life assessment of composite materials. Int J Damage Mech 8(4):339–354. https://doi.org/10.1177/105678959900800404
43. Vasiukov D, Panier S, Hachemi A (2015) Direct method for life prediction of fibre reinforced polymer composites based on kinematic of damage potential. Int J Fatigue 70:289–296. https://doi.org/10.1016/j.ijfatigue.2014.10.004
44. Wu Z, Wang X, Iwashita K, Sasaki T, Hamaguchi Y (2010) Tensile fatigue behaviour of FRP and hybrid FRP sheets. Compos Part B Eng 41(5):396–402. https://doi.org/10.1016/j.compositesb.2010.02.001

45. Xu HHK, Ostertag CP, Braun LM, Lloyd IK (1994) Effects of fiber volume fraction on mechanical properties of SiC-fiber/Si3N4-matrix composites. J Am Ceram Soc 77(7):1897–1900. https://doi.org/10.1111/j.1151-2916.1994.tb07068.x
46. Zhuang H, Wightman JP (1997) The influence of surface properties on carbon fiber/epoxy matrix interfacial adhesion. J Adhes 62(1–4):213–245. https://doi.org/10.1080/00218469708014570

# Predictive Engineering in Structural Application


**K. Balasubramanian, K. Sunitha, and N. Rajeswari**

*The best way to predict your future is to create it.*
—Abraham Lincoln

**Abstract** The wide variety of fiber reinforced composites are used in structural applications like in construction beams, columns; bridges, storage tanks, pipe lines and pressure vessels and also in other corrosion-resistant equipments. They find their extensive usage in industries, civil constructions, automotives, naval and marine applications with crucial differences in engineering loading conditions, operating conditions and environment. Although most of the fiber reinforced composites proclaims the advantages of high specific strength at low weight and greater stiffness with promising durability, due to the instantaneous undesirable load conditions, harsh handling or operating conditions that is when subjected to conditions beyond its working capability and change in environmental conditions, test the endurance to required performance and durability of the material. The well-known fact is that structural maintenance cost is a major expense in case of any industries or in Nation building process. Conventionally, the structural maintenance is consciously regulated on preplanned fixed schedules to ensure reliability. Most scheduled maintenance is designed to be very frequent to achieve a desirable level of safety against malfunction or failure. ***Predictive maintenance*** *monitors the performance and condition of equipment during normal operation to reduce the likelihood of failures.* The Predictive maintenance aims at low maintenance frequency by reducing the Reactive Maintenance without incurring much cost and time in Preventive Maintenance. With the application of sensor technology, advanced software tools for modeling, integrated simulation capabilities and data analytics, it is possible to sense the symptoms and predict the occurrence of structural dysfunctionality. When there is automatic and

K. Balasubramanian (✉)
Department of Mechanical Engineering, Bharath Institute of Higher Education and Research, Chennai, Tamilnadu, India
e-mail: balaraji1974@gmail.com

K. Sunitha · N. Rajeswari
Department of Mechanical Engineering, St. Peter's Institute of Higher Education and Research, Chennai, Tamilnadu, India

© Springer Nature Singapore Pte Ltd. 2021

M. Jawaid et al. (eds.), *Structural Health Monitoring System for Synthetic, Hybrid and Natural Fiber Composites*, Composites Science and Technology,
https://doi.org/10.1007/978-981-15-8840-2_10

continuous monitoring to sense or foresight the structural damage, this would enable to plan for maintenance activities in accordance with the predicted safety state of the structures rather than following traditional fixed schedule maintenance. When the collected predictive database is coupled with the maintenance decision-making, the Predictive Engineering is evolved. This requires the development of software model of the structure that have precisely the same behavior of the actual structural product. When it comes to synthetic, natural and hybrid fiber reinforced composites they behave differently with respect to structural, thermal, and fatigue properties. So they require dedicated modeling. The developed predictive digital model should remain synchronies in accordance with the entire product life cycle of real product. Predictive Engineering Analytics is a design and product development approach that uses computer integrated models, new software tools to let the simulation play active role in product design stage and predict the performance under nominal working conditions and also identify undesirable operating parameters and conditions that eventually leads to failure. With respect to the structural applications, from very early stage of design cycle itself, the Predictive Engineering Analytics predicts the behavior of the structural materials for all their functional requirements and changes in their physical and performance aspect on long run. This incorporates predictive functionalities into the system models, simulate their operations in system generated working conditions and the result information are fed back to design of structural elements. At the very early stage of product development cycle, the system modeling and simulation for testing enact a real time evaluation on the composite behavior in its application point. This type of system-based product development works towards reducing physical test, inspection and repair. The structural materials, monitoring machines and equipments are when connected by smart technologies, can also be accessed via cloud to predict the location and time of failures. This provokes maintenance actions thereby avoiding interruption in industrial process i.e. unnecessary downtime or even fatal accidents. The predictive Engineering has moved to an era where the material of the structure or product can remember the operating conditions and behavior of its operator, so that it can presume the next level of activities like prediction of failure and subsequent maintenance actions. The Predictive Maintenance is the most promising maintenance strategy that has proficiency to widen its scope as Predictive Engineering with more digital sophistications so as to develop materials for reliable structural applications.

**Keywords** Predictive maintenance · Condition monitoring · Predictive engineering · Non-destructive testing · Predictive modeling · Predictive engineering analytics

The Predictive Maintenance (PM) is the maintenance that predicts the occurrence of system components failures, followed by the activities to prevent the failures that are scheduled under the corrective maintenance. Predictive Maintenance (PM) aims at monitoring and recording the condition of equipment under normal operation to predict the likelihood of failures, inorder to repair or replace the components that are heading to failures and also to perform activities to eliminate the factors that contribute to predicted failures. PM is also known as Condition-Based Maintenance, where the determination of the deteriorating performance of components is identified and maintenance is carried out. This type of maintenance proclaims not only the prevention of unexpected failures, in addition promises the cost saving over scheduled preventive maintenance. The Preventive Maintenance, where the maintenance activities are scheduled based on previous life statistics data, but in contrast the Predictive Maintenance counts on actual existing condition of the equipment [1].

## 1 Predictive Maintenance and Condition Monitoring

The core activity of Predictive Maintenance is condition monitoring that includes continuous monitoring of systems during its operation cycle. The monitoring prospects the indication of the condition or health status of the system components in order to establish optimum operating conditions by appropriate safety maintenance [2]. The three feature of condition monitoring are:

- Online Condition Monitoring
- Periodic Condition Monitoring
- Remote Condition Monitoring

**Online Condition Monitoring**: Data is collected during all critical operations of the system including the start and end condition data. Example, machine condition data collected during change in operating parameters and when there is change in relative positioning of tool and workpiece.

**Periodic Condition Monitoring**: Trends are figured out of basic routine check up like oil measurement that can contribute to the clear cut indication of the condition of the operating system or machines.

**Remote Condition Monitoring**: Here the monitoring and recording of measurement data takes place from remote location away from the device. Thus the condition monitoring is performed without intruding in the midst of the intended operations of the device.

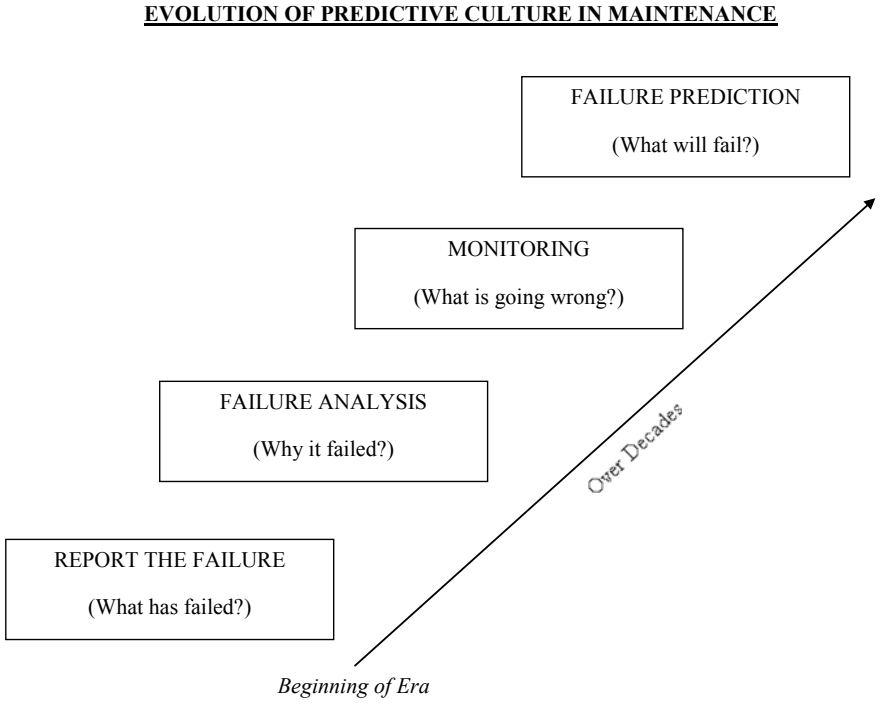


## 2 Benefits of Predictive Maintenance

- Cutting down the total cost of maintenance by eradicating the 'Reactive Maintenance' and on the other hand without incurring much cost and time on scheduled 'Preventive Maintenance' as well.
- Eliminating any unexpected equipments breakdowns that bring the whole system to halt.
- Reducing unnecessary damage to equipment by maintaining facilities at appropriate operating conditions at reduced maintenance labour cost and time.
- Minimizing the inventory of spare parts.
- Attaining high productivity as per scheduled work priority without any interruption to attend on any unplanned emergency maintenance activities [3].

Predictive Maintenance monitoring identifies the degrading conditions and derives trends to schedule for repair. The main features that are required for execution of PM are data collection, data processing, diagnosing, failure predictions or fault detection and scheduling for maintenance [2]. So here the basic point is to switch over from the conventional suffer and set right maintenance practice to predict and prevent maintenance approach. To assess the equipment or material condition PM employs

Non-destructive Testing technologies that include Visual Inspection, Vibration Analysis, Eddy Current Inspection, Thermo Graphic Inspection, Acoustic Inspection, Ultrasonic Inspection etc. [4].

## 3 Predictive Maintenance in Structural Materials

The wide variety of composites are used in structural applications like in construction beams, columns; bridges, storage tanks, pipe lines and pressure vessels and also in other corrosion-resistant equipments [1]. They find their extensive usage in industries, civil constructions, automotives, naval and marine applications with crucial differences in engineering loading conditions, operating conditions and environment. Although most of the composites proclaims the advantages of high specific strength at low weight and greater stiffness with promising durability, due to the instantaneous undesirable load conditions, harsh handling or operating conditions that is when subjected to conditions beyond its working capability and change in environmental conditions, test the endurance to required performance and durability of the material [5].

The well known fact is that structural maintenance cost is a major expense in case of any industries or in Nation infrastructure building process. Conventionally, the structural maintenance is consciously regulated on preplanned fixed schedules to ensure reliability. Most scheduled maintenance is designed to be very frequent to achieve a desirable level of safety against malfunction or failure. The Predictive Maintenance aims at low maintenance frequency by reducing the Reactive Maintenance without incurring much cost and time in Preventive Maintenance [5]. Establishing a Predictive Maintenance programme for structural materials, the required steps, include:

- Analyzing the need and installation history of structural components.
- Reviewing available records on component failures, material defects and threat on workplace safety.
- Establishing strategy to adopt PM.
- Making the stake holders aware about PM.
- Tracking the existing material inventory status.
- Selecting equipments and instruments for monitoring, recording, transferring and analysis of data.
- Framing system details based on individual structural components.
- Evaluating any existing proactive maintenance.
- Mapping the structural components that needed to be including for study and decision on tests to be carried out.

- Designing the program's criticality to decide PM frequency and nature of schedule.
- Checking for anticipated resources to establish PM.
- Designating safety personnel and labors with their individual roles and responsibilities for PM.
- Training the personnel and labors and also upgrading the existing equipments.
- Masterminding the PM program and incorporating it into the scheduling network.

## 4 General Working Strategy of PM

Predictive Maintenance employs condition-monitoring devices and equipment to evaluate performance of a system in real time. A significant element in any working model of PM at recent times is the Internet of Things (IoT). IoT enables for various aspects of a system to be web connected to share, analyze and utilize the data to perform together the intended function. IoT depends up on sensors to collect information, diagnosis it and determine the areas that need attention for predictive maintenance [2]. In case of Predictive Maintenance on machinery requires sensors for study on vibration, oil analysis, infrared imaging, and general equipment observation. Whereas in the case of the PM for structural application requires sensors predominately for checking the health status of the functional materials in terms of structural strains, vibrations, external loading, internal pressure, fatigue on long term loading, change in thermal behavior, sensors for monitoring humidity for material degradation by corrosion, sensors to detect cracks etc. [5]. Such Continuous monitoring on structural health provides ample data for identifying the real-time status of material properties that eventually contributes to maintenance planning and scheduling thereby eliminating the risk of possible disasters. The Structures to be monitored with sensors may include welded component, tanks, cranes etc. With the application of sensor technology, advanced software tools for modeling, integrated simulation capabilities and data analytics, it is possible to sense the symptoms and predict the occurrence of structural dysfunctionality [2].

Selection of correct techniques for carrying out structural condition monitoring is most crucial which is to be done by consulting with equipment manufacturers and considering the guidance of experts in condition monitoring. When there is automatic and continuous monitoring to sense or foresight the structural damage, this would enable to plan for maintenance activities in accordance with the predicted safety state of the structures rather than following traditional fixed schedule maintenance [2].

## WORKING STRATERGY OF PREDICTIVE MAINTENANCE

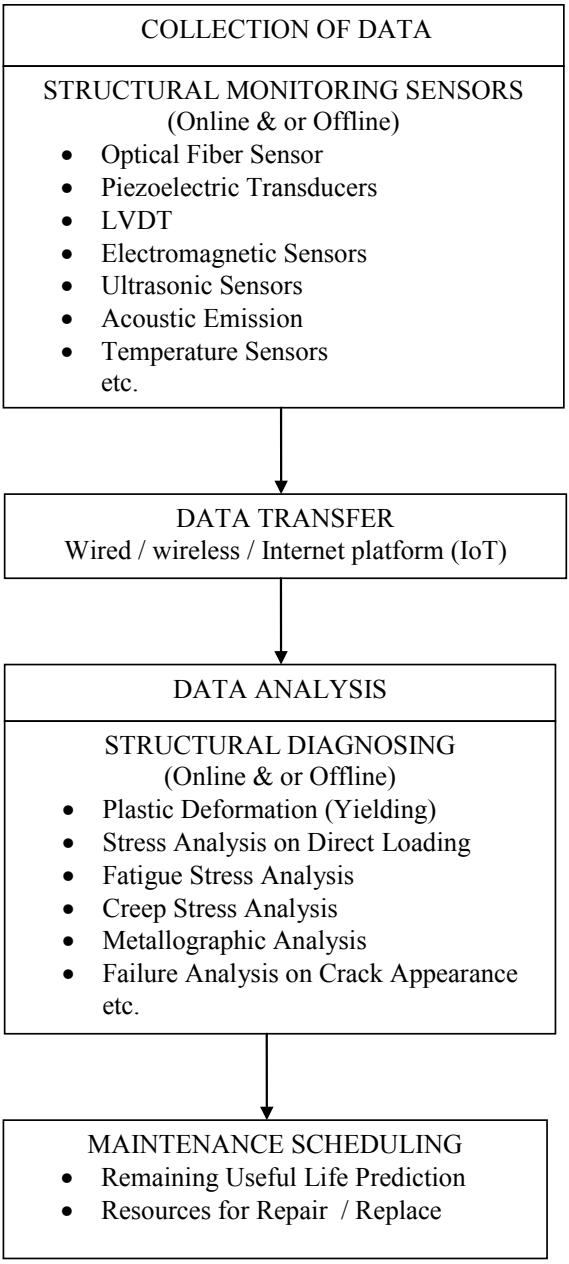

## 5 Monitoring Techniques and Sensors for PM

Latest developments in sensors have made possible for the Structural Health Monitoring (SHM) systems be successfully implemented in various structures like bridges, buildings, power plants, and aircrafts [1]. The sensors can be wired to wireless that are employed in the continual monitoring of structural materials by real time data gathering. For designing an efficient sensing system, the identification of appropriate kind of sensors is crucial. A well integrated networks of all sensors systems contributes to be existing current condition of the structure under usage by collecting measurements on various parameters like stress, strain, deformation, vibration, temperature etc. [3, 4].

There are numerous sensors which are basically from Non Destructive Testing and evaluation category is available for structural monitoring. Few among them that are widely used for fundamental parameters sensing are discussed below.

I. **Fiber Optic Sensors**:

Fiber optic sensors have been under great advancement in recent times. In structural materials, these sensors are used for strain monitoring, structural displacements, recording vibration frequencies and in measuring acceleration, pressure, temperature etc.

II. **Piezoelectric Accelerometer**:

A piezoelectric accelerometer is an electromechanical device accelerometer that works based on piezoelectric effect that produces electric charge when mechanical stress (due to acceleration) is applied. This is used to measure structural dynamic changes in terms of acceleration, low range fatigue shocks and vibration.

III. **Vibrating Wire Sensor**:

It is a transducer is comprises of vibrating wire with a tension spring. Any deformation in the structural elements leads to change in wire length due to the tension spring attached to it. So such disturbance causes resonance frequency in wire that is converted to sensible signals. It is used for monitoring strain and crack width measurements.

IV. **Linear Variable Differential Transformer (LVDT)**:

LVDT is an electromechanical sensor, employed for measuring minor scale linear displacements. Displacements ranging in few millimeters can be measured. In structural monitoring applications these LVDT sensors are used for recording displacements due to operating loads and temperature changes.

V. **Strain Gauging Sensor**:

It comprises load cell which converts any change in the dimension of the structural member to electric signals. It is used to measure the strain level in the structural materials.

VI. **Acoustic Emission Sensor**:

It is based on the principle that the Quantitative and qualitative properties of acoustic emission waves, (both sound and ultrasound waves) depend upon the material properties of generating sources and environmental factor. Acoustic emission sensor equipment is capable of identifying and analyzing acoustic emission waves through air gaps in cracks, leaks, knocks, etc. AE sensors are capable of picking up change in stress waves that are generated from continuous material and also from discontinuities or defects as well.

VII. **Temperature Sensors**:

The materials of structural members are exposed to the ambient temperature that affects the mechanical properties of the materials. Degradation of the materials due to environmental factors also occurs. Thermocouples are employed in the temperature sensors to measure the change in temperature at the points of interest at the structures.

In addition to the above discussed sensor, there exist vast varieties of sensor equipments for structural monitoring such as galvanostatic pulse method, electrochemical impedance spectroscopy, ultrasonic pulse velocity, surface penetration radar, X-ray radiography, infrared thermograph, etc. [3].

Data provided by these monitoring techniques are basically quantitative and discontinual with time and space. Such data is not sufficient to furnish the input requirements for future performance prediction. Latest advancement in remote sensing technologies are capable of providing real time data and analysis almost in continuous, time scale for the assessment of structural health status [6].

## 6 Predictive Engineering

When the collected predictive database is coupled with the maintenance decision-making, the Predictive Engineering is evolved. This requires the development of software model of the structure that has precisely the same behavior of the actual structural product. When it comes to synthetic, natural and hybrid fiber reinforced composites they behave differently with respect to structural, thermal, and fatigue properties [5]. So they require dedicated modeling. The developed predictive digital model should remain synchronies in accordance with the entire product life cycle of real product.

## 7 Predictive Modeling

Identification of deteriorating components and prediction of future performance is essential for evaluation of remaining service life. Due to earlier mentioned limitations, the data obtained from Non Destructive Examination and other condition monitoring techniques are inadequate for performance prediction [7]. Researchers are undertaken for development of predictive models for composite materials of varying ranges of complexity. These models are developed based on experimental data of predetermined multiple interacting physical conditions (inspection results through NDT and SHM) to predict the material behavior. Hence for such prediction, probabilistic approach modeling is most applicable [6]. Information provided through inspections is discontinuous in space and intermittent in time. Hence in these models the boundary limitations of their input parameters are accompanied with uncertainties, which limit their effective range of applications. These uncertainties in information should be prominently integrated with effective decision support tool for assessment of the deteriorating structures [8]. The uncertainty can be minimized by continuous updation on information is made available. The probabilistic predictive models, can be updated every time based on the results obtained from continuous monitoring and inspection that projects the actual performance of members in real time [6]. This would improve the reliability of the estimated future performance by minimizing the critical areas of uncertainty in the probabilistic models. So developed predictive models is capable of providing early foresight on potential area of failures and estimate the rate deterioration in the structural members.

With the development in software predictive modeling systems and increase in computing speed, the responses to stimuli of continuous real time scenarios are achieved at ease. The software works on the basis of carefully designed predictive models [8]. One of the effective approaches for handling with probabilistic evaluation and prediction of material failure is by the Bayesian approach. In recent time predictive performance by Bayesian model has gained its popularity over the precedents models like decision tree forecasting model, regression model and neural-network model [9]. The software predictive modeling is integral requisite of any Predictive Analytics.

## 8 Predictive Analytics

Predictive Analytics is a process of exercising data analytics to make predictions on future outcomes by using historical data. Predictive analytics develop statistical modeling and machine learning that captures and work on real time data to foresight the future performance [8]. Based on the predictions, decisions are taken for required actions to optimize the performance to avoid the predicted failure or malfunction. The predictive analytics can bring about future insights with an appreciable level of precision. The General steps involved in Predictive analytics are Data Collection, Data

Analysis, Statistics, modeling and deployment [9]. This basic predictive analytics workflow has been conveniently applied to predict the performance of the structural materials under use. The sophisticated predictive analytics tools and models enable us to peruse the past tested and current sensed data to reliably predict the future performance and forecast the failure of any structural member using predictive analytics, grid operators can turn this information into actionable insights [8].

## *8.1 Predictive Analytics Process for Structural Members*

Typical process flow steps of predictive analytics when applied for prediction of material performance for structural members are as follows:

1. **Data Collection**:

The information on the structural material is gathered from visual inspections and from previously conducted Non Destructive Testing and Evaluations. In addition the data is collected based on structural health monitoring techniques [7].

2. **Data Processing**:

The aggregation of different data sources is carried out. The generated data from early stage testing and evaluation and information from various subsystems i.e. various sensory data from intended points of structural member based on loading of member, temperature, humidity etc., are processed [8].

3. **Developing algorithm**:

It is the process of making the machine learn, wherein the processed data are statistically analysed and the critical parameters to be considered for assessment are integrated. The correlation of the governing factors of any materials such as grain microstructure, mechanical properties, load bearing capacity, its interaction and behavior with the environment are frame [7, 8].

4. **Predictive Model**:

An accurate predictive model is developed using framed algorithm that responds to the real time data received from sensors. Development and function of predictive model in perspective for structural members has already been discussed earlier [3, 9].

5. **Deployment of Model**:

The predictive model is integrated with the decision making systems. Based on the outcomes of the predictive analysis the decision for appropriate actions are taken to optimize the variables inorder to improve or sustain the betterment of the structures

and also suggestion to repair or replace any portion of the structural member if required are provided to prevent the failure of the sub structure or the whole [3, 9].

MATLAB and Simulink software are widely used for predictive analytics.

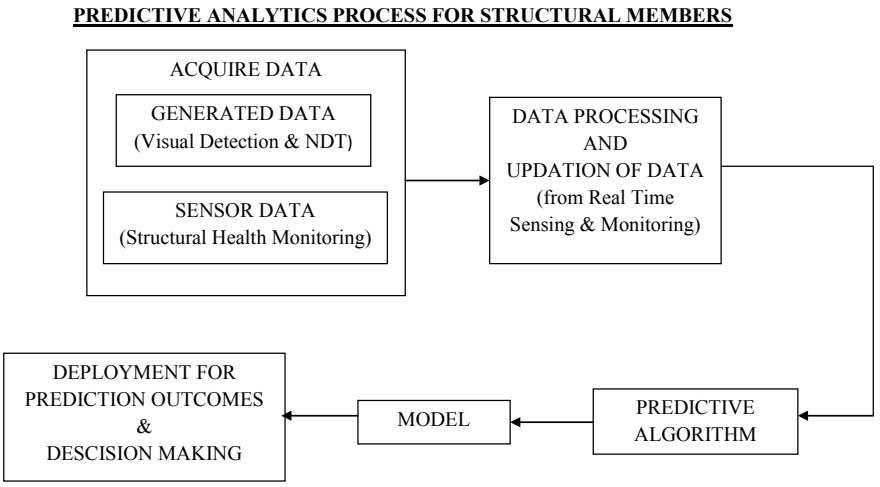


## 9 Predictive Engineering Analytics (PEA)

PEA is a design and product development approach that uses computer integrated models, new software tools to let the simulation play active role from the product design stage itself for prediction of the performance under nominal working conditions and identification of undesirable operating parameters that can eventually leads to failure.

PEA encompass multidisciplinary collaborative simulation and inspection tests associated with intelligent data computing and analytics, to develop digital clone that can predict the real time performance of the product throughout its lifecycle. The aim of implementing a predictive engineering analytics is to promote faster innovation on range of complex products with greater degree of performance [10]. PEA is regarded as upgraded evolution of product development strategy. PEA integrates various technologies including simulations for computational solid mechanics, computational fluid dynamics, finite element analysis, intelligent sensors and controls, testing, visualization, data analytics and prospects of creative design to establish product development engineering for complex systems [7]. In PEA approach, enables the manufacturers to build digital clones and control them in-sync with the real product to replicate responses in digital version with respect to real time stimuli in operating condition [10].

With respect to the structural applications, from very early stage of design cycle itself, the PEA predicts the behavior of the structural materials for all their functional requirements and changes in their physical and performance aspect on long run. This incorporates predictive functionalities into the system models, simulate their operations in system generated working conditions and the result information are fed back to design of structural elements [7]. At the very early stage of product development cycle, the system modeling and simulation for testing enact a real time evaluation on the material behavior in its application point. This type of system based structural product development works towards reducing physical test, inspection and repair. The structural materials, monitoring machines and equipments are when connected by smart technologies, can also be accessed via cloud to predict the location and time of failures [10]. This provokes maintenance actions thereby avoiding interruption in industrial process i.e. unnecessary downtime or even fatal accidents.

## 10 Conclusion

The Predictive Engineering has moved to an era where the material of the structure or product can remember the operating conditions and behavior of its operator, so that it can presume the next level of activities like prediction of failure and subsequent maintenance actions. The Predictive Maintenance is the most promising maintenance strategy that has proficiency to widen its scope as Predictive Engineering with more digital sophistications so as to develop materials for reliable structural applications.

## References

1. Anderson B, Kline T (2015). Predictive maintenance for infrastructure. Nuclear Plant J 36–48
2. Coleman C, Damodaran S, Chandramouli M, Deuel E (2017). Making maintenance smarter-predictive maintenance and the digital supply network, pp 1–21. Deloitte University Press. dup ress.deloitte.com
3. Romano P, Brito P (2016) Degradation monitoring systems for a BIM maintenance approach. Provisional https://doi.org/10.5772/intechopen.81433
4. Shahsavari V (2020) Structural health monitoring expert, sensors for structural health monitoring. Structural Health Monitoring Newsletter
5. Karbhari VM, Chin JW, Hunston D, Benmokrane B, Juska T, Morgan R, Lesko JJ, Sorathia U, Reynaud (2003) Durability gap analysis for fiber—reinforced polymer composites in civil infrastructure. ASCE J Compos Construct 7(3):238–247
6. Rafiq MI (2015) Structural health monitoring for maintenance management of deteriorating structures: current practice and state of the art. In: 2nd international & 6th national conference on earthquake & structures, ACECR of Kerman, Kerman, Iran
7. Guemes A, Fernandez-Lopez A, Pozo AR, Sierra-Perez J (2020) Structural health monitoring for advanced composite structures: a review. J Compos Sci 4(1):13, 1–15. https://doi.org/10.3390/jcs4010013
8. Edwards J (2019) Predictive analytics, transforming data into future insights. CIO

9. Jin Q, Liu Z, Bin J, Ren W (2019) Predictive analytics of in-service bridge structural performance from SHM data mining perspective: a case study. Hindawi Shock Vib Article ID 6847053 1–11. https://doi.org/10.1155/2019/6847053
10. Larsson J (2018) Predictive engineering analytics is about more than just big data. Global Simulation Product Marketing at Siemens PLM Software, Newsletter

# Preliminary Design of a Low-Resolution Thermography Camera System for Subsurface Defect Detection of a Thin Composite Plate; A Case Study for Composite Electric Bus Structure


**M. I. Hassim, F. Mustapha, M. Anwar, M. T. H. Sultan, N. Yidris, and A. Hamdan**

**Abstract** The use of electric vehicle especially electric bus in on the rise. Unfortunately, it still has a downside which is not having enough distance compared to the conventional bus which uses diesel as its energy source. One of the reasons that affect the distance the electric bus can travel is the weight of the bus. The lighter the bus, the longer it can travel. Because of that, a new way of building the chassis and bus body structure that uses the composite material to replace not just heavy but also rusty prone metallic material has been developed. Now that the weight has improved, it creates another problem where the current method of inspecting the quality of the product during manufacturing is not just error-prone, but also take a longer time than it is allocated. The available tool in the market is expensive and a lot of investment is needed to make it work with a large structure such as the bus that a small company could not afford. Due to that, this project is going to address the need by designing and developing a thermal imaging tool for composite damage detection. The design process is done by using a model-based systems engineering method to identify the needs of the user and develop the functional requirement it needs based on that.

M. I. Hassim · F. Mustapha (✉) · M. Anwar · M. T. H. Sultan · N. Yidris
Faculty of Engineering, Department of Aerospace Engineering, Universiti Putra Malaysia, Serdang 43400 UPM, Selangor Darul Ehsan, Malaysia
e-mail: faizalms@upm.edu.my

F. Mustapha · M. T. H. Sultan
Laboratory of Biocomposite Technology (BIOCOMPOSITE), Institute of Tropical Forestry and Forest Products (INTROP), Universiti Putra Malaysia, Serdang 43400 UPM, Selangor Darul Ehsan, Malaysia

F. Mustapha · N. Yidris
Aerospace Manufacturing Research Centre (AMRC), Universiti Putra Malaysia, Serdang 43400 UPM, Selangor Darul Ehsan, Malaysia

A. Hamdan
Structural Integrity and Monitoring Research Group (SIMReG), Faculty of Mechanical and Manufacturing Engineering, Universiti Tun Hussein Onn Malaysia, Parit Raja 86400, Batu Pahat, Johor, Malaysia

© Springer Nature Singapore Pte Ltd. 2021

M. Jawaid et al. (eds.), *Structural Health Monitoring System for Synthetic, Hybrid and Natural Fiber Composites*, Composites Science and Technology,
https://doi.org/10.1007/978-981-15-8840-2_11

Then, the structure of the tool is allocated to the functional requirement and eventually, the hardware needed for it to become a complete product is identified. Once the hardware has been identified, it now can be integrated and several conceptual housing designs are developed where the final selection of the design is selected by using the Pugh evaluation matrix method. The integrated hardware is then put to test to ensure the tool works as intended. Based on the experiment conducted, the tool can detect a sub-surface damaged-induced specimen up to 2 mm depth. More than that, a longer time is needed which is not productive. In conclusion, although the developed tool meets all its objectives, there is still room for improvement to make it work efficiently in the field.

**Keywords** Non-destructive test · Composite structure · Active thermography · Pulse thermography

## 1 Introduction

Composite material has been widely used in transportation especially in the aerospace industry due to the lightness and strength of the material. Not until the rise in demand for an electric vehicle especially the electric bus, the usage of such material in the construction of a bus was limited to aesthetical only. The performance of the electric bus is limited in terms of how far it can travel on a full charge and hence there is a lot of research conducted to study how to increase its performance.

One of the proposed ideas is by reducing the weight of the vehicle weight [1, 7, 8, 10]. By reducing the weight, the energy used to move the bus is reduced and hence it translated to energy-saving or improvement in efficiency and subsequently increases the distance it can travel [3, 5]. Because of that, a new way of building the chassis and bus body structure that uses the composite material which can be either synthetic, hybrid or bio-composite to replace not just heavy but also rusty prone metallic material has been developed (Fig. 1).

Now that the weight has improved, it creates another problem where the current method of inspecting the quality of the product during manufacturing is not just error-prone, but also take a longer time than it is allocated. The study is based on a real case study of an electric bus manufacturer Sync R&D Sdn. Bhd. (SRD) that build the bus using composite material. The process used is a vacuum-assisted resin transfer method (VARTM) which was first introduced and patented by [9].

A skilled person is needed to inspect the surface visually to find the defect and the process can take up to two to three days because of the huge size of the bus structure and this will affect the manufacturing quality and increase in the lead time. Hence there is a need for a better way to inspect, identify and detect the internal defects of the composite structure. If the defects can be found earlier, it can be fixed and thus reduce the likelihood of the large structure to be scrapped and save money to the manufacturer. Unfortunately, the available tool in the market is expensive and a lot


**Fig. 1** Composite monocoque chassis (with permission from Sync R&D Sdn. Bhd.)

of investment is needed to make it work with a large structure such as the bus that a small company could not afford.

Due to that, this paper is going to address the need by designing and developing a thermal imaging tool for composite damage detection where it is not only affordable but also portable and can be attached to a drone to easily inspect the damage on a large structure. The design process loosely followed a model-based systems engineering method. The first step is to identify the needs of the user. Then the functional analysis is done to come out with the system requirements. Then, the structure of the tool is allocated to the functional requirement and eventually, the hardware needed for it to become a complete product is identified. Once the hardware has been identified, it can be integrated, and several conceptual housing designs are developed where the final selection of the design is selected by using the Pugh evaluation matrix method. The integrated hardware is then put to test to ensure the tool works as intended.

## Thermography

Thermography is a method of obtaining an image of a thermal profile over the surface of an object. It uses a special camera that can detect thermal radiation in the form of infrared light. Infrared light is a long wavelength of light exists just beyond human visual perception. Whereas thermal radiation is an electromagnetic radiator that emitted by all matter above −273 °C (absolute zero) as a function of its temperature. It means, at around room temperature, most objects begin to emit this radiation at infrared wavelength.

The method has gained popularity throughout the years due to its effectiveness, low cost and ability to perform without contacting the object of interest [6]. This means it can monitor the performance of a moving machine without interrupting

its operation. There are two types of thermography method. The first one is passive thermography and the second one active thermography.

**Passive Thermography**

Passive thermography as the name implies is done passively. It means, the thermal camera is pointed to an object and the thermal radiation emitted from it is captured by the camera. It is commonly used for qualitative inspection to pinpoint thermal leakage in a building, measuring the temperature profile of a circuit board and insulated structures, a hot spot for detecting forest burning and many other things in the various industry.

**Active Thermography**

While passive thermography technique can only look at the surface, the active thermography can look beneath the surface, that is, detect structural detail below the surface. It is based on the heating principle (while cooling is also possible but not common) of the surface to be inspected. The heat is applied by either applying energy in a pulsed form or in a harmonic modulated way. The heat is then propagated inside the object and if there are any anomalies inside the object, it will affect the surface temperature, and this can be captured by the thermal camera.

**Pulse Thermography**

In the active thermography method, pulse thermography can be considered as one of the most popular methods because it is extremely easy to carry out which is the focus of this paper (Fig. 2).

The analysis of the result is a matter of analyzing the thermal images of the object as a function of time and looking for any anomalies in the captured response images. Where there is damage, the surface temperature will be higher compared to the surrounding. The pulse can last from a few milliseconds for high conductivity material such as metal to several seconds for a low conductivity material such as the composite.

Although the high energy of power is applied, because of the brief duration of the heating, the temperature rises is only a few degrees above the initial object temperature and hence prevents any damage to the object which is one the plus point for this method.

## 2 Methodology

The objective of this project is to develop a low cost portable conceptual design of the thermal imaging tool (thermal camera) to detect subsurface defect for composite bus structure.

This section contains the methodology that describes how to meet the objectives by explaining how the design and development, validation and verification of the thermal camera are conducted. There are six main steps involves which start from an

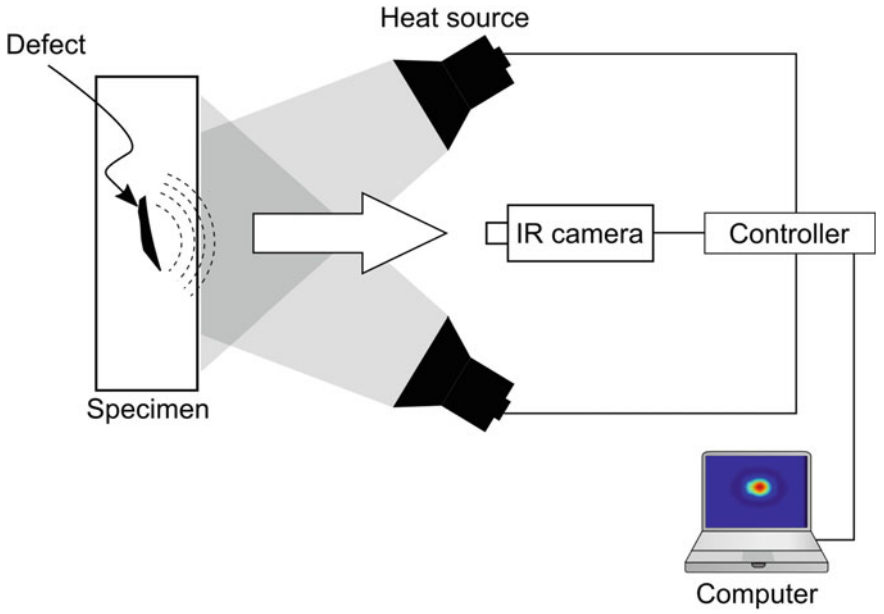


**Fig. 2** A typical Pulse Thermography test setup [4]

analysis of the stakeholder needs where the needs of the user are identified. Follows by the development of the requirements and the definition of the thermal structure to identify the hardware that needs to be used. Then the several conceptual designs are developed, the trade-off analysis is done to determine the best design and finally, experiments are conducted to ensure the design meets the objectives.

The methodology used to design and develop can be seen in Fig. 3 Step 1 until 3 is loosely based on the Model-Based Systems Engineering (MBSE) approach that uses SysML language to represent the idea in terms of diagrams. The approach is based on a functional analysis which is both familiar and intuitive to many practicing systems engineer where the requirements are based on the user needs. By doing so, it can be assured that the outcome can meet the objectives set for this project. While Table 1 describes in detail the activity in each step.

**Step 1: Analyze the Stakeholder Needs**

Based on the needs of the user and the objectives that need to be achieved, the system context and mission requirements are captured and are shown in Figs. 4 and 5 while Fig. 6 shown the stakeholder needs.

**Step 2: Analysis System Requirements**

Functional analysis is done by combining the use case diagram, textual scenarios and activity diagram and activity diagram with the support of swim lane where the activity diagram defines tasks that must be supported by the system and hence aid

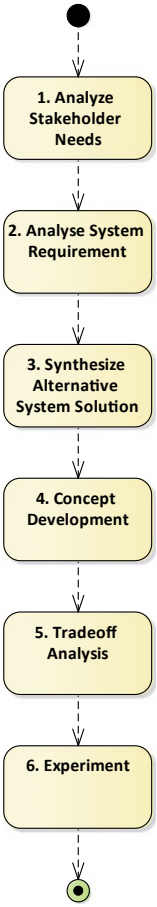


**Fig. 3** Methodology flow for design and development of the thermal camera. Modified from [2]

in the generation of functional requirements. Whereas, the swim lane will lead to requirements on elements that must exist in the system structure. Hence, there is no need to define the logical architecture of the thermal camera.

**Step 2a: System-Level Use Case**

From the use case diagram in Fig. 7, there are three actors outside the thermal camera boundary. The operator who is interested in operating the thermal camera, the thermal camera can have the option to be mounted on a drone and the thermography technique the thermal must be capable of delivering.

**Step 2b: Textual Use Case Description and Scenarios**

Use Case 1: Operate Thermal Camera

**Table 1** Description of activity. Modified from [2]

| Steps activity | | Overview |
|---|---|---|
| 1 | Analyze stakeholder needs (operation analysis) | Specifies the mission requirements that the thermal camera must support and the scope of the system in terms of a context diagram |
| 2 | Analyze system requirements (functional analysis) | Specifies the thermal camera requirements in terms of its input and output responses and other "black-box" characteristics needed to support the mission requirements |
| 3 | Synthesis candidate architectures | Allocates the logical components to physical components that are implemented in hardware |
| 4 | Concept development | Develop the conceptual design of the thermal camera housing |
| 5 | Tradeoff analysis | Performing Pugh evaluation matrix to choose the best design for the available concept |
| 6 | Experiment | Verify that the thermal camera is functioning and can meet the objectives of this project |

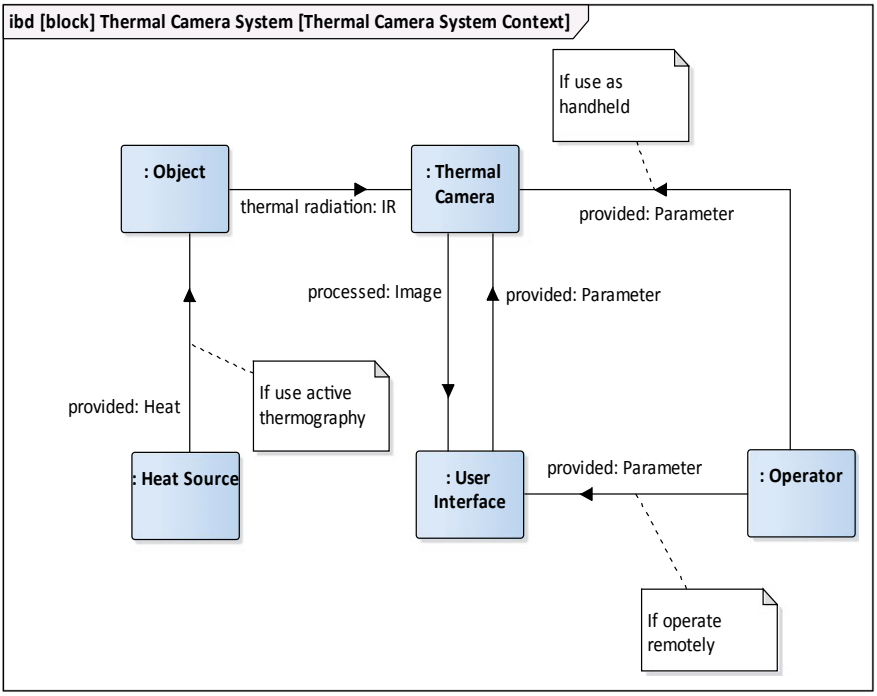


**Fig. 4** Methodology flow for design and development of the thermal camera. Modified from [2]

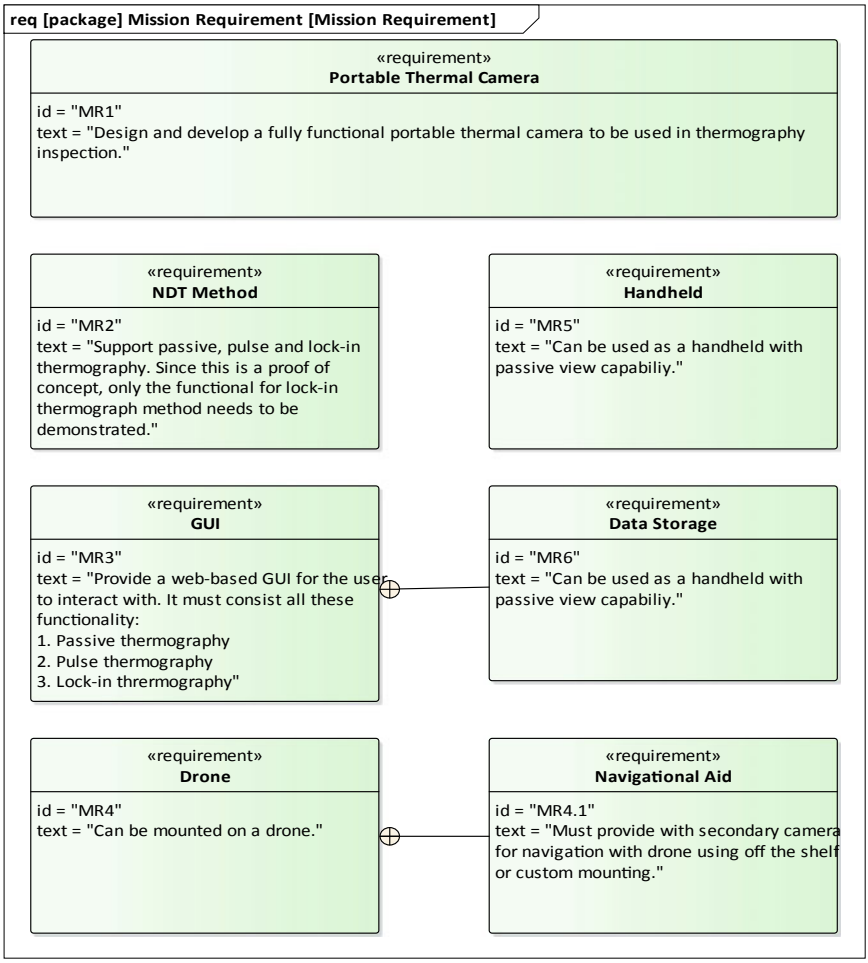


**Fig. 5** Top-level mission requirements

Scenario 1.1: The operator chose to mount the thermal camera on a drone, the camera must be easily mounted to the drone.

Scenario 1.2: The operator chose to use the thermal camera as a handheld tool, the handheld adaptor must firmly secure the thermal camera.

Use Case 2: Capture Thermal Image

Scenario 2.1: The operator chose to conduct passive thermography; the thermal camera must return with the right result.

Scenario 2.2: The operator chose to conduct pulse thermography; the thermal camera must send a pulse heating to the object of interest and return with the result

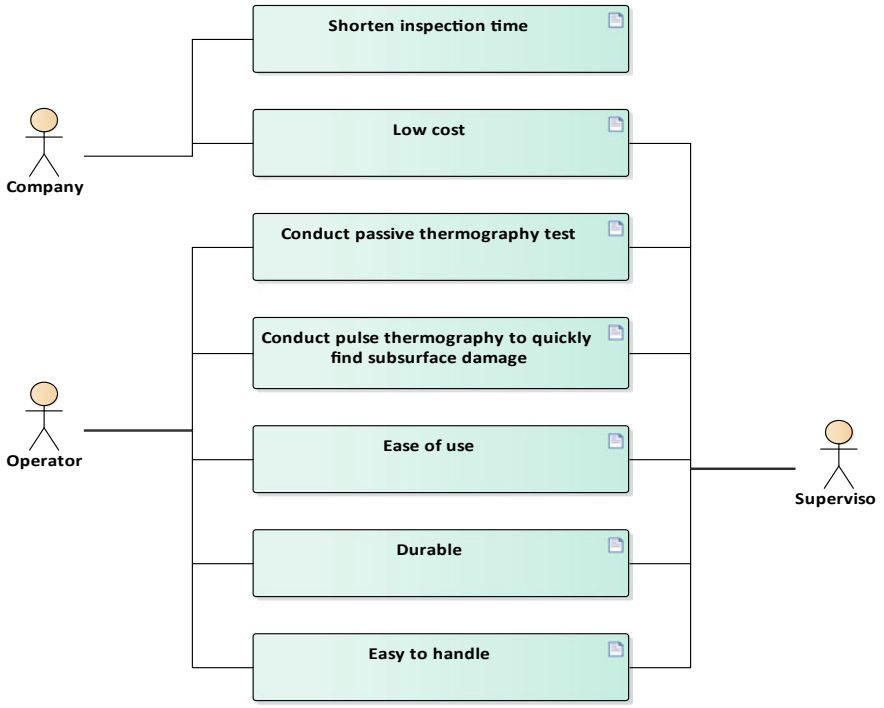


**Fig. 6** Stakeholder needs

Based on the scenarios defined above, it can be seen there are several new requirements that it captured.

1. There is a need to have a mounting that can handle both the handheld and drone operation mode.
2. There is a need to have a heat source to heat the object of interest
3. There is a need to have a user interface where the operator can select which mode to operate the thermal camera and there must be functions for the operator to change the settings of the test mode.

### Step 2c: Simplified Models of System Behaviour

The system's behavior as described in the previous section can be illustrated by using the activity diagram shown in Fig. 8.

The behavior for handheld usage is not shown here because the activity is simple. Just point the thermal camera to an object or scenery, and view the thermal image on a small built-in screen.

### Step 2d: Functional Requirements

Finally, the functional requirement (Fig. 9) can be derived from the use case, scenarios and activity diagram. In Fig. 10, the diagram shows how the functional requirements

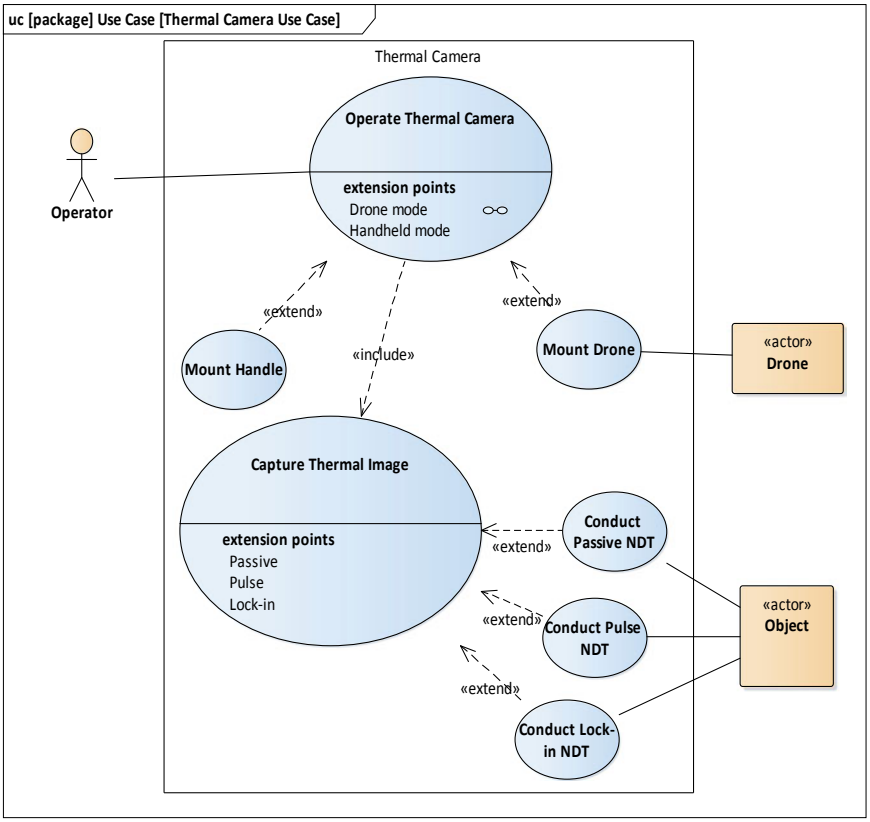


**Fig. 7** System-level use case

are traced back to the mission requirement ensuring confirmation that the functional requirements are meeting the main objective of this project.

### Step 3: Synthesize Candidate Physical Architectures

Based on the requirements defined in step 2, the physical architecture can be defined with the help of swim lane shows in Fig. 11 As can be seen in Fig. 12, the thermal camera is using Flir Lepton thermal module which is inexpensive and is the key to bring the cost down but unfortunately comes with a very low resolution which is 80px × 60px. Hence, the experiment is required to study if it can detect subsurface damage by using the pulse thermography method.

### Step 3a: Simplified Models of System Structure

Finally, the physical block can be mapped to actual components to be used in this project (Fig. 13). Although the power supply block is not mapped to the behavior in the previous section, it has to be there to satisfy the Power Source requirement.

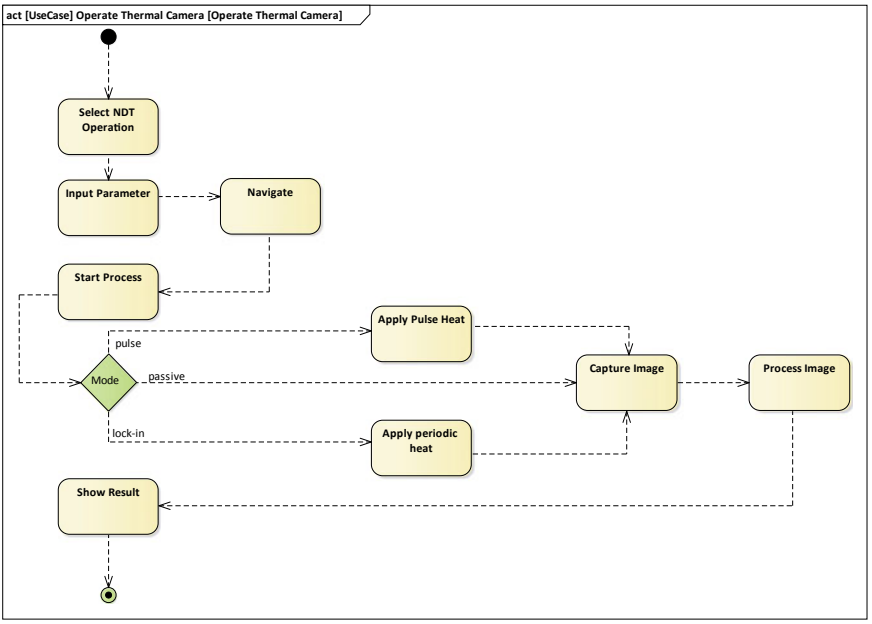


**Fig. 8** System behavior when mounted on the drone

### Step 4: Develop Concept Design

All the hardware has been selected in step 3. The only thing left that matters the most is the design of the housing. The housing design must be attractive and yet must be highly durable. Morphological Matrix is used to randomly generate ideas from the list of available options. Figure 12 shows the available combination while Fig. 14 shows the summary of possible combination for the thermal camera.

### Step 5: Tradeoff Analysis

Next, the Pugh evaluation matrix is used to select the best option to proceed with the prototype stage. Figure 15 illustrated the result of the process. It can be seen that the combination 3 gives the best alternatives that meet the needs.

### Step 5a: Final Concept

The final concept as selected by the Pugh evaluation matrix method is illustrated in Figs. 16 and 17. As mentioned previously, the focus is on the design of the housing as the hardware is already selected and mapped to the requirements.

### Step 5b: Actual Prototype

Based on the final concept selection, all the hardware is assembled to become one complete solution. As the main constraint is on the budget, it does not represent the

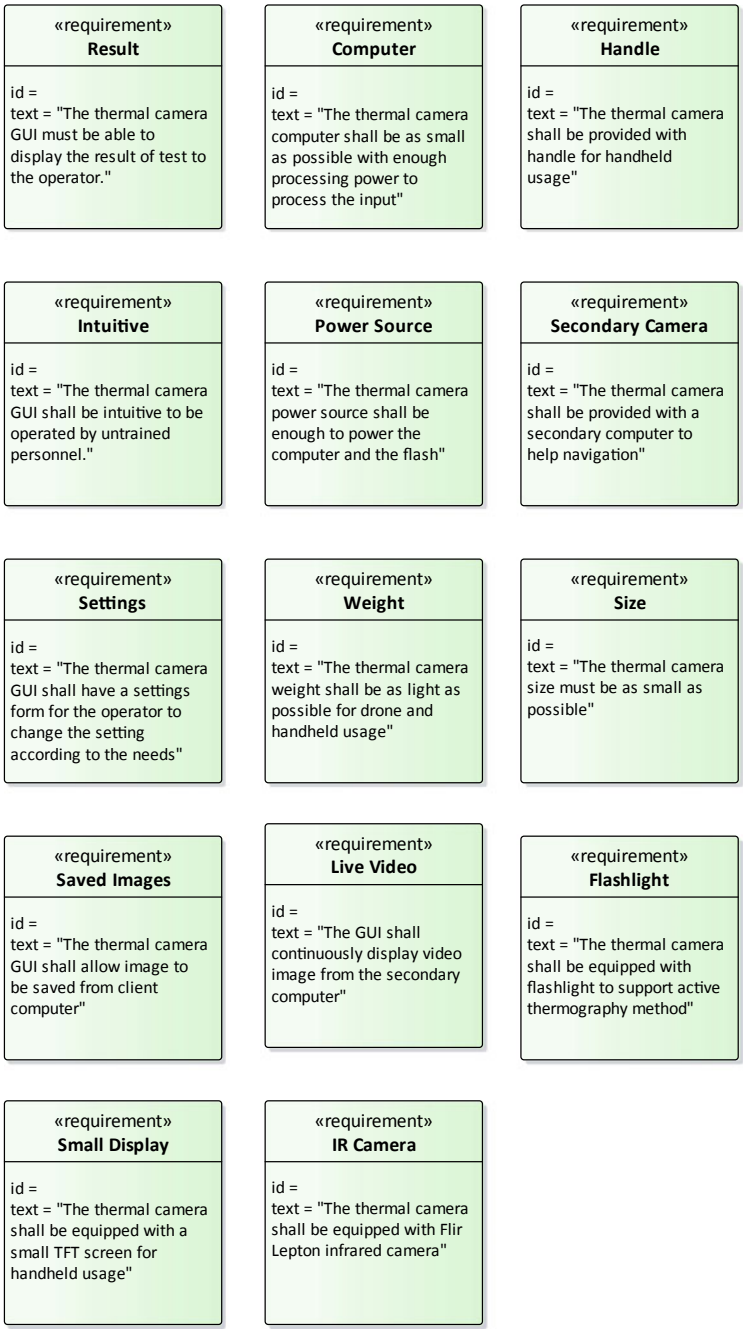


**Fig. 9** Functional requirements of the system

| Source \ Target | Computer | Flashlight | Handle | Intuitive | IR Camera | Live Video | Power Source | Result | Saved Images | Secondary Camera | Settings | Size | Small Display | Weight |
|---|---|---|---|---|---|---|---|---|---|---|---|---|---|---|
| Data Storage | ← | | | | | | | | | | | | | |
| Drone | | | | | | | | | | | | | | ← |
| GUI | | | | ← | | ← | | ← | ← | | ← | | | |
| Handheld | | | ← | | | | ← | | | | | ← | ← | ← |
| Navigational Aid | | | | | | | | | | ← | | | | |
| NDT Method | ← | ← | | | ← | | | | | | | | | |
| Portable Thermal Camera | | | | | | | ← | | | | | ← | | ← |

**Fig. 10** Relationship between functional requirement and mission requirements

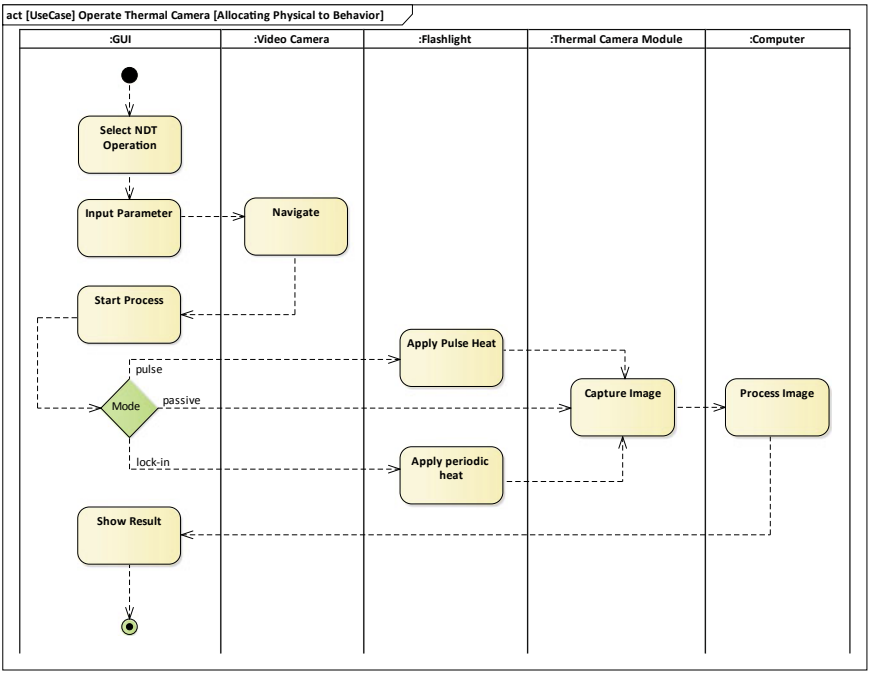


**Fig. 11** Allocating the physical block to behavior

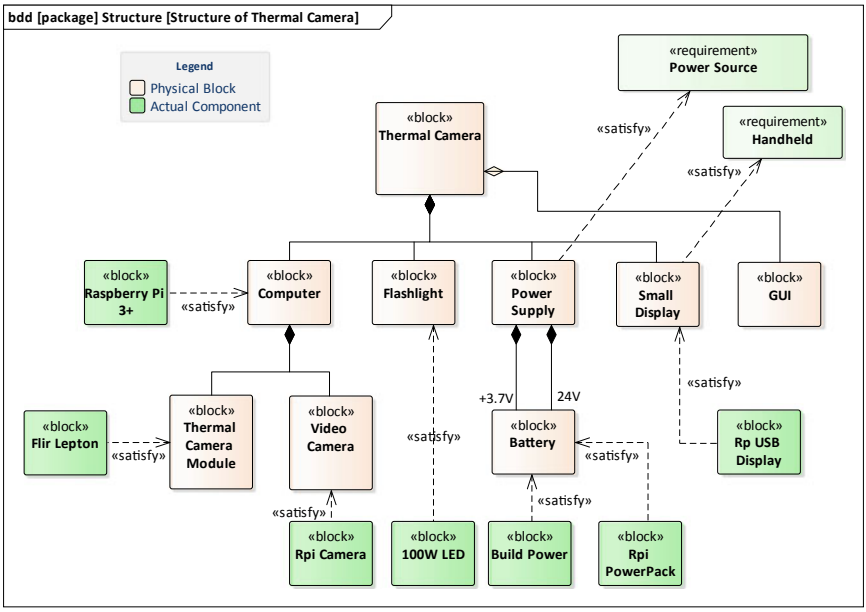


**Fig. 12** Mapping of the system structure to actual components

| | Housing | | | | Light Performance | Handle Locking Mechanism |
|---|---|---|---|---|---|---|
| Material | Shape | Grasp | Size | Protection | Number of LED | Type |
| Plastic | Flat | Smooth/Shiny | Compact | Rubber | 1 | Snap fit |
| Aluminium | Curve | Rubber layer | Medium | Thick thickness | 2 | Spring lock |
| Fibreglass | Combination | Combination | Bulky | None | 3 | Scre lock |

**Fig. 13** Morph matrix for the thermal camera

| | Cobination 1 | Combination 2 | Combination 3 | Combination 4 | Combination 5 |
|---|---|---|---|---|---|
| Material | Plastic | Aluminium | Plastic | Fibreglass | Aluminium |
| Shape | Flat | Combination | Combination | Curve | Flat |
| Grasp | Smooth/Shiny | Smooth/Shiny | Combination | Rubber layer | Combination |
| Size | Bulky | Medium | Medium | Bulky | Compact |
| Protection | None | None | Rubber | Thick thickness | None |
| Number of LED | 3 | 2 | 1 | 1 | 1 |
| Type | Screw lock | Spring lock | Snap fit | Snap fit | Screw Lock |
| Conceptual Sketching | 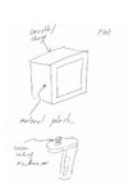 | 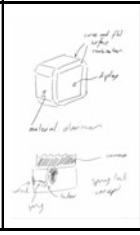 | 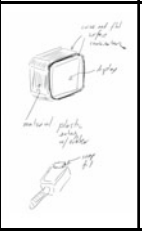 | 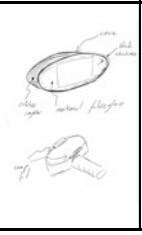 | 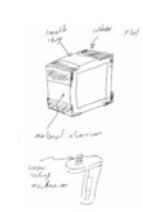 |

**Fig. 14** Summary of possible combination

| | Cobination 1 | Combination 2 | Combination 3 | Combination 4 | Combination 5 |
|---|---|---|---|---|---|
| Material | + | = | + | - | Datum |
| Shape | = | + | + | - | |
| Grasp | - | - | = | + | |
| Size | - | - | - | - | |
| Protection | = | = | + | + | |
| Number of LED | + | + | = | = | |
| Type | = | - | + | + | |
| Total "+" | 2 | 2 | 4 | 3 | |
| Total "-" | 2 | 3 | 1 | 3 | |
| Total "=" | 3 | 2 | 2 | 1 | |
| Rank | 3 | 4 | 1 | 2 | |

**Fig. 15** Pugh evaluation matrix with datum is combination 5

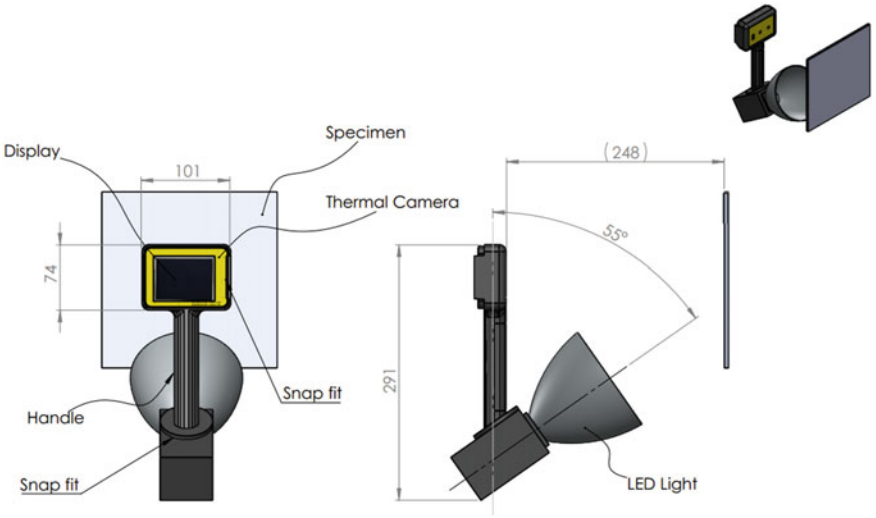


**Fig. 16** The thermal camera final concept

selected concept design 100% but the main functionality for it to conduct all the tests is there (Fig. 18).

### Step 6: Experiment

The test was done on passive and active pulse thermography. The image capture is then converted to gray color to enhance the defected area. Flat bottom hole glass fiber reinforcement composite (GFRP) were with different depth and diameter are used as a sample defect. The test setup is shown in Fig. 19 and the details are as follows:

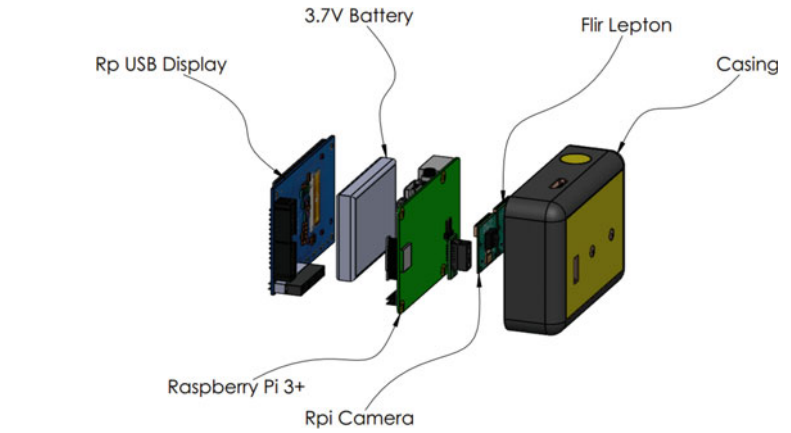


**Fig. 17** Internal components of the thermal camera

**Fig. 18** Various view of the thermal camera prototype


**Fig. 19** Initial test setup

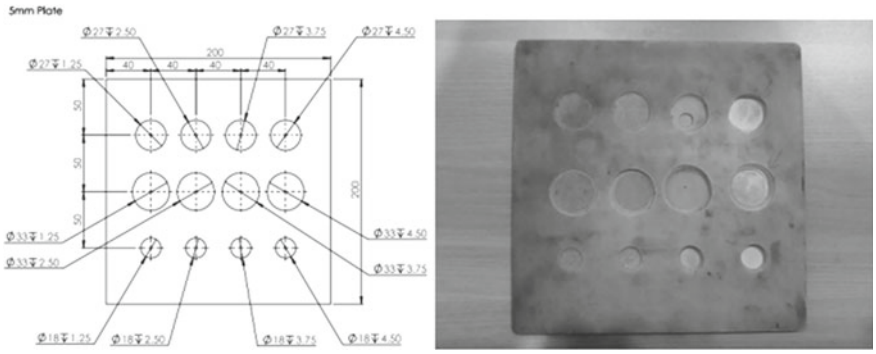


**Fig. 20** Specimen to be tested

1. Thermal camera—Without the housing with a measured distance from the specimen to the lens is 25 mm. This to ensure the whole specimen can be seen in the image.
2. Heat source—100 W LED arrange at a 35° angle pointing to the middle of the specimen.
3. Damage-induced specimen—A specimen made with fiberglass material with partial holes drill at the back; various diameter and depth (Fig. 20).

## 3 Results and Discussion

For the passive thermography test, not all of the defects were detected. This is due to no temperature difference between the specimen and the surrounding (Fig. 21).

For active pulse thermography, there are 4 different heating duration being tested:

**Fig. 21** Passive thermography on the specimen

1. Heating Pulse 5 s
2. Heating Pulse 15 s
3. Heating Pulse 20 s
4. Heating Pulse 50 s

Exposure to heat, two distinct categories can be observed. The image response of Fig. 22 which showed a low contrast and starting from the pulse duration of 10 s onwards (Fig. 23), the contrast from the temperature difference is noticeable.

Longer exposure to heat means there is enough time for the heat to be transferred from the light source to the specimen, but it seems after a while there is no significant advantage for the specimen to be exposed longer to the heat. This can be seen in Figs. 24 and 25. The increased pulse duration seems does not give any effect to the contrast. But with longer exposure, the damage depth can be penetrated further.

The first row on the top as seen in Fig. 25, the depth is about 0.5 mm, the second row, the depth is 1 mm and the third visible hole depth is 2 mm from the captured surface.

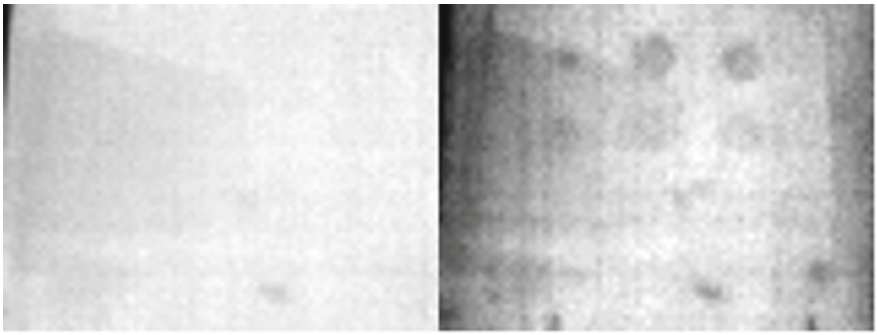

**Fig. 22** Right image taken at 0 s at left at 5 s

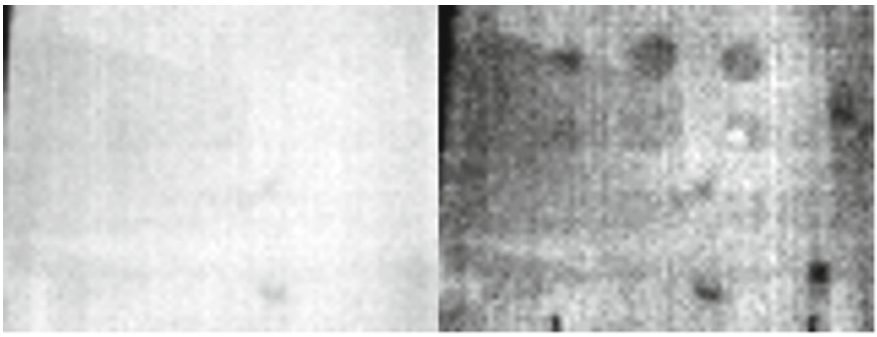

**Fig. 23** Right image taken at 0 s at left at 15 s

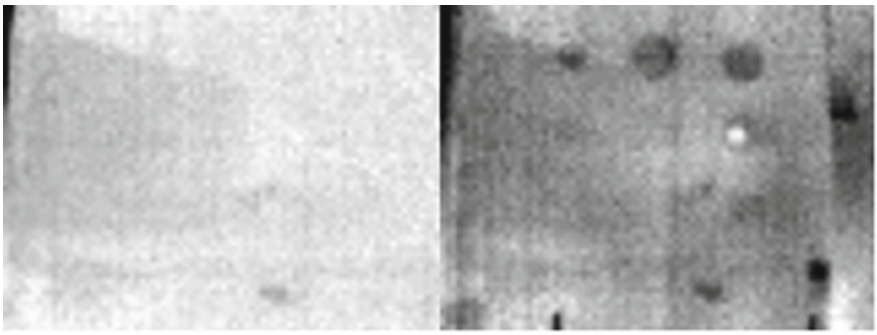

**Fig. 24** Right image taken at 0 s at left at 20 s

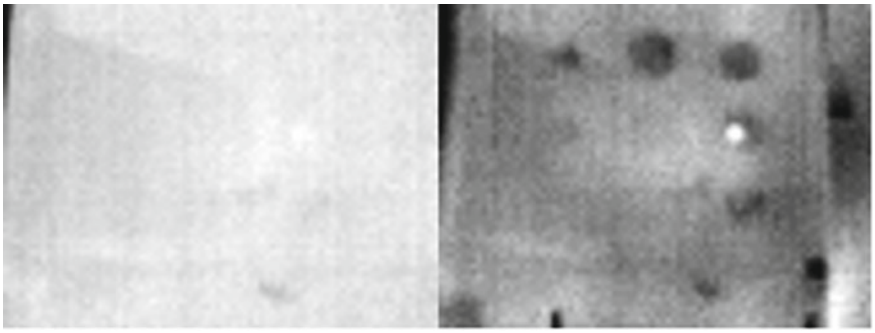

**Fig. 25** Right image taken at 0 s at left at 50 s

## 4 Conclusion and Recommendation

In conclusion, a fully functional portable thermal camera that can be used in thermography inspection has been developed. It can be used to successfully conduct passive and pulse thermography.

Although mounting to a drone is not shown, the thermal camera has the capability of doing so. It has a secondary video camera that can continuously feed to the user for ease of navigation. A secondary benefit of having a secondary video camera, the shape of the object can be easily identified since the Flir Lepton infrared thermal module has a very low resolution.

The handheld option is also available. Although the use is only limited, it is still useful to conduct passive thermography where it has a built-in small display.

### Recommendations

Increase the number of LED lights or increase the output power which currently is 100 W. By increasing the power, lesser time is needed to heat the object and hence the productivity can be increased. Furthermore, the contrast is much more visible. Also, increasing the number of lights, the blind spot, and uneven heat transfer can be compensated by repositioning the camera. But, an increasing number of led light will increase the weight. Handheld usage might be a pain to use. So, further study needs to be done to evaluate another type of light source and the quantity used.

As mentioned in the previous section, the Flir Lepton infrared thermal camera used has a very low resolution. The model version used was 2.5 and Flir Lepton has a new version 3.5 which quadruple the resolution of the 2.5 version where the pixelated on the image can be reduced. There is also a new breakout board that has more functionality. If the thermal camera needs to be used in a more professional environment or advanced research, it is recommended by the manufacturer to upgrade the module and the breakout board to the latest version.

The results from both of the design and development activity, and as well as the experiment shows that the thermal camera is successfully developed. As in many new product developments, more iteration is needed to ensure the product is fit to be used in the field.

## References

1. Butdee S, Vignat F (2008) TRIZ method for light weight bus body structure design analysis and modelling
2. Friedenthal S, Moore a, Steiner R (2015) A practical guide to SysML: the systems modeling language. Syst Eng
3. Helms H, Lambrecht U (2006) The potential contribution of light-weighting to reduce transport energy consumption. Int J LCA
4. Ibarra-Castanedo C, Bendada A, Maldague XPV (2007) Thermographic image processing for NDT. In: IV Conferencia Panamericana de END, pp 1–12
5. Joost WJ (2012) Reducing vehicle weight and improving U.S. energy efficiency using integrated computational materials engineering. JOM 64(9):1032–1038
6. Kroworz A, Katunin A (2018) Non-destructive testing of structures using optical and other methods : a review 12(April):1–17
7. Liu Q, Lin Y, Zong Z, Sun G, Li Q (2012) Lightweight design of carbon twill weave fabric composite body structure for electric vehicle
8. Ning H, Janowski GM, Vaidya UK, Husman G (2006) Thermoplastic sandwich structure design and manufacturing for the body panel of mass transit vehicle
9. Seemann WH, Springs O (1991) US5052906A. United States. https://patents.google.com/patent/US5052906A/en?assignee=Seemann+composite&oq=Seemann+composite
10. Vaidya U (2011) Composites for automotive, truck and mass transit, materials, design, manufacturing. DEStech Publications

# Mechanical Properties of Flax/Kenaf Hybrid Composites


**Noorshazlin Razali, Mohamed Thariq Hameed Sultan, Mohammad Jawaid, Ain Umaira Md Shah, and Syafiqah Nur Azrie Safri**

**Abstract** The aim of this work is to fabricate flax/kenaf hybrid composites and analyse their mechanical (tensile, flexural and compression), and scanning electron microscopy properties. Hybrid composites fabricated by using flax BL150, flax BL200 and kenaf, where the ratio of hybridisation of flax to kenaf is 30:70 by using hand lay-up techniques. The tensile tests, flexural test and compression test were performed using the test machine Instron. The morphological observation of tensile damaged sample of the composites was evaluated by Scanning Electron microscopy to ascertain the extent of the failure of composites. The results showed that the tensile, flexural compression properties of kenaf composites were improved by hybridization with flax fabrics. It is observed that Kenaf/Flax BL150/Kenaf display highest tensile strength whereas Flax BL150/Kenaf/Flax BL150 hybrid composites showed the highest tensile modulus as compared to kenaf composites. Flax BL200/Kenaf/Flax BL200 display highest flexural strength while Kenaf/flax BL 150/kenaf show highest flexural modulus due to better flexural properties of Flax. Flax BL200/Kenaf/Flax BL200 displayed highest compressive modulus while Flax BL150/Kenaf/Flax BL150 shows highest compressive stress than kenaf composite itself. The hybrid composites undergoes matrix cracking, fibre pull out and fibre breaking after the testing and being observed by using scanning electron microscope.

**Keywords** Flax fibre · Kenaf fibre · Hybrid composites · Mechanical properties · Scanning electron microscopy

N. Razali · M. T. H. Sultan (✉) · A. U. Md Shah
Department of Aerospace Engineering, Faculty of Engineering, Universiti Putra Malaysia, Serdang 43400 UPM, Selangor Darul Ehsan, Malaysia
e-mail: thariq@upm.edu.my

M. T. H. Sultan · M. Jawaid · A. U. Md Shah · S. N. A. Safri
Laboratory of Biocomposite Technology, Institute of Tropical Forestry and Forest Products (INTROP), Universiti Putra Malaysia, 43400 UPM Serdang, Selangor, Malaysia

M. T. H. Sultan
Prime Minister's Department, Aerospace Malaysia Innovation Centre (944751-A), MIGHT Partnership Hub, Jalan Impact, 63000 Cyberjaya, Selangor Darul Ehsan, Malaysia

© Springer Nature Singapore Pte Ltd. 2021

M. Jawaid et al. (eds.), *Structural Health Monitoring System for Synthetic, Hybrid and Natural Fiber Composites*, Composites Science and Technology,
https://doi.org/10.1007/978-981-15-8840-2_12

## 1 Introduction

The rapid growth of natural fibres to meet the global demands of alternative materials technologies has made remarkable progress. Natural fibres have generated potential environmentally friendly and economically efficient low cost engineering materials. Additionally, key advantages of natural fibres are their high strength, high dampening ratio and high stiffness per weight [1]. Natural fibres that are used in everyday products could contribute to an environmentally friendly planet. This is because natural fibres are considered to be a resource that can be renewed and completely biodegradable [2]. The tensile strength as well as the Young's modulus of natural fibres is generally lower than those of other fibres used in composite materials. However, the specific strength and density are quite comparable [3].

Natural plant fibres include fibrous materials extracted from both plant bast fibres and its core. This fibrous plant consists of kenaf *(Hibiscus cannabinus)*, jute *(Corchorus olitorius and Corchorus capsularis)*, industrial hemp, flax *(Linum usitatissimum)*, and ramie *(Boehmeria nivea)* [4]. The use of flax, hemp and kenaf are expanding very fast, while the usage of natural fibre is generally rising. Flax, hemp and kenaf are favoured due to their excellent combination of economic and functional properties [3]. The advantages of natural fibres compared to synthetic as example glass, Kevlar (aramid) and carbon are in terms of low density, low cost, and acceptable specific strength properties [3]. Eco-friendly composite materials including natural fibres have the potential to be the best, new materials of the modern century, and could be part of the solution to many global environmental issues.

Kenaf also known as *Hibiscus cannabinus L.* helps in conserving the environment and soil fertility. A research study showed that cultivation of one hectare of kenaf or jute plants will return 3.84 tons of biomass to the soil in the form of leaves, roots, and retting waste. Furthermore, it has the highest carbon dioxide absorption of any plant, and that is valuable in the prevention of global warming. Among the other natural fibres, kenaf fibre is particularly widely used in automotive applications. They have their own advantages over synthetic reinforcement materials. They are lower in cost, and non-toxic with low density [5]. Hybrid composites can be defined as the combination of two or more fibres in any reinforced matrix. There is lots of research on tensile and flexural testing of hybrid composites that has been conducted for various applications. Table 1 shows a few recent studies on hybrid composites for tensile test and flexural testing.

During recent years, the application of composite materials has expanding and spread in industries especially in aerospace structures [18]. Nowadays, natural fibres are widely used in many applications in order to replace synthetic fibres in structure and design. Therefore, the mechanical properties of a material must be known so that engineers can relate the measured strain in a material to its associated stress. Mechanical testing is used to determine the properties of a material. The understanding of their deformation behaviour is very important for encouraging their usage in structural and other applications. Thus, mechanical properties are determined from a tension or compression test. In this research, tension testing was used

**Table 1** Recent researches of tensile and flexure testing for hybrid composites

| Hybrid composites | Matrix | Fabrication method | References |
|---|---|---|---|
| Woven kenaf bast fibre/Oil palm empty fruit bunches | Poly hydroxybutyrate | Compressing molding | [6] |
| Flax/Basalt | Vinylester | Hand lay-up and resin infusion | [7] |
| Kenaf/Bamboo/Coir | Polylactic acid (PLA) polymer | Hot press | [8] |
| Glass/Flax | Modified soybean oil | Resin bath | [9 |
| Bamboo/Jute/Kenaf mat | Unsaturated polyester (UP) | Hand lay-up and compression molding | [10] |
| Oil palm/Woven jute fibers | Epoxy | Hand lay-up and hot press | [11] |
| Flax/Glass fiber | Phenolic resin | Compression molding | [12] |
| Flax/Hemp/Glass fibers | Epoxy | Vacuum infusion | [13] |
| Kenaf/Kevlar | Epoxy | Hand lay-up | [14] |
| Glass/Kenaf | Liquid epoxidised natural rubber | Hot press | [15] |
| Flax/Glass | Polypropylene (PP) | Injection molding | [16] |
| Kenaf/Fiberglass | Polyester | Hand lay-up and cold press | [17] |

to determine the mechanical properties of the fabricated materials. The most common tests performed on biocomposites are tensile tests, impact tests, flexural tests, and hardness tests.

The tensile test used in this research complied with ASTM standard, D3039/D3039M-95a [19]. Load or tensile stress is exerted in the form of a pulling force onto the material. Based on stress-strain graph from the tensile test, the material can be notified as being brittle or ductile. A ductile material like mild steel endures a large strain before rupturing [20]. ASTM offers better control of testing details that may cause variability; therefore, it is the preferred method. Results from the tension test were used to determine the elastic or tensile modulus, ductility, ultimate tensile strength (UTS) and yield strength. The maximum engineering stress in the sample known as tensile strength or ultimate tensile strength (UTS), can be determined using the maximum load at the point at which the load begins to decrease [21]. A tensile stress is applied to the end of the specimen. The straight-sided specimen provides no geometric stress-concentrated region, failure often occurs at or near the end of the grips. Other important factors that affect tension testing results include specimen preparation, specimen design tolerance, control of conditioning and moisture content variability. The flexural properties of biocomposites can also be identified using the flexure test based on the ASTM D790 standard test method [22]. The flexural test was conducted by 3-point loading with the load exerted at a controlled rate at the mid-span between the two points of supports.

Flax fibre is used to improve the mechanical properties of kenaf fibres. From previous research, flax is known as high strength fiber among natural fibers. From Table 1, not much research has been conducted on kenaf and flax hybrid composites. The usage of Kenaf has been wider from past few years in Malaysia because it is easy to get and environmentally friendly. Furthermore, according to Amar K., kenaf fibre has anisotropic mechanical properties that lead to a similar anisotropy in the composite materials [3]. The Young's modulus and tensile strength can be compared with those of traditional composites, and therefore the kenaf fibres were introduced as a good fibre for reinforcement in high-performance biodegradable composites. Kenaf has a high yield per acre, and according to Australia's CSIRO, can be 3 times the yields for Hemp. In addition, it has exceptional characteristics for papermaking, as less solvent, heat and time are required to pulp kenaf fibres because these fibres are not as tough as wood pulp and also contain less lignin. Kenaf can be easily pulped and bleached with relatively harmless chemicals, such as hydrogen peroxide. From previous literature review, it is indicated that no research has been reported on the tensile and flexural strength of kenaf/flax hybrid composites. Therefore, in this research, Kenaf and flax fibre were chosen in order to investigate the mechanical properties of their hybrid composites. The objective of this research is to determine the mechanical properties of kenaf composites, flax composites and the hybridisation of flax/kenaf fibre. It is important to identify these properties in order to identify the best combination for future research.

## 2 Methodology

### *2.1 Specimen Preparation*

Flax BL150, flax BL200 and kenaf were chosen for this research. "BL150" indicates the density of 150 g of flax/$m^2$, "BL200" indicates 200 g of flax/$m^2$. Figure 1 shows the differences in the structure of flax fibre types BL150 and BL200. All fibres


**Fig. 1** Flax BL150 and flax BL200

were used in woven form. The composites were prepared in the laboratories of the Engineering Faculty of Universiti Putra Malaysia (UPM). The fibres and epoxy resin were purchased from ZKK Sdn. Bhd.

The preparation procedure for this fibre consisted of material preparation, the lay-up process, and the cutting process using a CNC machine. In order to produce a square of flax/kenaf fibre material for the lay-up process, the kenaf and flax woven fibre was first cut into pieces of 300 mm long and 300 mm wide. A lay-up preparation was performed after the cutting process of the fibre. A square plate of smooth surfaced steel was needed as a base for the fabrication process. The surface of the steel needed to be as smooth as possible with no roughness. To make sure that the surface is smooth and free from debris, wax was used as a releasing agent to avoid the specimens sticking to the steel base after the curing process and to remove the unwanted rough surface from any small debris.

Flax and kenaf fabrics were placed as per layering sequence of hybrid composites. Figure 2 shows the stacking sequence of the hybrid composites. The resin that was used was a mixture of epoxy and hardener in 2:1 ratio, and was poured on each layer of fibre. Next, another piece of steel plate that had been wiped using wax was placed on top of the fibre followed by a load to ensure that the resin spread through all of the

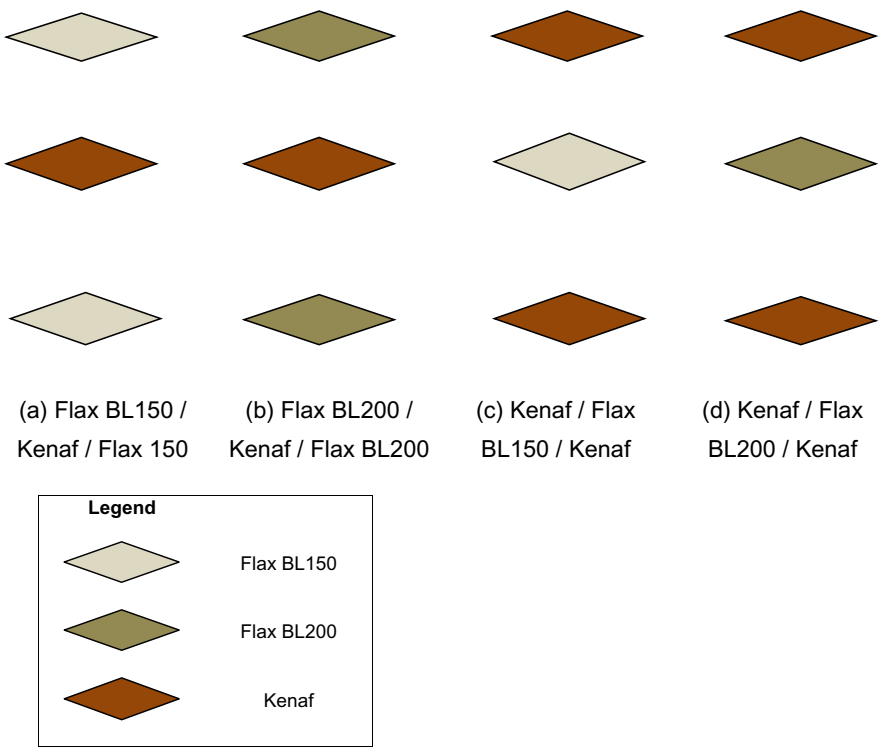


**Fig. 2** Stacking sequence of the hybrid composites

layers of the material. Load that has been used was 4 steel plates which each plate has weight of 150 N. The prepared hybrid composites left for 48 h for curing at room temperature (28–30 °C). Cured composite samples were cut into specific dimension as per standard for testing.

## 2.2 Tensile Test

The test was perform using the tensile test machine Instron 3382 100kN. To perform the tensile test, a sample of the composite material was made into a standard shape and size. The size of the test specimen was 20 mm × 120 mm with the ratio of the flax/kenaf hybridisation of 30:70 complying with ASTM standard, D3039/D3039M-95a [19]. This size was made according to the tensile test standard for polymer matrix composite materials, in which the fibre orientation is balanced and symmetrical. Measurements were taken of the initial cross sectional area of specimens, $A_0$, and the gauge length distance, $L_0$. A testing machine was used to put a tension load on the specimen at a very low constant rate until it reached failure point. The machine saved the load data while the testing was done.

The gauge length was set to 60 mm while the other 60 mm was in the gripping tools. The specimen was then stretched at a very low constant rate until it reached breaking point. The tests were done with a crosshead speed of 5 mm/min. The data were recorded and using Instron Bluehill software. The average values for Young's Modulus, maximum tensile stress and maximum tensile strain were deduced for each orientation. The results from the test were calculated and the mechanical properties of the composite are presented and discussed.

## 2.3 Flexural Test

The tests were performed using the Instron 3365 10 kN. To perform the flexural test, a specimen of the material was made into a standard shape based on ASTM D7264/D7264M-15 standard [22]. The specimen was placed on the two points of the support span and the load was applied at the centre of the specimen. Six composite specimens were tested for each sample. The gauge length was calculated based on the thickness of the sample using the following calculation:

$$\text{Gauge length (GL)} = 16 \times \text{thickness of the sample} \tag{1}$$


**Fig. 3** Samples for compression testing

## *2.4 Compression Test*

Compression test were performed using the Universal Testing Machine Instron 3382 which had 100 kN load cell. To perform this test, sample were cut into 12.7 mm × 12.7 mm as shown in Fig. 3, according to ASTM standard ASTM D695 (ASTM, 2015) with 1.3 ± 0.3 mm/min of crosshead speed. Five repeatability samples had been tested for each type of composites.

## *2.5 Scanning Electron Microscopy*

Scanning electron microscopy was used in order to observe damage and clarify the failure after tensile testing of the specimens. The samples were observed using Nova Nanosem 230 model FEI (USA). The adhesion between the layered of fibre and the matrix in the woven composites was further investigated by a micrograph of the cracking surfaces of the samples. The sample from the tensile test and flexural test was first cut to size (20 mm × 20 mm) at the crack section in order to be put in the scanning electron microscope. The samples were then coated with gold in order to see a clear image on the sample. Several magnification levels from were 100 to 600 times were used to examine the fracture sample from an overall view to a detailed view of the failure.

# 3 Results and Discussion

## *3.1 Tensile Properties*

All of the specimens were tested under the same test conditions. The data points for load, extension, tensile stress and tensile strain were taken until each of the specimens failed. Figure 4 shows the graph of load against extension from the average of five repeatability specimens of Flax BL150, Flax BL200, Epoxy, Kenaf, Flax BL150/Kenaf/Flax BL150, Flax BL200/Kenaf/Flax BL200, Kenaf/Flax BL150/Kenaf and Kenaf/Flax BL200/Kenaf. From the graphs, we can see that all specimens undergoes the same trend, which is in linear curves forms before it failed at certain maximum stress and certain maximum strain values for each sample that was tested. The linear curves suddenly drop when the specimens breaks at the maximum tensile stress that the specimen can withstand [23]. From the average of each type of specimen, flax BL200 had the highest value of load, 8340.25 N, and tensile stress 66.19 MPa needed before it exhibited failure modes. Kenaf had the lowest value of load, 3174.57 N, and tensile stress 28.34 MPa before it failed. It shows that flax BL200 needed more energy to break its fibre reinforcement than the kenaf composites. However, after both of the fibres were hybridize, the value of maximum tensile stress were higher for kenaf fibre hybrid with flax BL150, which is 41.06 MPa for Flax BL150/Kenaf/Flax BL150 and 44.40 MPa for Kenaf/Flax BL150/Kenaf as compared to kenaf hybrid with flax BL200, which is the value of maximum tensile stress is 35.45 MPa for Flax BL200/Kenaf/Flax BL200 and 26.85 MPa for Kenaf/Flax

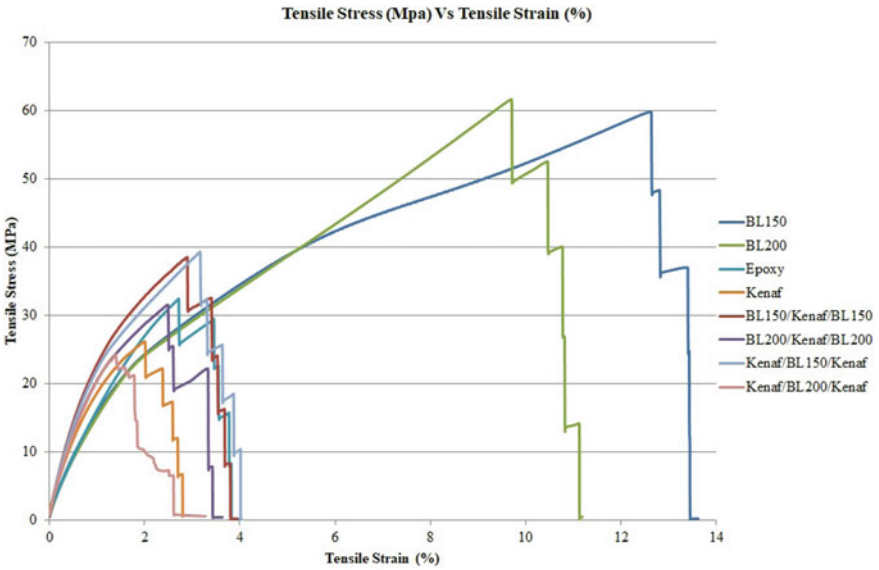


**Fig. 4** Tensile stress (MPa) against tensile strain (%)

BL200/Kenaf. The value of tensile stress of kenaf is improved after the kenaf fibre is being hybridized with flax, unless for sample Kenaf/Flax BL200/Kenaf that has a bit lower value than kenaf composites.

Figure 4 illustrates the average of tensile stress against tensile strain for all samples tested. Young's Modulus was determined from the slope of the graph of tensile stress against strain by using Eq. 2.

$$E = \frac{\text{Tensile Stress}}{\text{Strain}} \tag{2}$$

The values of Young's Modulus were detemined from the calculation of the slope of the graph. Tensile modulus explain the stiffness ability of the flax/kenaf hybrid composites. The data for the load at maximum tensile stress, tensile strain at maximum tensile stress and tensile extension at maximum tensile stress were also retrieved from the graphs.

Table 2 tabulated the average of the data of tensile properties of composites and hybrid composites. These are the tensile properties that were measured for all of the hybrid composites. Tensile properties of a composite material are influenced by fibre length, fibre strength, fibre/matrix interfacial bonding, fibre content, orientation, modulus, and fillers [24]. Tensile strength of the composite depends on the strength and modulus of fibres. The data tabulated in Fig. 5, clearly shows variation in the modulus of the different composites.

It is observed from Fig. 5, that hybrid Flax BL150/Kenaf/Flax BL150 showed the highest modulus, 2600.65 MPa, due to good bonding and arrangement between the flax fibre, kenaf fibre and epoxy. The modulus of the hybrid composites was higher than the modulus of pure fibre and pure epoxy composites. This shows that hybridisation between flax and kenaf fibre resulted in an increased modulus of the composites. The lowest modulus obtained from the tests was the pure flax BL150 composites at only 1072.74 MPa. The capability of the composite to bear load is enhanced as the tensile modulus is increased [25].

**Table 2** Data of the average tensile repeatability results

| | Modulus (MPa) | Tensile stress (MPa) | Tensile strain (%) |
|---|---|---|---|
| BL150 | 1072.74 (±65.08) | 61.13 (±1.11) | 13.11 (±0.43) |
| BL200 | 1181.39 (±73.92) | 66.19 (±2.77) | 10.76 (±0.76) |
| Epoxy | 1615.43 (±48.40) | 37.57(±2.97) | 3.57 (±0.53) |
| Kenaf | 2132.15 (±152.26) | 28.34(±1.28) | 2.56 (± 0.40) |
| Flax BL150/Kenaf/Flax BL150 | 2600.65 (±251.69) | 41.06 (±1.83) | 3.45 (±0.35) |
| Flax BL200/Kenaf/Flax BL200 | 2440.13 (± 271.56) | 35.45 (±1.92) | 3.01 (±0.63) |
| Kenaf/Flax BL150/Kenaf | 2390.80 (±104.45) | 44.40 (±6.02) | 3.93 (±0.67) |
| Kenaf/Flax BL200/Kenaf | 2564.86 (±267.41) | 26.85 (±1.26) | 1.80 (±0.50) |

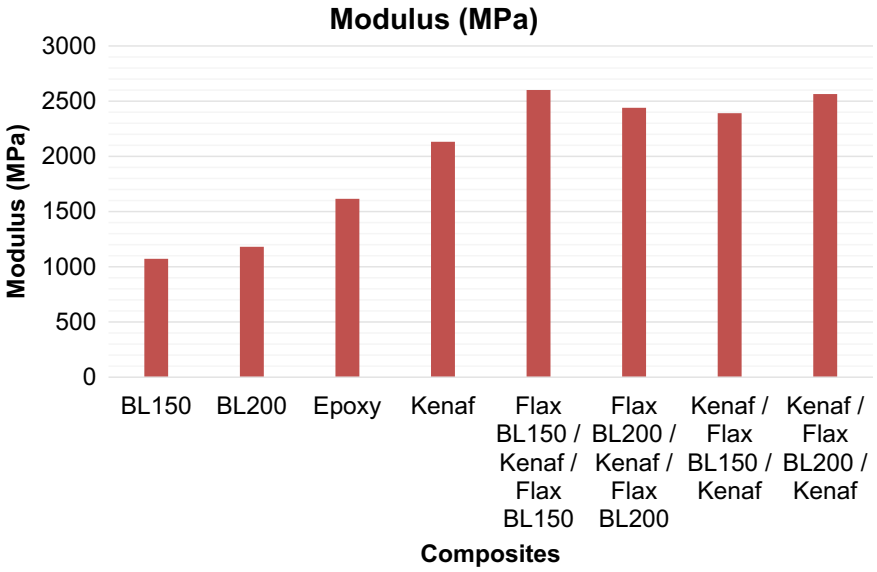


**Fig. 5** Modulus of the composites (MPa)

Hybrid composites have shown an improvement to the modulus and tensile strength of the composites compared to pure fibre composites. All of the pure composites such as Flax BL150, Flax BL200, Kenaf and epoxy had modulus values that were lower than 2200 MPa, while all of the hybrid composites (Flax BL150/Kenaf/Flax BL150, Flax BL200/Kenaf/Flax BL200, Kenaf/Flax BL150/Kenaf and Kenaf/Flax BL200/Kenaf) had modulus values of more than 2300 MPa. The modulus of the composites will influence the tensile strength value of the composites. The compatibility of the components in hybrid composites materials affects the mechanical properties of the material.

## *3.2 Flexural Properties*

During flexural loading on a sample of composite, the upper surface layer of a composite beam undergoes the maximum stress and deformation. As the beam bends under loading, the skin surface and the fibre elongate and shrink linearly from the loading point. While the load is applied, the upper surface is put into compression and the lower surface is put into tension. The internal component of the beam, which is the fibre, will put into shear and adhesion between fibre and matrix will reduce, resulting in debonding. When the applied load is at maximum, the matrix will crack and result in fibre breakage. The flexure load will suddenly decrease as the maximum load for the strength of the composite is exceeded. Table 3 shows the average data of maximum load, maximum stress and flex modulus that were retrieved from the testing.

**Table 3** Data of average flexural test

| | Maximum load (N) | Maximum stress (MPa) | Flex modulus (MPa) |
|---|---|---|---|
| BL150 | 182.65 (±8.09) | 61.64 (±2.73) | 2275.66 (±166.34) |
| BL200 | 187.31 (±3.51) | 57.56 (±1.08) | 2065.17 (±68.17) |
| Epoxy | 219.77 (±16.79) | 83.06 (±6.34) | 2955.60 (±307.09) |
| Kenaf | 146.81 (±14.26) | 48.67 (±4.72) | 3652.64 (±140.06) |
| Flax BL150/Kenaf/Flax BL150 | 196.84 (±19.31) | 64.13 (±6.29) | 3801.78 (±251.98) |
| Flax BL200/Kenaf/Flax BL200 | 211.63 (±27.63) | 73.38 (±9.58) | 4204.29 (±283.72) |
| Kenaf/Flax BL150/Kenaf | 223.37 (±26.43) | 64.94 (±7.68) | 4440.83 (±305.66) |
| Kenaf/Flax BL200/Kenaf | 144.21 (±23.18) | 43.26 (±6.95) | 3805.03 (±187.70) |

Figure 6 shows the graph of flexure stress against flexure strain from the average value of six repeatability specimens tested; which are Flax BL150, Flax BL200, Kenaf, Epoxy, Flax BL150/Kenaf/Flax BL150, Flax BL200/Kenaf/Flax BL200, Kenaf/Flax BL150/Kenaf and Kenaf/Flax BL200/Kenaf. The entire repeatability test towards the same types of sample shows the same pattern; as the flexure stress increased, the flexure strain also increased until the sample failed at a certain maximum stress. Accordance to Hooke's law, the curves indicate that the flexure

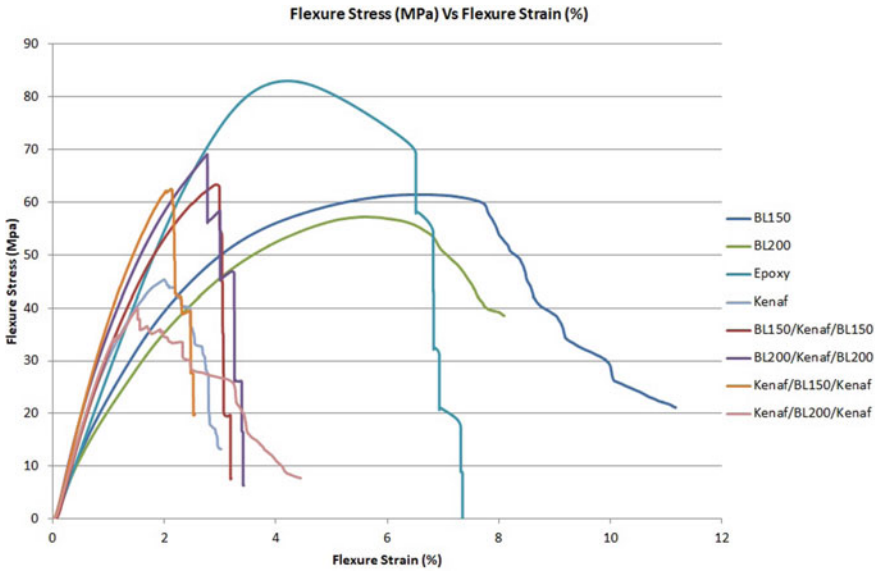


**Fig. 6** Flexure stress (MPa) against flexure strain (%)

stress increase proportionally to the strain until it extend to the proportional limit [26]. From the Fig. 6, it is clearly shows that epoxy have the highest value of flexure stress, while Kenaf/Flax BL200/Kenaf composites have the lowest value of flexure stress. Flax BL150 has the highest value of flexure strain and Kenaf/Flax BL200/Kenaf has the lowest value of flexure strain. It's clearly show that kenaf composites has been improved as the fibre were hybridized with flax shown an increased value of flexure stress and flexure strain in form of Kenaf/Flax BL150/Kenaf, Flax BL150/Kenaf/Flax BL150 and Flax BL200/Kenaf/Flax BL200. However, the hybrid Kenaf/Flax BL200/Kenaf has slightly lower in flexure stress and flexure strain value as compared to kenaf composites. This may due to the orientation of the fibre ply cannot whistand more exerted load pointed on the samples and the adhesion between matrix and fibre debonding much earlier. The presence of sufficient amount of fibres can provide an effective stress transfer between the reinforced fibres and the matrix [27]. Material with high value of flexural strength also has a good adhesion between the fibre and matrix [28]. The exact values of average from the repeatability test were calculated and the data is tabulated in Table 3.

From Table 3, it can be seen that Kenaf/Flax BL150/Kenaf sample need more load exerted before it break and failure which is 223.37 N load, while Kenaf composites only need 146.81 N load to break. The flexural modulus of the Kenaf/Flax hybrid composites with different layering patterns is compared in Fig. 7. The flexural modulus is a measure of resistance of bending deformation of the composites [29]. It was determined that none of the specimens were completely broken at peak load. From the average data, a chart of flex modulus was created to compare the flex modulus between the hybrid composites and the pure composites.

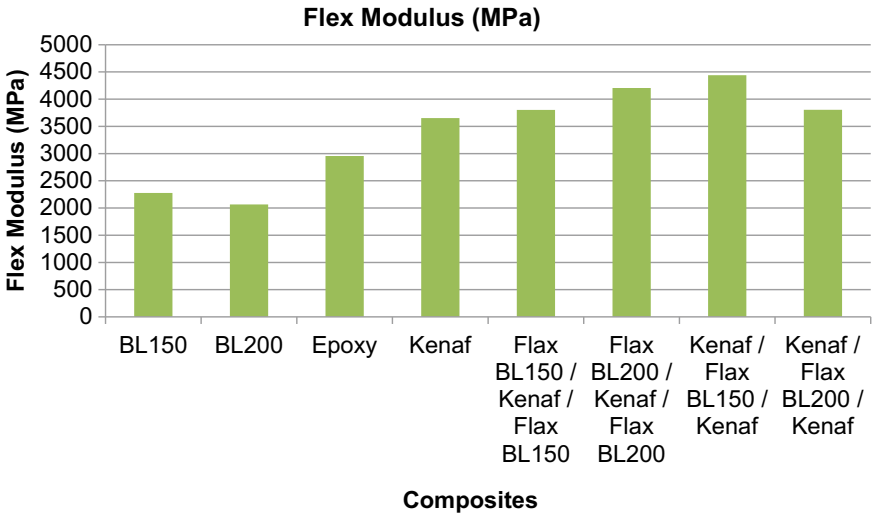


**Fig. 7** Flex modulus chart

From Fig. 7, it was observed that all of the hybrid composites had a higher flex modulus than the pure composites. All hybrid composites have the flex modulus more than 3800 MPa while all pure fibre composites has flex modulus lower than 3700 MPa. The combination of Kenaf/Flax BL150/Kenaf had the highest value of flex modulus, 4440.83 MPa, followed by Flax BL200/Kenaf/Flax BL200 with flex modulus 4204.29 MPa, Kenaf/Flax BL200/Kenaf with flex modulus 3805.03 MPa and Flax BL150/Kenaf/Flax BL150 with flex modulus 3801.78 MPa, while the pure Flax BL200 composites had the lowest value, 2065.17 MPa. This indicates that arranging woven flax fibre and kenaf leads to considerable improvement in the flexural modulus of the composites. It can be justified from the fact that flexural modulus is controlled by the strength of the layers of reinforcement. The hybridisation between flax and kenaf can increase the modulus and strength of the composites compared to the individual fibres themselves. The presence of flax in kenaf composites has proven improves the properties of the composites.

## *3.3 Compression Properties*

All of the tests were conducted under the same test procedure. Data of compressive stress, compressive strain and modulus were collected. The average data of repeatability compression testing were calculated and were presented in Table 4.

Young's modulus, E can be calculated by dividing the compressive stress by the compressive strain in the elastic region. From Table 4, it can be seen that Flax BL200/Kenaf/Flax BL200 has the highest average modulus value which is 1070.34 MPa followed by Kenaf/Flax BL150/Kenaf with 999.63 MPa, Epoxy with 982.94 MPa, Flax BL150 with 913.00 MPa, Kenaf/Flax BL200/Kenaf with 900.10 MPa, Flax BL150/Kenaf/Flax BL150 with 866.72 MPa and Kenaf with 783 MPa. The lowest value of compressive modulus is Flax BL200 which is only

**Table 4** Data of average compression test

| | Modulus (MPa) | Compressive stress (MPa) | Compressive strain (%) |
|---|---|---|---|
| BL150 | 913.00 (50.19) | 130.11 (2.27) | 0.20 (0.01) |
| BL200 | 770.91 (20.31) | 99.08 (1.39) | 0.20 (0.01) |
| Epoxy | 982.94 (376.60) | 63.57 (8.24) | 0.18 (0.13) |
| Kenaf | 783.00 (87.51) | 101.14 (0.93) | 0.23 (0.03) |
| Flax BL150/Kenaf/Flax BL150 | 866.72 (69.58) | 105.71 (4.16) | 0.22 (0.02) |
| Flax BL200/Kenaf/Flax BL200 | 1070.34 (54.20) | 90.24 (2.01) | 0.19 (0.01) |
| Kenaf/Flax BL150/Kenaf | 999.63 (47.98) | 95.49 (1.21) | 0.19 (0.01) |
| Kenaf/Flax BL200/Kenaf | 900.10 (6.21) | 96.17 (5.30) | 0.23 (0.01) |

770.91 MPa. It can be seen that, the modulus of the kenaf composites has been improved as flax fibre is added and hybrid with kenaf fibre.

Figure 8 illustrates the average value of compressive stress against compressive strain curves of the composites samples that undergoes compression testing. The graph demonstrates nonlinear behaviour. The compressive strength of the composites is based on the strength of the matrix and the fibre reinforcement. Flax BL150 has the highest compressive stress among the others samples tested which is 130.11 MPa. The lowest value of compressive stress is 63.57 MPa own by epoxy. As we know, epoxy is much brittle by itself without any reinforcement with fibres. The combination of Flax BL150/Kenaf/Flax BL150 improved a bit of compressive strength of kenaf while the other hybrid composites has lower value of compressive stress than kenaf composites. Generally, most of composites specimens that undergoes compression testing will have a failure by compression and by shear at the load point. From Fig. 8, it clearly shown that most of the sample undergoes a shear compression type of failure. The composites materials have a high compressive strength because they are highly compressed, face failure and brittle microparticles of the matrix will increase the fibre shear rate [30].

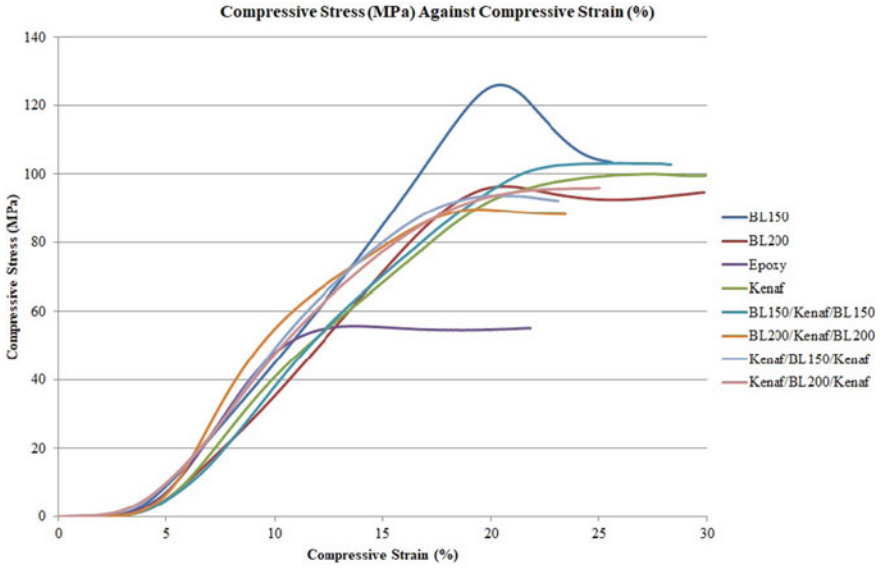


**Fig. 8** Compressive stress (MPa) against compressive strain (%)

### 3.4 *Scanning Electron Microscopy from Tensile Testing Samples*

Scanning electron microscopy (SEM) was used to determined the fracture of tensile, flexural and compression damage in more detail. It can capture a micro image up to 30,000 times of magnification. In this study, the fractures from the testing were magnified up to 600 times in order to observe the fibre breakage and matrix cracking. The scanning electron microscopy images shown in Fig. 9 detailed the structural, morphological features and type of damages occurred on the composites during mechanical testing. In overall, it was observed that the types of failure were mainly on the matrix cracking and fibre breakage. As fibres used were all in the type of woven, the fibre breakage can be seen clearly from the images. It's reveal the poor adhesion in the laminates, which result in fibre pull-out, indicating the poor strength under high load. Just epoxy undergoes matrix cracking only because no present of fibre in it. SEM images illustrated typical brittle plastic nature, with smooth exterior surface and crack in between that indicating poor resistance of the matrix against load or stress exerted on the samples [31]. The fibres and matrix will bend under

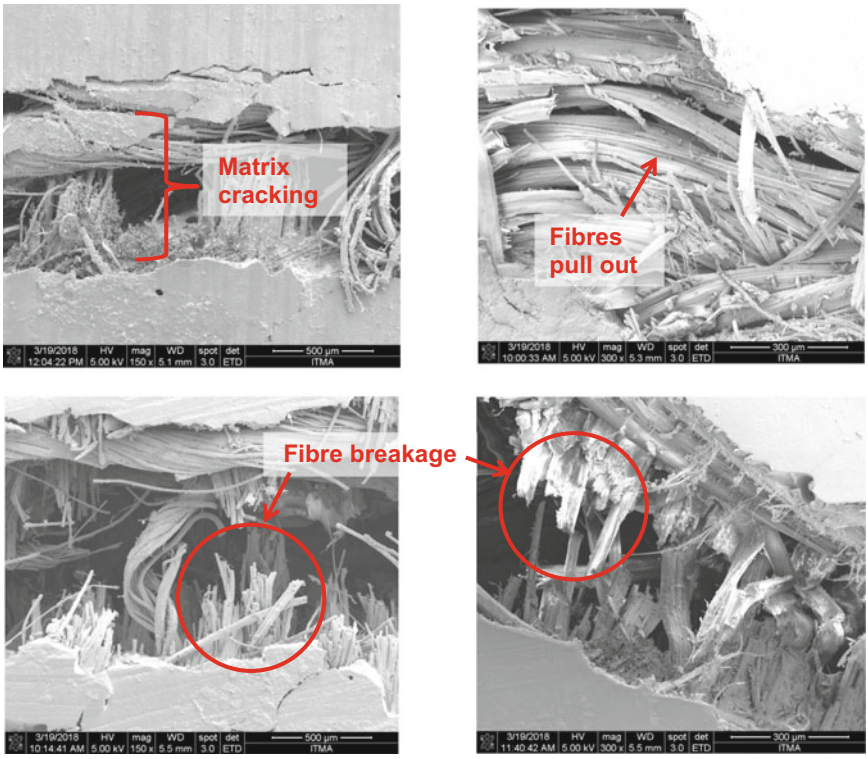


**Fig. 9** The type of failure after tensile testing on the composites

flexure load and compressed under compressive load until it fail to withstand the load. This induces stress concentration on the interface of the fibre/matrix that can creates micro cracks in the matrix and it spread in transverse direction causing fibre fracture. It continues until the woven composites were fractured completely.

## 4 Conclusions

The effect of woven flax fabrics and kenaf reinforced epoxy composites on tensile and flexural properties was studied with different layering patterns of fibre with the same weight ratio of 30:70. From the tensile test results, the hybrid composites made from flax/kenaf has better tensile strength and tensile modulus with minimum increment at 25% and 12%, respectively. From the flexural test results, the flax/kenaf hybrid composites have better flexural strength and flexural modulus with minimum increment at 32% and 4%, respectively. It was clearly determined from the results that the addition of woven flax fibre into pure kenaf composites improved the tensile, flexural and compression properties of the hybrid composites. It was also found that the tensile modulus of the hybrid Flax BL150/Kenaf/Flax BL150 were the highest compared to all the other composites, while Kenaf/Flax BL150/Kenaf has the highest flex modulus and Flax BL200/Kenaf/Flax BL200 has the highest compressive modulus. The stacking sequence pattern of flax/kenaf/flax and kenaf/flax/kenaf affected the flexural, tensile and compression properties of that hybrid composite. Kenaf and flax fibre exhibited superior properties as hybrid reinforcement for polymeric composites under tensile, flexural and compression loading conditions compared to the pure fibres themselves. In this research, we saw how the flax improved the properties of kenaf and vice versa. Moreover, there is a possibility of replacing synthetic fibres such as glass with these hybrid composites for tensile and flexural applications. It is very important to study the tensile, flexural and compression properties of new composites before they are ready to use in various applications especially in structural applications.

**Acknowledgements** This work is supported by UPM under GP-IPS grant, 9486400. The authors would like to thank the Department of Aerospace Engineering, Faculty of Engineering, Universiti Putra Malaysia and Laboratory of Biocomposite Technology, Institute of Tropical Forestry and Forest Products (INTROP), Universiti Putra Malaysia (HICOE) for the close collaboration in this research.

## References


1. Specialists Bcomp. Natural fiber specialists. Bcomp Technology. http://www.bcomp.ch/10-0-natural-fibers.html. Accessed 23 Nov 2019
2. CSIR (2009) What are natural fibers? Council for Scientific and Industrial Research. Food and Agriculture Organisations of United Nations. http://www.csir.co.za/Grips/fibres.html. Accessed 22 Dec 2019
3. Mohanty Amar K, Misra Manjusri, Drzal Lawrence T (2005) Natural fibers, biopolymers, and biocomposites. CRC Press, Florida, p 2004058580
4. Derasid Z, Abdullah A (2012) What is kenaf. Kenaf Everise. Everise Crimson (M) Sdn Bhd. http://www.kenaf-everise.com.my/Kenaf_Everise/What_is_Kenaf.html. Accessed 26 June 2019
5. Raman Bharath VR, Vijaya Ramnath B, Manoharan N (2015) Kenaf fibre reinforced composites: a review. ARPN J Eng Appl Sci 10(13):5483–5485
6. Razali N, Sultan MTH, Safri SNA, Basri S, Yidris N, Mustapha F (2014) High velocity impact test on glass fibre reinforced polymer (GFRP) using a single stage gas gun (SSGG)—an experimental based approach. Appl Mech Mater 564:376–381. https://doi.org/10.4028/www.scientific.net/AMM.564.376
7. ASTM D 3039-14 (2014) Standard test method for tensile properties of polymer matrix composite materials. Annual Book of ASTM Standard 15:03. https://doi.org/10.1520/D3039_D3039M-14
8. Shah AUM, Sultan MTH, Jawaid M, Cardona F, Talib ARA (2016) A review on the tensile properties of bamboo fiber reinforced polymer composites. BioResouces 11(4). https://doi.org/10.15376/biores.11.4.Shah
9. Ghassan TK (2006) Material properties and characterisation. Manuf Syst Eng Ser 6:1–22. https://doi.org/10.1007/0-387-23291-5_1
10. ASTM D7264/D7264M-15 (2015) Standard test method for flexural properties of polymer matrix composite materials. ASTM International, West Conshohocken, PA. 15(03). https://doi.org/10.1520/d7264_d7264m-15
11. Salleh Z, Yunus S, Masdek N, Taib Y, Azhar I, Hyie K (2018) Tensile and flexural test on kenaf hybrid composites. Paper presented at the IOP conference series: materials science and engineering
12. Bahtiar WM (2012) Investigation on the mechanical and physical of treated and untreated woven sugar-palm fibre reinforced composites. Master Thesis of Faculty of Mechanical Engineering, Universiti Tun Hussien on Malaysia
13. Nurazzi NM, Khalina A, Sapuan SM, Rahmah M (2018) Development of sugar palm/glass fibre reinforced unsaturated polyester hybrid composites. Mater Res Express 5(4):045308
14. Jumahat A, Amir W, Soutis C, Kasolang S (2014) Flexural response of nanoclay-modified epoxy polymers. Mater Res Innov 18(sup6), S6-280–S286-285
15. Sapuan SM, Lok HY, Ishak MR, Misri S (2013) Mechanical properties of hybrid glass/sugar palm fibre reinforced unsaturated polyester composites. Chin J Polym Sci 31(10):1394–1403. https://doi.org/10.1007/s10118-013-1324-4
16. Haque M, Rahman R, Islam N, Huque M, Hasan M (2010) Mechanical properties of polypropylene composites reinforced with chemically treated coir and abaca fiber. J Reinf Plastics Compos 29(15):2253–2261
17. Assaedi H, Alomayri T, Shaikh FUA, Low IM (2015) Characterisation of mechanical and thermal properties in flax fabric reinforced geopolymer composites. J Adv Ceramics 4(4):272–281. https://doi.org/10.1007/s40145-015-0161-1
18. Mahendrakumar N, Thyla PR, Mohanram PV, Sabareeswaran A, Manas RB, Srivatsan S (2015) Mechanical and dynamic properties of nettle polyester composite. Mater Express 5(6):505–517. https://doi.org/10.1166/mex.2015.1263
19. Saba N, Paridah M, Abdan K, Ibrahim N. (2016) Effect of oil palm nano filler on mechanical and morphological properties of kenaf reinforced epoxy composites. Construct Build Mater 123, b, 133–138

20. Khoshnava SM, Rostami R, Ismail M, Rahmat AR, Ogunbode BE (2017) Woven hybrid biocomposites: Mechanical properties of woven kenaf bast fibre/oil palm empty fruit bunches hybrid reinforced poly hydroxybutyrate biocomposite as non-structural building materials. Construct Build Mater 154:155–166. https://doi.org/10.1016/j.conbuildmat.2017.07.189
21. Fragassa C, Pavlovic A, Santulli C (2017) Mechanical and impact characterisation of flax and basalt fibre vinylester composites and their hybrids. Compos Part B. https://doi.org/10.1016/j.compositesb.2017.01.004
22. Yusoff R, Takagi H, Nakagaito AN (2016) Tensile and flexural properties of polylactic acid-based hybrid green composites reinforced by kenaf, bamboo and coir fibers. Ind Crops Products 94:562–573. https://doi.org/10.1016/j.indcrop.2016.09.017
23. Morye SS, Wool RP (2005) Mechanical properties of glass/flax hybrid composites based on a novel modified soybean oil matrix material. Soc Plastic Eng 407–416. https://doi.org/10.1002/pc.20099
24. Hojo T, Xu Z, Yang Y, Hamada H (2014) Tensile properties of bamboo, jute and kenaf mat-reinforced composite. Energy Proc 56:72–79. https://doi.org/10.1016/j.egypro.2014.07.133
25. Jawaid M, Abdul Khalil HPS, Abu Bakar A (2011) Woven hybrid composites: tensile and flexural properties of oil palm-woven jute fibres based epoxy composites. Mater Sci Eng, A 528:5190–5195. https://doi.org/10.1016/j.msea.2011.03.047
26. Zhang Y, Li Y, Ma H, Yu T (2013) Tensile and interfacial properties of unidirectional flax/glass fiber reinforced hybrid composites. Compos Sci Technol 88:172–177. https://doi.org/10.1016/j.compscitech.2013.08.037
27. Petrucci R, Santulli C, Puglia D, Sarasini F, Torre L, Kenny JM (2013) Mechanical characterisation of hybrid composite laminates based on basalt fibres in combination with flax, hemp and glass fibres manufactured by vacuum infusion. Mater Design 49:728–735. https://doi.org/10.1016/j.matdes.2013.02.014
28. Yahaya R, Sapuan SM, Jawaid M, Leman Z, Zainudin ES (2014) Mechanical performance of woven kenaf-kevlar hybrid composites. Reinf Plastics Compos 33(24):2242–2254. https://doi.org/10.1177/0731684414559864
29. Muhammad YH, Ahmad S, Abu Bakar MA, Mamun AA, Heim HP (2015) Mechanical properties of hybrid glass/kenaf fibre-reinforced epoxy composite with matrix modification using liquid epoxidised natural rubber. J Reinf Plastics Compos 34(11):896–906. https://doi.org/10.1177/0731684415584431
30. Arbelaiz A, Fernandez B, Cantero G, Llano-Ponte R, Valea A, Mondragon I (2005) Mechanical properties of flax fibre/polypropylene composites. Influence of fibre/matrix modification and glass fibre hybridization. Compos Part A Appl Sci Manuf 36:1637–1644. https://doi.org/10.1016/j.compositesa.2005.03.021
31. Ghani MAA, Salleh Z, Hyie KM, Berhan MN, Taib YMD, Bakri MAI (2012) Mechanical properties of kenaf/fiberglass polyester hybrid composite. Proc Eng 41:1654–1659. https://dx.doi.org/10.1016/j.proeng.2012.07.364

# Effect of Stacking Sequences on the Energy Absorption Performances of the Rectangular-Shaped Crash Boxes Reinforced Hybrid Composites


**Al Emran Ismail and Justin Anak Empaling**

**Abstract** In this work, the effect of fiber type stacking sequences and the inclined angle of two rectangular tubes on the crashworthiness performances are investigated. Three type of fiber materials are used such as kenaf, glass and carbon fibers. These fibers are wetted with resin and wrapped over the mold. Three stacking sequences are implemented such as Kenaf-Carbon-Glass (KCG), Glass-Kenaf-Carbon (GKC) and Carbon-Glass-Kenaf (CGK) fiber configurations. Hand layout technique is used to fabricate the tubes where epoxy resin is used to harden the fibers. The composite tubes are positioned vertically and compressed quasi-statically at 5 mm/min to obtain their force-displacement curves. Based on the experimental works, it is found that fiber stacking sequences played an important role is increasing the specific energy absorption (SEA) capability and the introduction of inclined sides of rectangular tubes also improve the SEA. However, 8° side inclination angle attained higher level of force ratio compared with others.

**Keywords** Energy absorption · Hybrid fiber composites · Crushing, crash boxes

## 1 Introduction

Composite materials are commonly used in most of engineering applications especially in automotive and aerospace industries. The selection of composite materials due to high strength-to-weight ratio. In stead of this, composite materials capable to absorb impact or crush energy more than steel materials through multiple toughening mechanisms. Due to sustainable approaches, natural fiber is progressively used to replace synthetic fiber due to environmentally friendly materials. Therefore, natural and synthetic fibers are combined to consider the advantages and disadvantages of these fibers.

A. E. Ismail (✉) · J. A. Empaling
Faculty of Mechanical and Manufacturing Engineering, Universiti Tun Hussein Onn Malaysia (UTHM), Batu Pahat, Johor, Malaysia
e-mail: emran@uthm.edu.my; al.emran.ismail.77@gmail.com

© Springer Nature Singapore Pte Ltd. 2021

M. Jawaid et al. (eds.), *Structural Health Monitoring System for Synthetic, Hybrid and Natural Fiber Composites*, Composites Science and Technology,
https://doi.org/10.1007/978-981-15-8840-2_13

Yahaya et al. [1] studied the effect of layering sequence on the mechanical properties of woven kenaf-aramid hybrid laminated composites. There are three mechanical tests are conducted such as tension, flexure and impact. It is confirmed that layering sequences affected the mechanical performances. For further information on the fiber hybridization in polymer composites such information can be found here [2].

In term of crashworthiness performances, several works in open literature are found such as Kim et al. [3] investigated the crushing behaviors of composite circular tubes with different reinforcing fibers. They compared the tubes made of carbon, Kevlar and their hybridization. It is found that hybrid and non-hybrid has different effect on the crashworthiness performances and it is also suggested that if energy absorption capability and post-crush integrity are simultaneously required, the hybrid composite tubes are the best material condition. In summary, Supian et al. [4] reviewed the influence of hybrid fibers reinforced thermoset polymer composite in energy absorption tube applications. The combinations of natural and synthetic fibers exhibited more desirable option of failure modes therefore capable to absorb more energy during impact collisions.

Hamza et al. [5] also studied the influence of geometric shape on the deformation performance of natural jute/epoxy specimens under axial quasi-static compression. The corrugated and circular cross-sectional samples with three layers exhibited stable and progressive deformation failure mechanisms. The failure modes associated with these samples were lamina bending, friction effect, axial cracks with delamination. The corrugated configuration tube can be considered as the most favorable compared to the circular configuration tube, which showed the higher of SEA and CE value of 22 J/g and 81% respectively. Thus, the jute/epoxy composite tube is possible to be utilized as an energy absorption device. In another work, Ismail and Kamarudin [6] numerically investigate the phenomena of hybrid composite tubes under quasi-static compression. Changing the elliptical aspect ratio improved the performance of specific energy absorption.

Therefore, this paper presents the influence of stacking sequences and side-angle of rectangular tubes under compression. Three important crashworthiness parameters such as specific energy absorptions and force ratios are extracted from the force-displacement curves. Crushing mechanisms are also observed during the progressive collapses.

## 2 Methodology

### *2.1 Composite Fabrications*

In this work, experimental studies are conducted on the rectangular tubes under quasi-static compressive loading. The sizes of tubes are 107 × 74 × 140 mm and the molds are prepared according to these sizes. On the other hand, two sides of the tubes are inclined at specific angles such as 0°, 4°, 8°, 12° and 16° as shown

in Fig. 1a, b reveals the completed hybrid composite tube. Hand-layup technique is used to fabricate composite tubes where fiber strands are firstly wetted with the resin and wrapped around the mold. A release agent is used and applied to the surface of mold to prevent sticking between two composite and mold surfaces. During the wrapping processes, three type of fibers are used such as kenaf, glass and carbon fibers and only three layers are considered as tabulated in Table 1. One the processes are accomplished; they are cured for 24 h for fully hardened and removed from the mold.

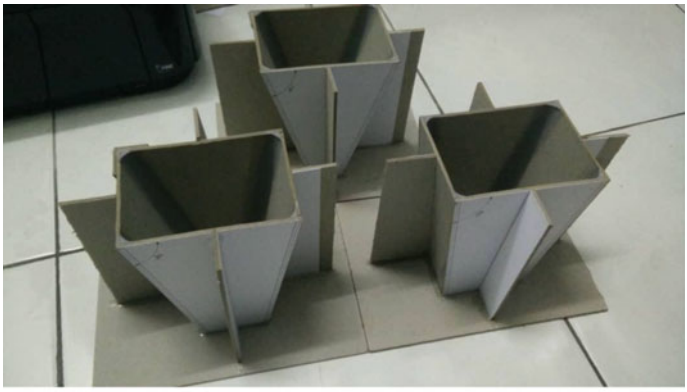

(a)

(b)

**Fig. 1** **a** Mold used to fabricate the composite tubes and **b** Completed composite tube

**Table 1** Type of composites and geometry parameters

| Type of samples | Fiber sequences | Side angles, θ | Weight, (gram) |
|---|---|---|---|
| H1 | KCG | 0° | 192 |
| H2 | | 4° | 182 |
| H3 | | 8° | 176 |
| H4 | | 12° | 165 |
| H5 | | 16° | 150 |
| H6 | GKC | 0° | 218 |
| H7 | | 4° | 209 |
| H8 | | 8° | 201 |
| H9 | | 12° | 174 |
| H10 | | 16° | 164 |
| H11 | CGK | 0° | 207 |
| H12 | | 4° | 198 |
| H13 | | 8° | 194 |
| H14 | | 12° | 192 |
| H15 | | 16° | 186 |

## 2.2 Quasi-Static Compression Tests

Quasi-static compression test is conducted using Universal Testing Machine (UTM) with a constant cross-head displacement of 5 mm/min. Samples are positioned axially between two flattened rigid plates and they are quasi-statically compressed and the force and displacement data are recorded automatically. The tubes are compressed approximately at 75% of total height. Figure 2 shows the compression processes at initial stage (Fig. 2a) while Fig. 2b indicates the failure occurred somewhere during the progressive collapses.

## 2.3 Crashworthiness Performances

Performances of energy absorbing materials can be measured through their specific energy absorption (SEA), Peak or maximum force and mean force. These parameters can be obtained from the force-displacement curves. For an example, the energy absorption is determined using the area under the force-displacement curves as in Eq. (1):

$$\text{SEA} = \frac{\text{Energy Absorbed, E}}{\text{Mass of Material Crushed, m}} = \frac{\int_{x,\text{start}}^{x,\text{end}} F dx}{m} \tag{1}$$

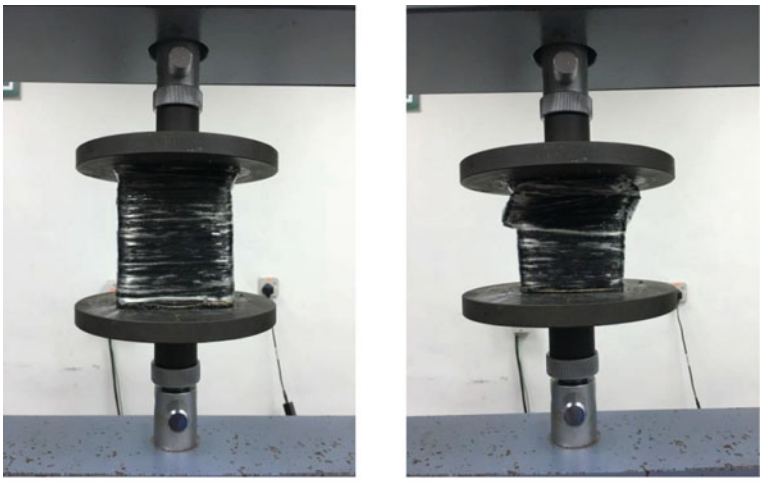


**Fig. 2** **a** Compression process at the initial stage, and **b** Progressive collapse during the compression process

Force ratio or some other called crush efficiency (CE) is defined as in Eq. (2):

$$Force\ ratio = \frac{F_{mean}}{F_{peak}} \tag{2}$$

Peak or maximum force is identified as the highest force experienced during the event and it is the potential force to cause the injury to the occupants or pedestrian in a crash situation. One of the main purposes is to reduce the level of peak force relative to the mean force.

## 3 Results and Discussion

### *3.1 Force-Displacement Responses*

Figure 3 shows the responses of force-displacement curves of three different fiber stacking sequences under quasi-static compression. For each hybrid condition, different side inclination angles, θ are varied. Based on the experimental observations, fiber stacking configurations played an important role in increasing the responses of force-displacement curves. Kenaf-Carbon-Glass (KCG) fiber reinforced composites (as in Fig. 3a) produced the lowest resistance while Carbon-Kenaf-Glass (CKG) fiber reinforced composites (as in Fig. 3c) attained the highest resistance to the compressive deformations. It is also observed samples 16° (H5, H10 and H15)

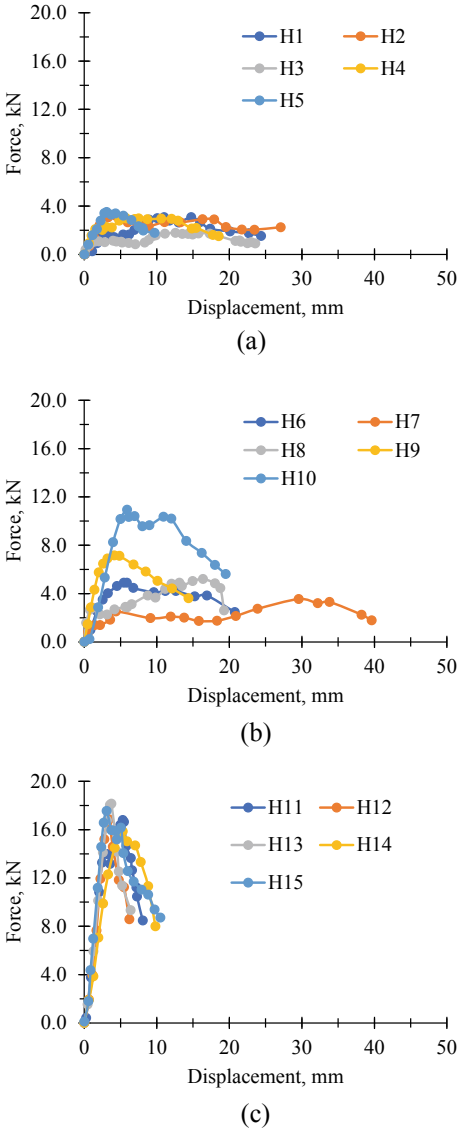


**Fig. 3** Force-displacement curves of hybrid fiber reinforced composites, **a** Kenaf-Carbon-Glass fiber reinforced composites, **b** Glass-Kenaf-Carbon fiber reinforced composites and **c** Carbon-Glass-Kenaf fiber reinforced composites for different angles of tube

sided tubes produced higher force-displacement curves compared with other type of composites. Figure 4 reveals the progressive collapse of H2 typed composite tube. After the elastic deformation, the tube experienced localized failure at the location just below the upper end and estimated approximately 50 mm from the top end. Further loading, localized buckling occurred producing large composite fragmentations. Large composite fragmentations responsible for lower force-displacement responses.

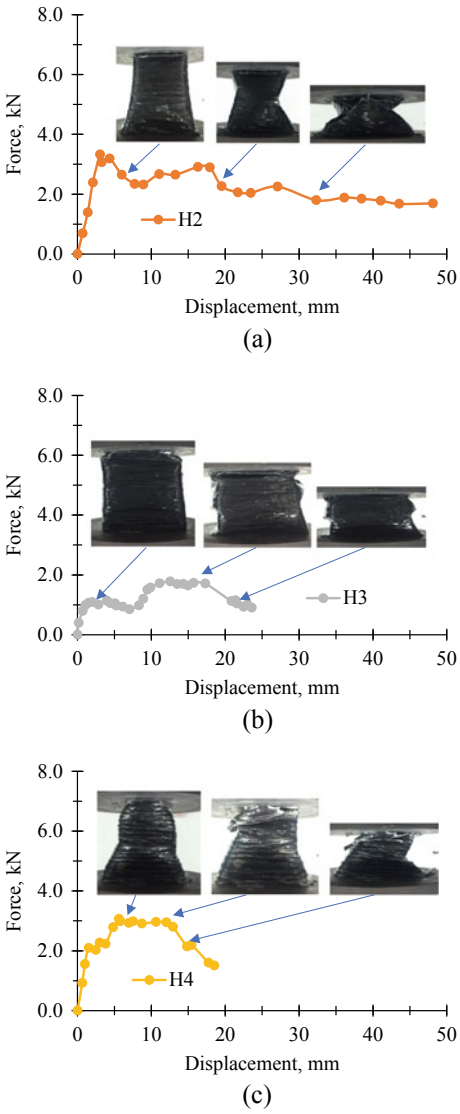


**Fig. 4** Progressive collapse of H2 hybrid composite tube

## *3.2 Specific Energy Absorptions*

Specific energy absorption (SEA) is determined according to Eq. (1). SEA indicates that the capabilities of composite tubes to absorb compression energy. The energy absorption is then divided with the weight of crushed material to produce the specific energy absorption (SEA). Based on Fig. 5, it is observed there is a strong effect of inclined angles played significant role where increasing such angles capable to

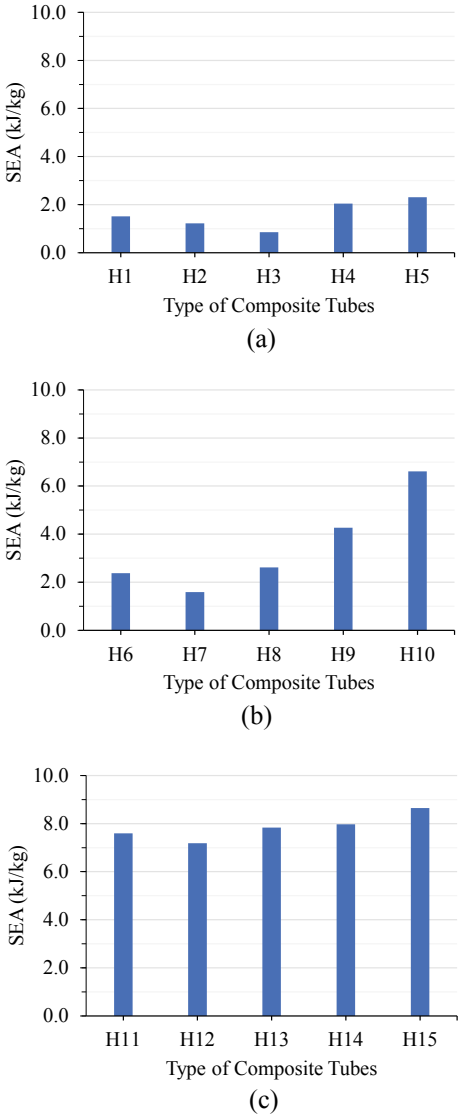


**Fig. 5** Specific energy absorption of hybrid fiber reinforced composites, **a** Kenaf-Carbon-Glass fiber reinforced composites, **b** Glass-Kenaf-Carbon fiber reinforced composites and **c** Carbon-Glass-Kenaf fiber reinforced composites for different angles of tube

increase the performance of energy absorptions for all hybrid sequences. This is indicated that the angles acted as crush initiators where it is able to initiate the crushing process and on the other hand preventing the global buckling to occur. This behavior is important since it is capable to enhance the energy absorption performances.

Based on Fig. 5a, it is revealed that lower SEA can be obtained if KCG configuration is used. When the crush initiator is introduced, the trend of SEA is increased slightly as the angle of side inclination of the tubes increased. Similar pattern of SEA increment can be seen for GKC stacking sequence is selected except the level of SEA

is relatively higher for the case of KCG condition as shown in Fig. 5b. For the case of CGK sequence as in Fig. 5c, higher SEA can be obtained however the effect of inclined angles seem to be insignificant since the increment of SEA is almost similar.

### *3.3 Force Ratio*

Figure 6 shows the effect of fiber stacking configurations on the force ratio when the angle of tubes is varied. The force ratio is defined as in Eq. (2). The peak force, $P_{peak}$ means the maximum force occurred during the crashing processes. The force ratio should be as high as possible to control energy absorption efficiency without causing much damage or injury to the passengers or pedestrians. Equation (2) indicates that if the force ratio is less than 1.0, it is revealed that the mean or average force is less than the peak force. On the other hand, the capability to absorb the energy is less efficient.

Figure 6a shows the force ratio for the case of KCG configurations. It is seemed that the force ratio is reduced as the tube angles increased indicating that higher tendency of tubes to experience catastrophic failure. Similar trends are also observed for other fiber configurations as in Fig. 6b, c. It is also revealed that the samples of H3, H8 and H13 attained the highest level of force ratio for a similar group of fiber configurations especially for KCG and GKC hybrid composite tubes. The angle of 8° is the best inclination angle can be used as a crush initiator in order to maintain higher force ratio.

## 4 Conclusion

From experimental results conducted on the hybrid composite tubes subjected to quasi-static compression, several conclusions can be listed as below:

1. It is found that fiber stacking sequences played an important role in determining the specific energy absorption (SEA) capability.
2. The most stand-out sided angle of rectangular tubes is 8° specially to attain higher level of force ratio.
3. It is also observed that large composite fragmentations contributed lower value of SEA while small fragmentation produced higher SEA.

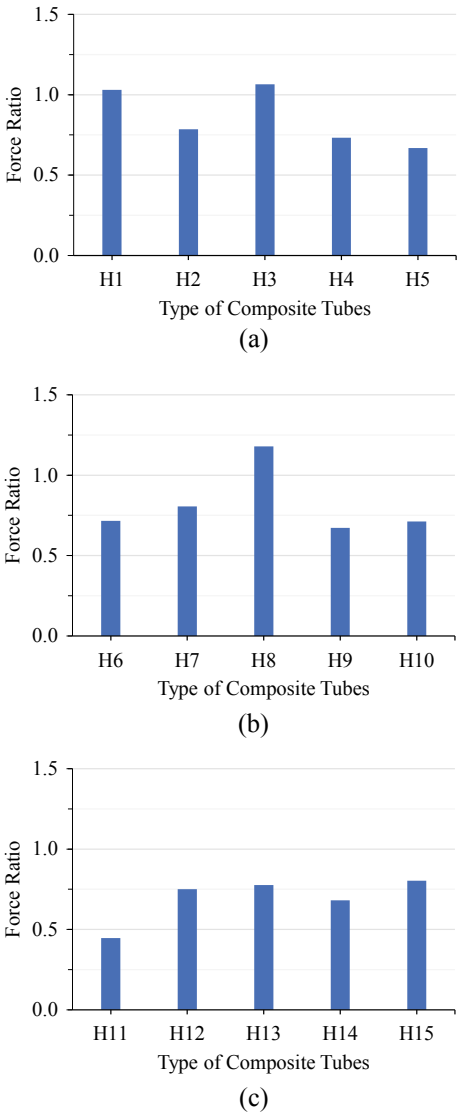


**Fig. 6** Force ratio of hybrid fiber reinforced composites, **a** Kenaf-Carbon-Glass fiber reinforced composites, **b** Glass-Kenaf-Carbon fiber reinforced composites and **c** Carbon-Glass-Kenaf fiber reinforced composites for different angles of tube

## References

1. Yahaya R, Sapuan SM, Jawaid M, Leman Z, Zainudin ES (2015) Effect of layering sequences and chemical treatment on the mechanical properties of woven kenaf-aramid hybrid laminated composites. Mater Des 67:173–179
2. Swolfs Y, Gorbatikh L, Verpoest I (2014) Fibre hybridisation in polymer composites: a review. Compo: Part A 67:181–200
3. Kim Jung-Seok, Yoon Kyuk-Jin, Shin Kwang-Bok (2011) A study on crushing behaviours of composite circular tubes with different reinforcing fibers. Int J Impact Eng 38:198–207

4. Supian ABM, Sapuan SM, Zuhri MYM, Zuhri ES, Zainudin ES, Ya HH (2018) Hybrid reinforced thermoset polymer composite in energy absorption tube application: a review. Defence Technol 14:291–305
5. Hamza SS, Yuhazri Yaakob M, Ismail AE, Absi SMA (2019) influence of geometric shape on the deformation performance of natural jute/epoxy specimens under axial quasi-static compression. Test Eng Manag, 719–732
6. Ismail AE, Kamarudin K-A (2019) Modeling of crushing mechanisms of hybrid metal/fiber composite cylindrical tubes. In: Modelling of damage processes in Biocomposites, fibre-reinforced composites and hybrid composites. Woodhead Publishing Series in Composites Science and Engineering (2019) 27–39

# Energy Absorption of Tilted Rectangular Composite Crash Boxes


**Al Emran Ismail and Muhammad Syafiq Abdul Rahman**

**Abstract** This paper presents the investigation of energy absorption of tilted rectangular crash boxes fabricated using fibers (natural or synthetic) reinforced composites. Three types of fiber are used such as glass, carbon and kenaf fibers which are then immersed into polyester resin before they are wrapped around the mold. Quasi-static compression is used to crush the composite tubes and force-displacement responses are obtained. Two important parameters are considered such as specific energy absorption and force ratio. Based on the experimental studies, it is found that kenaf fiber reinforced composites attained higher capability of energy absorption compared with other type of fibers while increasing the tilted angles capable to increase the force ratio and therefore increasing the energy absorption performances.

**Keywords** Energy absorption · Hybrid composite · Crash boxes

## 1 Introduction

The crash box plays important roles to manage crushing energy during a collision event. This device is generally positioned at the frontal end of the vehicle. There are two paramount important factors affecting the performance of crash boxed for examples geometry of the crash boxes and materials used to construct them. The influence of these factors is summarized in [1, 2]. Due to the high strength-to-weight ratio, composite materials are used especially in automotive industries. For crushing applications, composite is the primary choice since it is capable to absorb more impact energy relative to metal. This is due to the fact that composite materials offer various kind of toughening mechanisms.

An investigation on energy absorption of natural and hybrid fibres under quasi-static compression are conducted in [1]. In term of failure modes and load-displacement curve, the circular geometry is considerably better than the square

A. E. Ismail (✉) · M. S. A. Rahman
Faculty of Mechanical and Manufacturing Engineering, Universiti Tun Hussein Onn Malaysia, Batu Pahat 86400, Johor, Malaysia
e-mail: emran@uthm.edu.my; al.emran.ismail.77@gmail.com

© Springer Nature Singapore Pte Ltd. 2021

M. Jawaid et al. (eds.), *Structural Health Monitoring System for Synthetic, Hybrid and Natural Fiber Composites*, Composites Science and Technology,
https://doi.org/10.1007/978-981-15-8840-2_14

geometry. The effect of fibre orientations on energy absorption is also studied by Hu et al. [2]. They prepared the prepreg material and rolled over the steel mandrel and then cured into an autoclave where the material or fibre orientations are varied to study the effect on the energy absorption. Two types of tests are used such as static and dynamic compression tests. It is found that the variation of peak force can be divided into two when orientations are increased. If the value below than 45°, the peak force decreases while if the value greater than 45° the peak force increases. On the other hand, for the specific energy absorption, there is an insignificant effect when the different value of fibre orientations is used.

Several review papers can be found in [3] to summarize the fibre hybridization in polymer composites. This paper focused on the performances of tensile strength for hybrid fibre-reinforced composites and stated that the effect of fibre hybridization on tensile strength is full understanding. However, under a more complex condition such as flexural, impact and fatigue tests are not well known. More extensive works must be conducted to study the influence of fibre hybridization on the experimentations. Alkbir et al. [4] also reviewed the fiber properties and crashworthiness of natural fibre-reinforced composites. They summarized that several previous experiments have been carried out to investigate natural fiber reinforced composite tubes and exhibited that these natural fibre-reinforced composites have an advantage of good energy absorption and probably be replaced the synthetic fiber in the near future.

Research advances of the crashworthiness performances of thin-walled energy absorbers is summarized by Baroutaji et al. [5]. They stated that modifying the shape of geometry is always considered as an effective way for enhancing the crashworthiness capability of materials and structures. This includes considering the use of multi-cell composite inside the tube and also the used of functional graded materials. This is important to control the mechanism of progressive collapses. The study of woven type natural fiber on the crushing behavior can also be found in [6, 7].

In this work, different types of fiber are used to fabricate rectangular tubes considering tilted angles at one end. These angles are assumed to act like crush initiators. The fibers such as glass, carbon and kenaf are wetted with polyester resin and wrapped around the molds. Once the composite tubes are hardened, they are positioned vertically and compressed quasi-statically to obtain their force-displacement responses. Then, the specific energy absorption and force ratio are determined and discussed in the relation with the collapse mechanisms.

## 2 Experimentation

### *2.1 Composite Preparations*

The shape and dimension of the crash box are based on the actual device obtain directly from the commercial vehicle. In general, the size of the crash box is 107 × 74 × 140 mm. However, in this work two-sided angles are varied in order to investigate

the effect on the performances of energy absorption such as 0°, 4°, 8°, 12° and 16°. Five molds are prepared to produce the crash boxes as shown in Fig. 1.

The hand-layout method is used to fabricate the composite tubes where the fibers are immersed into epoxy resin bath and wrapped around the mould. A release agent is also used to prevent stick between fibers and the mold. Three types of fibers is used in the form of strands such as glass, carbon and kenaf fibers. These fibers wetted by polyester resin are wounded around the mould three times to produce three-layered composite tubes. Table 1 summarizes the parameters involved during composite preparations.

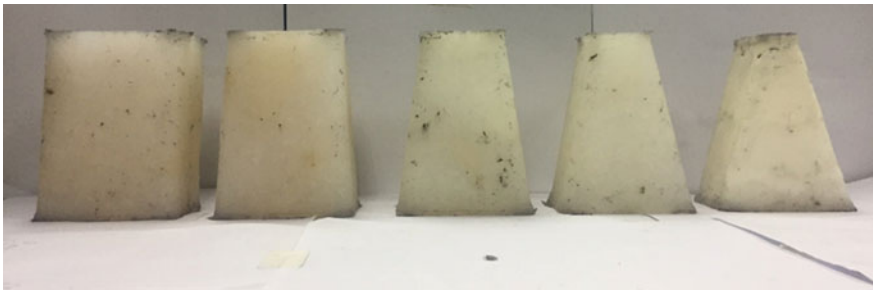

**Fig. 1** Molds used to fabricate the composite tubes (0°, 4°, 8°, 12° and 16°) (from left to right)

**Table 1** Composite tubes parameterizations

| Type of samples | Fibers | Side angles, θ | Weight, (gram) |
|---|---|---|---|
| S1 | Glass | 0° | 129 |
| S2 | | 4° | 118 |
| S3 | | 8° | 112 |
| S4 | | 12° | 106 |
| S5 | | 16° | 78 |
| S6 | Carbon | 0° | 105 |
| S7 | | 4° | 99 |
| S8 | | 8° | 88 |
| S9 | | 12° | 79 |
| S10 | | 16° | 74 |
| S11 | Kenaf | 0° | 136 |
| S12 | | 4° | 132 |
| S13 | | 8° | 107 |
| S14 | | 12° | 125 |
| S15 | | 16° | 114 |

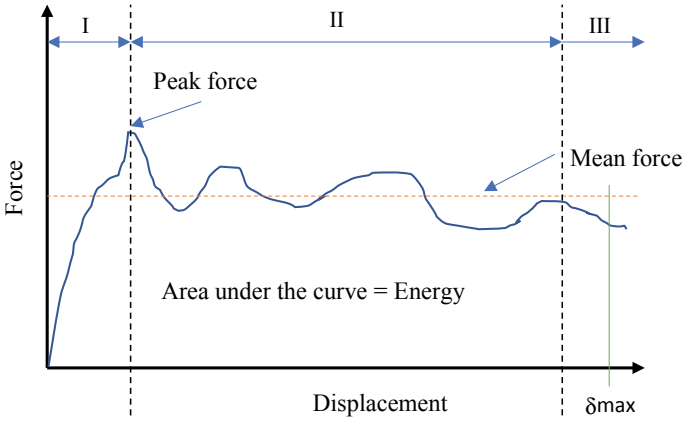


**Fig. 2** Schematic diagram of the force-displacement curve

## *2.2 Quasi-Static Compression Test*

A compression test is conducted using Universal Testing Machine (UTM). Composite tunes are positioned vertically between two flattened rigid plates. The bottom plate is stationary while the upper plate is moving downward at a constant cross-head displacement of 5 mm/min. During compression, force and displacement are automatically recorded and plotted as shown in Fig. 2.

Force-displacement curve is valuable to extract the following parameters:

$$\text{Energy absorption, } E = \int_0^{\delta max} P(\delta) d(\delta) \tag{1}$$

$$\text{Mean load, } P_m = \frac{E}{\delta_{max}} \tag{2}$$

$$\text{Crush load efficiency, } CFE = \frac{P_m}{P_{max}} \times 100 \tag{3}$$

# 3 Results and Discussion

## *3.1 Progressive Collapse of Composite Tubes*

Figures 2 and 3 reveal the progressive collapses of composite tubes under quasi-static compression. According to Fig. 2 the schematic diagram of a typical force-displacement curve, the curve can be divided into three main regions. The first region

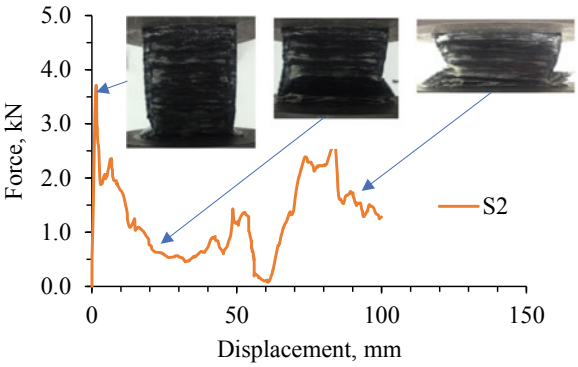


**Fig. 3** Force-displacement curves of fibreglass reinforced tubes sample S1

(I), it is an elastic deformation where the force is linearly proportional to the displacement. Once further loading is continued, the first plastic or fracture occurred indicating a sudden drop of force. The fluctuation of forces is taken place to show that multiple progressive fractures occurred as shown in region II. The last or final is region III, this region produced the lowest energy absorption capability since a huge amount of force is applied to accumulate an insignificant amount of displacement.

Figure 3 represents the sample S1 where the rectangular sides are not tilted. It is meant there is no triggering mechanism is used as a result higher peak force can be observed. However, on the other hand, large force drop occurred. According to collapse mechanism, localized buckling occurred in the approximately at the tube middle point which is responsible for large force drop.

## *3.2 Force-Displacement of Composite Tubes*

For the case of 8° tilted rectangular tube designated as sample S3, the fracture initiated at the upper end of the tubes. This is as expected since the narrow-ended tube acts a crush initiator. As compared with Figs. 3 and 4 shows that the collapse of the tube is more stable and in control manner since the force drop after the peak force is insignificant. Same goes to sample S6 as in Fig. 5, where there is no crush initiator. Large force drop can be observed where based on the observation, it can be seen that localized buckling occurred at the middle height of the tube during the compression. Large force drops also contribute to lower the efficiency of energy absorption performances.

Figure 6 shows the responses of force-displacement curves for various tilted angles and for a different type of fibers. In comparison, synthetic fiber reinforced composites show more stable in term of the way of collapses where there is low force fluctuation during region II as in Figs. 6a, b. On the other hand, Fig. 6c shows the responses of force-displacement curves for kenaf fibre-reinforced composite tubes. For this type of composite, large force drops and force fluctuations can be observed even

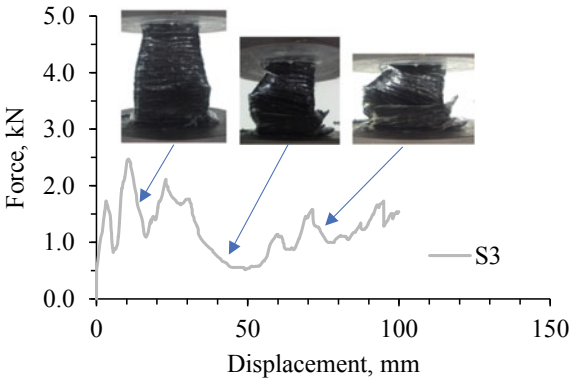


**Fig. 4** Force-displacement curves of fibreglass reinforced tubes sample S3

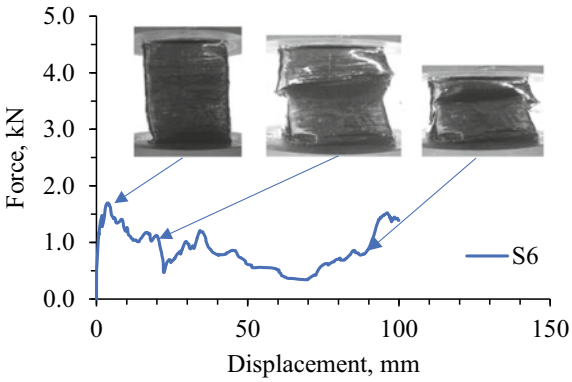


**Fig. 5** Force-displacement curves of fibreglass reinforced tubes sample S6

though crush initiator is used. Based on the observation, large force drop and force fluctuations are observed as a result of large composite fragmentation during the collapses.

### *3.3 Effect of Sided-Rectangular Tubes on the Specific Energy Absorption and Force Ratio*

Figure 7a shows the effect of tilted rectangular tube angles on the specific energy absorption for different type of fibers. In general, there is no significant effect on the glass fiber composites when tilted angles are introduced. However, for carbon and kenaf fiber composites the specific energy absorptions increased when the angles are increased. In term of force ratio as shown in Fig. 7b, all of the composites used are below than 1.0 indicating that the peak force is always greater than the mean force. However, the force ratio is seen to slightly increase when the tilted angles increase. This is shown the importance of crush initiator where the function is to

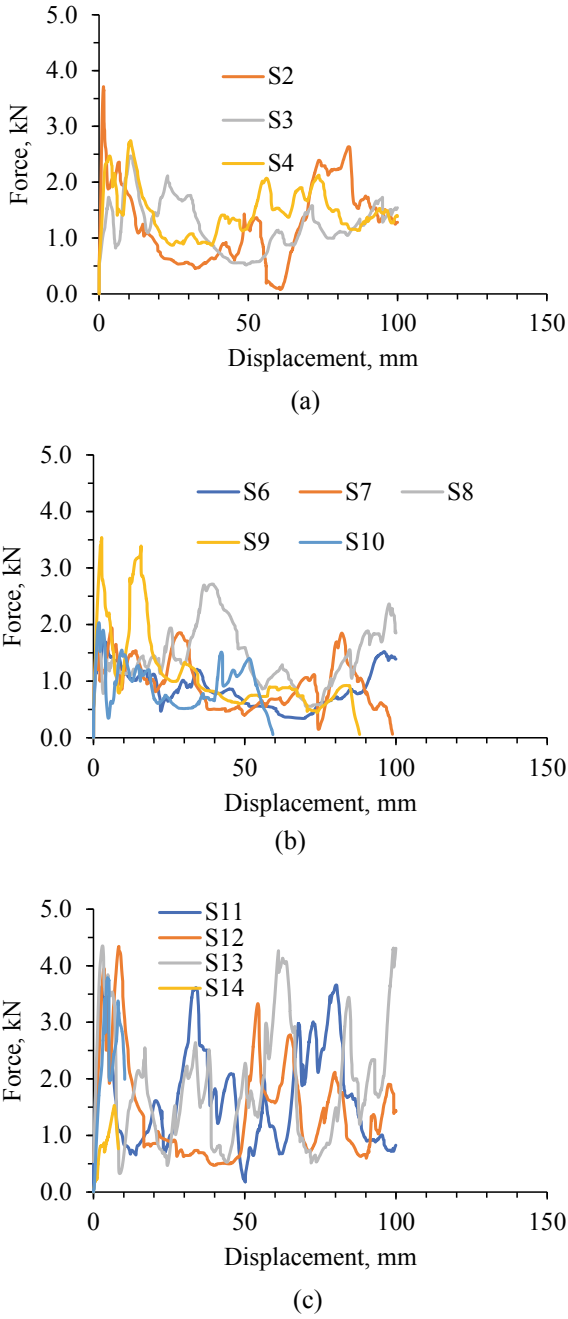


**Fig. 6** Force-displacement responses of **a** glass fiber, **b** carbon fiber and **c** kenaf fibre-reinforced composite tubes

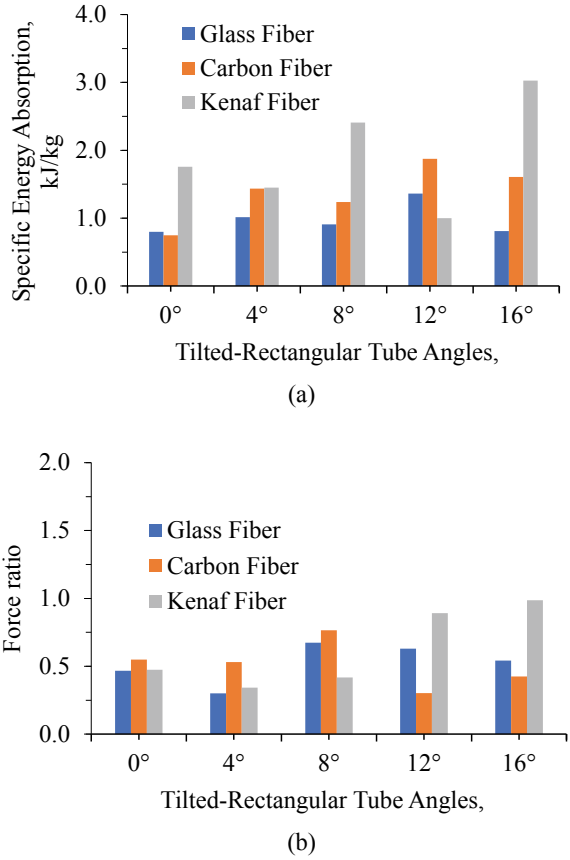


**Fig. 7** Effect of tilted-rectangular tube angles on **a** Specific energy absorption, and **b** Force ratio

reduce the peak force and therefore increasing the mean force. This behaviour of forces responsible to increase the energy absorption performances as revealed in Fig. 7a.

## *3.4 Effect of Fiber Types on the Specific Energy Absorption and Force Ratio*

The influence of the type of fibers on the specific energy absorptions (SEA) and force ratio can be found in Fig. 8 respectively. In general, the performances of SEA are determined by the type of fibers. In Fig. 8a, it is observed that kenaf fiber reinforced composites produced higher number of SEA compared with other types of composites. It is also found that the introduction of crush initiator or tilt-ended tubes capable to increase the SEA. This is due to the fact that crush initiator acts to reduce the severity of localized buckling occurs on the tube walls.

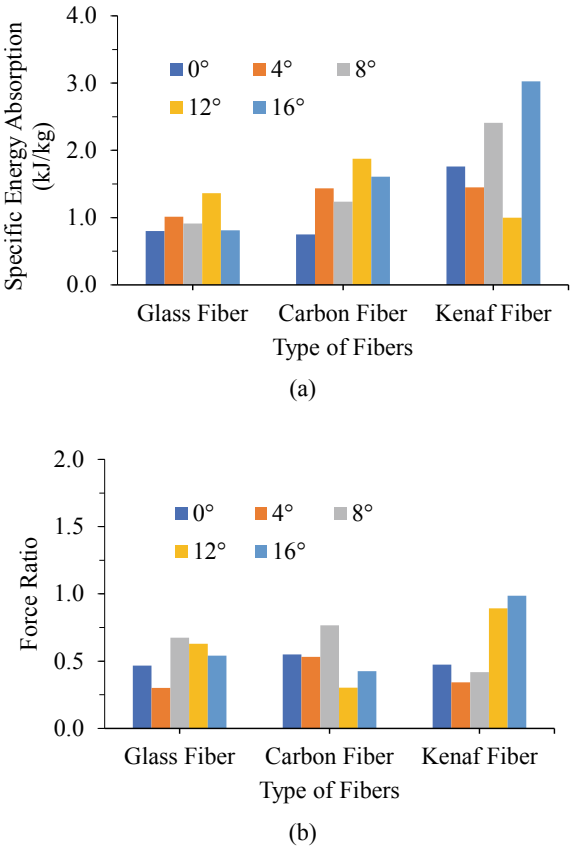


**Fig. 8** Effect of type of fibers on **a** Specific energy absorption and **b** Force ratio

Another indicator as shown in Fig. 8b, the force ratio can also be used to determine the level of SEA. If the force ratio is low, it can be observed that the SEA is also low. For both glass and carbon fibers, the force ratio is relatively lower than the force ratio for kenaf fibers. This is why in general the SEA for kenaf fiber composites are relatively higher than other types of composites.

## 4 Conclusion

Quasi-static compression tests are conducted experimentally on the rectangular tubes fabricated using a different type of fibres and tilted-side angles. During the compression, force-displacement curves are extracted and analyzed to obtain the specific energy absorption and force ratio. It is found that tilted angles played an important role in increasing the specific energy absorption and force ratio. Kenaf fiber is observed to offer higher specific energy absorption performances compared with

other types of composites. In term of force ratio, there is an insignificant effect on the force ratio. Sizes of composite fragmentations are also determined the performance of energy absorption.

**Acknowledgements** Authors acknowledge Universiti Tun Hussein Onn Malaysia (UTHM) for sponsoring this works.

## References

1. Albahash ZF, Ansari MNM (2017) Investigation on energy absorption of natural and hybrid fiber under axial static crushing. Compos Sci Technol 15:52–61
2. Hu D, Zhang C, Ma X, Song B (2016) Effect of fiber orientation on energy absorption characteristics of glass cloth/epoxy composite tubes under axial quasi-static and impact crushing condition. Compos: Part A 90:489–501
3. Swolfs Y, Gorbatikh L, Verpoest I (2014) Fibre hybridization in polymer composites: a review. Compos: Part A 67:181–200
4. Alkbir MFM, Sapuan SM, Nuraini AA, Ishak MR (2016) Fibre properties and crashworthiness parameters of natural fibre-reinforced composite structure: a literature review. Compos Struct 148:59–73
5. Baroutaji Ahmad, Sajjia Mustafa, Olabi Abdul-Ghani (2017) On the crashworthiness performance of thin-walled energy absorbers: Recent advances and future developments. Thin-Walled Struct 118:137–163
6. Ismail AE, Sahrom MF (2015) Lateral crushing energy absorption of cylindrical kenaf fiber reinforced composites. Int J Appl Eng Res 10(8):19277–19288
7. Khalid SNA, Ismail AE, Zainulabidin MH, Tajul Arifin AM, Hassan MF, Ibrahim MR, Rahim MZ (2018) Mechanical performances of twill kenaf woven fiber reinforced polyester composites. Int J Integr Eng 10(4):49–59

# Numerical and Experimental Assessment Of Water Absorption of Red Mud-An Industrial Waste Reinforced Sisal/Polyester Hybrid Polymer Composite


**S. Vigneshwaran, M. Uthayakumar, V. Arumugaprabu, and R. Sundarakannan**

**Abstract** The fundamental point of the investigation is to examine the water absorption qualities of highly alkaline red mud (a waste created during the production of alumina) reinforced sisal/polyester hybrid composite. Composites are fabricated at a different percentage of red mud (0, 10, 20 and 30%) utilizing the compression moulding process. Manufactured composites are inspected for water absorption qualities. Water absorption test is done using three unique waters, such as ocean water, ordinary water and distilled water. Redmud inclusion decreased the water absorption of the composites but the increment in redmud reinforcement increases the water absorption. The water absorption behavior of the composite is explored with the numerical model—Fick's law of diffusion. The water absorption model was found to follow the Fickian behavior for each of the three water used. The composites are analyzed through Scanning electron microscopy (SEM) for understanding the surface failure and fiber damage.

**Keywords** Redmud · Sisal fiber · Hybrid composite · Void · Water absorption

S. Vigneshwaran · M. Uthayakumar (✉) · V. Arumugaprabu · R. Sundarakannan
Kalasalingam Academy of Research and Education, Krishnankoil, India
e-mail: uthaykumar@gmail.com

S. Vigneshwaran
e-mail: s.vigneshwaren@gmail.com

V. Arumugaprabu
e-mail: v.arumugaprabu@klu.ac.in

R. Sundarakannan
e-mail: sundarakannan.r@gmail.com

© Springer Nature Singapore Pte Ltd. 2021

M. Jawaid et al. (eds.), *Structural Health Monitoring System for Synthetic, Hybrid and Natural Fiber Composites*, Composites Science and Technology,
https://doi.org/10.1007/978-981-15-8840-2_15

## 1 Introduction

Natural fiber reinforced polymer composites are utilized in different open-air applications owing to their improved performance with minimal cost and eco-benevolence. Despite the fact that they are more appealing than synthetic fibre-reinforced polymers, their poor moisture resistance property limits their utilization in different open-air application. The water absorbed by the natural fiber polymer composites influences the mechanical quality of the composites by affecting the fiber reinforcement and matrix material [1]. To extend the life of natural fiber composites it is fundamental to improve the water-resistance property of the composites. Several researches addressed that hybridization in polymer composites can increase the composites water resistance property [13]. Hybridization in polymer composites can be accomplished by the addition of at least one fiber or filler or filler with fiber in a matrix. By hybridization, the composites can be developed with a balanced performance at low cost [18]. Inclusion of filler particles in the fiber composite enhances the mechanical performance which can likewise increase the water resistance property [8]. Utmost care should be taken in selecting the filler or fiber reinforcement which should be suitable for practical requirements and economical [22].

Removal of redmud is a significant issue to be addressed around the world. To meet the aluminium need all through the world the production of alumina has expanded which reliably expanded the red mud. Red mud is made out of mineral oxides which vary on the proportion from the geological region [10]. These wastes are isolated from the living space zone and dumped in an enormous sum in landfills. At present as a result of the lack in disposal capacity and ecological issues, these wastes have been tried for their potential utilization in different applications [20]. In composite material fabrication red mud has been utilized as a potential reinforcement material. Several researchers examined the adequacy of redmud support in cement [9, 12], metal matrix composite [17] and polymer composites [23, 14] utilized redmud as a filler material in a polyester matrix and studied the composite tensile, impact and hardness property. Addition of redmud in the matrix increased the impact strength to 47% when compared to the pure polyester matrix. In another work Prabu et al. [15] reinforced redmud in banana-fibre composite and found increased mechanical performance. Satapathy and Patnaik [21] reported an increase in the wear performance of the polyester composites owing to the reinforcement of red mud. Rachchh et al. [16] noticed an improvement in the mechanical and buckling characteristic of coir fiber reinforced polymer composite on redmud inclusion.

In this manner, redmud has been effectively reinforced in the natural fiber composites and enhancements in properties were recorded, also the red mud composites were suggested for different auxiliary applications [24]. In such a cause it becomes more essential to find the durability of the composites to the environmental conditions. Understanding this the current work is focused on studying the water absorption behavior of the redmud particle added natural fiber (sisal fiber) reinforced polyester hybrid composite. The significance of redmud reinforcement in the water intake behavior of the composite in correlation with the kinetic and water absorption was studied.

## 2 Materials and Methods

Composite plates of size 300 × 127 × 3 mm having 40% fiber reinforcement and redmud of three rates (0, 10, 20 and 30%) were fabricated utilizing press moulding. The selected natural fiber is sisal fiber which is used in the form of randomly arranged long fiber mat brought from Tokyo Corporation, India. For particle reinforcement, the industrial waste red mud is used which is obtained from the NALCO, India. The matrix material used for the present investigation is unsaturated polyester purchased from Vasavibala Resins Private limited, India. Wax was applied throughout the mould for making the composite removal process easy. Initially, the matrix is blended with red mud thoroughly. Then as preferred by the makes unsaturated polyester with the catalyst (methyl ethyl ketone peroxide) and accelerator (Cobalt naphthenate) were taken in the proportion of 100:1:1 and completely blended. The blended mixture is applied over the fiber placed in the mould. Utmost care was taken to avoid the formation of air traps. Finally, the mould is closed and compressed at a pressure of 200 kg/cm$^2$ and left to cure for 4 h. After curing, the composite was removed from the mould and was then cut to the required dimensions. The composition of matrix, filler and fiber is shown in Table 1.

### *2.1 Characterization of Material Properties*

#### 2.1.1 Density and Void Fraction

The void percentage of the composites is found through Eq. 1.

$$\text{Void fraction} = \frac{\rho_{th} - \rho_{exp}}{\rho_{th}} \tag{1}$$

$\rho_{th}$ and $\rho_{exp}$ are the theoretical density and experimental density of the composites. The experimental density is found through the Archimedes principle and the theoretical density is calculated through following Eq. 2 [19].

**Table 1** Details of Fabricated composite

| S. No | Composition | Designation |
|---|---|---|
| 1 | 60 wt% Polyester + 40 wt% Sisal fiber + 0 wt% Redmud | SR |
| 2 | 50 wt% Polyester + 40 wt% Sisal fiber + 10 wt% Redmud | SR10 |
| 3 | 40 wt% Polyester + 40 wt% Sisal fiber + 20 wt% Redmud | SR20 |
| 4 | 30 wt% Polyester + 40 wt% Sisal fiber + 30 wt% Redmud | SR30 |

$$\rho_{th} = \frac{1}{\left(\frac{W_{fiber}}{\rho_{fiber}}\right) + \left(\frac{W_{matrix}}{\rho_{matrix}}\right) + \left(\frac{W_{filler}}{\rho_{filler}}\right)} \quad (2)$$

where, $W_{fiber}$, $W_{matrix}$ and $W_{filler}$ is the weight percentage of fiber, filler and matrix in the composite respectively, $\rho_{fiber}$, $\rho_{matrix}$ and $\rho_{filler}$ is the density of fiber, filler and matrix in the composite respectively.

## 2.2 Water Absorption Test

The water absorption test was carried out as per ASTM D570-98 standard. The SR composites of dimension 25 × 25 × 3 mm were used for testing. The composites were immersed in the water medium for 30 days at room condition. Intermittently the samples were taken out one after one and cleaned for expelling moisture from the surface, at that point weighted. Similarly, all the samples were weighted intermittently at 1, 2, 3, 4, 5, 6, 7, 8, 9, 10, 15, 20, 25, 30 days' submersion until saturation point. For every composite, three samples were tested and the average was noted. Finally using the weight of the tested composites ($w_o$-weight of the SR composite before immersion and $w_1$-after immersion) water absorption percentage is calculated through Eq. 3 [7],

$$\text{Percentage of water absorption} = \frac{(w_1 - w_0)}{w_0} \quad (3)$$

## 2.3 Kinetics of Water Absorption

The water absorption phenomenon of fiber composites is categorized by three major characteristics [13] which includes: (i) Transmission of water molecules through the minute gapsin the polymer chain, (ii) Transmission by capillary transportation—where the water molecules diffuse through the voids and fibre-matrix interfacial region, (iii) Final diffusion is through the micro-cracks in the matrix material developed because of the compounding process. However, these phenomena were active and important in understanding the water absorption behavior, yet it becomes vital to perform diffusion analysis according to Fick's theory [6]. Water absorption behavior can be explained by several mechanisms for composite material. But in case of better analysis the diffusion mechanism is well correlated. The diffusion mechanism was postulated by Fick's theory. This includes three cases [5]

i. Case-i or Fickian diffusion
ii. Case-ii
iii. Case-iii or Non- Fickian diffusion (Intermediate of case i and case ii)

All these three diffusion characteristics can be differentiated by means of sorption curve drawn with the aid of the data collected from water absorption test conducted, which is also represented by Fick's equation [11],

$$\frac{M_t}{M_m} = Kt^n \tag{4}$$

where $M_t$is the percentage of water absorbed at time t, $M_m$ is the maximum water absorption at the equilibrium point, k and n are kinematic constants. The values of n explain the diffusion mechanism of the material water absorption as case i ($n = 0.5$), case ii ($n \geq 1$), case iii ($0.5 \leq n < 1$) [5]. The constant k value represents the relation between time and saturation point. Higher and lower water absorption is the function of the diffusion rate of water molecules. By using Fick's diffusion coefficient (D), the rate of water molecules diffusion can be found. Fick's diffusion coefficient is used to determine the water sorption and water molecule penetration behaviour [7] which can be determined using the Eq. 5 using specimen thickness (h), maximum water absorbed at equilibrium point ($M_m$) and slope (ɵ) of curve plotted against $M_t$ and t [11].

$$D = \pi \left( \frac{h\theta}{4M_m} \right)^2 \tag{5}$$

The sorption coefficient (S) determining the solubility related to water absorption can be determined by the following Eq. 6 [11],

$$S = \frac{M_m}{M_t} \tag{6}$$

Meanwhile, the Permissible Coefficient (P) can be calculated by multiplying the Fick's diffusion coefficient (D) and the sorption coefficient (S),

## 3 Result and Discussion

### *3.1 Water Absorptions*

It is well known that both the redmud and the sisal fiber were hydrophilic. To find the durability of composites in water-based applications, the composites samples were subjected to the water absorption test. From the test results, the water absorption percentage of composites in normal water, seawater, and distilled water are found which is shown in Fig. 1. The water absorption percentage of the unfilled composites was higher in all the three different water. All the composites showed the linear increase in water intake at the initial stage and then water intake becomes slow until

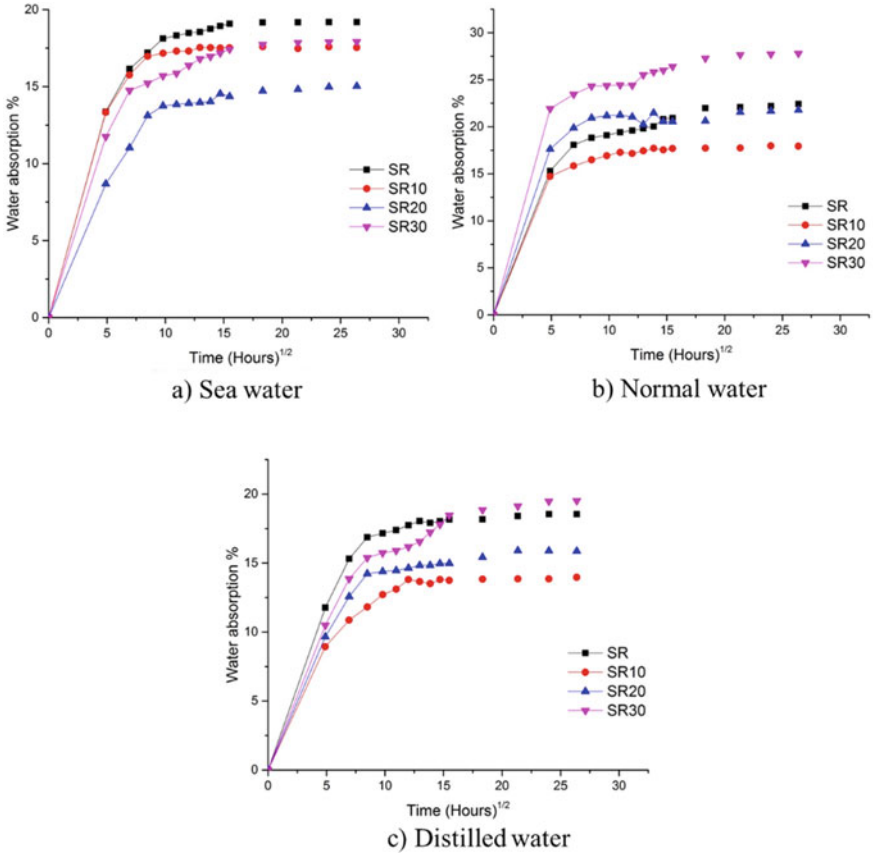


**Fig. 1** **a** Water absorption curves for Sea water immersion, **b** Water absorption curves for Normal water immersion, **c** Water absorption curves for Distilled a water immersion

it attains the saturation level. The filled composites showed reduced water absorption because of the good bonding of fiber, filler and the matrix material. Also, it is noticed that at increasing the redmud content to 20% and 30% the water absorption percentage increases. This could be due to the aggregation of red mud particle in the matrix, phase separation and formation of voids on the composite structure.

## *3.2 Diffusion Mechanism and Fitting of Fick's Diffusion Law*

Table 2 shows the calculated kinematic parameters k and n value from the fitting curves plotted against $M_t/M_m$ and time using experimental data. For all the three different waters, the value of n was found to be close to 0.05 which explains the Fick's diffusion behaviour. This concludes that the fitness of the experimental data with the

**Table 2** Diffusion kinematic parameters n and k

| S. No | Specimen | n | | | k | | |
|---|---|---|---|---|---|---|---|
| | | Normal water | Distilled water | Seawater | Normal water | Distilled water | Seawater |
| 1 | SR | 0.5304 | 0.5001 | 0.5246 | 0.027 | 0.024 | 0.023 |
| 2 | SR10 | 0.5210 | 0.5008 | 0.5190 | 0.026 | 0.022 | 0.019 |
| 3 | SR20 | 0.5346 | 0.4993 | 0.5187 | 0.028 | 0.028 | 0.023 |
| 4 | SR40 | 0.5112 | 0.5179 | 0.5361 | 0.029 | 0.027 | 0.024 |

Fickian diffusion model. Larger k value denotes the attainment of equilibrium at the minimum time [4]. The value of k on SR10 composites was minimum when compared to the SR composites in all three waters. This proves the efficiency of filler material against water absorption. The main reason could be the addition of redmud particles restricts water penetration through the fibers. The k value is high for groundwater immersion indicating that the high interaction of water molecules with the composites than the water molecules present in the sea and distilled water.

Higher water absorption was noted after 96 and 120 h and this may because of the propagation of cracks in the surface and separation of fiber from the matrix. Debonding occurs as the material starts swelling because of the high intake of water. Further prolonged immersion leads to the dissolution of soluble matters presents in the fiber such as hemicellulose, pectin and other soluble contents. This is absorbed through the colour variation of water in unfilled composites. After 168 h the SR20 and SR30 composites showed severe changes in the watercolour. The watercolour changes to red which indicates the filler dissolution. At this stage, the SR20 and SR30 composites showed higher water intake. Although there is some material loss due to immersion, there is an increase in the weight percentage since water absorption is higher than the material loss.

Up to a certain time, the water absorption percentage was high and this is because the water intake by the surface cracks present in the composite. The reason behind this mechanism is highly related to the sisal fiber characteristics. Since the sisal fiber is hydrophilic it readily absorbs the water, which turns the fibers to swells. The swelling in fibers develops the stress in the matrix which results in cracks propagation. Due to prolonged immersion, the water molecules break the bond and enter the fiber region. The increase cellulose content in the fibers allows more water intake which causes composites failure through delamination of fiber from the matrix. The water molecules easily affect the fiber matrix bonding region and weak the fiber lead to delamination. Figure 2 shows the delaminated fiber from the matrix.

Table 3 presents the calculated diffusion coefficient (D) and permissible coefficient (P). The diffusion coefficient calculated is similar as the results reported in various composite materials [2, 3] where the diffusion coefficient value varies between $10^{-8}$ to $10^{-9}$ ($mm^2/s$). The diffusion coefficient of the composites varies for all the three waters used owing to the difference in water molecules diffusion rate. Higher the

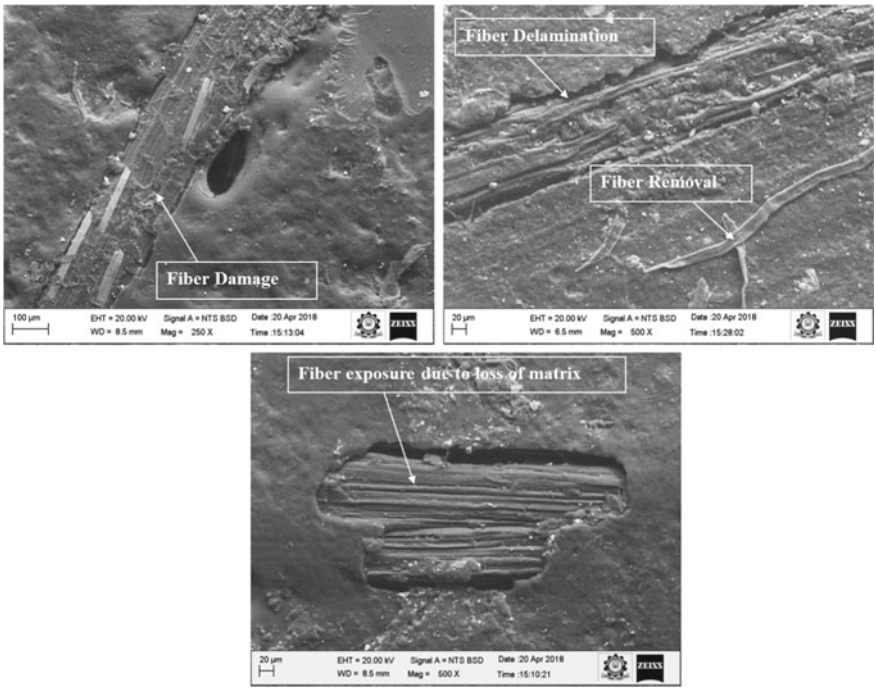


**Fig. 2** Fiber damage due to normal water immersion on unfilled composite

diffusion coefficient indicates the faster attainment of the equilibrium state of moisture absorption. The unfilled composites have a higher diffusion coefficient than the 10% redmud filled composite in all the three water immersion test. This explains the ability of redmud reinforcement against water diffusion through the composites. But in case of increasing the redmud to 20% and 30% the diffusion coefficient increases. This is because the increase in the redmud percentage allows the water molecules to diffuse easily through the micro cracks and voids (Fig. 3a) in the composite surface. Development of micro cracks was severe in the unfilled composites than the filled composite (Fig. 4a). Attack of water molecules removes the matrix from the surface more easily in the unfilled composites (Fig. 3b). The redmud particle in the matrix of SR10 composite develops the good bonding with the matrix which restricts the flow of water molecules into the fibers. The increased redmud percentage in the composite SR20 and SR30, the surface of the composite consists of redmud accumulated regions where the development of crack was severe (Fig. 4b). Through these regions the water molecule easily diffuses and forms cracks in the surface.

**Table 3** Calculated diffusion coefficient (D) and permissible coefficient (P)

| S. No | Specimen | Sorption coefficient (S) | | | Diffusion Coefficient (D) × $10^{-8}$ ($mm^2/s$) | | | Permissible Coefficient (P) × $10^{-8}$ ($mm^2/s$) | | |
|---|---|---|---|---|---|---|---|---|---|---|
| | | Normal water | Distilled water | Sea water | Normal water | Distilled water | Sea water | Normal water | Distilled water | Sea water |
| 1 | SR | 1.077 | 1.114 | 1.151 | 5.91 | 3.52 | 2.36 | 6.36 | 3.92 | 2.71 |
| 2 | SR10 | 1.168 | 1.112 | 1.044 | 5.00 | 3.12 | 2.57 | 5.84 | 3.46 | 2.69 |
| 3 | SR20 | 1.180 | 1.108 | 0.969 | 5.76 | 4.78 | 1.99 | 6.79 | 5.30 | 1.93 |
| 4 | SR30 | 1.238 | 1.110 | 1.137 | 6.90 | 5.39 | 1.45 | 8.54 | 5.98 | 1.64 |

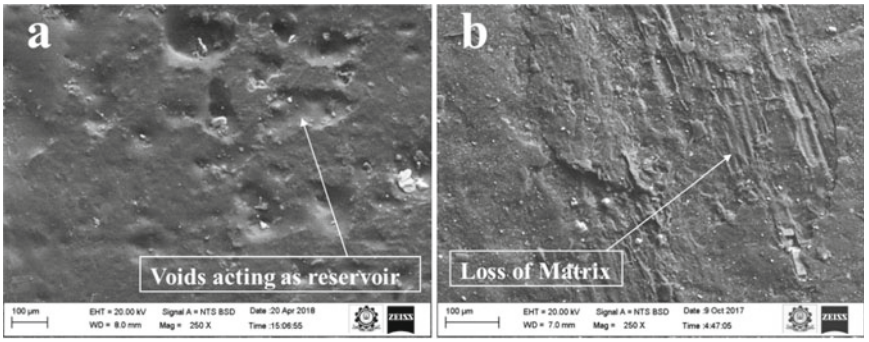


**Fig. 3** Voids and matrix removal due to normal water immersion on unfilled composite

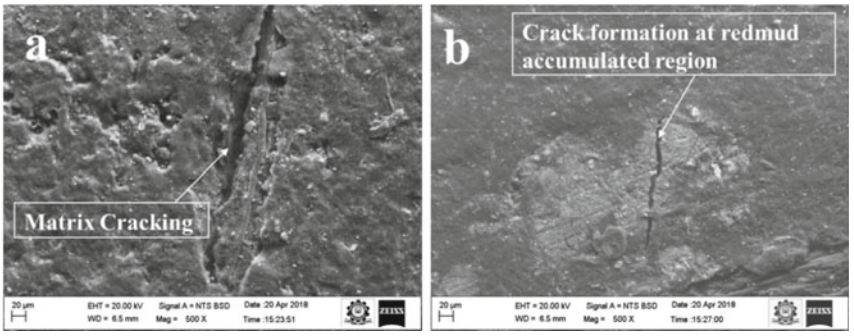


**Fig. 4** Development of cracks due to normal water immersion on **a** Unfilled composite **b** SR30 composite

## *3.3 Void Fraction Influence on Water Absorption*

The void fraction of the SR composites with its density is shown in Table 4. The density of the composites increased with the red mud addition and correspondingly the voids also increased. Density increased is the main reason for the reinforcement

**Table 4** Void fraction and water absorption percentage

| S. No | Designation | Theoretical Density ($gm/cm^3$) | Experimental Density ($gm/cm^3$) | Void Fraction (%) | Water absorption percentage (%) | | |
|---|---|---|---|---|---|---|---|
| | | | | | Normal water | Distilled water | Sea water |
| 1 | SR | 1.1851 | 1.1482 | 3.1161 | 18.54 | 22.42 | 30.34 |
| 2 | SR10 | 1.2604 | 1.1790 | 6.4557 | 13.97 | 17.93 | 23.97 |
| 3 | SR20 | 1.3458 | 1.2525 | 6.9327 | 15.87 | 21.79 | 28.21 |
| 4 | SR30 | 1.4437 | 1.2884 | 10.759 | 19.51 | 27.81 | 34.36 |

of hard red mud particle. The void in the composites is mainly because of the red mud particle clustering. At increased weight percentage the red mud particle sticks together and developed particle clustering. In the particle clustered area the matrix has poor bonding and developed pores and voids. Because of these reasons the voids are found to be high at increased red mud percentage. Presence of void reduces the composite strength. In the present investigation, it is noted that the water absorption percentage increases on increase in the voids. However, for the unfilled composite the void fraction is low yet water absorption increases owing to the direct contact of water molecules with fiber. But in the red mud reinforced composites, red mud restricts the direct attack of water molecules. So compared to unfilled composites the water absorption was low on filled composites even at the high void percentage. However, on increasing the red mud reinforcement the water absorption was increased owing to the high red mud agglomeration in the composites. The water molecules enter into the red mud agglomerated areas and contact the fiber reinforcement which increases the water absorption percentage corresponding. In all the water medium 30wt% red mud composite showed increased water absorption percentage.

## 4 Conclusion

From the investigation of water absorption characteristics of red mud sisal fiber composites following conclusions were drawn:

- Hybridization of redmud with sisal fiber reduced the moisture absorption of the composites. Filled composite with 10% redmud addition showed better water resistance than the unfilled composite which has 20%, 25% and 8% reduction in water absorption when compared to unfilled composite at distilled, normal and seawater respectively. Composite with 20% and 30% redmud percentage increases the water intake.
- The diffusion coefficient (D) was high for 30% redmud filled composite in the normal water immersion which was 28% higher than distilled water immersion and 78% higher than seawater immersion.
- Increases in voids increase the water absorption percentage. SEM analysis on the water absorption tested specimens reveals the development of cracks in the matrix surface and fiber delamination and damage. Prolonged immersion in water causes separation of fiber layers.

## References


1. Akil HM, Cheng LW, Mohd Ishak ZA et al (2009) Water absorption study on pultruded jute fibre reinforced unsaturated polyester composites. Compos Sci Technol 69:1942–1948
2. Anbukarasi K, Kalaiselvam S (2015) Study of effect of fibre volume and dimension on mechanical, thermal, and water absorption behaviour of luffa reinforced epoxy composites. Mater Des 66:321–330
3. Athijayamani A, Thiruchitrambalam M, Natarajan U, Pazhanivel B (2009) Effect of moisture absorption on the mechanical properties of randomly oriented natural fibers/polyester hybrid composite. Mater Sci Eng A 517:344–353
4. Boukettaya S, Alawar A, Almaskari F et al (2018) Modeling of water diffusion mechanism in polypropylene/date palm fiber composite materials. J Compos Mater 52:2651–2659
5. Chen RS, Ab Ghani MH, Salleh MN et al (2015) Mechanical, water absorption, and morphology of recycled polymer blend rice husk flour biocomposites. J Appl Polym Sci 132:41494
6. Deepak JR, Arumugaprabu V, Manikandan V (2021) Effect of Moisture on the resistance of sansevieria cylindrica-reinforced vinyl ester composites. J Test Eval 49:20180827
7. Dhakal HN, Zhang ZY, Richardson MOW (2007) Effect of water absorption on the mechanical properties of hemp fibre reinforced unsaturated polyester composites. Compos Sci Technol 67:1674–1683
8. Geetanjali D, Sandhayarani B (2016) Physical, mechanical and water absorption behaviour of coir fiber reinforced epoxy composites filled with $Al2O_3$ particulates. IOP Conf Ser: Mater Sci Eng 115:012012
9. Liu RX, Poon CS (2016) Utilization of red mud derived from bauxite in self-compacting concrete. J Clean Prod 112:384–391
10. Liu X, Zhang N (2011) Utilization of red mud in cement production: a review Waste management & research: the journal of the international solid wastes and public cleansing association. ISWA 29:1053–1063
11. Mrad H, Alix S, Migneault S et al (2018) Numerical and experimental assessment of water absorption of wood-polymer composites. Measur: J Int Measur Confeder 115:197–203
12. Nikbin IM, Aliaghazadeh M, Charkhtab S, Fathollahpour A (2016) Environmental impacts and mechanical properties of lightweight concrete containing bauxite residue (red mud). J Clean Prod 172:2683–2694
13. Panthapulakkal S, Sain M (2007) Studies on the water absorption properties of short hemp—glass fiber hybrid polypropylene composites. J Compos Mater 41:1871–1883
14. Prabu VA, Johnson RDJ, Amuthakkannan P, Manikandan V (2017) Usage of industrial wastes as particulate composite for environment management: Hardness, Tensile and Impact studies. J Environ Chem Eng 5:1289–1301
15. Prabu VA, Uthayakumar M, Manikandan V et al (2014) Influence of redmud on the mechanical, damping and chemical resistance properties of banana/polyester hybrid composites. Mater Des 64:270–279
16. Rachchh NV, Misra RK, Roychowdhary DG (2015) Effect of red mud filler on mechanical and buckling characteristics of coir fibre-reinforced polymer composite. Iran Polym J 24:253–265
17. Rajesh S, Rajakarunakaran S, Sudhakara Pandian R (2012) Modeling and optimization of sliding specific wear and coefficient of friction of aluminum based red mud metal matrix composite using Taguchi method and response surface methodology. Mater Phys Mech 15:150–166
18. Raghavendra G, Ojha S, Acharya SK, Pal SK (2016) A comparative analysis of woven jute/glass hybrid polymer composite with and without reinforcing of fly ash particles. Polym Compos 37:658–665
19. Rout AK, Satapathy A (2012) Study on mechanical and tribo-performance of rice-husk filled glass-epoxy hybrid composites. Mater Des 41:131–141
20. Samal S, Ray AK, Bandopadhyay A (2013) Proposal for resources, utilization and processes of red mud in India—a review. Int J Miner Process 118:43–55

21. Satapathy A, Patnaik A (2010) Analysis of dry sliding wear behavior of red mud filled polyester composites using the taguchi method. J Reinf Plast Compos 29:2883–2897
22. Sundarakannan R, Arumugaprabu V, Manikandan, Vigneshwaran S (2020) Mechanical property analysis of biochar derived from cashew nut shell waste reinforced polymer matrix 6:125349
23. Vigneshwaran S, Uthayakumar M, Arumugaprabu V (2019) Development and sustainability of industrial waste-based red mud hybrid composites. J Clean Prod 230:862–868
24. Vigneshwaran S, Uthayakumar M, Arumugaprabu V (2019) Solid particle erosion study on redmud—An industrial waste reinforced sisal/polyester hybrid composite. Materials Research Express 6:065307